Design and Implementation of an off-grid PV drive system for small-scale fresh produce cooling

by

Jason Avron Samuels

Thesis presented in partial fulfilment of the requirements for the degree of Master of Engineering (Electrical and Electronic) in the Faculty of Engineering at Stellenbosch University

Department of Electrical and Electronic Engineering,
University of Stellenbosch,
Private Bag X1, Matieland 7602, South Africa.

Supervisor: Dr. J. M. Strauss

December 2017

Declaration

By submitting this thesis electronically, I declare that the entirety of the work contained therein is my own, original work, that I am the sole author thereof (save to the extent explicitly otherwise stated), that reproduction and publication thereof by Stellenbosch University will not infringe any third party rights and that I have not previously in its entirety or in part submitted it for obtaining any qualification.

Date: December 2017

Abstract

Design and Implementation of an off-grid PV drive system for small-scale fresh produce cooling

J. Samuels

Department of Electrical and Electronic Engineering,
University of Stellenbosch,
Private Bag X1, Matieland 7602, South Africa.

Thesis: M.Eng (E & E)

December 2017

The implementation of a PV drive system is discussed in this thesis with the focus on fresh produce cooling for small-scale farmer. A background study is presented, which firstly addresses hunger and food insecurity through emphasis on one of the mentioned six causes of hunger, namely, food waste. Further focus is placed on cooling and, specifically, solar cooling. Therefore, the relevant factors pertaining to cooling and solar energy as a power source are presented, adding to the background study.

Thereafter, the project details are outlined which states the research significance as the investigation of feasibility, in terms of cost and performance, of the design and implementation of PV drive systems, using the proposed development process. With that being said, the design of the PV drive system, elevation of low-voltage solar PV energy and cost-effective implementation were evaluated.

In a high-level project overview the project parts are presented for the designed and implemented PV drive system, with the focus on the solar energy source and the cooling application. Similarly, the proposed development process is discussed through which the drive system was implemented. In effect, this process entails using off-the-shelf subsystems, as far as possible, to construct the drive system with only the necessary self-built subsystems. The drive system consists of the following self-built subsystems, namely the DC-DC converter and control module, and a commercial VSD, with integration between these subsystems.

As the main means of voltage elevation, from the low-voltage solar PV source, the focus is placed on DC-DC converters. Furthermore, a comparison of DC-DC converters are made, with the defined criteria for the project, for the most suitable converter. For easier comparison, the converters are grouped and their advantages and disadvantages are presented. Ultimately, a converter choice was made.

The chosen converter, the resonant push-pull converter, was thoroughly discussed, analysed and specifically designed for the project. Furthermore, this theoretical design of the converter was firstly simulated, for confirmation, before physical construction proceeded. Thereafter, converter tests were done to verify the design through various measurements. Most importantly, the converter output voltage range and efficiency were measured and verified to a satisfactory degree.

The system control module allowed for proper operation of the converter and, moreover, the integration of the PV drive subsystems. Furthermore, the microcontroller-based control module is discussed and the implemented algorithms are presented for optimal energy transfer; these algorithms were expressed in flow diagrams. In addition, transient control results are shown for start-up and load variations for verification.

After verification of the main subsystems, the complete PV drive system was operated throughout a whole day with an appropriate load, to ensure proper conclusions are made. Unfortunately, a cooling system could not be acquired for testing. Details for the demonstration are presented, which include the specific equipment used and results for the operation. Moreover, the results present a fully operational drive system from a low-voltage solar PV energy source able to drive the appropriate load, which demonstrates successful performance. However, the drive system included performance shortfalls, which are discussed and for which recommendations were provided.

With the drive system operational, conclusions were made, regarding cost and performance, in comparison with other similar systems. In addition, the research objectives and aims were evaluated. After evaluation, although the PV drive system could be designed and implemented to a successful measure with regards to performance, it fell short regarding cost in comparison with the compared systems. Therefore, the proposed PV drive system, with the development process followed, is not completely feasible in implementation -to the degree described- for fresh produce cooling for small-scale farmers.

Uittreksel

Ontwerp en toepassing van 'n nie netwerkgeskakelde FV aandryfstelsel vir kleinskaalboerdery vars oes en opbrengs verkoeling

J. Samuels

Departement Elektriese en Elektroniese Ingenieurswese,
Universiteit van Stellenbosch,
Privaatsak X1, Matieland 7602, Suid Afrika.

Tesis: M.Ing (E & E)

Desember 2017

Die implementering van 'n fotovoltaïese (FV) aandryfstelsel word bespreek in die tesis met die fokus op die verkoeling van vars produkte in kleinskaalboerdery. 'n Agtergrondstudie is aangebied wat eerstens hongersnood en voedselonsekerheid aanspreek met die klem op een van die ses genoemde oorsake van hongersnood, naamlik, voedselvermorsing. Verdere fokus is geplaas op verkoeling, spesifiek sonverkoeling, en die relevante faktore van verkoeling en sonenergie as bron is aangebied, in byvoeging tot die agtergrondstudie.

Daarna is die projek besonderhede getoon wat die navorsingsbelang verklaar as die uitvoerbaarheidsondersoek, in terme van koste en uitvoering, van die ontwerp en toepassing van FV aandryfstelsels, met die voorgestelde ontwikkelingsproses. Met dit gesê, is die ontwerp van die FV aandryfstelsel, die verhoging van die laespanning FV sonenergie bron en koste-effektiewe toepassing geëvalueer.

In 'n hoëvlak projekoorsig is die projekdele aangebied vir die ontwerp en toepassing van die FV aandryfstelsel met die fokus op die sonenergie as bron en die voerkoelingstoepassing. Soortgelyk is die voorgestelde ontwikkelingsproses bespreek waardeur die FV aandryfstelsel toegepas is. In effek bevat die proses die gebruik van van-die-rak substelsels, so ver mootlik, om die FV aandryfstelsel saam te stel met net die nodige selfgeboude substelsels. Die aandryfstelsel bestaan uit die volgende selfgeboude substelsels, naamlik, die g.s.-g.s. omsetter en die beheermodule, en 'n kommersieële veranderbare spoed aandrywer (VSA), met integrasie tussen die substelsels.

As hoof manier van spanningsverhoging, vanaf die laespanning FV sonenergiebron, is die fokus geplaas op die GS-GS omsetter. Nog meer is 'n vergelyking van g.s.-g.s. omsetters gemaak, met die gekose kriteria vir die projek, vir die mees gepaste omsetter. Om die vergelyking makliker te maak is die omsetters gegroepeer en hulle voordele en nadele getoon. Uiteindelik is 'n omsetterkeuse gemaak.

Die gekose omsetter, die resonante stoot-trek omsetter, is deuglik bespreek, geanaliseer en ontwerp spesifiek vir die projek. Nog meer, is die teoretiese ontwerp van die omsetter gesimuleer, vir bevestiging, voordat die fisiese samestelling voortgegaan is. Daarna is omsettertoetse gedoen om die ontwerp te bevestig deur verskeie metings. Mees belanglik

is voldoende bevestiging van die omsetter se uittreespanningsbereikmetings en doeltreffendheidmetings.

Die stelselbeheermodule het toegelaat vir behoorlike werking van die omsetter en, nogmeer, die integrasie van die FV aandryfstelseldele. Boonop is die mikrobeheerdergebaseerde beheermodule bespreek en die toegepaste algoritmes aangebied vir optimale energieoordrag; hierdie algoritmes is deur vloeidiagramme uitgedruk. Verder is die oordragsbeheerresultate getoon, van die omsetteraanskakeling en lasvariasies, vir bevesting.

Na bevestiging van die hoofsubstelsels is die volledige FV aandryfstelsel bedryf vir 'n volle dag met 'n toepaslike las om te verseker dat gepaste gevolgtrekkings gemaak is. Ongelukkig is 'n verkoelingsstelstel nie verkry vir toetse nie. Besonderhere vir die demonstrasie is aangebied wat die informasie oor die spesifiek toerusting en resultate van die volle dag se bedryf insluit. Nog meer is die resultate aangebied van 'n werkende aandryfstelsel van 'n laespanning FV sonenergiebron om 'n toepaslike las aan te dryf, wat suksesvolle uitvoering demonstreer. Alhoewel die FV aandryfstelsel suksesvolle werking toon, is tekortkominge in werksverrigting waargeneem en bespreek met die nodige aanbevelings.

Met die FV aandryfstelsel operasioneel, is gevolgtrekkings gemaak met betrekking tot koste en uitvoering saam, in vergelyking met ander soortgelyke stelsels. Nog meer is die navorsingsuitsette en navorsingsdoelwitte geëvalueer. Na die evaluering, alhoewel die FV aandryfstelselontwerp en toepassing tot suksesvolle uitvoeringsmate getoon is, val dit kort in terme van koste in vergelyking met soortgelyke stelsels. Dus is die voorgestelde FV aandryfstelsel met die ontwikkelingsproses gevolg, nie volledig uitvoerbaar in toepassing -tot die mate beskryf- vir vars produk verkoeling by kleinskaalboerdery nie.

Acknowledgments

I would like to express my sincere gratitude and appreciation to the following people and organisations:

- Dr. Strauss for his wisdom, guidance, support and patience throughout the thesis duration. His passion and attitude was truely a driving force of inspiration for myself;
- My family and friends for their support and assistance;
- The financial assistance of the National Research Foundation (NRF) towards this research is hereby acknowledged. Opinions expressed and conclusions arrived at, are those of the author and are not necessarily to be attributed to the NRF;
- The university E & E workshop staff; and
- finally, our heavenly Father.

Contents

Declaration i

Abstract ii

Uittreksel iv

Contents vii

List of Figures xi

List of Tables xvi

1 Introduction 1
- 1.1 Hunger and food insecurity . . . 1
- 1.2 Food waste . . . 3
- 1.3 Cooling . . . 3
  - 1.3.1 Food refrigeration . . . 3
  - 1.3.2 Solar-cooling . . . 3
  - 1.3.3 Compressors . . . 4
- 1.4 Solar PV as an Energy source . . . 5
- 1.5 Introduction to the project . . . 8
- 1.6 Research question . . . 9
- 1.7 Problem statement . . . 9
- 1.8 Research aims . . . 9
- 1.9 Research objectives . . . 10
- 1.10 Significance of the Research . . . 10
- 1.11 Scope of the Research . . . 11
- 1.12 Proposed execution project . . . 11
- 1.13 Thesis outline . . . 12

2 High-level project overview 13
- 2.1 Introduction . . . 13
- 2.2 Development process . . . 14
- 2.3 Input source for the project . . . 14
  - 2.3.1 Introduction . . . 14
  - 2.3.2 Resources for electricity . . . 15
  - 2.3.3 Solar PV . . . 15
  - 2.3.4 Input source specifications . . . 15
  - 2.3.5 Cost of modules . . . 16
  - 2.3.6 Safety . . . 16

2.4 Drive system . . . 16
2.4.1 Introduction . . . 16
2.4.2 Voltage Elevation . . . 16
2.4.3 Control module . . . 16
2.4.4 Variable speed drive . . . 17
2.5 Cooling application . . . 17
2.5.1 Small scale farming . . . 17
2.5.2 Refrigeration . . . 18
2.6 Project specifications . . . 18
2.7 Research project execution . . . 19

3 DC-DC converter 20
3.1 Introduction . . . 20
3.2 DC-DC converters: A brief overview . . . 21
3.2.1 Introduction . . . 21
3.2.2 Elevation factors . . . 22
3.2.3 From linear to switching power supplies . . . 22
3.3 Resonant converter: a brief overview . . . 23
3.4 Criteria of the DC-DC converter choice . . . 24
3.5 Non-isolated converter group . . . 25
3.5.1 Boost converter . . . 25
3.5.2 Interleaved Boost Converter . . . 26
3.5.3 Z-source Converter . . . 27
3.5.4 Clamp-mode Coupled-Inductor Buck-boost Converter . . . 27
3.5.5 Hybrid DC-DC Converter . . . 28
3.6 Isolated converter group . . . 29
3.6.1 Full-bridge converter with half-bridge diode rectifier, center-tap . . . 29
3.6.2 Full-Bridge converter with full-bridge diode rectifier . . . 31
3.6.3 Full-bridge converter with soft-switching . . . 31
3.6.4 Full-Bridge Boost Converter . . . 32
3.6.5 Push-pull Converter . . . 33
3.7 Resonant converter group . . . 35
3.7.1 Series-loaded Resonant DC-DC Converters: . . . 35
3.7.2 Resonant push-pull converter . . . 35

4 Resonant push-pull converter 37
4.1 Introduction . . . 37
4.2 Circuit layout and steady-state analysis . . . 38
4.3 The operation of the converter . . . 39
4.3.1 The non-overlapping region . . . 39
4.3.2 The overlapping region . . . 47
4.4 Design of resonant push-pull converter . . . 52
4.4.1 The design procedure . . . 52
4.4.2 The Specific design procedure of the project . . . 53
4.4.3 The design of the components used in the converter . . . 55
4.4.4 Integration of additional circuitry . . . 60
4.5 Simulation of the design . . . 61
4.5.1 Introduction to Simplorer . . . 61
4.5.2 Brief description of the simulation elements . . . 61

4.5.3 Simulated results . . . 62
4.5.4 Evaluation of simulated results . . . 66
4.6 Construction of the converter . . . 66
4.6.1 PCB design . . . 66
4.6.2 PCB assembly (Manufacturing) . . . 68
4.7 Results . . . 70
4.7.1 Measurements . . . 70
4.7.2 Evaluation of measurements . . . 78

5 System control 79
5.1 Introduction . . . 79
5.2 Control module . . . 80
5.2.1 Control module description . . . 80
5.2.2 Microcontroller . . . 80
5.2.3 The chosen microcontroller . . . 81
5.2.4 Microcontroller peripherals . . . 82
5.2.5 Specific control capabilities . . . 82
5.2.6 PWM . . . 83
5.2.7 Measurements . . . 83
5.2.8 ADC . . . 83
5.2.9 Current measurement circuit design . . . 84
5.2.10 Voltage measurement circuit design . . . 84
5.2.11 Implemented communication methods . . . 85
5.3 Energy flow algorithm concepts . . . 86
5.3.1 Voltage regulation . . . 86
5.3.2 Input power control . . . 86
5.3.3 Output speed control . . . 86
5.4 Order of the algorithm . . . 87
5.4.1 Outline of operation and modes . . . 87
5.4.2 No-operation mode . . . 87
5.4.3 Voltage control mode . . . 87
5.4.4 MPPT mode . . . 88
5.4.5 VSD mode . . . 88
5.4.6 Speed and duty cycle control integration . . . 89
5.4.7 Flow diagrams . . . 90
5.5 Control results . . . 98

6 Results of implemented application 99
6.1 Introduction . . . 99
6.2 Practical implementation . . . 100
6.2.1 Brief overview of subsystems' roles and specifications . . . 100
6.2.2 Aim of demonstration . . . 100
6.2.3 Description of demonstration . . . 100
6.2.4 Results of full load start-up tests . . . 105
6.2.5 Results of full-day operation test . . . 107

7 Conclusion 108
7.1 Introduction . . . 108
7.2 Chapter reflections . . . 108

7.2.1 Chapter 1 . . . 108
7.2.2 Chapter 2 . . . 108
7.2.3 Chapter 3 . . . 108
7.2.4 Chapter 4 . . . 108
7.2.5 Chapter 5 . . . 109
7.2.6 Chapter 6 . . . 109
7.3 Project evaluation . . . 109
7.3.1 Research objectives evaluation: Performance . . . 109
7.3.2 Research aims evaluation: Performance and cost . . . 110
7.3.3 Research question evaluation . . . 111
7.3.4 Shortcomings . . . 111
7.4 Recommendations . . . 112

Appendices **113**

A List of abbreviations **114**

B Power supply **115**

C Control signals **116**

D Motors **120**
D.1 Induction motor vs Brushless DC motor . . . 120
D.1.1 Induction motor . . . 120
D.1.2 Brushless DC motor . . . 120
D.1.3 Comparison between the motors . . . 121
D.1.4 The use of three-phase systems . . . 121

E DC-DC converter : Temperature observation **122**

F Flow diagrams: Full view **124**

G Component financial information **130**

H Output voltage:Start-up attempts before noon **132**

I Output voltage: Start-up attempts after noon **134**

List of References **136**

List of Figures

1.1 Schematic representation of the PV drive system, indicating interactions between various subsystems. . . . 12

2.1 Schematic representation of the PV drive system, indicating interaction between various subsystems. . . . 13
2.2 Variable speed drive . . . 17
2.3 Separate compressor and motor cooling system, including a condenser . . . 19

3.1 Schematic representation of the PV-drive system, indicating interaction of the DC-DC converter between subsystems . . . 20
3.2 The boost converter topology . . . 26
3.3 A two-phase interleaved boost converter with coupled inductors . . . 26
3.4 Z-source converter . . . 27
3.5 Clamp mode coupled-inductor buck-boost converter . . . 28
3.6 Non-isolated boost converter with a high voltage gain for non-isolated on-line UPS . . . 29
3.7 Full-bridge converter: Center-tap connected half bridge diode rectifier . . . 30
3.8 Rectifier configuration: Half-bridge diode rectifier . . . 30
3.9 Full-bridge converter: Full-bridge diode rectifier . . . 31
3.10 Soft-switching Full-bridge Converter . . . 32
3.11 Isolated full-bridge boost converter with voltage doubling rectifier . . . 33
3.12 The push-pull converter topology . . . 34
3.13 The series-loaded resonant DC-DC converter . . . 35
3.14 Resonant Push-Pull converter: which include active clamp circuits and a voltage doubler . . . 36

4.1 Schematic representation of the PV-drive system, indicating interaction between subsystems . . . 37
4.2 Resonant Push-Pull converter . . . 38
4.3 Mode 1 of the non-overlapping operation . . . 40
4.4 Mode 2 of the non-overlapping operation . . . 40
4.5 A current summation of the resonant capacitor currents making up the secondary winding current . . . 41
4.6 Mode 3 of the non-overlapping operation . . . 43
4.7 Inductor voltage over a half period operating below 50 %duty cycle . . . 45
4.8 Non-overlapping control and power signals . . . 46
4.9 Mode 1 of the overlapping operation . . . 47
4.10 Mode 2 of the overlapping operation . . . 48
4.11 Mode 3 of the overlapping operation . . . 49

4.12 The voltage across the inductor for a half period, the overlapping operation . . 50
4.13 Overlapping control and power signals 51
4.14 The center-tap transformer, indicating the number of turns 58
4.15 Integration of converter with the additional circuitry 60
4.16 The switch current of S1 at 35 %duty cycle 62
4.17 The switch current of S1 at 50 %duty cycle 62
4.18 The switch current of S1 at 65 %duty cycle 62
4.19 The switch current of S1 at 35 %duty cycle 63
4.20 The switch current of S1 at 50 %duty cycle 63
4.21 The switch current of S1 at 65 %duty cycle 63
4.22 The switch current of S3 at 35 %duty cycle 64
4.23 The switch current of S3 at 50 %duty cycle 64
4.24 The switch current of S3 at 65 %duty cycle 64
4.25 The switch current of S3 at 35 %duty cycle 65
4.26 The switch current of S3 at 50 %duty cycle 65
4.27 The switch current of S3 at 65 %duty cycle 65
4.28 Schematic view of the gate-drive circuitry 66
4.29 Schematic view of the measurement circuitry 67
4.30 Schematic view: The resonant push-pull converter in Altium 67
4.31 Digital view: The resonant push-pull converter in PCB Altium 67
4.32 Photo: The resonant push-pull inductor 68
4.33 Photo: The resonant push-pull transformer with only one winding, disassembled 68
4.34 Photo: The resonant push-pull transformer with only one winding, assembled 68
4.35 Top view of the resonant push-pull converter 69
4.36 Photo: The resonant push-pull converter from the right side 69
4.37 Photo: The resonant push-pull converter from the left side 69
4.38 Photo: The resonant push-pull converter from the back 69
4.39 Photo: The resonant push-pull converter from the front 69
4.40 The measured output voltages against to the measured input voltages under load (less than 300 W) at various duty cycles 70
4.41 The measured output voltages against the measured input voltages under no-load at various duty cycles 70
4.42 Comparison of output voltage measured from MCU and Multi-meter 71
4.43 Comparison of output voltage measured from MCU and Multi-meter 71
4.44 Comparison of output voltage measured from MCU and Multi-meter 71
4.45 Comparison of input voltage measurements from MCU and Multi-meter 72
4.46 Comparison of input voltage measurements from MCU and Multi-meter 72
4.47 Comparison of input voltage measurements from MCU and Multi-meter 72
4.48 Comparison of input current measurements from MCU and Multi-meter 73
4.49 Comparison of input current measurements from MCU and Multi-meter 73
4.50 Comparison of input current measurements from MCU and Multi-meter 73
4.51 Comparison of output current measurements from MCU and Multi-meter . . . 74
4.52 Comparison of output current measurements from MCU and Multi-meter . . . 74
4.53 Comparison of output current measurements from MCU and Multi-meter . . . 74
4.54 Inductor voltage: Input voltage of 60 V at 65 %duty cycle. 75
4.55 Inductor voltage: Input voltage of 60 V at 50 %duty cycle. 75
4.56 Inductor voltage: Input voltage of 60 V at 35 %duty cycle. 75
4.57 Diode voltage: Input voltage of 50 V at 35 %duty cycle. 76
4.58 Diode voltage: Input voltage of 50 V at 50 %duty cycle. 76

4.59 Diode voltage: Input voltage of 50 V at 65 %duty cycle. 76
4.60 Capacitor clamp voltage: Input voltage of 55.7 V and 4.4 A from the PV source 77
4.61 Capacitor clamp voltage: Input voltage of 60 V and 9.8 A from the Controlled source 77
4.62 Capacitor clamp voltage : Input voltage of 80 V and 14.8 A from the Controlled source 77
4.63 Efficiency: Measured with input voltage 80 V and 550 V output voltage and measured with input voltage 50 V and 550 V output voltage 78

5.1 Schematic representation of the PV-drive system, indicating an interaction between subsystems. 79
5.2 Schematic representation of the control module. 80
5.3 The control module. 81
5.4 Daisy chain connection of master and slave devices 85
5.5 The basic MODBUS RTU message structure 85
5.6 Control loop: Verification of input voltage. 90
5.7 Control loop: Voltage control (Part 1). 91
5.8 Control loop: Voltage control (Part 2). 92
5.9 Control loop: Load or speed control. 93
5.10 Control loop: Maximum power point tracking (Part 1). 94
5.11 Control loop: Maximum power point tracking (Part 2). 94
5.12 Control loop: Speed adjustment (Part 1). 95
5.13 Control loop: Speed adjustment (Part 2). 96
5.14 Control loop: Shutdown. 97
5.15 Output voltage transient: Start up at the light-load condition. 98
5.16 Output voltage transient: Start-up at the no-load condition. 98
5.17 Output voltage transient: The voltage regulation with light load changes after start-up. The magnification indicates the load connection. 98

6.1 Schematic representation of the PV drive system, indicating interaction between various subsystems 99
6.2 Photo: The Yokogawa digital power meter. 101
6.3 Photo: The PV panels used as the input source. 101
6.4 Photo: The AVR debugger. 101
6.5 Photo: The extra airflow fan. 102
6.6 Photo: The multi-meters. 102
6.7 Photo: The control module. 102
6.8 Photo: The resonant push-pull DC-DC converter is shown plugged in. 103
6.9 Photo: The VSD. 103
6.10 Photo: The whole built setup. 103
6.11 Photo: Power sources and oscilloscopes. 104
6.12 Photo: The front view of the industrial fan. 104
6.13 Photo: The induction motor used to run the fan. 104
6.14 Photo: The industrial fan, used as a load. 104
6.15 Photo: The industrial fan and induction motor, a side view 104
6.16 Output voltage transient: Start-up of the system increasing the speed to maximum load, in the morning. 105
6.17 Output voltage transient zoomed in: Start-up of the system increasing the speed to maximum load, in the morning. 105

6.18 Output current transient: Start-up of the system increasing the speed until maximum load, in the morning. . . . 105
6.19 Output voltage transient: Start-up of the system increasing the speed until maximum load, in the afternoon. . . . 106
6.20 Output voltage transient zoomed in: Start-up of the system increasing the speed until maximum load, in the afternoon. . . . 106
6.21 Output current transient: Start-up of the system increasing the speed until maximum load, in the afternoon. . . . 106
6.22 The PV drive system is operated throughout a day. . . . 107

B.1 Photo: The resonant push-pull inductor . . . 115

C.1 Control signals: 35 %Duty cycle . . . 116
C.2 Control signals: 50 %Duty cycle . . . 117
C.3 Control signals: 65 %Duty cycle . . . 118
C.4 Control signals: 35 %Duty cycle dead-time between S1 and S3 . . . 119
C.5 Control signals: 50 %Duty cycle dead-time between S1 and S3 . . . 119
C.6 Control signals: 65 %Duty cycle dead-time between S1 and S3 . . . 119

E.1 Temperature distribution: The diodes heatsinks at 47.9 degrees Celsius. . . . 122
E.2 Temperature distribution: The transformer windings at 47.2 degrees Celsius. . 122
E.3 Temperature distribution: The transformer windings at 79.2 degrees Celsius . . 122
E.4 Temperature distribution: The transformer windings at 76.4 degrees Celsius . 122
E.5 Temperature distribution: The converter. . . . 123
E.6 Temperature distribution: Heatsinks. . . . 123
E.7 Temperature distribution: Heatsinks, with temperature of left heatsink as 68.8 degrees. . . . 123
E.8 Temperature distribution: Heatsinks, with temperature of right heatsink as 60.7 degrees. . . . 123

F.1 Control loop: Verification of input voltage. . . . 124
F.2 Control loop: Voltage control. . . . 125
F.3 Control loop: Load or speed control. . . . 126
F.4 Control loop: Maximum power point tracking. . . . 127
F.5 Control loop: Speed adjustment. . . . 128
F.6 Control loop: Shutdown. . . . 129

G.1 Schematic representation of the PV drive system, indicating interaction between various subsystems . . . 131

H.1 Output voltage transient zoomed in: Start-up of the system increasing the speed until maximum load, in the morning - Attempt 1. . . . 132
H.2 Output voltage transient zoomed in: Start-up of the system increasing the speed until maximum load, in the morning - Attempt 2. . . . 132
H.3 Output voltage transient zoomed in: Start-up of the system increasing the speed until maximum load, in the morning - Attempt 3. . . . 133
H.4 Output voltage transient zoomed in: Start-up of the system increasing the speed until maximum load, in the morning - Attempt 4. . . . 133
H.5 Output voltage transient zoomed in: Start-up of the system increasing the speed until maximum load, in the morning - Attempt 5. . . . 133

I.1 Output voltage transient zoomed in: Start-up of the system increasing the speed until maximum load, in the morning - Attempt 1. 134
I.2 Output voltage transient zoomed in: Start-up of the system increasing the speed until maximum load, in the afternoon - Attempt 2. 134
I.3 Output voltage transient zoomed in: Start-up of the system increasing the speed until maximum load, in the afternoon - Attempt 3. 135
I.4 Output voltage transient zoomed in: Start-up of the system increasing the speed until maximum load, in the afternoon - Attempt 4. 135
I.5 Output voltage transient zoomed in: Start-up of the system increasing the speed until maximum load, in the afternoon - Attempt 5. 135

List of Tables

2.1 Basic electrical design parameters 18

5.1 Speed adjustments for different speed ranges 89
5.2 Speed adjustments for different speed ranges 89

Chapter 1

Introduction

1.1 Hunger and food insecurity

Food insecurity is an outcome of inadequate access to safe and nutritious food necessary for normal development and growth, resulting in chronic undernourishment and hunger. Between 2014 and 2016, an estimated 795 million people across the globe were determined to be undernourished. Most of the affected people were living in developing regions. Increased food availability, accessibility, quality sufficiency and quantity are required to ensure positive nutritional outcomes and long-term food security. Good nutrition plays a vital role in human development; people who receive adequate nutrition are more likely to realize their potential and seize existing opportunities. Furthermore, good governance and political stability create an environment conducive to food security. [1].

Central to the fight against hunger is economic growth-socio-economic elements that enable food security include economic growth, agricultural productivity, and social protection. Thus, due to a higher wage threshold, higher unemployment rate and labor demand, richer countries are less susceptible to food insecurity [1].

Social protection systems and programmes that focus on nutrition, health, and education as well as distribution schemes that promote food security plays a vital role in the fight against hunger. Public policies support the management of food resources and implementation of correct practices and techniques . Improved agricultural productivity plays a key role in increasing food availability and thus improving food security. As agricultural productivity increases, more food is grown. As a result, farmers become more competitive and can generate more income. Higher productivity reduces the price of staple foods and thus increases access to basic food items [1].

In addition, when small-holder and family farmers have the opportunity to sell food at markets, this facilitates the movement of food from surplus to deficit areas, thus ensuring food availability. When food is sold at markets, price signals are transmitted to farmers, giving them indications of how to adjust their production. Not only do farmers selling produce rely on markets to make an income, buyers rely heavily on these markets as a source of affordable food. Improving access to marketing opportunities can have a positive impact on productivity [1].

Small-holder agriculture and family farming are central to reducing poverty and hunger [2]. The majority of poor and hungry people in the developing world reside in rural areas. In 2011, the International Labour Organisation (ILO) stated that this figure is nearly eight out of ten people [3]. Growth in small-holder agriculture and family farming has positive effects on economic and nutritional development in these rural areas [2].

However, food insecurity is one of the outcomes of consumers demanding more food than producers are able to supply. Abdalla (2007) highlights the importance of mobilizing agriculture to rapidly increase food production to meet the growing population needs. He also mentions the value of improving the integration of public, private and informal actors to enable better food security services to the needy with appropriate food pricing schemes and policies. Food availability is negatively affected by problems within the agricultural supply chain. Recurring low productivity and frequent natural disasters contribute to frustration in the supply chain

Issues in the spectrum of demand are related to a lack of food entitlement (poverty), because of weak economic growth; irregular and poor balanced income; unemployment; failure in proper governance and failure to manage supply. Other factors further complicating the fight against hunger are rapidly growing populations, diseases (such as HIV) and constraints in implementation (lack of financial resources) [4].

Technological developments, promotion of agriculture and rural development have a positive impact on the productivity of small-holder farmers and thus poverty reduction. Most of the poor live in rural areas and use agricultural and rural activities as a basis for their livelihoods and depend on the agricultural sector for their income. Therefore, agricultural and rural development is vital to achieving economic growth [5].Most people who are undernourished live in Asia and Africa, and their food security depends on agricultural production and income [4]. It is therefore arguable that *"agricultural development by small farmers in conjunction with policies to enhance the capabilities of the poor to access food, offers the best hope of a swift reduction in mass poverty and hunger"* [5].

Although the world produces enough food to feed its entire population of seven and a half billion people, there are still one in eight people that live in hunger. The World Food Programme (WFP) highlights the following as the main causes of hunger [6]:

- The poverty trap, which is a situation where people living in poverty experience its negative effects in a recurring cycle because they cannot afford certain necessities. These necessities include food and tools. The inability to buy food or tools for work hinders the development of a person living in poverty. This hindrance leads to physical weakness and an inability to earn an income that could help them escape poverty and hunger.

- Lack of investment in agriculture, including lack of infrastructure particularly in developing countries which limits yield and accessibility to food. Investment in agriculture is effective in the reduction of hunger.

- Climate and weather, in the form of natural disasters (droughts, floods, and storms) can have negative consequences for the hungry in developing countries.

- War and displacement conflicts disrupt farming and food production. As fighting forces people to flee, they need to find food while displaced from their homes.

- Unstable markets, wherein the instability of food prices make it difficult for the poor to access food.

- Lastly, food wastage contributes to hunger as one-third of all food produced is never consumed. This means that resources that are used in producing food that is not consumed are wasted. This leads to the unnecessary addition of greenhouse gases to the atmosphere, which has consequences for the climate and, ultimately, for food production. Food waste is further investigated in the following section.

1.2 Food waste

Globally, it was recorded that 40% of food produced was lost before it reached the markets. Lack of refrigeration technology and sustainable energy sources contributes to crops going to waste post-harvest. Insufficient refrigeration contributes to economic loss specifically to small-scale farmers who lose produce and income. Therefore, there is an urgent need to develop refrigeration systems with a focus on cost-effective design and implementation for small-scale farming communities [7].

Furthermore, fresh produce can spoil in hot climates, due to poor storage facilities and lack of cooling infrastructure [8]. Therefore, there is a need to explore and develop alternatively-powered cold-storage for rural communities.

1.3 Cooling

1.3.1 Food refrigeration

Refrigeration is significant for the food industry. Refrigeration allows preservation and storage of perishable products until they are sold [9].

Cooling slows down the chemical reactions and breakdown by bacteria. The bacteriological nature of food spoilage was determined by Pasteur [10] and others in the mid-nineteenth century. To reduce the amount of free moisture leading to bacterial activity, produce must be stored at below the minimum temperature for growth of micro-organisms [9].

Evaporative cooling impacts the temperature and weight of warm produce. When cooling warm produce, temperature and humidity related control methods need to be carefully considered, as freezing or cooling produce does not produce any improvements. When refrigerated, the product will be kept near the condition it was in before it entered the cooling process. Therefore, refrigeration keeps produce fresher for longer and prevents wastage by preservation in cold stores [9].

1.3.2 Solar-cooling

There exists a link between peak solar gain and peak cooling demand. It is therefore possible to produce cooling which coincides with the demand thereof by using solar energy. Solar-powered cooling, applied in this manner, is a potential technology for domestic, commercial and industrial buildings [11].

Solar cooling is a technology using solar radiation energy to provide a cooling application. There are typically three parts to a solar cooling scheme; a means to harness the energy of the sun, a plant to produce cooling and a process of heat rejection [11].

The need for solar-powered cooling systems exists as many buildings in hotter climates require cooling. Low-energy sustainable cooling applications are needed as an alternative to traditional methods. Cooling systems using solar thermal and solar photovoltaic (PV) energy have been presented by Best [12] and Maidment [11]. Solar thermal powered cooling is used to energize absorption cycles and solar PV powered cooling is used in vapor, compression refrigeration cycles. The use of these system results in having a low or zero reliance on grid-networks [12].

PV-compression systems drive vapor compression refrigeration systems through the direct current (DC) electricity converted from solar radiation. The DC power produced

is inverted to AC to produce shaft power for a electromechanical compressor. Although PV has efficiency-limitations, according to Best and Pilatowski, these systems are good options due to the lower cost and higher coefficient of performance (COP) of cooling systems, although PV has efficiency-limitations [12].

The Solaire project achieved results that presented promise in creating a viable cooling system. In the project, a 1.2 kW array was used to power a 1 kW prototype air-conditioner. Satisfactory results were achieved for various climatic conditions and food products [11].

In a study funded by the European Union, it was stated that there is significant potential for solar cooling technology in the capacity range of less than 20 kW. The study investigated current and future potential, creating a database of installed application and implementations [11].

1.3.3 Compressors

In the refrigeration cycle, four parts are present, namely evaporation, expansion, condensation and compression. Compression is the one part of the refrigeration cycle that remained a key focus as the drive system will be directly connected to the compressor. The purpose is to compress low-pressure gas from the evaporator and raise it to a high-pressure suitable for the condenser [13].

There are two main types of compressor configurations, namely positive displacement, and dynamic compressors. In positive displacement compressors, the pressure increase is achieved by physically reducing volume. In dynamic compressors, the velocity is increased and decreased in a way that changes pressure and the temperature [14].

There are millions of hermetic compressors in domestic refrigerators and freezers, with sizes ranging up to tens of kW. Below a power range of 5kW, single-phase motors, instead of three-phase motors, are used in locations where there is no availability of three-phase supply. There are three different ways to enclose compressors namely open, semi-hermetic and fully-hermetic compressors [14].

The semi-hermetic compressors have extended crankshafts integrated with the rotor of the drive motor. The drive motor stator is fitted within the extended crankcase. Semi-hermetic compressors are built in a wide range of sizes for both commercial and industrial markets [14].

While semi-hermetic compressors are still manually accessible, inaccessible fully-hermetic compressors also exist. The motor and compressor are sealed within a steel shell; this restricts access for repair or maintenance. Fully-hermetic compressors operate at a two-pole synchronous motor speed, usually 2900 rpm for a 50 Hz supply. Semi-hermetic run at a four-pole speed of 1450 rpm [14].

Using a variable speed drive (VSD) provides speed variability in a controllable way and speed limitations can be maintained using this control. The large start currents are reduced or mitigated by the rotationally slow starting and gradual speed increase of the VSD controlled shaft [14].

DC motors are used for small compressors. AC to DC conversion is required when using the grid as an input source. Frequency differs across countries; the DC motor is universally suitable because the frequency is not limited. There is a need for small compressors driven by low-voltage DC supplies. Typical cases include batteries or solar cells, where there is grid electricity, for small boats or mobile homes [14]. The failure of a motor within an enclosed system may damage other vital components. This may lead to products decomposing and serious contamination of the system. However, protective devices can be fitted to mitigate this risk [14].

Open compressors have a shaft extended from the crankcase to external drive capability using motors. Open compressors require a gland or a seal. When ammonia is used as a refrigerant, open-drive compressors are required because ammonia is not compatible with copper wiring and/or components. Coupling with the compressor may be direct to the shaft of the motor or via a belt drive. The shaft seal usually comprises a rotating ring of carbon with a highly polished metal facing ring, with the whole assembly being well lubricated. The carbon ring is spring loaded to allow for slight movement of the shaft [14].

1.4 Solar PV as an Energy source

Conversion from sunlight to electricity is completed using PV semiconductor materials, in most cases, pure crystalline silicon is used. They are called PV because of the ability of these semiconductor materials to convert the energy contained in photons of light into electrical energy [15].

In developed countries, the deployed PV systems are based on grid-connected topologies since the grid is very stable. For developing countries, this is not the case, where the grid is intermittent or some of the population have no connection to the grid. This is the reason renewable off-grid solutions are sought after [16].

The main reasons behind the search for alternative energy solutions are increasing power requirements and demands, the high cost of fossil fuels and the environmental impact of their use in generating electricity. It is for these reasons that the development of sustainable and affordable energy resources that are not harmful to the environment remains imperative [16].

The use of PV as a source of electricity for rural areas is a favorable alternative to the national grid. PV off-grid systems are essential for rural electrification. The following factors contribute toward the support of small-scale generation: accessibility, load demand, the fight against poverty and leapfrogging [17].

- Accessibility: Renewable small-scale generation is preferred for remote areas that, due to the unfeasible costs involved remain unreachable by the main, national grid [18].
- Load demand: The demand load in rural areas is very low, thus a small-scale system is more suitable [19].
- The fight against poverty: The continued focus on poverty-based strategies drew attention to probable links between energy and poverty which underlines the importance of improving living conditions through energy services. Electricity was thus considered as the main component in programmes geared towards rural development, using scale-small generation as the preferable option [20].
- Leapfrogging: Learning from what has already been done, rural areas can implement and incorporate the most advanced technologies for electrification [21]. Leapfrogging entails the observation of successful technological implementation, incorporating the advanced implementation stages while skipping earlier stages of unsuccessful advancement. PV small-scale generation is one such example [22].

Adding to the background of the study, the following points outline various applications and systems in which the PV-source has been used. The components and concepts

used in some of these applications, specific to the proposed cooling application, are included in the following chapter. PV has been used for electrification, solar-cooling, water pumping and small-scale off-grid systems for households and is discussed more in depth in the following sections:

- **Off-grid Electrification using Solar PV in a rural area in Malaysia**

  Researchers, M. Fahmi and D. Isa et al, implemented the use of PV energy systems for rural households. It is essential that further research is conducted in order to discover and develop innovative technologies to extract the maximum solar energy to be used to fulfill demands.

  A 2 kW system was implemented in the form of a solar off-grid cabin. The investigation was conducted into the possible replacement of current diesel generators with PV systems to supply power to houses in rural areas. All the usual household power-needs were combined and designed to be supplied for by the PV system. The PV system comprised of panels, a charge controller, an inverter, sensors and an electronic-load. The total load used, representing the household power-need, was implemented by using an electronic-programmable load. The system was tested for 3 days against the average rural household. The researchers concluded that the system was able to supply sufficient power to the rural household [23].

- **Off-grid Electrification using Solar PV in a rural area as an affordable solution in Sub-Saharan Countries**

  The financial feasibility of implementing an off-grid PV system for rural areas was investigated. The study was conducted for the Sub-Saharan African (SSA) area. In 2012, the percentage of people without access to electricity in SSA was 35.3%. Five major issues were investigated, namely cost-effectiveness, affordability, financing, environmental impact and poverty alleviation [24].

  Diesel generators are most frequently used as they are conventional and low cost compared to solar PV. They have greater reliability and provide income-generating possibilities from the electricity produced [24].

  The initial investment of a 100 W solar PV system could be alternatively spent on a 1.2 kW diesel generator. Diesel generators have higher running costs, but as stated, the generated electricity could be used for activities such as water pumping, milling, and irrigation or income generating activities [24].

  However, the main reason consumers from rural areas cannot afford a solar PV system is due to their inability to pay the credit whilst burdened with the strain of operations and maintenance costs. Authors S. Baurzhan and G. Jenkins concluded that off-grid solar PV systems for rural communities of SSA would not be financially feasible unless entities from abroad are to subsidize them [24].

  Authors outline two important advantages that PV systems have over diesel generators. PV is less detrimental to the environment than diesel generators. Furthermore, the cost of PV systems will eventually drop below that of diesel generators as the cost of PV systems is decreasing annually[24].

- **Solar PV used in small-scale power systems**

  The design an off-grid 2 kW solar PV system was designed by Bouzguenda and Omair et al, from King Faisal University in Saudi Arabia. Their study presented

the potential use of solar PV and a successful design methodology. They concluded that high ambient temperatures and shading losses reduced system performance [25].

The study was done in Saudi Arabia where according to figures given by Chatham house, approximately 70% of the energy consumption goes to air conditioning [26]. Bouzguenda and Omair et al, state that the reason why air-conditioning constitutes such a high percentage of energy consumption is that of cooling-unit inefficiency coupled by the frequent use of cooling units in the summer during which there are very high temperatures [25].

A stand-alone solar PV system was designed and presented with a proposed methodology for technical and economic analysis. The system was sized to 2 kW and the design-methodology was based on five stages. These included power needs, followed by the PV system type and the specific surroundings, a shading analysis and system layout and sustainability constraints [25].

Finally, an economic analysis was conducted based on the aforementioned stages. The design and methodology were implemented with energy storage. The focus of the study was on the specific geographical site, shading, and cost [25].

Qaiser et al [16] proposed the design and implementation of a low-cost, efficient and robust maximum power point tracking (MPPT) based charge controller that is suited for stand-alone or backup PV applications for small power-levels. The converter used a microcontroller. The paper focused on the charge controller. The charge controller did maximum power point tracking and charged the batteries. A Buck-boost topology charge controller was implemented because the topology is easily implemented and has simplified control. The implementation was found to be successful as it was tested through charging batteries at various voltages with good results [16].

- **Solar PV used in pumping applications**

Economic analysis of Photovoltaic powered water pumping and desalination without energy storage for agriculture

The economic feasibility of battery-less PV water pumping and desalination systems was investigated and modeled using simulations. The simulation was performed hourly, simulating PV pumping and desalination at variable loads [27].

Solar PV was compared to other energy sources such as diesel and the grid. Multiple inverter topologies were simulated as well. The economic analysis results showed that solar PV based systems fared better for water pumping than diesel-based systems. However, economically grid-based systems fared even better than PV based systems due to electrical costs [27].

PV water pumping has been investigated and proves to be technically feasible to operate with commercial systems. Jones et al evaluated medium to large-scale, variable speed, directly coupled with PV pumping and desalination systems. PV array sizes ranged from 15 to 120 kW for pumping and desalination systems. Compared to previous studies, larger-scale simulated system sizes, along with system optimization resulted in a cost reduction in PV- powered systems [27].

The PV systems simulated were without battery banks, thus pumping and desalination would not continue during the night or in low sunlight conditions. Therefore,

the operation of the systems was adjusted, using an inverter-controller to charge the inverter frequency to suit the available PV power for maximum efficiency and reliability. The adjustments were in speed, flow rate, and pumping head, to match the power available from the PV source [27].

- **An Effective Induction Motor Control for Photovoltaic Pumping**

  For the application of PV pumping, Vitorino et al published a paper on effective induction motor control. PV technology is most promising for low-power distributed electrical generation. The decrease in price per peak watt for PV panels is a very attractive feature [28].

  In the paper, a battery-less pumping system with PV as input source is proposed as batteries are heavy, expensive and have one-fifth of the lifetime of a PV panel. The PV pump-storage system would store energy as potential energy using water-storage that could be utilized later [28].

  The system would be made out of five components, namely the PV panels, a DC-DC converter, a DC-AC inverter, a three-phase induction motor and lastly, a centrifugal pump. This is the general make-up of a PV system, except for the last two components which are application-specific [28].

  The induction motor provides the electromechanical power conversion fed by an inverter drive. Sensorless methods are used to maximize the potential energy of water pumped for the available solar energy [28].

- **Solar used in cooling applications**

  In recent years the research and development of solar refrigeration technologies have gained global interest because they offer desirable advantages. The first advantage is the alleviation of harmful environmental effects of traditional refrigeration machines. Secondly, the coinciding with solar radiation supply with the regular peak demand in cooling is an advantage previously mentioned [29].

  Solar energy can power a refrigeration cycle through its conversion to electricity or heat. In a review conducted by Fan et al, it is stated that more interest has been found in solar thermal-driven refrigeration technologies than in solar photovoltaic-driven refrigeration technologies due to the lower efficiency and fairly high initial cost of the PV system. However, in this project, developments are made regarding photovoltaic-powered refrigeration for small-scale farmer produce using the proposed drive-system, which has implications that will be discussed later [29].

1.5 Introduction to the project

A power conversion system was built to power a cooling system for small-scale farmers. The field of application would be agriculture, specifically powering a cooling system for small-scale farming. The cooling system was powered by PV solar panels. The PV system voltage was increased to a suitable voltage required to power the cooling system

Certain voltage level requirements need to be met in order to drive retail cooling systems with VSDs. When using PV panels to power such systems the number of panels needed to build up the voltage level required is extensive and consequently expensive. To decrease the number of panels and expenses required, a DC-DC converter could be designed, built and implemented. The converter is then designed to increase the output

voltage of the system to meet the voltage requirement of the VSD for the cooling system.

There are a few problems to discuss in the field of application regarding the project. The major ones are:

- Pricing
- Voltage level elevation
- Implementation of new technology (power electronics) in the field of agriculture.

The ability of small-scale farmers to successfully produce and deliver fresh-produce has been negatively affected by a number of factors. One of which is the inability to store fresh produce for a period of time between harvesting and marketing. It has been argued that small-scale farmers lose a substantial percentage of their fresh produce or their income due to an absence of proper cooling facilities. This project forms part of a multidisciplinary effort (along with horticulturists, civil engineers, etc.) to establish affordable cooling facilities that can address this problem.

1.6 Research question

Using the proposed development process, is the design and implementation of off-grid PV drive systems feasible for small-scale farmer fresh produce cooling?

This project aims to reveal the necessary requirements for implementing a cost-effective cooling system for small-scale farmers, where many of these farmers are found in rural areas (at least where the supply of energy is restricted or inaccessible). Part of the answer will, therefore, have to address the use of alternative energy sources, with the focus for this study being photovoltaic energy sources. To provide a proper answer the following needs to be considered:

- What is necessary for a drive system supplied from photovoltaic energy sources to successfully drive such a cooling and refrigeration system?

1.7 Problem statement

Using the proposed development process, is it feasible to design and implement off-grid PV drive systems for small-scale farmer fresh-produce cooling that is cost-effective?

1.8 Research aims

In order to practically address the research questions above in such a way that the result may be used to practically evaluate cooling and refrigeration systems, the following research aims have been identified:

- To design and build a drive system supplied from photovoltaic energy sources for a cooling system requiring a few kilowatt of power. This aim would enable the evaluation of the ability to drive cooling systems and to propose possible improvements or alternative approaches in future.

- To investigate, propose and practically demonstrate the ability to drive commercially available cooling systems for energy supply restricted applications driven by the drive system as expressed in the first aim. This aim will again enable the evaluation of the feasibility of powering cooling systems with PV drive systems and will possibly aid in future research relating to small-scale fresh produce farming.

This thesis documents the design and implementation of an off-grid PV drive system for a cooling system. The drive system needs to be able to increase the PV array voltage, so that it is suitable for the application. The project was aimed at small-scale farmers, thus the financial aspect of the project contributed heavily to the direction of the project.

Further aims include:

- The designing the PV drive system;
- elevating the PV array voltage; and
- the implementation of cost-effective technology power electronics in the field of agriculture.

1.9 Research objectives

The following research objectives are envisaged to address the research aims:

- To design and to implement a DC-DC converter to supply commercial VSD from solar photovoltaic modules. This action arises from the fact that the maximum voltages possible from photovoltaic modules, especially in lower power applications, are not sufficient in the application to drive normal single-phase and three-phase motors as found in off-the-shelf commercially available cooling systems.
- To design and to implement a micro-controller based control systems to control the DC-DC converter as well as a VSD to ensure optimal application of energy flow.
- To establish a combined system of the various subsystems mentioned above to evaluate and to prepare for application as part of a cooling system.
- To adapt a commercially available cooling system for variable drive/energy restricted application and to apply this cooling system as part of an energy restricted application.
- To evaluate the entire system in the field as part of a multidisciplinary effort to help address the problems faced by small-scale farmers.

1.10 Significance of the Research

The research was done in the form of a feasibility study. This was done to determine whether the use of off-the-shelf products with a self-built converter, power and control units could be used to implement an off-grid PV drive system able to power a cooling system used in small-scale farming. After designing and implementing the system, feasibility or the lack thereof will be the significance of the research. Any contribution made, in terms of small-scale farming refrigeration drive systems, would ultimately be in aid of alleviating food insecurity and hunger.

1.11 Scope of the Research

The feasibility of the design and implementation of cost-effective PV drive off-grid systems for small-scale farmer, fresh produce cooling will be investigated. A drive system will be built to provide power and control for the application consisting of a DC-DC converter, a control module, and a commercially available VSD. Once manufactured, the system will be tested with PV panels and various loads leading up to the implementation of the cooling system.

1.12 Proposed execution project

In the investigation to determine the feasibility of the implementation of a designed PV drive system, the research methods will be stated for the development process, for rural farming produce cooling.

Qualitative research methods will be followed in order to select important parts of the PV drive system. Investigations will be carried out in order to gather information about certain converters and control units (Micro-controllers). The gathered information will be compared in a qualitative manner to determine the most suitable design to implement.

Quantitative research methods will be followed, in which off-grid PV system section components need to be defined and designed. These will include theoretical design, simulations of the converter's theoretical design and measurements of the converter parameters. The results of these methods will be used in the evaluation of the converter design.

Manufacturing will commence once Printed circuit boards (PCB) have been designed and populated. Thereafter, a testing phase will begin of the designed electronic circuits (converters and control unit) with various load-conditions and input sources. A second testing phase will be done moving closer to the proposed sources and load conditions until implementation is done with the PV source and cooling-load application. Lastly, observations and measurements of the development and implementation process will be documented.

1.13 Thesis outline

A short description of each of the chapters in this thesis:
Chapter 2 gives a high level - detailed overview of the research project
Chapter 3 discusses the DC-DC converter and provides a comparative review of various converters. These converters are evaluated according to the stated criteria. In closing, a DC-DC converter choice is made for the project.
Chapter 4 describes the hardware design of the chosen DC-DC converter and shows the results of the implemented DC-DC converter.
Chapter 5 describes the control of energy-flow of the system.
Chapter 6 presents the implementation and application of an experimental system.
Chapter 7 concludes the project through the provision of an evaluation and necessary recommendations.

Figure 1.1 will be used as a visual indication of the systems involved or being discussed in the relevant chapter. It will be shown at the start of each chapter, highlighting the focused system or systems in black.

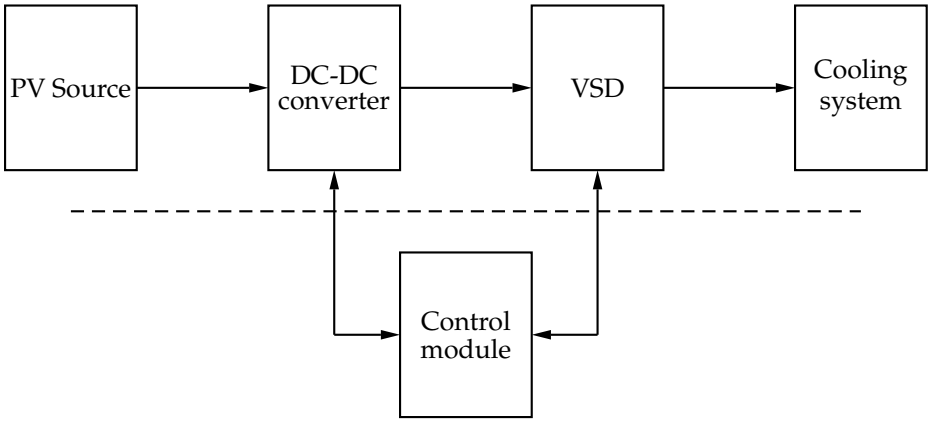

Figure 1.1: Schematic representation of the PV drive system, indicating interactions between various subsystems.

Chapter 2

High-level project overview

2.1 Introduction

This chapter entails a brief layout of the project and provides the research overview. Firstly, the development process of the project is presented in section 2.2. Parts of the research project are discussed namely, the input source in section 2.3 and the drive system section 2.4. The latter, in subsection 2.4.2, expanding on the voltage elevation of the input source. The application of voltage elevation for the project is discussed in section 2.5, which is small-scale farming refrigeration. The project's main electrical specifications are stated in section 2.6. Lastly, the integration of these parts for the project is outlined in section 2.7. Figure 2.1 illustrates the system and the interaction of subsystems.

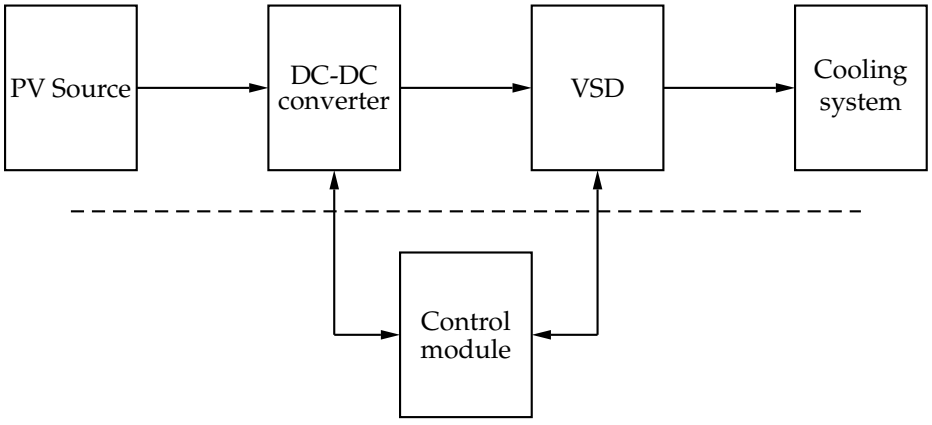

Figure 2.1: Schematic representation of the PV drive system, indicating interaction between various subsystems.

This system is aimed at small-scale farming communities, and the detail will be presented in this chapter in subsection 2.5.1. In this section, the system will be discussed and explored from every angle. A holistic overview will be provided, stating the detail of each part of the system from the input source, through to the increase in DC voltage. Thereafter, the chapter will outline the AC-conversion of the DC voltage. Lastly, the cooling system, which is the application for which the increased AC voltage is required, will be discussed. The focus of this chapter was to state the development process followed for the implementation of the PV drive system for small-scale farm produce cooling. This was carried out in order to determine the viability of the process.

This system contains many crucial parts from the supply through to the load, which will be briefly discussed below. PV was chosen as the input source; the voltage is increased and regulated using a DC-DC converter. With the voltage now elevated to a usable magnitude, the DC voltage is made AC with a VSD. The control module is the central control unit governing system execution, mainly between the DC-DC converter and the VSD. This is done in order to drive an off-grid the cooling system load for small-scale farmers.

2.2 Development process

Smallholder farms face multiple problems, which include limited access to electricity, lack of agricultural technology, lack of adequate produce storage and cooling facilities. The development of technology as a solution to a multiplicity of simultaneous problems is worth investment [30]. This is the focus of the project and the proposed development process.

The objective is to verify feasibility for the development a PV drive system for a cooling application aimed at small-scale farmers. This will be completed using the development process followed for this project.

The development process entails the use of commercial products (as far as possible) in integration with necessarily designed subsystems to implement the PV drive system. The decisions and their justifications made following this development process will be stated. An evaluation of these decisions and alternatives to negative outcomes thereof will be provided.

In order to implement a cost-effective drive system, commercial components were used as far as possible. These commercial components include the PV array and the VSD. The DC-DC converter and the control module were designed and built for use with the commercial components. The converter's supplementary circuitry includes power, measurement, gate-drive and isolation circuitry.

Integration of the system is achieved by having a central control module that monitors and controls the drive system. The control module designed controls the converter and the VSD. The VSD speed is adjusted and the converter output voltage is regulated by Maximum Power Point Tracking (MPPT). These are the two main control objectives forming part of the energy flow from the source to the load. The control module provides other functions as well, for example, measurement of the input and output currents and voltages.

2.3 Input source for the project

2.3.1 Introduction

The rural community areas do not have sufficient electricity supply. Reasons for the insufficiency of supply include the intermittency of the electricity grid, the inability of the grid to reach the rural areas and limited access to electricity grid facilities. Governments cannot afford an expansion of their national grids, thus leading to limited access and failure to provide such areas with electricity.

2.3.2 Resources for electricity

Conventional grid electricity is generated using resources that may impact the environment negatively. These resources include coal and natural gas and are being used to generate electricity. However, these sources are not renewable, are being depleted and may produce waste harmful to humans [31].

Although well-priced, the use of non-renewable resources for electricity generation for grid networks poses a threat to the environment, with these sources, electricity is mostly provided to urban, near-urban and developed areas where with the electricity grid is reachable. Limited or no access is provided to the rural communities, which need electricity as well. Therefore, an energy source is needed that is mobile, not limited to the reaching range of the conventional grid, affordable and easily replenishable [22].

Renewable energy sources are easily replenished and are not harmful to the environment in their generation of electricity. These sources are used to generate and provide electricity, regardless of access to the grid. These sources use mobile equipment and can provide electricity to rural communities and areas where the conventional grid is unable to reach [22, 31].

These sources are still being improved in terms of technology, cost, and implementation. This makes it a very competitive market, as manufacturers are progressing in developments which reduce cost and pricing [24]. Renewable energy sources that are currently used and researched are wind, solar, pump-storage and many others (geothermal, tide/ocean, Hydroelectric, and biomass). The focus of the proposed development process is solar and specifically solar PV.

2.3.3 Solar PV

To implement solar PV as a source of electricity for rural areas is a viable option as it is easy to set up and able to provide the necessary electricity that rural communities need for certain applications. It does not negatively impact the environment when generating electricity. In terms of solar PV, a substantial amount of physical space is needed for module installation. Solar PV modules have low efficiencies but there is no pollution produced during the generation of electricity [15].

In summary, solar PV is mobile in its setup, making it highly accessible. The source, the sun, is abundant and able to supply the needed electricity through PV, for various applications. Disadvantages of solar PV include high cost and low efficiencies. Major advantages include minimal pollution, the source is naturally renewable and is still being researched and developed, meaning future price drops [[15].Solar PV as input source is a sustainable source of energy as the sun is abundant (with high insolation levels in SSA) [24]. A PV drive system was developed for cooling purposes aimed at rural small-scale farming communities.

2.3.4 Input source specifications

For this project, a medium power level of 1.5 kW was designed for. This power level equates to six 250 W, 35 Vmpp PV panels. The DC-DC converter was designed to operate with an input voltage range of 50 V to 120 V, which could be made up of six panels in certain connection configuration. Certain series and parallel configurations were needed making up this voltage range, for example, 3 strings in parallel of 2 panels each in series.

2.3.5 Cost of modules

This starting capital cost of solar PV equipment such as panels can be very intense. The price of a 250 W from Renesola is R 2,625.00 [32]. This is the cost of the PV modules to match the specifications of 550 V and 1.5 kW. Building this power capacity with the above stated 250 W panels, 6 panels are required. This brings the total panel cost of the panels to an estimate of R 15,750.00.

2.3.6 Safety

The use of a few panels, in the correct configuration, provides a relatively small accessible input voltage. This means, that unforeseen contact or accidents with the power source would be relatively harmless and not fatal, as opposed to higher input voltages. The voltage is elevated and applied in a usable manner within the drive-system which would not be accessible.

2.4 Drive system

2.4.1 Introduction

The drive system design used contains a self-built combination of a control module and a DC-DC converter, used with a commercially bought VSD. The proposed design features a central control module, which provides integration between the DC-DC converter with the VSD, above many other functions. This allows a controlled voltage input to the VSD from the DC-DC converter using solar PV as the input source.

2.4.2 Voltage Elevation

PV panels are low-voltage sources and are often used for domestic and industrial applications [33]. These applications require higher voltage input sources, which means that there needs to be some sort of voltage increase or voltage elevation from the PV panels to the application, in order to power these applications with a suitable voltage. DC-DC converters are suitable for voltage elevation energy-efficiently. DC-DC converters will be fully discussed in chapter 3.

A combination of solar PV with a DC-DC converter provides compatibility and mobility, as the required voltage of the application can be easily achieved while operating in an optimum power range. Without a converter, a matchup of connection configurations (series and parallel connection) is required in voltage and power. To extract maximum power would require a load match at a specific voltage. Therefore, use of a converter is advantageous [15].

2.4.3 Control module

The control module is a central part of the drive system. It provides communication, control of switches, the ability to take in measurements and processing them. These measurements are used to execute the necessary algorithms. This module observes and monitors the output and input voltages and currents. Based on these measurements, the DC-DC converter regulates its output voltage for the VSD. Providing a sufficient voltage as input to the VSD - the VSD speed is controlled by the control module through

communication. Basic speed control is implemented. The control module will be discussed in more detail in chapter 5.

2.4.4 Variable speed drive

From the converter, a regulated DC output voltage is supplied. A VSD was chosen, providing a way to integrate the elevated input source voltage with the cooling application, including an option for speed control. It does this by supplying the load, typically a motor, with variable frequency AC power.

VSDs take in DC-power or AC-power. This power, whether DC or AC goes through a rectification stage, using diodes. After the power has gone through this rectification stage, it is built up in a capacitor. The voltage built up in this capacitor is called the DC-Bus voltage. Using this DC-bus voltage and pairs of transistors, an AC output voltage is produced. The frequency of the AC output voltage is adjusted by the VSD, to a user set-frequency. This is done by switching the transistors on or off at specific times.

The output of the VSD is perceived by the three-phase motor as a sinusoid with the variable frequency. The VSD does this by modulating the DC-bus voltage through switching the transistors on and off. It produces a sinusoidal output per each phase.

The VSD, known as an adjustable-speed motor drive, eliminates power losses by adjusting the motor speed to appropriately supply a variable load. Mohan et al give the example of an adjustable-speed motor drive used with a motor-driven pump. Energy is conserved by not letting the motor run at a constant speed over a time-period for a variable load, but by adjusting the speed [34].

A VSD schematic is shown below in figure 2.2 [35], the input of the diagram could be AC or DC building a DC link when powered. Thereafter, an inversion stage is presented. This inversion stage is used to create a PWM waveform that is controlled and is seen by the motor as sinusoidal.

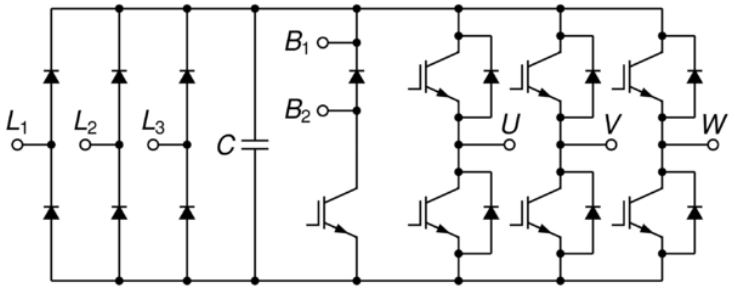

Figure 2.2: Variable speed drive

.

Since VSDs are typically used with three-phase motors two popular motor types exist. These are discussed in Appendix D, including a mention of three-phase systems.

2.5 Cooling application

2.5.1 Small scale farming

Smallholder farmers, as defined by V.Barends, are farmers who have low yields, produce more products than is needed for their own consumption and are the direct link with

consumers, or supply directly to retail groups who process and market the produce [36].

84 % of farms worldwide, 570 million farms, operate on less than 2 hectares. This illustrates the role and the importance of the smallholder farmer. In the developing world, these types of small-farms provide income, employment, and food to billions of people [30].people [30]. These same parts of the world house a large fraction of the hungry people in the world. The 500 million smallholder farms in the developing world provide close to 80 % of the produced food in Asia and Africa south of the Sahara. Yet these smallholders are the group that accounts for the poorest and hungry in the world. They live in rural areas and agriculture is the main way to make a living. Therefore, improvement and investment in the development of technologies that will help smallholder farmers are helpful to the people who most need it in the world.

Smallholder farmers face many challenges; they are faced with a lack of access to energy and above many other issues, they lack the infrastructure for storage which leads to food loss. Support in these areas will lead to helping and uplifting smallholder farm communities. Supporting such farmers to increase their productivity could lead to the improvement of income, in turn leading to agricultural growth. Providing support for food insecurity increases the ability of smallholder farmers to produce and sell, this enhances their ability to provide nutrition. Their livelihoods can be improved with better access to energy, which is achieved by the promotion and implementation of rural renewable energy use. Lastly, food availability can be improved through investment into storage infrastructure [30].

The proposed product is aimed to contribute to achievement of these outcomes. The project is aimed at smallholder farmers, where the development of a cold storage/cooling system is provided powered by renewable energy. The cooling system is driven by solar PV using a drive system that elevates the panel voltage. This drive system provides control and communication as well, by monitoring outputs.

2.5.2 Refrigeration

The cooling application that this project aims at developing uses a vapor-compression refrigeration system. The system uses a separate compressor and three-phase motor. The compressor and motor are coupled using belts or directly coupled (special couplings) via their shafts. The motor connects to a VSD through which the control of the refrigeration system is provided. Refrigeration systems and such technologies are needed by smallholder farmers, helping them to effectively store and cool produce. The results and implementation of the application will be displayed in chapter 6. In figure 2.3 below, an image of a refrigeration system is shown, containing a condenser at the back and an open compressor and motor coupled using belts.

2.6 Project specifications

Table 2.1: Basic electrical design parameters

Parameters	
Input voltage range	50 V - 120 V
Output voltage range (VSD input voltage)	550 V - 600 V
Power	1500 W (Six 250 W PV panels)

Figure 2.3: Separate compressor and motor cooling system, including a condenser

In order to power and control a cooling system, the above described electric parameters were to be used as input supply into a VSD, the whole drive system is used in integration with a control module that controls to the VSD and to the DC-DC converter, doing processing on the measurements it monitors. This is the proposed design to power a cooling system driven by PV, for small-scale farmers to cool fresh produce.

2.7 Research project execution

Figure 2.1 illustrates the project in the main system and how the subsystems work together. The input source is a PV array and provides a voltage that ranges from 50 V to 120 V, depending on the configuration of the array and temperature of the module [37]. As seen in the diagram, this input feeds into the DC-DC converter. The DC-DC converter is controlled by the control module, through control signals sent to gate-drivers for the converter switches. The control module measures input and output power by monitoring the converter parameters, able to implement control methods. Control methods to be implemented include maximum power point tracking and voltage regulation. The output of the DC-DC converter is used by the VSD. The VSD is controlled and monitored by the control module and is connected to the cooling system, powering it at optimum power.

In the following chapters, the parts will be discussed in more detail, starting with the DC-DC converter in chapter 3.

Chapter 3

DC-DC converter

3.1 Introduction

This chapter describes the DC-DC converter. A comparison is made between converters investigated for implementation, leading up to the selection of the specifically proposed converter. An overview of DC-DC converters, switch-mode, and resonant converters is discussed in sections 3.2 and 3.3, respectively. The criteria used for the converter choice are stated thereafter in section 3.4. A few converters are chosen, grouped together and then compared. The groups contain basic DC-DC converters, featured in sections 3.5 and 3.6, and resonant converters in section 3.7. In chapter 4, the design and operation of the proposed converter are discussed in-depth.

Figure 3.1 shows the system and its interconnection. The main focus of the chapter is the DC-DC converter, highlighted in black.

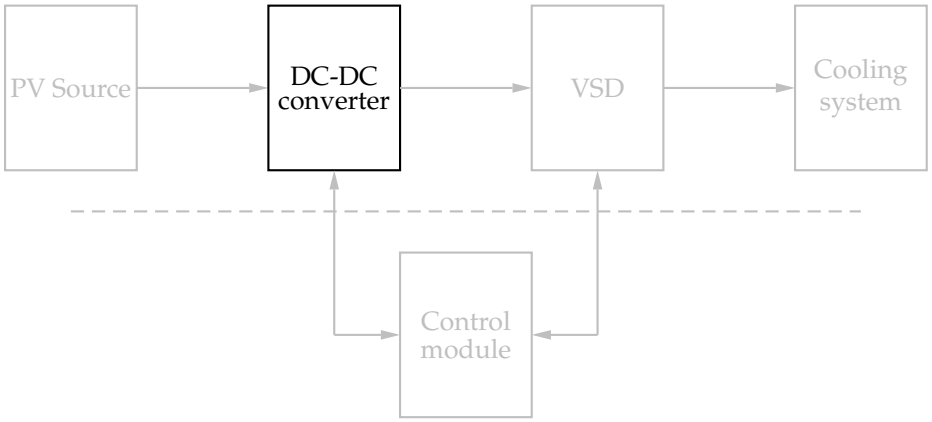

Figure 3.1: Schematic representation of the PV-drive system, indicating interaction of the DC-DC converter between subsystems

The DC-DC converter plays a key role in the PV drive system. This converter would be used to provide a high voltage output from the lower PV panel voltage, in a safe and controlled manner. The converter should be able to operate within a wide input-voltage range providing a high voltage gain throughout. This should be done cost-effectively and energy-efficiently, which are important factors in order to implement the PV drive system for small scale farming. The feasibility of the proposed PV drive system implementation by small scale farm communities is ultimately investigated.

The converter choice was based on the set criteria. The criteria are fully presented later in this chapter in section 3.4. A summary of the criteria to be met to fulfill the requirements of the project are given below as:

- A high-voltage gain from low-voltage input,
- wide input voltage range,
- high efficiency, and
- low in cost.

3.2 DC-DC converters: A brief overview

3.2.1 Introduction

The advances in power electronics in the last few decades have made it possible to achieve great feats [38]. Previously, such technology has only been used in military and space applications, due to of cost and reliability implications. Since the early 1970s, advances in semiconductor devices led to the switching converter becoming a popular choice [39]. Developments in power electronics in the last 40 years have seen advances in electric motor applications. Motors can now be powered from various sources and at various frequencies [38]. Moreover, the versatility and flexibility in power electronic developments resulted in the development of even newer and better applications. The progress of high-power electronic components has led to an increase in reliability and decrease in cost [38].

Furthermore, rapid population growth and advances in technology have increased electrical power consumption, from 1.5 million MW in 1940 to a projected 5 million MW in 2000 [40]. It is predicted that almost 75 % of the electrical power will be processed by power electronics, about 3.8 million MW in 2000 [40]. The frequent use of power electronics indicates the need for the development of energy and cost-efficient applications, incorporating power electronics such as the DC-DC converter.

A DC-DC converter is a device, consisting of electronic and magnetic components, that takes in a certain DC input voltage and produces a certain output voltage. The output is dependent on the device-topology and control. Control is primarily implemented by gate-drivers through transistors and diodes used for conduction of current flow, where desired [34]. These converters often contain inductors and capacitors as filters. These components serve as energy-storage elements in the circuit as well. Similarly, converters can contain transformers, where a greater increase or decrease in the input voltage level to output voltage level is needed [34].

A normal DC-DC converter operation has a DC stage, an AC stage, and another DC stage. The transformer is inserted after the converter's AC stage. After this AC stage, a rectification stage occurs. For these two stages to take place, the transistor and the diode are used. The transistor is used as a simple switch in the circuit, functioning in both an on-state and an off-state. This provides the AC stage from the DC input, which can then be used by a transformer to scale the voltage. Typically, after this process, rectification is achieved by using diodes in combination with a filter capacitor and filter inductor. From the DC input, through the alternating stage and rectification, a DC output is obtained and changed in voltage level. This is how the DC-DC converter takes one DC voltage level to another, using the described components [34, 39].

Converters can operate in three conduction modes, namely in a continuous-conduction mode, a discontinuous-conduction mode and a boundary-conduction mode which exists between the previous two modes. The continuity (whether discontinuous or continuous) relates to the inductor current flow. However, if the inductor current never reaches zero, the conduction mode is continuous. On the other hand, if the inductor current reaches zero for a duration before the end of the period, its conduction mode is discontinuous. When the inductor current-flow reaches zero precisely at the end of the switching period, the conduction mode is the boundary condition between discontinuous- and continuous-conduction [34]. These modes need to be taken into account as they define the design of components for the DC-DC converter.

3.2.2 Elevation factors

The use of DC-DC converters to elevate voltage levels are very useful for applications that need a higher voltage-level powered by low-voltage sources. Using DC-DC converters in conjunction with low-voltage sources, such as PV panels, creates an alternative way of powering commercial or industrial applications. The magnitude of the conversion ratio depends on a few parameters, such as:

- The duty cycle;
- the transformer winding ratio (if the topology includes a transformer);
- the output diode and capacitor configuration; and
- lastly, placement of components.

3.2.3 From linear to switching power supplies

DC-DC converters are presented as the main components required for switching power supplies [34]. Therefore, the switching power supply will be investigated in this study, as it is essentially seen as a DC-DC converter.

Switching power supplies are able to provide regulation of output voltages, isolation and multiple outputs differing in voltages. Linear power supplies were used traditionally, as it is a power supply using a 50 Hz or 60 Hz transformer and the transistor in its active region [34].

In linear power supplies, a transformer is used providing electrical isolation and delivering output in the desired range. However, the low-frequency transformer is one of the shortcomings of linear power supplies; they are large in size and weight. Another vital shortcoming is the efficiency of the supply that ranges from 30 - 60 %. A significant amount of power loss occurs because the transistor operates in its active region. These supplies do have advantages, for instance, simplicity in circuitry in small power ratings and they do not produce a large electromagnetic interference (EMI). These advantages, unfortunately, do not outweigh the shortcomings, but these shortcomings do lead to a greater appreciation for the switching power supply and the DC-DC converter [34].

The emergence of the switching power supply was due to improvement in the linear supply components and transistor operation methods [34].

The major advantages of using switching power supplies, compared to linear power supplies, are:

- The transistors are used as switches: By being used in an on or off state, power losses by transistors are reduced, instead of being used in an active region (operating constantly between an on and off state) [34];
- the high-frequency transformers are used: Using high-frequency transformers, as opposed to 50 Hz or 60 Hz transformers, results in a reduction of the size and weight of the supply [34]; and
- the higher efficiency, in ranges of more than 70 - 90 % [41].

Using switching power supplies has some negative implications, which include the increase of complexity in design and control [41], as well as the prevention of high-switching frequency EMI [34]. The common switching power supply topologies include the buck, boost, buck-boost, Cuk, flyback, push-pull, half-bridge and full-bridge converters. These converters have many variations, which improves on the basic converter [34, 40]. The focus will be placed on converters where the DC level voltage is increased from input to output.

Two of the major objectives in switching converter design are to improve conversion efficiency and to increase power-packing density. At higher switching frequencies, the size and weight of the reactive components are reduced, increasing power packing density. However, there are limitations to this, as the switching frequencies of converters cannot be increased infinitely. This is due to excessive switching losses in the converter as high switching frequencies, for example, 1 MHz, are approached using pulse-width modulated control. Heat-sinks will be required with excessive switching losses, and this will offset the net reduction in magnetic size. The predominant switching losses, at high frequencies, will be the capacitive turn-on losses in the metal oxide semiconductor field effect transistor (MOSFET). Ang [39] presents the example of a power MOSFET with a drain-source capacitance of 100 pF, turning on at 500 V. The losses calculate to 12.5 W at 1 MHz. This is excessive for switching losses. The resonant converter offers a solution to this problem and is described in the following section.

3.3 Resonant converter: a brief overview

The discussed converters are all pulse-width modulated (PWM) converters. This means that power is processed in a pulse form. However, power can be processed in a sinusoidal form as well. This is called resonance conversion [40], which is used in resonant converters.

For resonant converters operating in continuous conduction mode, the frequency is shifted either towards or away from resonance to vary the output voltage. In discontinuous conduction mode, a fixed on-time pulse is used, but with varying frequency. In effect, all resonant control circuits keep the pulse width constant and vary the frequency whereas all PWM control circuits keep the frequency constant and vary the pulse width [40].

In resonant power supplies, a transformer leakage inductance can be utilised for soft-switching, which reduces losses, as these leakage inductances are usually unwanted in switch-mode power supplies. Therefore, the design of these transformers should still be carefully considered [34].

The common resonant topologies are load-resonant and quasi-resonant converters. Load-resonant converters have inductor-capacitor (LC) resonant tank circuits. The resonant tank generates oscillating voltage and current, applied to the load. The resonant tank controls the power flow to the load, which is directed by the comparison in switching

to the resonant frequency. This means that the ratio of switching frequency to resonant frequency is important. This ratio determines the mode of operation, meaning the type of inductor current flow or conduction. The switching frequency is set and changed by self-controlled switches [34].

The load-resonant converters can be categorized into one of two groups as voltage-source series-resonant converters and current-source parallel resonant converters, with further subdivided groups as series and parallel loaded resonant converters. These groups each have advantages, such as for the former, inherent overload protection and, for the latter, not being sensitive to load variations [39].

On the other hand, quasi-resonant converters incorporate an LC resonant tank circuit which changes the shape of the voltage and current waveforms of the switching transistor from square to sinusoidal. The resonant tank is incorporated and built around the switch, hence the name quasi-resonant switches. This results in device turn-on or turn-off at zero-voltage or zero-current conditions. Zero-current switching (ZCS), quasi-resonant switches are used to reduce turn-off losses and eliminate switch stress [40]. Turn-on losses are reduced by zero-voltage switching (ZVS) quasi-resonant switches. These switching methods, ZCS and ZVS, are known as soft-switching. The voltage or current of the switching device used is zero at the switching transition. All commonly-used converters can be converted to quasi-resonant converters by replacing the switches with quasi-resonant switches [34, 39]. Important to note is that, at zero voltage, or zero current, the converter switches, transistors, and diodes can be changed in the state (On to off or off to on) resulting in minimal power loss.

Furthermore, the main advantage of resonant converters is that they incorporate the parasitic components and transistor capacitances into the converter topology. However, the resonant converter components generally do need to handle higher voltages and currents compared to pulse-width modulated switching converters. In addition, EMI may be unpredictable; as a result, resonant converter output voltage regulation is needed [39].

In summary to clarify, resonant converters fundamentally incorporate an adjustment made to the frequency instead of adjusting the duty cycle, to control the output voltage. This means that the period length of the converter is changed, thus changing the frequency. In switch-mode converters, the on and off times are adjusted, with the period kept constant. Resonant methods and converter modifications have been used for development in advanced switching converters. Resonant soft-switching is one of the concepts adding to the development of this project, leading to improvements in efficiency, power density, and reliability of converters [42].

3.4 Criteria of the DC-DC converter choice

With the above stated, the converter choice needed careful consideration as there are many DC-DC converters with different topologies for various applications. It was important for this study to choose a DC-DC converter that would fulfill the following criteria:

- The input and output parameter range: The converter needed to be able to work, within a certain wide range for the input and high output range as stated for the specific application. The application was a PV based application. The input range would have to be between 50 V and 120 V, and the output voltage needed to be regulated to 550 V for a Y-connection and 380 V for a delta connection;

- the cost: The manufacturing cost of the converter was to be kept low, to have a cost-effective converter whilst meeting the converter specifications;
- the complexity of design: The converter-design was to be simple and easily implementable, to avoid making mistakes in the manufacturing of the converter;
- the power level: The amount of power that the converter can deliver to adequately supply the load and still be functional is important. A small-scale power rating was specified to be able to power a small cooling load;
- the efficiency: The power supplied to the load needed to be at high-efficiency to ensure optimal conversion of the input power; and
- the added learning-value of the converter choice: This criterion relates to the value that the converter could add in using it in the project. Therefore, an advanced converter needed to be chosen that met the above-mentioned criteria, instead of a basic converter. This investigated and evaluated the integration of advanced converters with the proposed PV drive system.

Different topologies exist and comparison needs to be done to fulfill criteria needed. Therefore, multiple converters are presented and thoroughly compared in the following section. The voltage gain from input to output is dependent on the components and the configurations used the in converter. The below-mentioned converters were chosen based on their ability to step up the voltage, their efficiencies, and the power capacity. Furthermore, their advantages and disadvantages are stated. These converters will be presented in groups, including slight variations or modifications of converters. Classifying the converters into groups was difficult as they could be sorted in many ways. Under these circumstances, the converters were categorised into the following groups: non-isolated, isolated and resonant converter groups.

3.5 Non-isolated converter group

3.5.1 Boost converter

The boost converter includes an inductor, diode, a transistor (power switch) and a capacitor, all of which, are used to increase the voltage level. From the inductor volt-balance law, the following equation is achieved stating the output voltage with regard to the input voltage and the duty cycle [40], as

$$V_{out} = \frac{V_{in}}{(1-D)}.$$

The converter is simple, with a low input ripple current. High-efficiencies can be reached with the boost converter, of typically 80 %. The converter does, however, lack isolation and has high output ripple [40].

Boost converters are mainly used in regulated DC power supplies and regenerative breaking. This converter provides an output voltage that is always greater than its input voltage [34].

When the switch of the converter is on or closed, the diode is turned off and the inductor connected to the source is isolated from the rest of the circuit. The inductor then stores the energy from the input source. Consequently, the output energy is a result

of the input source with the added stored energy from the inductor. This occurs when the switch is opened and the diode conducts [34].

When operating, the boost converter needs a load connected to the output capacitor, without which, the output voltage will continue to increase until the components break [39]. The converter is shown below in figure 3.2.

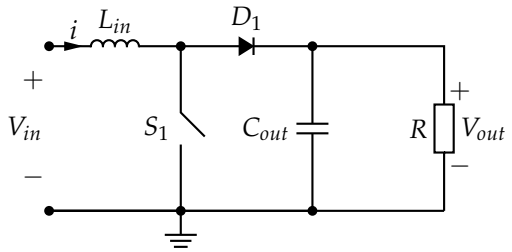

Figure 3.2: The boost converter topology

An increased output voltage can be achieved, but the boost converter is limited in power because of high peak current stress on the diode and the switch [40]. The converter is limited to the output voltage and maximum duty cycle. Therefore, a high output voltage cannot be obtained from a low input voltage. Although some advantages for the converter do exist, these are the main reasons this converter was not chosen.

3.5.2 Interleaved Boost Converter

The simple boost converter remains inefficient because of the high current and voltage stress on the switch and the severe diode reverse-recovery losses when operating in continuous conduction mode. An interleaved boost converter (IBC) with more than one phase takes care of these high stresses, sharing them among the phase legs.

The input ripple current is inherently low, because of the input side inductors. Current is divided into the two interleaved branches [43]. The interleaved operation contributes to the low input current and low output voltage ripple [44]. Hence, a cascaded topology reduces voltage and current stress [45]. An additional multiplier stage could also be added to IBC [46]. The converter design results in a simple circuit [47]. The interleaved boost converter is shown below in figure 3.3.

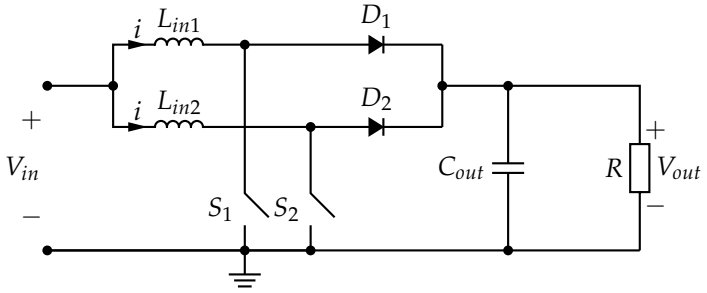

Figure 3.3: A two-phase interleaved boost converter with coupled inductors

A decrease in efficiency as the load increases can be seen in the IBC [48]. The design involves careful set-up, adjustment of inductor turns and calculation of the capacitor parameters.

Interleaving has high power potential, modularity, and reliability. The optional beneficial use of a coupled inductor means reduced core and winding losses as well [45].

With the above said, the interleaved boost converter fulfills most technical requirements and is a strong competitor as converter choice for the project. It has low input current stresses, has a simple design, a low semiconductor device count and is reliable. The output voltage is defined as a number of phases in terms of n, shown as

$$V_{out} = \frac{V_{in}}{(1 - nD)}.$$

The modified interleaved boost converter, with an addition of the coupled inductor, fulfills the voltage increase requirement [48], from low to high voltage. It also fulfills the power level requirement, in a range of 1.5 kW [45]. These are met apart from each other, but not together. The IBC, without coupled inductors, has a low voltage gain [49] and cascading the boost converter has a negative effect on the efficiency. This is a result of the amount of power processing stages [50]. The converter is considered as a basic converter as well, therefore not being chosen although it has many advantages as stated above.

3.5.3 Z-source Converter

The Z-source converter is a very interesting converter as it has unique features. These features include both voltage and current source compatibility and the ability to operate in boost or buck-boost modes. This versatile converter contains only two switching devices, two transistors, and four energy storage components, two inductors and two capacitors. It was stated that the Z-source converter can reduce cost and improve reliability. The converter is suitable up to the power-level of 3 kW [51]. The output voltage of the converter can be expressed as

$$V_{out} = \frac{(1 - D)}{(1 - 2D)} V_{in}.$$

The converter, though being in the correct power range and able to reduce cost, is a complex converter to implement in terms of design and control. Therefore, it was not chosen for this project. The Z-source converter is shown below in figure 3.4.

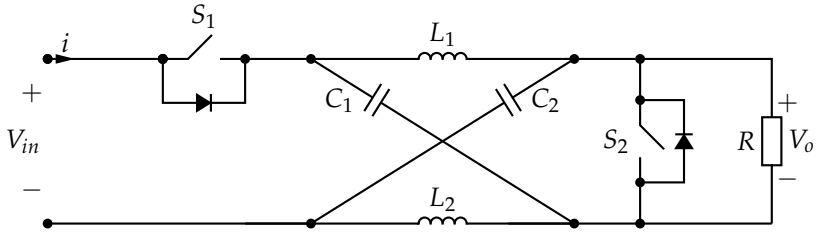

Figure 3.4: Z-source converter

3.5.4 Clamp-mode Coupled-Inductor Buck-boost Converter

Q. Zhao and F. lee [52] presented a family of high step-up DC-DC converters. These converters would be used in non-isolation applications, with high-efficiency and voltage gain.

Problems like large input current and high output voltage were stated as major concerns. Severe reverse-recovery was stated as a minor concern in output diodes, because of high output voltages.

Converters that include coupled inductors could be used to achieve a high voltage gain. One problem with these converters is the leakage energy that induces high voltage stress on switches. This leads to large switching losses and EMI problems. Incorporating an active-clamp circuit would solve the problem by recycling the leakage energy. This comes at a cost of efficiency and complexity [52].

The family of converters that Zhao and Lee proposed were high step-up, high-efficiency clamp-mode converters shown below in figure 3.5, which is the Clamp mode coupled-inductor buck-boost converter.

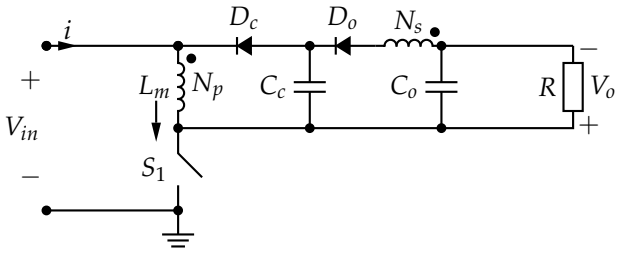

Figure 3.5: Clamp mode coupled-inductor buck-boost converter

These converters do not work with extreme duty ratios. The increase in losses and complexity associated with active-clamp circuits are drawbacks. The incorporated clamp circuit is made from one diode and a capacitor. This reduces cost and complexity compared to traditional active-clamp circuits. This results in a lesser switch voltage stress because the leakage energy is recycled and does not induce voltage spikes [52].

For the clamp-mode coupled-inductor boost converter, a snubber was required. The leakage inductance of the coupled-inductor resonates with the parasitic capacitance of the output diode when the switch turns on, this causes an increased voltage. A snubber is needed to reduce the output rectifier peak voltage. The clamp mode inductor boost converter of 1 kW reached efficiency ranges of 90 to 92 % [52].

The clamp-mode coupled-inductor boost converter does not have a wide enough input voltage range. The converter was designed to a power level below the required power level of the project; furthermore, the output voltage is not high enough. Therefore, although the converter has advantages stated above and could be seen as a basic converter, it was not chosen for the project.

3.5.5 Hybrid DC-DC Converter

The converter is to be run from a battery, able to supply a high voltage for uninterrupted power supply (UPS) systems. The non-isolated design presents higher efficiency. This is due to the size increase of the system because of isolation transformers [50].

A high step up in voltage was done, using a design that does not include a transformer. To power, the UPS system a DC bus voltage of 700 VDC - 800 VDC is required. This bus voltage feeds to an inverter which is connected to the UPS [50], presented below in figure 3.6

A battery with voltages ranging between 63 VDC and 81 VDC was increased to an output of 710 V. This power capacity of the design is 1.55 kW. Advantages of the proposed

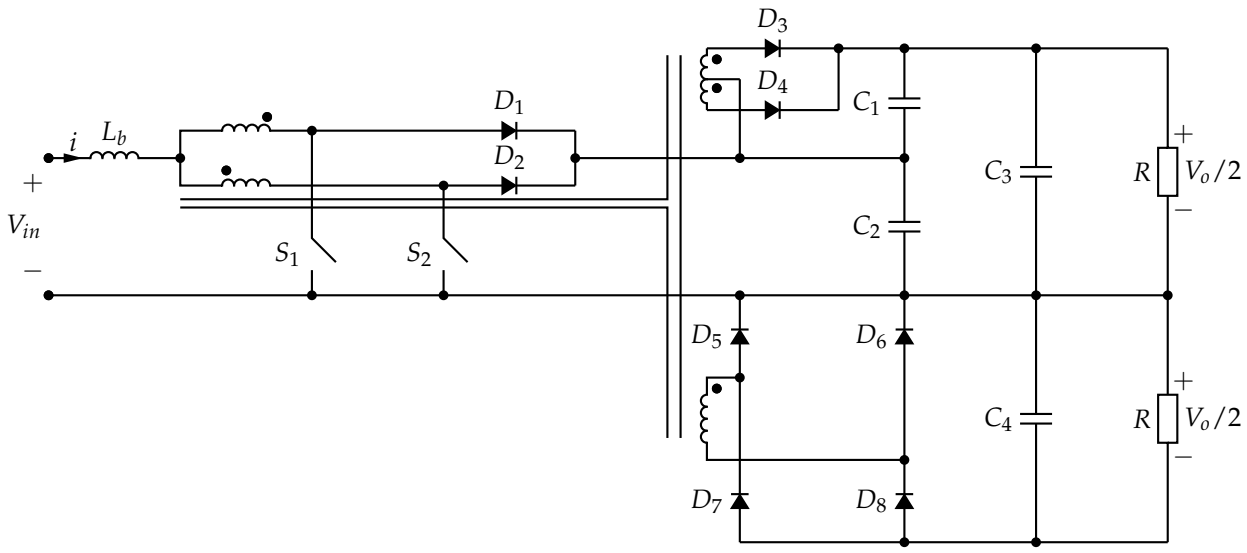

Figure 3.6: Non-isolated boost converter with a high voltage gain for non-isolated on-line UPS

converter include low input current ripple. The volume and weight reduction of input inductor operate within a double switching frequency, because of the 2 phases. Snubbers are not necessary, only a fraction of the output voltage appears across the switches and they are clamped by the output capacitor. Disadvantages of the converter include a direct current path between the source and the DC-link capacitors and without isolation [50].

Authors state that the proposed design could be used for renewable energy applications. The design contains various components. The efficiencies ranges from 89 - 91.5 % [50].

Although the converter efficiency exceeds the suitable power level, the voltage increase done by the converter is also more than required. This could be corrected by controlling regulation to another output voltage. This converter is suitable for a battery powered application, which could be used in development for stand-alone systems [50]. Unfortunately, the research project does not include any battery storage and the converter contains 10 switching devices, which are expensive. From a cost and complexity perspective, the converter was not chosen for the research project, although certain vital criteria were met.

3.6 Isolated converter group

3.6.1 Full-bridge converter with half-bridge diode rectifier, center-tap

The full-bridge converter contains a number of 4 transistor switches, which makes it suitable for power capacities of several kilowatts. The switches are controlled in groups of two, being switched on simultaneously with the groups out of phase. S1 and S4 make a group, as does S2 and S3. When this is done, the input voltage magnitude appears across the primary winding, reducing peak currents [40]. The full-bridge converter with a center-tap is shown below in figure 3.7.

The converter has a high parts count but is suitable for high power applications. It contains isolation and switches that are rated at the input voltage of the source. The full-bridge converter is an industry favorite for high output power converters [41]. The

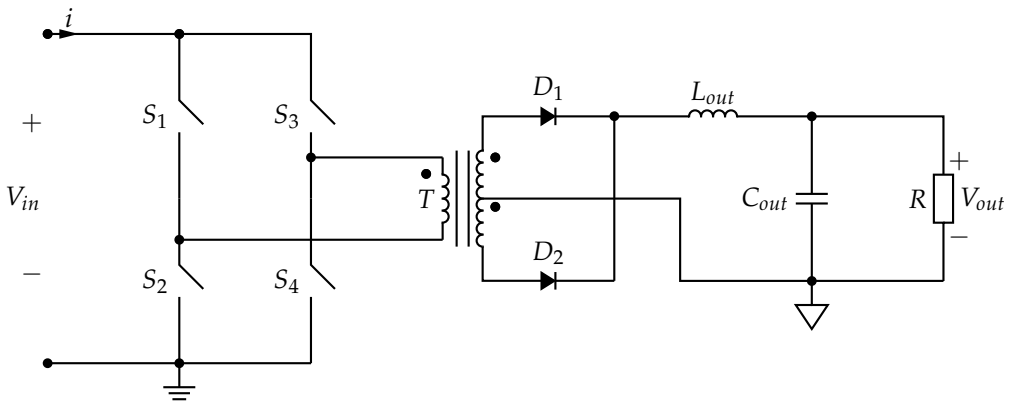

Figure 3.7: Full-bridge converter: Center-tap connected half bridge diode rectifier

volt-second balance of the filter inductor for one half of the switching period gives the following

$$\frac{V_{out}}{V_{in}} = 2\frac{N_2}{N_1}D.$$

The rectification configuration used in this converter is the half-bridge diode rectifier. The diodes used must be able to handle a minimum reverse voltage; otherwise, failure of these components will occur. Through analysis, each diode must be able to handle twice the input voltage multiplied by the turn's ratio. This is illustrated below in the diagram of the rectifier and the equations. In the instance where D2 is conducting as illustrated below D1 is reverse-biased.

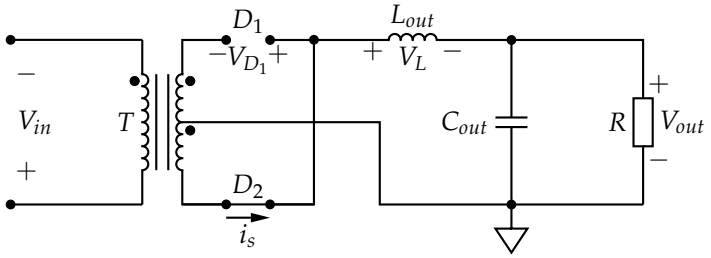

Figure 3.8: Rectifier configuration: Half-bridge diode rectifier

The reverse voltage that D1 needs to handle to avoid failure can then be calculated with Kirchoff's voltage law Figure 3.8 shows V_{D1}, which consists of the voltage across the diode, the output voltage, and the referred input voltage

$$V_{D1} = \frac{N_2}{N_1}V_{in} + V_L + V_{out}.$$

As the inductor voltage is $V_L = \frac{N_2}{N_1}V_{in} - V_{out}$, the reverse voltage across D1 is

$$V_{D1} = 2\frac{N_2}{N_1}V_{in}.$$

The input voltage can be replaced with the $\frac{V_{out}}{V_{in}}$ for this converter,

$$V_{D1} = \frac{V_{out}}{D}.$$

3.6.2 Full-Bridge converter with full-bridge diode rectifier

The full-bridge converter without soft-switching has much to offer. Being suitable for power-levels up to 5 kW [53], its transformer core is utilized bi-directionally and the voltage stress on the power switches is equal to the input voltage [41]. The use of four switches are justified at higher power levels. The full-bridge converter is stated as a good choice by Redl et al [53] for such power levels. This converter can achieve high efficiencies [54] but operate at a duty-cycle maximum of 50%. The converter contains a high number of semi-conductor devices [55]. Input ripple current and leakage inductance problems could exist with this converter, as the design does not include leakage energy alleviating circuitry or an input inductor. The converter includes a full-bridge diode rectifier, which is the main difference between this converter and the aforementioned full-bridge converter. This rectifier reduces the voltage that each diode needs to be able to handle a reverse voltage. This is an advantage, but more components are added meaning a greater cost. A circuit schematic is shown in figure 3.9.

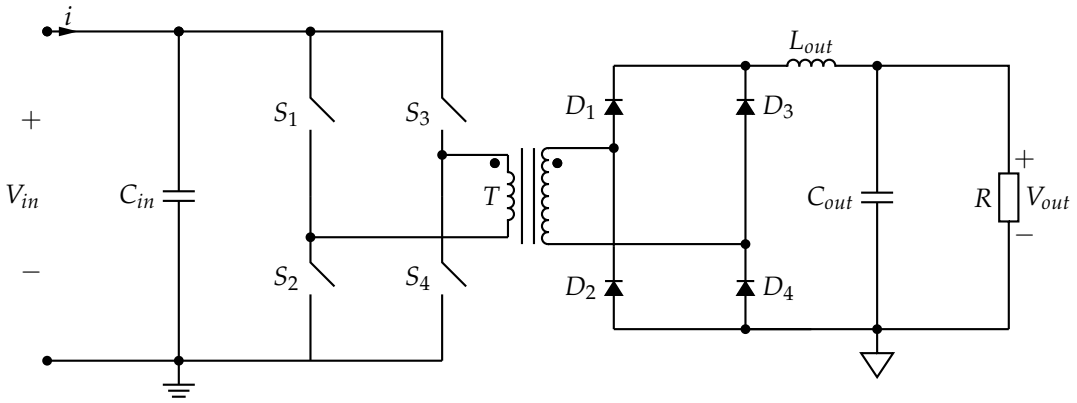

Figure 3.9: Full-bridge converter: Full-bridge diode rectifier

The Full-bridge converter (applying to both the half-bridge and full-bridge rectifiers) is suited for the application but was simply not chosen as it is limited by its duty cycle, lacks alleviation of leakage energy which could cause damage.

3.6.3 Full-bridge converter with soft-switching

R.Redl et al [53], presented a 1.5 kW converter. The converter had an output of 60 V at 25 A. The input source for the experiment was a regulated 370 V source. Using this converter with a PV input requires a number of PV panels connected in series.

Voltage-overshoot and ringing caused by transformer leakage inductance interacting with the diode reverse-recovery process can lead to possibly damaging components and losses, decreasing efficiency. To prevent such consequences diodes with low di/dt could be used to control voltage-overshoot. Resistive capacitive (RC) snubber connected across the diodes are an option which reduces ringing, but in an inefficient way [53].

Soft-switching helps alleviate switching losses in converters. Some of the advantages that soft-switching contribute are high efficiencies, simpler analysis, better use of components (power transistors and diodes) and simpler power circuits as stated by Redl et al [53].

The converter contains all the main characteristics of the above-mentioned topology. Many components are included in this design. The design contains clamping diodes,

which limit the junction of the transformer resulting in the reduction of switching losses and voltage stress of the diodes. The commutating inductor connected in series with the transformer helps with transistor soft-switching. The added inductor and clamping diodes do contribute to the complexity of the design [53]. The converter has an efficiency of 95%. A circuit schematic is shown in figure 3.10.

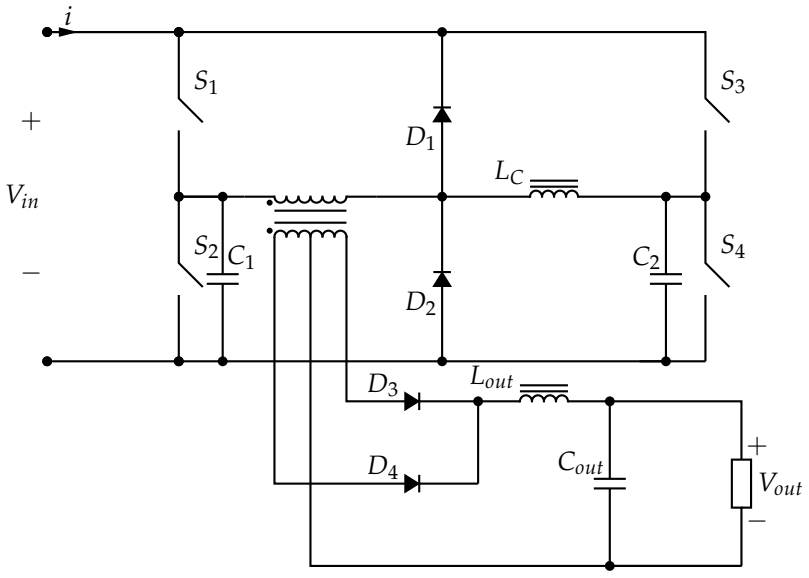

Figure 3.10: Soft-switching Full-bridge Converter

This converter was not chosen to be used in the PV drive-system. This is the conclusion as the converter was designed for a high input voltage capacity. The drive-circuit is very complex, although stated as simple [53]. The control circuitry is also outdated. Using this converter for the project would not contribute any significant value, although the design contains many beneficial concepts like soft-switching and overshoot alleviation.

3.6.4 Full-Bridge Boost Converter

In 2008 Nymand and Andersen [56] published a new approach to high efficiency isolated full-bridge boost converters. This was for high-power low-voltage fuel cell applications. These authors stated that high efficiencies of 96-98 % were able to be realized for a 1.5 kW full-bridge boost converter by reducing transformer leakage inductance through better winding methods, namely interleaving of primary and secondary windings. Interleaving of the primary winding with sections of the secondary winding reduces the transformer leakage inductance and the AC resistances [56].

High currents flow through the transformer's primary winding when working with high-power low-voltage applications. This requires the primary windings to have large copper cross sections. Nymand and Andersen used foil windings to provide large copper cross sections. The full-bridge boost converter is shown below in figure 3.11.

This converter is characterized by the ability to reduce current ripple and minimalize voltage stress. The use of boost converters inherently provides low current ripple as the inductor is placed on the input side. The output diode is placed across the capacitors resulting in minimum voltage stress [56].

In 2010, Nymand and Andersen [57] published a report looking at same topic regarding high efficiency isolated full-bridge boost converters, with more detailed interleaving

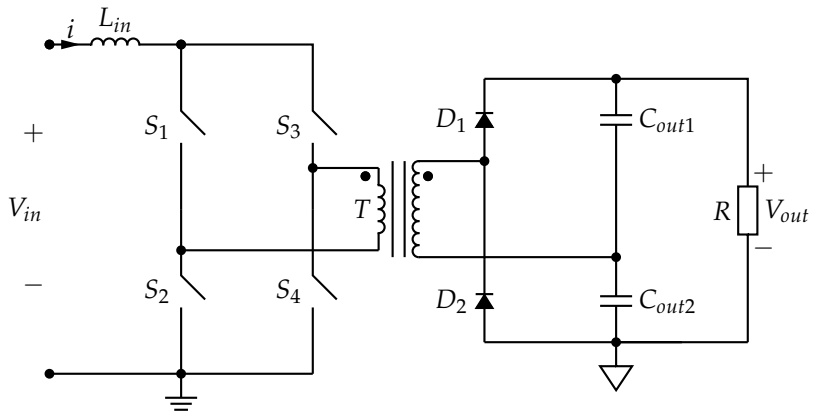

Figure 3.11: Isolated full-bridge boost converter with voltage doubling rectifier

configurations. They showed how the resistance decreases with an increase in the amount of interleaved intersections. The use of Litz wire was stated to be impractical and difficult, as the required copper cross section is large. The Litz wire would lead to increased DC resistance as it would contain a large number of strands.

The complexity of this converter lies in the interleaving process of the transformer winding, which was foil windings. Using this type of winding configuration reduces transformer losses. Lower AC resistance and leakage inductances contribute to a reduction in the transformer losses. With the precise layout of the primary side and low leakage inductance, clamp circuits can be eliminated [56].

The converter topology published by Nymand and Andersen [57] takes low-voltage high-current inputs to high-voltage outputs, at high efficiency. This was the type of voltage elevation needed for this research project, using low-voltage high-current sources, such as fuel and solar cells.

The isolated full-bridge boost converter is suitable in power-level for the application. Efficiencies are as high as 98 % for the 1500 W output power converter with 30 V to 50 V input voltage and the output voltage of 400 V, all DC voltage levels. Although the transformer design for this converter reduces the leakage inductance, it was not chosen for this project due to the transformer design complexity, the output voltage is shown below, where n is the turns-ratio and D is the duty cycle ($0.5 \leqslant D \leqslant 1$), as

$$V_{out} = \frac{nV_{in}}{(1-D)}.$$

3.6.5 Push-pull Converter

The Push-pull converter is a transformer-containing topology, where the input source is connected to the transformer primary winding center-tap [41]. As seen below, the converter contains two switches, a transformer, two diodes and a LC-filter. The two switches are connected at either side of the transformer primary winding. The diodes are connected to either side of the secondary transformer side going to the filter [40]. The two switches are turned on and off, out of phase including dead time. They ensure the magnitude of the input voltage appears across the appropriate center-tap section. The connected center-tap section sees the input voltage, of the turned-on switch. The voltage is increased by the transformer ratio, rectified and filtered [40]. Current flows through the primary side when that switch is turned on. Concurrently, one of the center-tapped

secondary side halves begins to conduct. The current flows to the load, through the respective forward biased diode [40]. The risk of core saturation is reduced because the current flows through the primary winding in opposite directions. This means that the core material is driven in both flux polarities, positive and negative. Therefore, the core is used more efficiently. The converter is also able to generate output power capacity of numerous hundreds of watts, as it contains two switches. The control needs to be done with precaution, as the switches may not conduct at the same time, otherwise, components could be damaged during operation [40]. If the converter contains asymmetry because of non-ideal different components, the core will eventually saturate. A volt-second balance of push-pull circuit's output inductor yields the expression below as

$$V_{out} = 2nDV_{in}.$$

The converter contains isolation and low output ripple, with a typical efficiency of 75 %. It does, on the negative side, contain a high parts count and the possibility of cross conduction of the switches, which could be catastrophic [40]. The push-pull topology is shown in figure 3.12 .

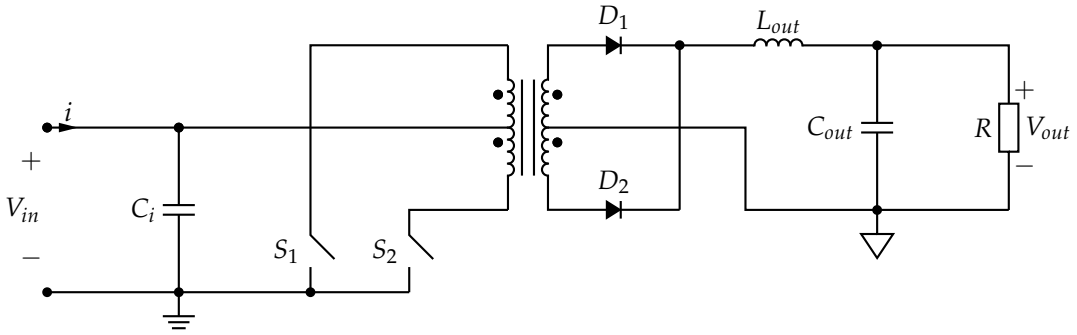

Figure 3.12: The push-pull converter topology

The inductor current rises linearly for the on-time of the switch through the D1, then both switches are off. When both the switches are off, the inductor current is split between the half-windings of the secondary side and decreases. The on-time of T1, with T2 off, and the off-time of both switches, add up to half of the switching period. The next half of the switching period consists of the same circuit behavior and current, but that T2 is conducting, while T1 is off. This means that diode D2 is on and diode D1 is off [34]. The volt-second balance yields the following for one half of the switching period

$$\frac{V_{in}}{V_{out}} = 2\frac{N_2}{N_1}D,$$

where D is the duty cycle for $0 < D < 0.5$ is

$$D = \frac{t_o n}{T_s}.$$

The duty ratio is to be kept less than 0.5 (meaning less than 50 % on) to avoid both switches being on simultaneously. This would create a short current with a possibility of damaging the circuit. In practice, switching times of the two switches will differ slightly. This causes an imbalance in the switch currents, possibly leading to flux imbalance and core saturation. In the push-pull converter, this can be eliminated with current-control [34].

The converter was not chosen as it has duty cycle limitations and transformer core saturation is a possibility. The power range of the converter does not suite the criteria and a high voltage output is not easily attainable, only through a large transformer ratio.

3.7 Resonant converter group

3.7.1 Series-loaded Resonant DC-DC Converters:

Resonant converter contains resonant components as stated in section 3.3. The series-load resonant (SLR) DC-DC converter has a resonant-tank impedance which depends on the operating frequency. This means that regulation of the output voltage is done by controlling the switches at specific frequency [34]. Depending on the switching frequency, the output voltage will be regulated. Below is a schematic of the series-loaded resonant DC-DC converter, in figure 3.13

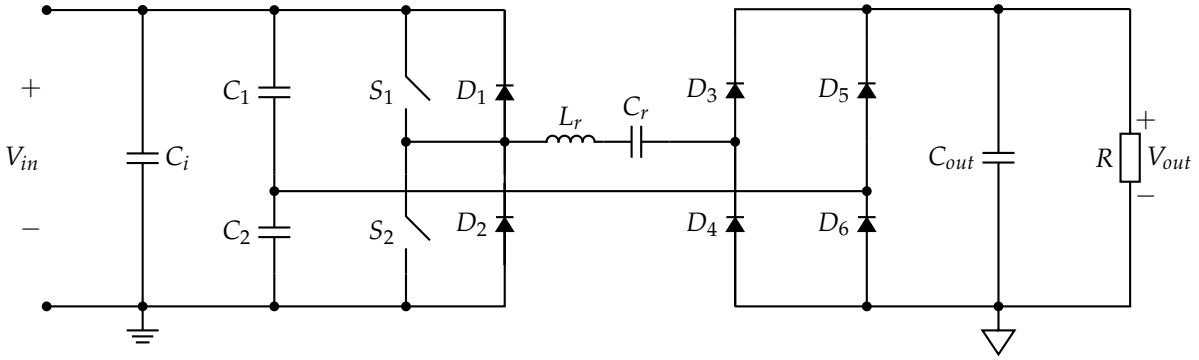

Figure 3.13: The series-loaded resonant DC-DC converter

From the [34], it is shown that the output voltage cannot exceed half of the input voltage, given as the expression below, as

$$V_o \leqslant \frac{V_{in}}{2}.$$

The converter does have advantages of resonance and isolation, however, was not chosen as it would not be able to provide the needed output voltage from low-voltage source.

3.7.2 Resonant push-pull converter

The proposed converter is a combination of the current-fed push-pull converter and quasi-resonant converter. The Resonant push-pull converter does soft-switching using LC-resonance similar to resonant converters, resulting in a minimal to zero power loss when switching [34]. The resonant push-pull converter has inherent advantages of the current-fed push pull converter with the disadvantages of the converter addressed. These disadvantages include voltage spikes caused by the leakage inductance of the transformer, high-voltage stress on the diodes and diode reverse-recovery problems [33]. The resonant push-pull converter is shown below in figure 3.14.

By soft-switching the diodes, the loss caused by the reverse-recovery is reduced. The implemented secondary side voltage doubler configuration increases the conversion ratio and reduces the voltage stress on the diodes, to the output voltage. Lastly, the voltage

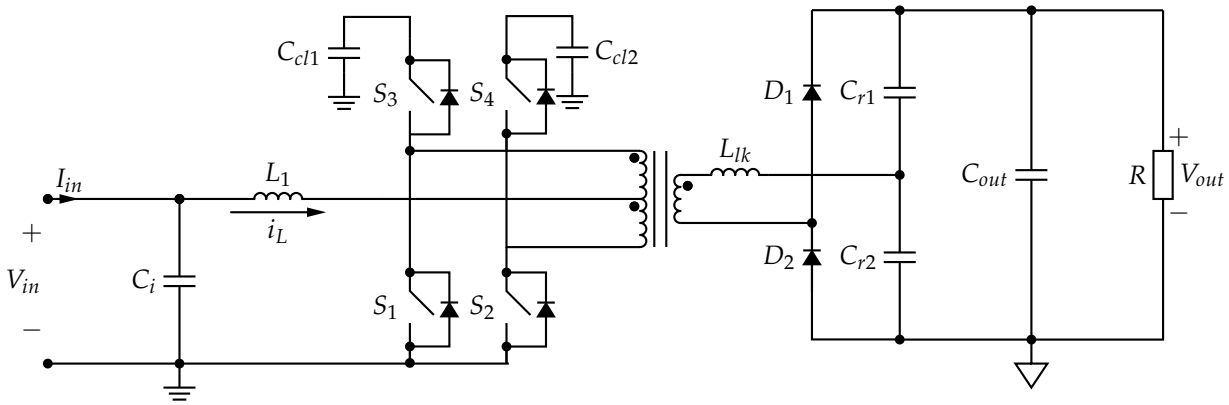

Figure 3.14: Resonant Push-Pull converter: which include active clamp circuits and a voltage doubler

spikes caused by the transformer leakage inductances are clamped by the active-clamp capacitors placed at the drain of the high-side transistors [33].

The advantages of the resonant push-pull converter are high-voltage conversion ratio and low input current ripple, at high efficiencies. The choice of diode output configuration adds to the high conversion ratio. The converter operates for duty cycles ranging between 0 and 100 %, which is uncommon for most DC-DC converters which operate only for duty cycles less than or equal to 50 % [41], this gives the converter a wider input operating range. The ripple current tends to zero, as the converter operates closer to 50 % of the duty cycle. The output voltage of this converter is easily controlled through a gate-drive circuity at any duty cycle. An analysis was done, by the authors using the high step-up resonant converter implemented for an application requiring 1.5 kW as output power. The converter was tested with input voltage range between 30 V and 60 V, and an output voltage of 350 V. This input range is within the range of common PV solar panel maximum power point (MPP) and output voltages, which makes it a suitable converter for PV input sources. Experimentally the authors showed the proposed converter to have a minimum efficiency of 95.5 % at the full-load condition for minimum voltage [33]. The output voltage of the converter is expressed as

$$V_o = n\frac{2V_i}{1-D}.$$

The resonant push-pull converter was the chosen converter, as it met all of the requirements in the defined criteria. It is able to take a low-voltage input of a wide range and produce an output voltage that is suitable. Equally important, the converter operates at high efficiency and is advanced in implementation and design, as it incorporates pulse and resonant conversion. Therefore, this chosen converter for the project will be discussed in more detail in chapter 4 of this study.

Chapter 4

Resonant push-pull converter

4.1 Introduction

The resonant push-pull converter is presented and demonstrated in this chapter, thus the emphasis of the chapter will not be on the control of the converter. The control of the converter will be discussed in chapter 5 of the study. Section 4.2of this chapter outlines the layout of the circuit, assumptions about the converter and characteristics of the switches used in the project. The operation of the converter is then discussed in 4.3. This section is divided into two sections, one discussing the non-overlapping region and the other discussing the overlapping region of operation. The converter design and its components are presented in section 4.4.This presentation consists of the theoretical design of all components used in the converter and the practical design of the magnetic components in the converter. The simulated results of the converter are then presented and discussed in section 4.5. After simulation, the converter was built and tested.

Therefore, in section 4.6, the construction of the converter is presented. The results of the implemented resonant, push-pull converter are presented in section 4.7.1, the closing measurements section

Figure 4.1 demonstrates the interconnection of the system and precludes a discussion and evaluation of the chosen DC-DC converter. The converter's design, simulation, and results will also be presented.

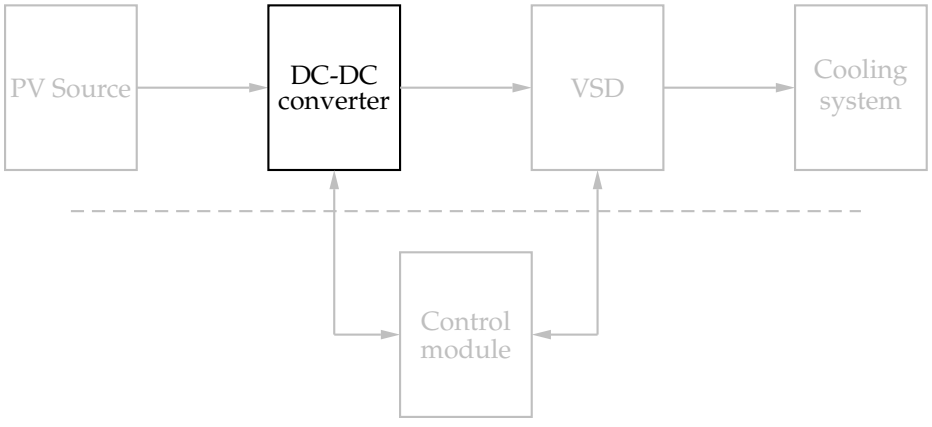

Figure 4.1: Schematic representation of the PV-drive system, indicating interaction between subsystems

The resonant push-pull converter has low primary side conduction loss, due to the input current being distributed through the switches. In addition to the reduction of conduction loss, low on-resistance switches are used, and through an active-clamp circuit, the voltage across the switches is contained.

Conduction loss is further reduced by addressing and alleviating the challenge of reverse-recovery. Reverse-recovery in diodes occurs when the diode switches off and a negative current is present for a moment [41]. As the diodes commutate softly on the secondary side reverse-recovery loss does not occur. In addition, reduction in transformer turns-ratio is realized through the use of the voltage doubler rectifier, doubling the conversion ratio. All of these factors contribute to the overall efficiency of the resonant push-pull converter [33].

4.2 Circuit layout and steady-state analysis

The primary side of the converter features a bus capacitor and boost-inductor, with the inductor connected in series with the primary center tap of the transformer. The main switches are connected to the primary side, and the active-clamp circuits composed of capacitors and auxiliary switches. On analysis, the transformer is modeled as ideal because it has a leakage inductance and zero magnetizing currents. This can be achieved by neglecting the magnetizing inductance of the transformer in order to simplify analysis. The magnetizing inductance is neglected as it is large and the transformer is bi-directionally excited, thus the magnetizing current is regarded as zero. To the secondary side of the transformer, a voltage-doubler rectifier is applied. This includes diodes and resonant capacitors. Figure 4.2 below illustrates the chosen converter.

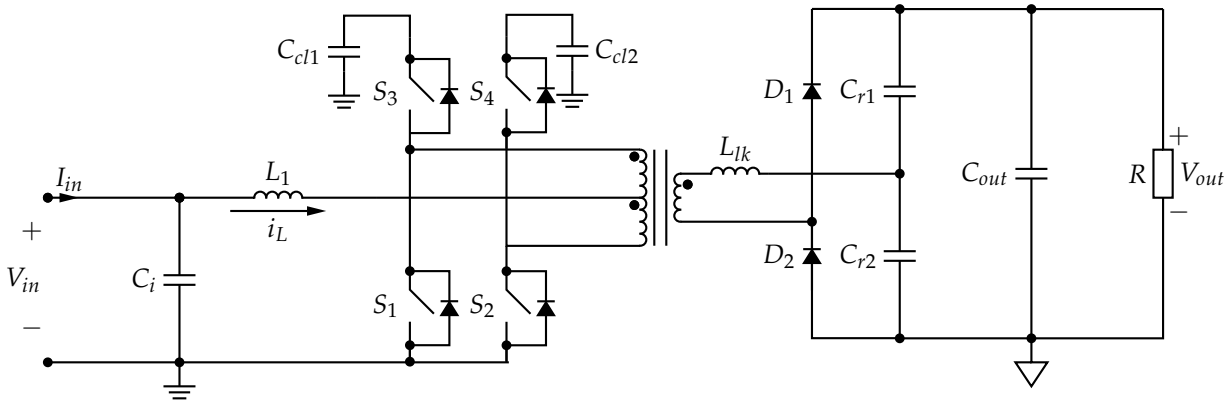

Figure 4.2: Resonant Push-Pull converter

Assumptions

All the transistor switches are treated as ideal. The output voltage is constant over one switching period, as the output capacitor capacitance is sufficiently large. For symmetrical operation, the clamp capacitors are equalized in terms of capacitance and the resonant capacitors are further equalized in capacitance. The clamp capacitors are made sufficiently large to make the ripple components negligible

Switch operation

The four switches are driven using gate-drive circuitry and PWM signals. These signals

are adjustable in duty cycle. The main switches S1 and S2 are driving 180 degrees out of phase with each other. The auxiliary switches, S3 and S4, are driven complementarily to the main switches S1 and S2, respectively.

The converter operates in a non-overlapping and an overlapping region. When the duty cycle of less than 50 % is used, the converter operates in the non-overlapping region. In this region, S1 and S2 are not on simultaneously. When the duty cycle of greater than 50 % is used, the converter operates in the overlapping region. In this region S1 and S2 are on simultaneously. Utilising both the regions and moving from one to another, the converter could operate using a larger range of input voltage. The switch-operation of all the switches is presented in section 4.3.

4.3 The operation of the converter

4.3.1 The non-overlapping region

Six topological modes are present over one switching period, T_s. These modes repeat periodically. Although there are six modes, it is only necessary to describe three of the modes because the other three are analogous to the three that will be described.

The principle of operation for D $<$ 50 % is such that it contains the modes of the converter signals, illustrating when devices are conducting and when resonance is terminated. This is useful in order to understand the operation of the converter throughout a switching period. The operation is illustrated through equations, circuit diagrams, and waveforms. Mention is made to certain time-stamps which define the modes presented, for example, t_0. These time-stamps are illustrated at the end of the discussion of the non-overlapping region in figure 4.8 which presents control and analog signals.

Mode 1, from t_0 to t_1: The primary current i_{p1} flows through S_3 and the primary current i_{p2} flows through S_2 proceeding to mode 1. The switch S2 is turned off at t_0 and i_{p2} stops flowing through it. The current i_{p2} continues to flow through D_{s4}, the body diode of S_4, until S_4 is turned on, after a certain amount of dead time. i_{p2} then flows through S_4. From t_0 to t_1, the current through the inductor i_L decreases linearly, since the voltages across the windings are zero and the clamp capacitor voltage V_C is greater than the input voltage V_i. i_L can then be expressed as

$$i_L(t) = I_L(t_0) - \frac{V_C - V_i}{L}(t - t_0).$$

The flow of currents in the converter for mode 1 is illustrated in figure 4.3 below. i_L is equally divided between S_3 and S_4, since the magneto-motive forces in the windings sum up to zero, as shown in the following equation

$$i_{S3}(t) = i_{S4}(t) = -\frac{i_L(t)}{2}.$$

S_3 is turned off towards the end of mode 1 and its body diode D_{S3} starts conducting during the short period of dead time.

Mode 2, from t_1 to t_2: S_1 is turned on at t_1 and $0.5V_C$ is the voltage across the center-tapped winding, on the primary side. i_L increases linearly through the inductor as V_i is now higher than $0.5V_C$, as shown in the equation below

$$i_L(t) = I_L(t_1) + \frac{V_i - 0.5V_C}{L}(t - t_1).$$

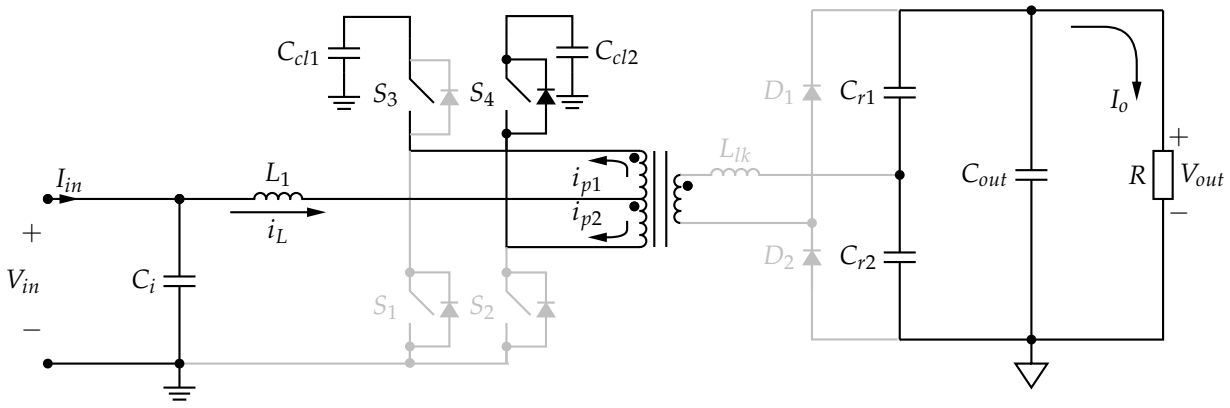

Figure 4.3: Mode 1 of the non-overlapping operation

The diode D_1 is conducting and the leakage inductance L_{lk} resonates with the resonant capacitors, as the current i_s flows through, on the secondary side. The input power is transferred through the transformer to the output load in this way. The flow of currents in mode 2 is illustrated in figure 4.4 below.

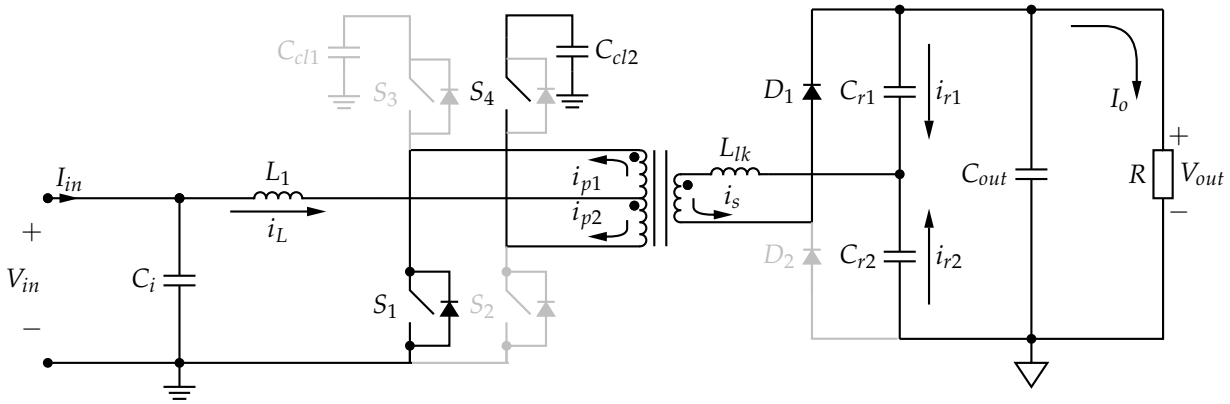

Figure 4.4: Mode 2 of the non-overlapping operation

The following equations describe the voltage across the leakage inductance equating to the difference between the secondary winding voltage and one of the resonant capacitors, as

$$L_{lk}\frac{di_s(t)}{dt} = nV_C - v_{Cr1}(t). \tag{4.1}$$

The output voltage is the sum of the resonant capacitor voltages, expressed as

$$V_o = v_{Cr1}(t) + v_{Cr2}(t). \tag{4.2}$$

Applying the Kirchoff current law and illustrated in figure 4.5, at the node where the resonant capacitors meet, the secondary winding current can be described as

$$i_s(t) = i_{Cr1}(t) + i_{Cr2}(t). \tag{4.3}$$

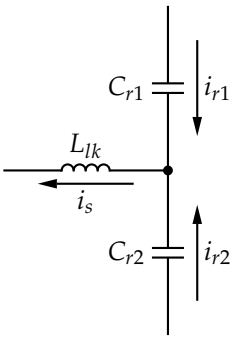

Figure 4.5: A current summation of the resonant capacitor currents making up the secondary winding current

Equation 4.3 can be further expressed, in terms of the definition of current through a capacitor, as

$$i_s(t) = C_{r1}\frac{dV_{Cr1}(t)}{dt} + C_{r2}\frac{dV_{Cr2}(t)}{dt}. \tag{4.4}$$

The resulting or effective resonant capacitance is written as

$$C_r = C_{r1} + C_{r2}. \tag{4.5}$$

Assuming that both resonant capacitor voltages are the same for the time period, the effective resonant capacitance can be used in the secondary winding current equation. Using the subsequent equations 4.4 and 4.5, the secondary winding current is shown as

$$i_s(t) = C_r\frac{dV_{Cr1}(t)}{dt}. \tag{4.6}$$

The equations for the leakage inductance and the secondary winding current are a set of equations that are equivalent to an under-damped series-resonant circuit [34]. The same solutions of the set for the under-damped circuit can, therefore, be applied to equations L_{lk} and I_s. The solutions of equations 4.1 and 4.6 are shown, respectively as

$$i_s(t) = i_s(t_1)cos[\omega_r(t-t_1)] + \frac{nV_C - v_{Cr1}(t1)}{Z_r}sin[\omega_r(t-t_1)] \tag{4.7}$$

and

$$V_{Cr1}(t) = nV_c - (nV_c - V_{Cr1}(t_1))cos[\omega_r(t-t_1)]) + Z_rI_{L0}sin[\omega_r(t-t_1)]. \tag{4.8}$$

The transformer turns-ratio is n, given by

$$n = \frac{N_2}{2N_1}.$$

The initial values of these equations for the time period are $v_{Cr1}(t_1) = V_{Cr1}(t_1)$ and $i_s(t_1) = 0$.

The final solutions of equations 4.7 and 4.8, including the initial values are the resonant capacitor voltage as

$$V_{Cr1}(t) = nV_c - (nV_c - V_{Cr1}(t_1))cos[\omega_r(t - t_1)] \tag{4.9}$$

and the secondary current is then expressed as

$$i_s(t) = \frac{nV_C - v_{Cr1}(t1)}{Z_r} sin[\omega_r(t - t_1)]. \tag{4.10}$$

Furthermore, equation 4.7 and equation 4.8 were obtained without derivation or explanation from equation 4.1 and equation 4.6 respectively by [33]. Therefore, the short derivation and explanation showing the in-between steps were included by the researcher. The following is from [33]. The peak value of the secondary current is given by

$$I_{s,peak} = \frac{nV_C - v_{Cr1}(t1)}{Z_r}. \tag{4.11}$$

Therefore equation 4.10 can be rewritten, using equation 4.11, as

$$i_s(t) = I_{s,peak} sin[\omega_r(t - t_1)]. \tag{4.12}$$

The angular velocity and resonant impedance [34] are given by

$$Z_r = \sqrt{\frac{L_{lk}}{C_r}} \tag{4.13}$$

and

$$\omega_r = \frac{1}{L_{lk}C_r}. \tag{4.14}$$

The output load current is equal to half the secondary winding current since the resonant capacitances are the same. This yields the following current relations

$$i_{Cr1}(t) = -i_{Cr2}(t) = 0.5i_s(t) = i_o(t) \tag{4.15}$$

The input inductor current is split into the two primary side currents from the center-tap as seen in figure 4.4. The sum of the magneto motive forces of all the windings is zero. This yields the following switch currents,

$$i_{s1}(t) = i_{p1}(t) = \frac{i_L(t)}{2} + ni_s(t)$$

and

$$i_{s4}(t) = -i_{p2}(t) = -\frac{i_L(t)}{2} + ni_s(t).$$

Mode 3, from t_2 to t_3: The inductor current is still increasing linearly and divides equally between S_1 and S_4 at t_2, as expressed by

$$i_{s1}(t) = i_{p1}(t) = \frac{i_L(t)}{2}$$

and

$$i_{s4}(t) = -i_{p2}(t) = \frac{i_L(t)}{2}.$$

The flow of currents is shown in figure 4.6, for mode 3.

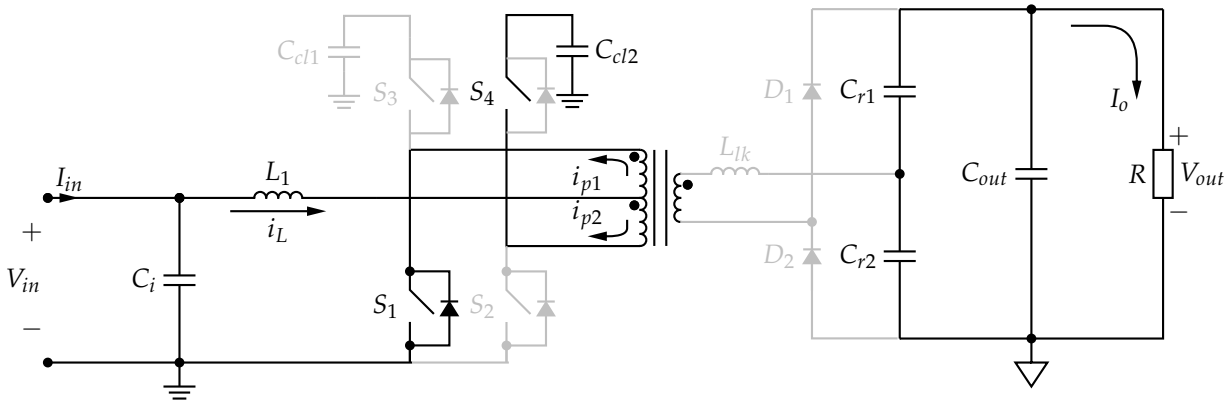

Figure 4.6: Mode 3 of the non-overlapping operation

The current through D_1 becomes zero since the resonance ends; therefore the secondary winding current is zero. Upon the termination of resonance in the circuit's secondary side, D1 can be turned off resulting in ZCS at t_3, since the current i_{D1} is zero. This mitigates any potential losses caused by reverse-recovery of the diode.

The operations of modes 1, 2 and 3 represent the first half period. The operations of modes 4, 5 and 6 representing the second half period are analogous to 1, 2 and 3, respectively. This concludes the operation of the non-overlapping region in terms of modes. Other important properties will be defined for this region.

The average output current of the half-period is calculated below from equation 4.12 and equation 4.15 as

$$\begin{aligned} I_o &= \frac{2}{T_s}\int_{t_2}^{t_1} \frac{I_{s,peak}}{2} sin[\omega_r(t-t_1)]dt \\ &= -\frac{I_{s,peak}}{\omega_r T_s} cos[\omega_r(t-t_1)]\Big|_{t_1}^{t_2} \\ &= \frac{I_{s,peak}}{\omega_r T_s}[cos[\omega_r(t_1-t_1)] - cos[\omega_r(t_2-t_1)]] \\ &= \frac{I_{s,peak}}{\omega_r T_s}[1 - cos[\omega_r(t_2-t_1)]] \\ &= \frac{I_{s,peak}}{\omega_r T_s}[1 - cos[\frac{2\pi}{T_r}(t_2-t_1)]] \\ &= \frac{I_{s,peak}}{\omega_r T_s}[1 - cos[\frac{2\pi}{T_r}(t_2-t_1)]], \end{aligned} \tag{4.16}$$

since $(t_2 - t_1) = \frac{1}{2}T_r$,

$$\begin{aligned} &= \frac{I_{s,peak}}{\omega_r T_s}[1 - cos[2\pi\frac{1}{2}]] \\ &= \frac{I_{s,peak}}{\omega_r T_s}[1 - cos[\pi]] \\ &= \frac{2I_{s,peak}}{\omega_r T_s}. \end{aligned} \tag{4.17}$$

The derivation in 4.16 and 4.17 was not obtained from [33], but was derived by the researcher. This derivation gives a relationship between the peak secondary winding current and the average output current, substituting $\frac{2}{T_s} = \omega_s$ into equation 4.16 as

$$\begin{aligned} I_o &= \frac{2I_{s,peak}}{\omega_r T_s} \\ &= \frac{\omega_s I_{s,peak}}{\omega_r \pi}. \end{aligned} \tag{4.18}$$

With $I_{s,peak}$ as the subject, equation 4.17 can be written as

$$I_{s,peak} = \frac{I_o \omega_r \pi}{\omega_s}. \tag{4.19}$$

where ω_s represents the angular switching frequency. The peak secondary current was described earlier in equation 4.11 , equating it with equation 4.19 yields,

$$I_{s,peak} = \frac{nV_C - v_{Cr1}(t1)}{Z_r} = \frac{I_o \omega_r \pi}{\omega_s}.$$

From equation 4.8, the average voltage across the resonant capacitor is $V_{Cr1}(t) = nV_c$. Therefore using,

$$\frac{nV_C - v_{Cr1}(t1)}{Z_r} = \frac{I_o \omega_r \pi}{\omega_s}. \tag{4.20}$$

the voltage ripple over the resonant capacitor can be expressed using 4.20, as

$$\Delta V_{Cr1} = nV_C - v_{Cr1}(t1) = \frac{I_o Z_r \omega_r \pi}{\omega_s}.$$

The mode 2 time interval from t_2 to t_3 is when the resonance takes place and can be adjusted by the angular resonant frequency and is minimized at $D = D_{min}$. D1 is reverse-biased at t_3, this means that i_{D1} needs to reach zero by t_3 to minimize conduction loss.

The critical angular resonant frequency, at $D = D_{min}$, to ensure ZCS and minimum conduction loss must satisfy

$$i_s(t_3) = I_{s,peak} sin(\omega_{rc} D_{min} T_s) = 0. \tag{4.21}$$

From equation 4.21 the sin-function must be equal to 0, therefore the argument of the sin-function, $(\omega_{rc} D_{min} T_s)$, can be equal to π. This is expressed as

$$2\pi f_{rc} D_{min} T_s = \pi. \tag{4.22}$$

The critical resonant frequency with respect to the switching frequency and to the minimum duty cycle for minimum conduction loss from equation 4.22 is then

$$f_{rc} = \frac{f_s}{2D_{min}}. \tag{4.23}$$

Having obtained the critical resonant frequency, the chosen frequency of resonance needs to be greater than the calculated value of the critical resonant frequency. The reason for this is that zero current switching through the diodes can then be obtained.

Resonant capacitance can then be chosen using equation 4.14. It is expressed as an inequality, as the chosen resonance capacitance needs to be greater than the capacitance at the critical frequency for ZCS, yielding

$$C_{rc} < \frac{1}{{\omega_{rc}}^2 L_{lk}}. \tag{4.24}$$

As the net change in inductor current is zero, the average inductor voltage over one switching period is equal to zero. This is known as the Volt-second balance law. The Volt-second balance law of the inductor of the half period is illustrated in figure 4.7 and expressed as

$$(V_i - V_c)(0.5 - D) + (V_i - 0.5V_c)D = 0. \tag{4.25}$$

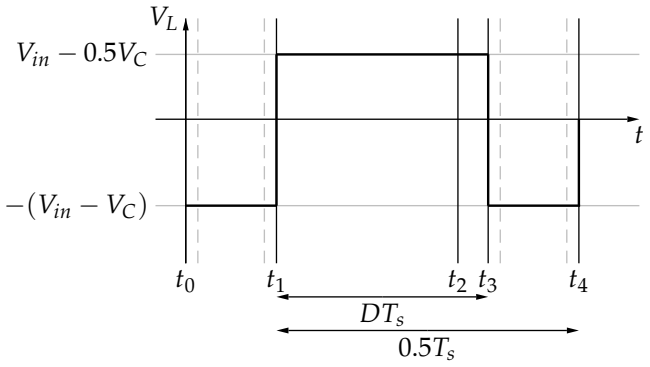

Figure 4.7: Inductor voltage over a half period operating below 50 % duty cycle

Therefore, from equation 4.25 the clamp voltage is expressed as

$$V_c = \frac{V_i}{1 - D}. \tag{4.26}$$

The resonant capacitors' voltages, v_{Cr1} and v_{Cr2}, are both equal to the average value of nV_C, yielding from equation 4.2 the output voltage as

$$V_o = v_{Cr1}(t) + v_{Cr2}(t) = nV_C + nV_C = 2nV_C. \tag{4.27}$$

Therefore, the output voltage is given, using equations 4.2 and 4.26, as

$$V_o = n\frac{2V_i}{1 - D}. \tag{4.28}$$

Lastly, the ripple current is defined by observing mode 1. The current over the time interval through the inductor is $-\frac{V_C - V_i}{L}$. The time interval of mode 1 is $(0.5 - D)T_s$. The expression for the ripple current of the inductor is

$$\Delta I_L = \frac{V_c - V_i}{L}(0.5 - D)T_s. \tag{4.29}$$

The ripple current of the inductor can be rewritten in terms of the output voltage, using equations 4.28 and 4.29 as

$$\Delta I_L = \frac{V_o D(0.5 - D)}{2nf_s L} \tag{4.30}$$

In figure 4.8 presented below from [33] the switch control-signals, voltage and current signals are shown for the non-overlapping region. In it, firstly, the four control signals of the switches are shown for this region, followed by the secondary side current, diode current through D_1 and the output current. These are all sinusoidal due to resonance. The inductor current is then shown and currents through one main switch and one auxiliary switch. Finally, the voltage through D_1 is illustrated.

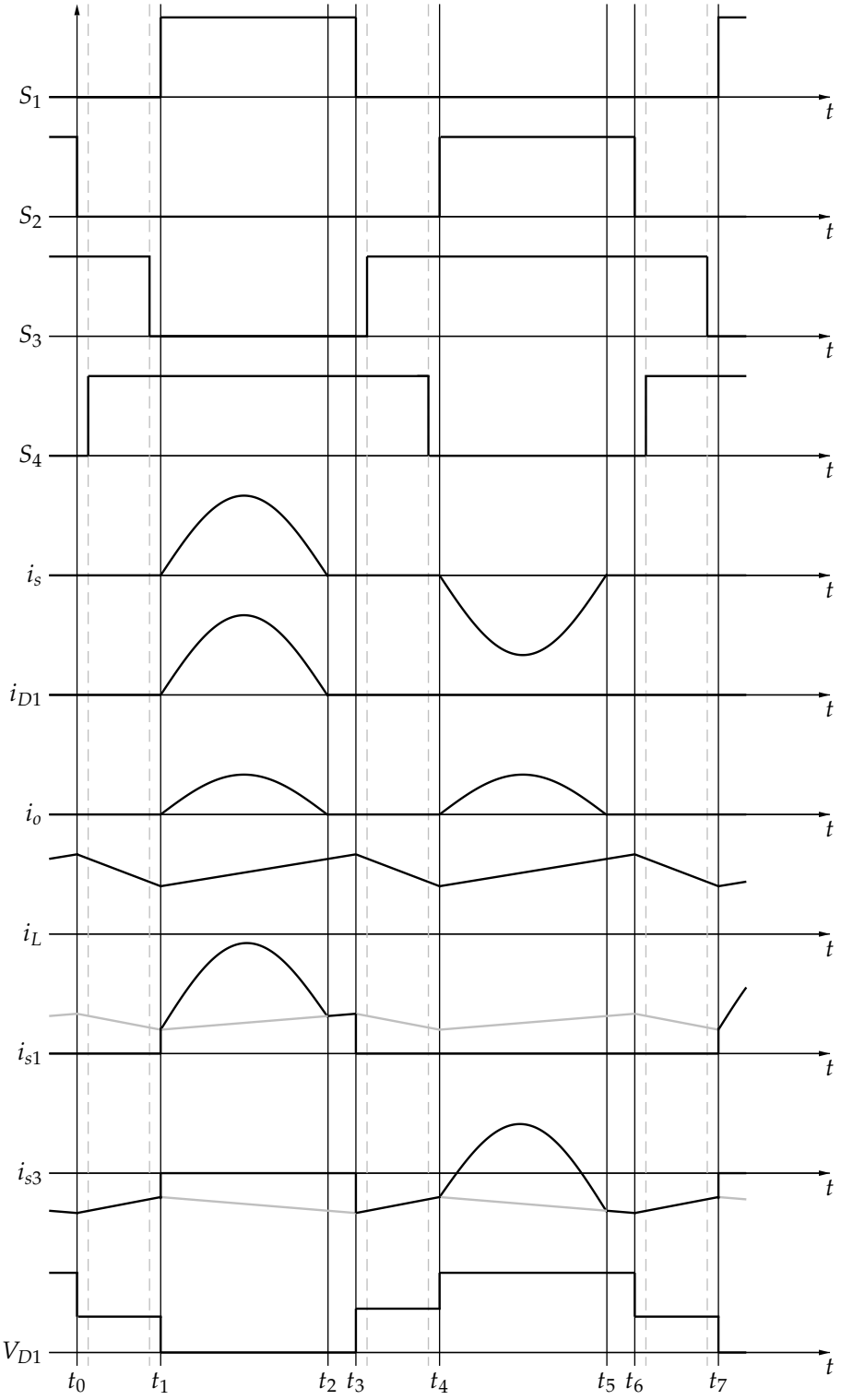

Figure 4.8: Non-overlapping control and power signals

4.3.2 The overlapping region

Six topological modes exist over one switching period, T_s, as it was for the non-overlapping region. These modes repeat periodically. It is only necessary to describe three of the modes, as the other three are analogous to the three that will be described. The principle of operation for D $>$ 50% will be presented through equations, diagrams and waveforms. Illustrated at the end of the discussion for the overlapping region is figure 4.13. This figure presents the control and analog signals related to this region and illustrates the time-stamps to be mentioned.

Mode 1, from t_0 to t_1: The primary current i_{p1} flows through S_2 and the primary current i_{p2} flows through the body diode of S_3 proceeding to mode 1. The switch S_1 is turned on at t_0 and i_{p2} stops flowing through the body diode of S_3. As the current i_{p1} flows through S_2 and i_{p2} flows through S_1, both main switches are conducting. This means that their on-times overlap. There is zero voltage across the windings of the transformer. Therefore, the current through the inductor i_L increases linearly from t_0 to t_1 and is equally divided flowing through both switches. The current flow is illustrated in figure 4.9 and the inductor and switches currents are expressed mathematically as well.

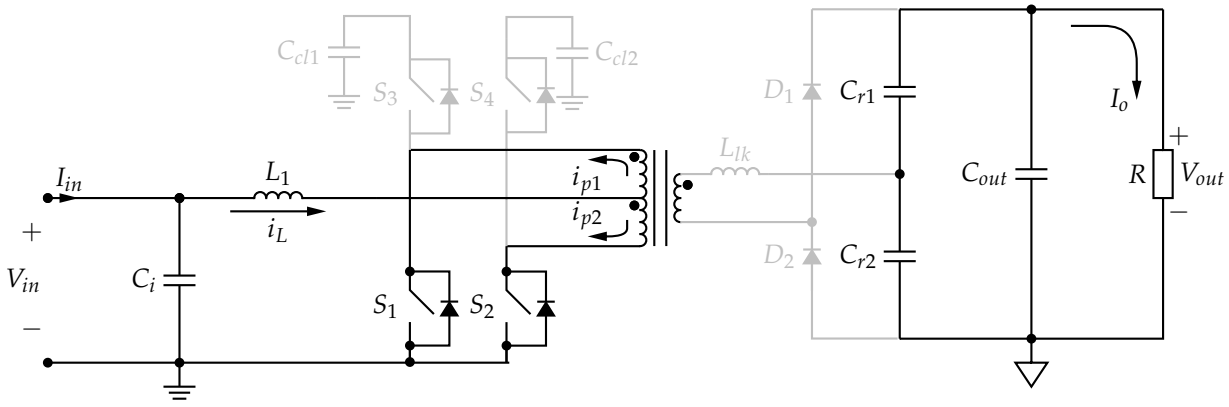

Figure 4.9: Mode 1 of the overlapping operation

$$i_L(t) = I_L(t_0) + \frac{V_i}{L}(t - t_0)$$

$$i_{S_1}(t) = i_{S_2}(t) = \frac{i_L(t)}{2}$$

Mode 2, from t_1 to t_2: S_2 is turned off at t_1, the body diode of S_4 conducts and $0.5V_C$ is the voltage across the center-tapped winding, on the primary side. S_4 is turned on, while its body diode conducts after a short dead time, shown in figure 4.10. i_L decreases linearly through the inductor as V_i is now less than $0.5V_C$, shown in the equation below as

$$i_L(t) = I_L(t_1) - \frac{0.5V_C - V_i}{L}(t - t_1)$$

The diode D_1 is conducting and the leakage inductance L_lk resonates with the resonant capacitors, as the current i_s flows through, on the secondary side. The input power is transferred to the output load through the transformer in this way.

This mode is similar to mode 2 of the non-overlapping region, so are the equations used to describe the mode. The following equations describe i_s and v_{Cr1}, the derivation will not be presented again as it is the same as for previous region's mode 2. The derivation parts are presented in 4.16 and 4.17. The final solutions, including the initial values, are

$$V_{Cr1}(t) = nV_c - (nV_c - V_{Cr1}(t_1))cos[\omega_r(t - t_1)] \tag{4.31}$$

and

$$i_s(t) = \frac{nV_C - v_{Cr1}(t_1)}{Z_r} sin[\omega_r(t - t_1)]. \tag{4.32}$$

The peak value of the secondary current is given, from equation 4.32 as

$$I_{s,peak} = \frac{nV_C - v_{Cr1}(t_1)}{Z_r}. \tag{4.33}$$

also written, therefore, from equation 4.31 as

$$i_s(t) = I_{s,peak} sin[\omega_r(t - t_1)]. \tag{4.34}$$

The output load current is equal to half the secondary winding current since the resonant capacitances are the same. This yields the current relationships of the secondary side as

$$i_{Cr1}(t) = -i_{Cr2}(t) = 0.5i_s(t) = i_o(t).$$

The currents flowing through the switches S_1 and S_4 are obtained as

$$i_{s1}(t) = i_{p1}(t) = \frac{i_L(t)}{2} + ni_s(t)$$

and

$$i_{s4}(t) = -i_{p2}(t) = -\frac{i_L(t)}{2} + ni_s(t).$$

These currents are represented above, as the sum of the magneto motive forces of all the windings is zero, therefore yielding these switch currents. The schematic diagram representation, in figure 4.10 shows the flow of the currents for this mode. The input inductor current is split into the two primary side currents from the center-tap. On the secondary side, the diode D_1 conducts and the secondary inductor current flows through the resonant capacitors and output load.

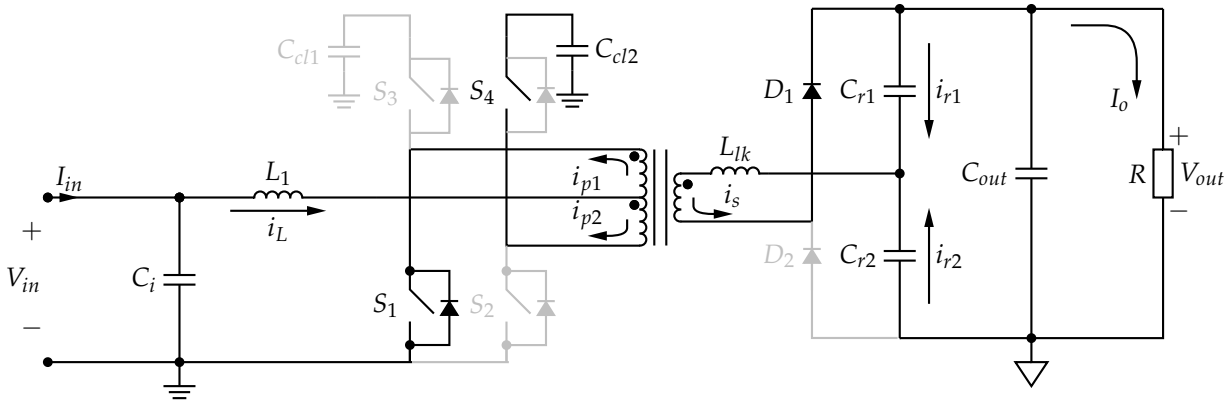

Figure 4.10: Mode 2 of the overlapping operation

Mode 3, from t_2 to t_3: The current through D_1 becomes zero since the resonance ends. Therefore, the secondary winding current is zero and the inductor current divides equally between S_1 and S_4. D_1 can be turned off resulting in ZCS at t_3, since the current i_{D1} is zero. This mitigates any losses potentially caused by reverse-recovery of the diode. This is shown in figure 4.11.

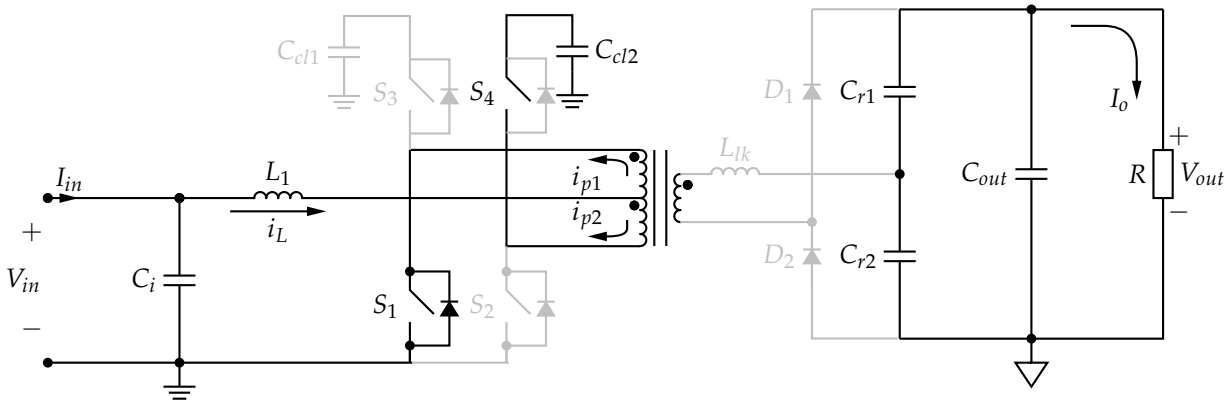

Figure 4.11: Mode 3 of the overlapping operation

The operations of modes 1, 2 and 3 represent the first half period. The operations of modes 4, 5 and 6 representing the other half period are analogous to 1, 2 and 3, respectively. This concludes the operation of the overlapping region. Other important properties will be defined for this region. As in the previous region, the peak secondary current is obtained and the derivation will not be presented again as it is the same as the previously stated equation 4.16. It is given as

$$I_{s,peak} = \frac{\pi I_o \omega_r}{\omega_s}.$$

The clamp capacitor voltage is obtained using the volt-second balance law during the half period, including the input voltage and the duty cycle. The Volt-second balance law of the inductor of the half period is

$$(V_i)(D - 0.5) + (V_i - 0.5V_c)(1 - D) = 0. \tag{4.35}$$

The inductor voltage of a half period is shown below in figure 4.12, from which equation 4.34 is derived. Simplifying equation 4.35 and solving for the clamp capacitor voltage, the following is obtained.

$$V_C = \frac{V_i}{1 - D}. \tag{4.36}$$

From the above-stated resonant capacitor voltage in equation 4.31, the average value of it is $v_{Cr1} = nV_C$. This is the same for the other resonant capacitor voltage. Since the output voltage can be defined in terms of the resultant resonant capacitor voltages as $V_o = 2nV_C$, using equation 4.36, the output voltage is defined in more detail as

$$V_o = n\frac{2V_i}{1 - D}. \tag{4.37}$$

The time of resonant termination can be changed by ω_{rc} and is minimized at $D = D_{max}$. To mitigate the conduction losses of the D1, the current through it has to reach

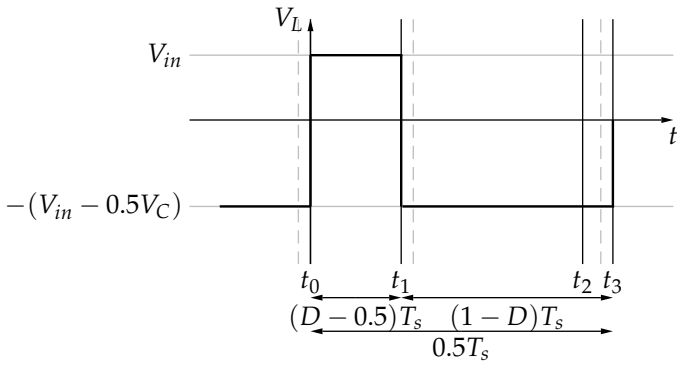

Figure 4.12: The voltage across the inductor for a half period, the overlapping operation

zero at t_3. From the previously stated secondary current in equation 4.33, the frequency that will result in both ZCS and mitigated diode conduction loss at $D = D_{max}$ must satisfy the following

$$i_s(t_3) = I_{s,peak} sin[\omega_{rc}(1 - D_{max})T_s] = 0. \tag{4.38}$$

The critical frequency, f_{rc}, is then obtained from equation 4.38. The argument of the function can be equal to π, therefore yielding

$$f_{rc} = \frac{f_s}{2(1 - D_{max})}. \tag{4.39}$$

As for the previous mode, in order to achieve ZCS, the resonant capacitance must satisfy the inequality

$$C_r < \frac{1}{\omega_{rc}^2 L_{lk}}.$$

This means that zero diode current will be reached before t_3 if the above inequality is satisfied. Since the difference between the ends of both the on-times of the main switches is $(D - 0.5)T_s$, the ripple current for mode 1 can be defined as

$$\Delta I_L = \frac{V_i}{L}(0.5 - D)T_s \tag{4.40}$$

The ripple current can be rewritten, using equation 4.37 in equation 4.40 as

$$\Delta I_L = \frac{V_o(D - 0.5)(1 - D)}{2nf_sL}. \tag{4.41}$$

In figure 4.13 presented below from [33] the switch control-signals, voltage and current signals are shown for the overlapping region. As previously shown for the non-overlapping region, the four control signals of the switches are shown, followed by the secondary side current, diode current through D_1 and the output current. These are all sinusoidal due to resonance. The inductor current is then shown as well as currents through one main switch and one auxiliary switch. Finally, the voltage through D_1 is illustrated.

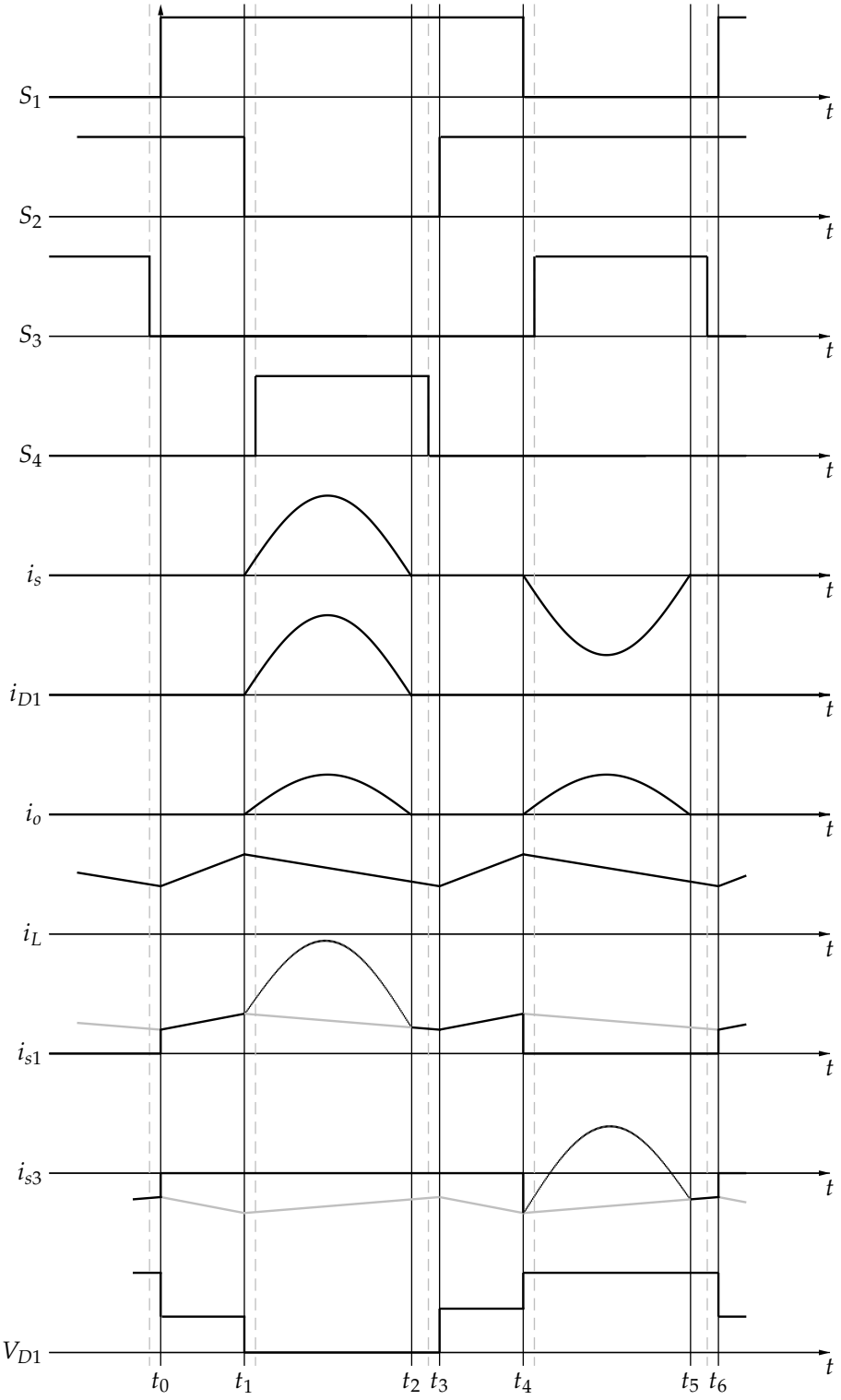

Figure 4.13: Overlapping control and power signals

4.4 Design of resonant push-pull converter

4.4.1 The design procedure

A basic design procedure for the resonant push-pull converter is offered by authors, Kim and Kwon [33]. This procedure was followed and was completed for a given switching frequency, input voltage range and fixed output voltage. The procedure is stated below.

1. Choose the clamp capacitor voltage, V_C. The voltage stress constraint for the primary switches will be determined by V_C. A guideline of 1.5 times greater than the maximum input voltage or lower is suggested by the authors, to use low-on resistance switches.

2. The duty cycle range is obtained using the input voltage ranges from equation 4.26.

3. The transformer turns ratio is selected using equations 4.26 and 4.28, yielding

$$n = \frac{V_o}{2V_C}. \tag{4.42}$$

4. The critical resonant frequency is calculated using equations 4.23 and 4.39. The higher of the two calculated resonant frequencies are used to ensure ZCS throughout the entire input voltage range.

5. The resonant capacitance of both resonant capacitors is determined using equation 4.24; these capacitances are chosen to be the same. The leakage inductance is estimated or measured from the transformer. The clamp capacitances are chosen to be of greater proportion to the resonant capacitors. This is to ensure that resonance can be neglected between leakage inductance and the clamp capacitors using the following inequality

$$C_c > n^2 C_{rc}. \tag{4.43}$$

6. The input inductance is determined from the maximum input current ripple. The maximum current ripple is obtained using equations 4.30 and 4.41, respectively. The inductances are expressed below as

$$L = \frac{V_o D(0.5 - D)}{2nf_s \Delta I_{L,max}}, \tag{4.44}$$

for D $<$ 0.5, and the following for D $>$ 0.5 as

$$L = \frac{V_o (D - 0.5)(1 - D)}{2nf_s \Delta I_{L,max}}. \tag{4.45}$$

The inductance is calculated for the D_{min}, D_{max} both defined in (2), $D = 0.25$ and $D = 0.75$. The largest inductance is chosen among these.

7. The remaining components are then chosen according to voltage and current stresses. The voltage stress maximum across the secondary side diodes is the output voltage V_o, which is then chosen accordingly. Trade-offs are to be made in the choice of semiconductor devices to be used. The trade-off regards power conversion efficiency and cost of the converter.

4.4.2 The Specific design procedure of the project

The converter input voltage range was $V_i = 50{-}120$ V and operated at switching frequency f of 40 kHz. An output voltage range of $V_{out} = 500{-}600$ V and a maximum power capacity of 1500 W was specified for the design.

1. As $V_i = 120$ V is the maximum of the input voltage range and using the guideline of less than a 1.5 multiple of the input voltage, a maximum clamp capacitor voltage of $V_C = 180\ V$ is calculated. A voltage less than this was selected, $V_C = 150$ V.

2. The duty cycle was calculated for both the minimum and maximum input voltages respectively as $V_{i,min} = 50$ V and $V_{I,max} = 120$ V, with the chosen clamp capacitor voltage as $V_C = 150$ V. Using equation 4.26 with the duty cycle as the subject yields

$$D = 1 - \frac{V_i}{V_C}.$$

   The maximum duty cycle is then calculated as $D_{max} = 66,7\ \%$, using the minimum input voltage. The minimum duty cycle is then calculated as $D_{min} = 20\ \%$ using the maximum input voltage.

3. The turns-ratio, from equation 4.42 is calculated as using the maximum output voltage, 600 V, and the clamp capacitor voltage, 150 V, as

$$n = \frac{V_o}{2V_C} = \frac{600}{2(150)} = 2.$$

4. The critical frequency, with $f_s = 40$ kHz, using equation 4.23 is calculated as

$$f_{rc} = \frac{f_s}{2D_{min}} = \frac{40 \times 10^3}{2(0.2)} = 100 \times 10^3$$

   Using equation 4.39 is calculated as

$$f_{rc} = \frac{f_s}{2(1 - D_{max})} = \frac{40 \times 10^3}{2(1 - 0.667)} \cong 60 \times 10^3$$

   From the above calculated critical frequencies, the higher frequency is chosen to ensure soft-switching of the diode for the entire duty cycle range. Therefore $f_{rc} =$ 100 kHz.

5. Resonant capacitances are calculated based on the above-chosen f_{rc} and the transformer leakage inductance, using inequality 4.24. The leakage inductance was initially chosen as $L_{lk} = 1\ \mu H$, as it needs to be estimated or measured. It was chosen to be small so as to have minimum negative effects on the efficiency. Calculation of the resonant capacitance yielded

$$C_{rc} < \frac{1}{{\omega_{rc}}^2 L_{lk}}$$

$$C_{rc} < \frac{1}{2\pi {f_{rc}}^2 (1)(10^{-6})}$$

$$C_{rc} < \frac{1}{(2\pi(100)10^3)^2(10^{-6})}$$

$$C_{rc} < 2.53303 \times 10^{-6}.$$

The initial resonant capacitance was obtained as $C_{rc} = 2.53303$ μH. L_{lk} was measured after the transformer was wound, this will then change the initial resonant capacitance for the same critical frequency, to ensure soft-switching. This change in capacitance will be presented after the presentation of the transformer design and testing. The clamp capacitance is not effected by the changed L_{lk}.

From equation 4.43, the clamp capacitance is calculated as

$$C_c > n^2 C_{rc} = (2)^2(2.53303)(10^{-6}) = 10.13212 \times 10^{-6}.$$

The capacitance for the clamp capacitors was chosen as $C_c \cong 10$ μH.

6. Input inductance was calculated for the overlapping and non-overlapping regions of operation. This was done for various duty cycles and with a chosen ripple current. The chosen input ripple current is $\Delta I_L = 1$ A. The maximum calculated inductance from the variously calculated inductances will be chosen. For the duty cycles less than 50 %, specifically, 20 % and 25 % inductance was obtained from equation 4.44 using

$$L = \frac{V_o D(0.5 - D)}{2n f_s \Delta I_{L,max}}$$

as

$$L = \frac{(600)(0.2)(0.5 - 0.2)}{2(2)(40)(10^3)(1)} = 225 \times 10^{-6}$$

for D = 0.2 and for D = 0.25 as

$$L = \frac{(600)(0.25)(0.5 - 0.25)}{2(2)(40)(10^3)(1)} = 234.375 \times 10^{-6}.$$

For the duty cycles greater than 50 %, specifically 66.7 % and 75% from equation 4.45 the inductance was obtained using

$$L = \frac{V_o(D - 0.5)(1 - D)}{2n f_s \Delta I_{L,max}}$$

as

$$L = \frac{(600)(0.667 - 0.5)(1 - 0.667)}{2(2)(40)(10^3)(1)} = 208.541 \times 10^{-6}$$

for D = 0.667 and for D = 0.75 as

$$L = \frac{(600)(0.75 - 0.5)(1 - 0.75)}{2(2)(40)(10^3)(1)} = 234.375 \times 10^{-6}.$$

Therefore the maximum inductance is $L = 234.375$ μH, for a ripple current of 1 A.

A ripple current of 5 A was chosen, as a more realistic value and a decreased inductance. For the duty cycles, less than 50 %, specifically 20 % and 25 % inductance was obtained from equation 4.44 using

$$L = \frac{V_o D(0.5 - D)}{2nf_s \Delta I_{L,max}}$$

as

$$L = \frac{(600)(0.2)(0.5 - 0.2)}{2(2)(40)(10^3)(5)} = 45 \times 10^{-6}$$

for D = 0.2 and for D = 0.25 as

$$L = \frac{(600)(0.25)(0.5 - 0.25)}{2(2)(40)(10^3)(5)} = 46.875 \times 10^{-6}.$$

For the duty cycles greater than 50 %, specifically 66.7 % and 75% from equation 4.45 the inductance was obtained using

$$L = \frac{V_o(D - 0.5)(1 - D)}{2nf_s \Delta I_{L,max}}$$

as

$$L = \frac{(600)(0.667 - 0.5)(1 - 0.667)}{2(2)(40)(10^3)(5)} = 41.7082 \times 10^{-6}$$

for D = 0.667 and for D = 0.75 as

$$L = \frac{(600)(0.75 - 0.5)(1 - 0.75)}{2(2)(40)(10^3)(5)} = 46.875 \times 10^{-6}.$$

Therefore, the maximum of 46.875 μH was chosen as the input inductance for a 5 A ripple current.

4.4.3 The design of the components used in the converter

With the converter design from the previous section, various parameters were obtained and defined for the components used in the converter. The component parameters obtained were the resonant and clamp capacitance values, the input and resonant inductances, ripple current and the transformer turns ratio. All the components need to be sized and selected to correct specifications to ensure that failure due to excessive voltage or current for that specific component does not occur. For the magnetic components, more design is needed, as they require windings, have material-dependent cores and are frequency-dependent. The component will be evaluated with similar components and the best component will be chosen. The chosen component needs to meet the specifications regarding power requirements, ability to achieve outcome and efficiency. A components description will follow.

Component description

All components must be able to handle the maximum stresses of voltage and current. They are chosen to handle slightly over-specified parameters to avoid unnecessary failure due to accidental and excessive power being applied or transferred.

At the input side, where the Solar PV modules are the source, a sufficiently large capacitor is chosen and placed as a DC-bus capacitor to ensure a nearly constant DC input voltage. The capacitor has a 3900 μF capacitance and is rated at 200 V.

The primary side input inductor was calculated as $L \cong 45\ \mu H$. The design of the inductor is present further on, discussing the core selection and turns number. The inductor handles the current ripple from the input PV source, ensuring inherently low input current [56].

The clamp circuit limits the maximum voltage across the four switches. The purpose of the clamp circuit is to clamp surges of the voltage across the switches. The energy stored in the leakage inductance that causes these surges is then recycled [58]. The specific transistors used as switches in the design are MOSFETs. MOSFETs that are able to handle 200 V are chosen, as $V_{Cmax} = 150\ V$ is the maximum drain-source voltage that will appear across the MOSFETS.

They have a very low on resistance and can transition relatively fast between on and off states [41]. The clamp capacitors of the clamp circuits are rated at 250 V and are film-type capacitors. Film capacitors are rated for large currents, without being exceptionally large in size.

The transformer is one of the main voltage elevation components implemented with a turn-ratio of 2, with a double primary side center-tap configuration and a single secondary winding. The design for the transformer will be later presented. The transformer leakage inductance is used with the resonant capacitors, resonating to provide soft-switching capabilities. The resonant capacitors are very small compared to the clamp capacitors avoiding any unnecessary resonance. These resonant capacitors were chosen to be $C_{cr} = 0.8\ \mu H$ able to handle 400 V each.

The secondary side diodes need to be rated at 800 V, able to at least handle the output voltage as such a magnitude will be applied across the diode as reverse voltage. Lastly, a sufficiently large capacitor at the output is needed ensuring a low ripple voltage and near constant output voltage. The capacitors are rated at 800 V, a current of 2.5 A and a capacitance of 110 μH.

Inductor design

The inductance was calculated as $L_{in} = 46.875\ \mu$H, using equation 4.41. In order to build such an inductor, a core needs to be chosen that is suitable for the application, followed by a calculation of the number of windings and thickness. The core defines the number of windings. Moreover, the core material of the core defines when saturation occurs. The following expression can be used to obtain L from [59] as

$$L = \frac{(\mu_e)(\mu_0)(N)^2(A_e)}{l_e}.$$

The above equation includes the effective magnetic length l_e, the effective magnetic cross section A_e and the effective permeability μ_e. AL is the inductance factor, which represents all of the described parameters, yielding

$$L = (AL)(N)^2. \tag{4.46}$$

To calculate the number of turns, N, for the inductor, the equation 4.46 can be rewritten with N as the subject, as

$$N = \sqrt{\frac{L}{AL}}. \tag{4.47}$$

To see whether the inductor will be saturating the Ampere's current law is used, with the magnetic flux density as the subject of the equation, yielding

$$B_{sat} = \frac{\mu N i_{peak}}{l}.$$

Using the equation 4.47 and Ampere's law, various cores were investigated in order to choose the right one. They were compared to match the calculated inductance and ripple current, and to ensure saturation does not occur, of $L = 45$ μH and $\Delta I_L = 5$ A.

Inductor design choices					
Core types	Ind[μH]	AL[nH]	Number of turns	B[T]	ΔI_L[A]
Toroidal-core (26)	45	169	17	0.5	5
ETD-core 59	45	5	3	1.4239	5
E-core 36, with 1mm gap	45	0.183	16	0.70372	5
E-core 36, with 2mm gap	45	0.1083	21	0.4618	5
E-core 36, with 2mm gap	21.2268	0.1083	14	0.3	12
E-core 36, with 2mm gap	14	0.1083	11	0.25	17

Ferrite and iron power cores are included in the table presented. From an Epcos data book, the saturation magnetic flux density is $B_{sat} \cong 450-500$ mT [59] for ferrite materials. The saturation magnetic flux density is $1.2 - 1.5$ T for iron powder materials [60]. From table 4.4.3, and the magnetic flux density saturation limits, the Toroidal core (26) was chosen. It was chosen, as the core does not saturate, that is, surpass the saturation flux density, and the ripple current is not too high. The ferrite core E 36 is a valid option for a core to be used, but the ripple current is too high. The Toroidal core remains the best choice, mainly as saturation B is high.

After the numbers of turns have been decided, the thickness of the conductor for the windings can be determined. The current density is used together with the specified current through the winding in order to define the parameters of the conductor. The area of the conductor is defined as

$$A_{cond} = \frac{i_{peak}}{J}.$$

where J is the current density, $\frac{A}{mm^2}$ is the SI units for current density. A current density of 4 $\frac{A}{mm^2}$ was chosen. A current density choice between 0.1 - 8 $\frac{A}{mm^2}$ is typical for power converters [61]. The area of the wire, with the peak input current, is calculated as

$$A_{cond} = \frac{35}{4} = 8.75mm^2.$$

For a round conductor the radius is

$$A_{cond} = \pi r^2 = 8.75mm^2.$$

$$r = \sqrt{\frac{8.75}{\pi}} = 1.6688953.$$

The thickness of the round conductor in diameter is $d \cong 3.34$mm. A square conductor, was used instead that satisfies the calculated need area $A_{cond} = 8.75mm^2$.

Transformer design

The transformer was designed using Faraday's law to define the number of turns, as

$$E = (N)(A_e)\frac{dB}{dt}. \tag{4.48}$$

The core choice is made first, which defines the physical parameters, the area, and the saturation limit for the design by the core material. With the switching frequency and duty cycle range defined, Faraday's law can be used to calculate N. Making N the subject of equation of Faraday's law, with the minimum input voltage and maximum duty cycle, yields

$$N_P = (V_{d,min})\frac{\Delta t}{(A_e)\Delta B} = (V_{d,min})\frac{T_{on,max}}{(A_e)\Delta B}. \tag{4.49}$$

ΔB is the change in magnetic flux density and is equal to twice the peak flux density, $\Delta B = 2B_{max}$ [41]. The peak flux density for the N72 ferrite material is $B_{max} \cong 3500$ G, which makes the change in magnetic flux density $\Delta B = 7000$ G [59]. To ensure that saturation does not occur, the core should be utilized below the $\Delta B = 7000$ G. For the design of this transformer, $\Delta B = 3800G$ is chosen as it is below the saturation threshold, therefore $B = 1900$ G.

The single primary winding was calculated as 5.96217 turns, shown below

$$N_P = \frac{(50)(25)(10^{-6})(0.667)(10^8)}{(3.68)(3800)} \cong 5.96217, \tag{4.50}$$

and was chosen practically as 6 Turns. With the calculated turns ratio of 2 from equation 4.42 and the $n = \frac{N_s}{2N_p}$, the secondary winding number of turns is calculated as $N_s = 24$ turns, of which the center-tap configuration is illustrated below in figure 4.14.

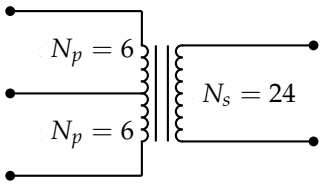

Figure 4.14: The center-tap transformer, indicating the number of turns

The primary inductance can be calculated using the number of turns and the AL-value of the core, using equation 4.46, for each half of the center-tap as

$$L_p = (AL)(N)^2 = (5.3)(6)^2 = 190.8\mu H$$

Transformer winding thickness

With an applied time-varying current in a conductor generating a magnetic field, eddy currents are created in turn by the magnetic fields. These eddy currents tend to shield the conductor interior from the applied current and the magnetic fields, as they flow in the opposite direction in the conductor interior. The shielding is minimal at the surface of the conductor and decays exponentially in relation to the distance toward the conductor interior. Therefore, the current density is maximum at the surface of the conductor. This is the skin-effect [34]. The characteristic decay length is the skin depth, which is defined as

$$\delta = \sqrt{\frac{2}{\omega\mu\sigma}},$$

where ω is the angular frequency of the magnetic field, μ the permeability and σ the conductivity of the material (copper). As seen, the skin depth is inversely proportional to frequency [34].

If a conductor is chosen to be much larger than the skin depth, the current density decays toward the interior and the surface of the conductor would carry most of the current, a layer of nearly one skin depth [34].

To mitigate effects caused by the skin effect, conductors are used that is smaller than the skin depth in diameter, d. As the exponential decay occurs from both ends of the conductor cross-section the diameter should be $d \leqslant 2\sigma$ [34]. Litz wire was used to wind the transformer as it consists of a bundle of smaller conductors and the skin depth can be used to define the size of these smaller conductors, mitigating the skin effect.

With the conductivity $\sigma = 5.96 \times 10^7 \Omega$.m, and permeability, $\mu_0 = 1.256629 \times 10^{-6}$ H/m, of copper and a switching frequency of 40 kHz, the skin depth is calculated as

$$\delta = \sqrt{\frac{2}{(2\pi)(40000)(5.96)(10^7)(\mu_0)}} = 0.32596202 \times 10^{-3}.$$

With a skin depth of 0.326 mm, the diameter could be chosen as $d \leqslant 0.652$ mm, to mitigate the skin effect. Litz wire with a thickness of 2.4 mm was used, containing a bundle of 70 smaller conductors. The conductors were 0.2 mm each, which is sufficiently within range of the skin depth inequality.

Flux unbalance

In the hysteresis loop the transformer operates along the loop when it is magnetized. After each switching cycle, the operating point of the transformer should return to the original starting point. Flux unbalance occurs when the voltage-second product of the windings are not equal. This is caused by unequal duty cycles and turns-ratios [33]. The operation becomes lopsided, as the magnetizing core does not return to the original starting point in the loop after a switching cycle. After numerous cycles, the core will reach saturation. This means that the core will not be able to the handle the applied voltage from the in-put. When in saturation, the switching devices are subjected to high currents and voltage situations, leading to damage to these devices [62].

Applying a current-limit control on the converter through the switches is a way flux imbalance can be prevented and is described as one of the external measures that can be taken. It is difficult to implement current-control for multiple switches as the current increase is complex [33].

The second measure to mitigate flux imbalance is to include a DC block capacitor in series with the primary winding of the transformer. These capacitors have to be large to handle the voltage and current. This is undesirable [63].

The resonant push-pull converter utilises an inherent corrective mechanism provided through the two clamping capacitors. A voltage drop is caused at the transformer center tap when a larger switch current than load demand is flowing. The inductor decreases the voltage of the clamp capacitor in operation, resulting in the voltage drop. The voltage-second product in the half-period is then decreased, bringing the switch current down [33].

With this, the main design of the converter is concluded. On the same PCB additional circuitry was implemented in order to measure voltages and currents; and to provide gate-drive signals for the MOSFETs. These circuits are discussed in the following segment.

4.4.4 Integration of additional circuitry

Figure 4.15 presents the converter in schematic detail and the integration between the parts of the PV drive system. The aim of this figure is to show and emphasize the relationship between the converter and the additional circuitry.

The converter is presented as the central component; and through the dashed line dividing the figure, galvanic isolation is shown. Through the transformer in the converter, isolation is provided creating two ground planes, namely the primary and the secondary ground plane.

On the PCB where the resonant push-pull converter is placed, the input source and the output load are both measured. The measurements are made on the different ground planes and then taken to the primary ground plane to be processed by the MCU. Opto-couplers are used to transmit the secondary side measurements to the primary side. There-

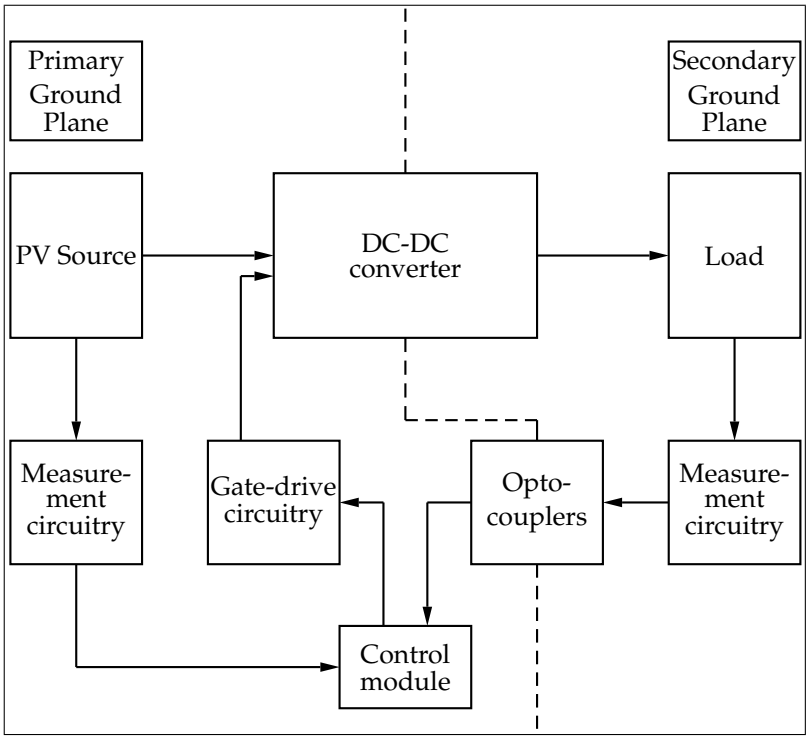

Figure 4.15: Integration of converter with the additional circuitry

fore, the input and output parameters can be measured.

On the primary side of the transformer, as the switches are referenced to the primary ground, the gate-drive circuitry is included. The MCU supplies the gate-drive circuitry with control signals and power is provided as well. The output signals, of the gate-driver circuitry, are then used to control and the MOSFETs. More detailed schematics are shown in section 4.6.

4.5 Simulation of the design

4.5.1 Introduction to Simplorer

After the theoretical design shown in sections 4.3 and 4.4 from [33], the resonant push-pull converter was simulated. The converter was simulated using ANSYS Simplorer, which is able to analyze complex power electronics systems. The purpose of the simulation was to verify the theoretical analysis and the converter modes of operation before building the converter. Simplorer is an advanced simulation programme. It contains both basic electrical elements and real-world manufacturer elements, making the simulation more specific and accurate. Elements are able to be designed and programmed as well.

4.5.2 Brief description of the simulation elements

The simulation elements represent the components used in the converter design. As previously mentioned, they can be designed or formed if they are not found in Simplorer. The components designed or formed for the simulation of the resonant push-pull converter are described below.

The PV source was modeled using a diode and a current source. The source current of the current source was set with the saturation current and the thermal voltage of the diode to model specific parameters.

MOSFETs were chosen, as MOSFETs would be used in the design of the converter, and not just generic switches. The MOSFETs were controlled by gate-drivers that were manufacturer elements, the LM5114 gate-driver. These specific gate-drivers were not used in the design but helped in the simulation. The gate-drivers were provided with control signals through basic PWM elements, which act as substitutes for the MCU control signals. The duty cycle could be adjusted for specific converter operation and dead-time could be implemented.

The transformer used in the converter was not found in the Simplorer. Therefore, a primary center-tapped converter needed to be constructed in the simulation. This was done by appending transformers. In Simplorer, primary and secondary windings exist separately and must be connected forming the transformer. These primary and secondary windings were used to create the resonant push-pull transformer. To form a center-tapped primary, two of the primary windings were connected in parallel. Each of the primary windings connected together with their associated secondary windings. The secondary windings were then connected in series to form one secondary winding. Therefore, forming a center-tapped primary winding with a single secondary winding.

The rest of the converter components like the inductors, capacitors, diodes and loads were used as generic components. The converter could be implemented to a sufficient extent in the simulation.

4.5.3 Simulated results

The converter could be observed and monitored through voltage and current plots in Simplorer to confirm the converter design given by [33]. The simulation proved satisfactory to verify the design and to proceed with the building of the converter. Control methods to regulate the converter were not implemented in the Simplorer.

Figures 4.16, 4.17 and 4.18, present the voltage across and current through the switch S1 a at duty cycle of 35 % (non-overlapping), 50 % and 65 % (overlapping) for one period. The shape of the current signals is similar to that of the discussed converter presented in [33].

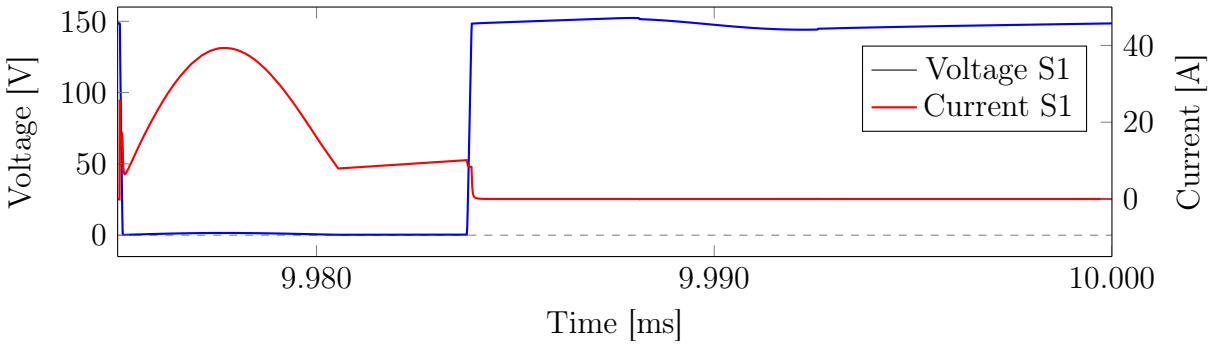

Figure 4.16: The switch current of S1 at 35 % duty cycle

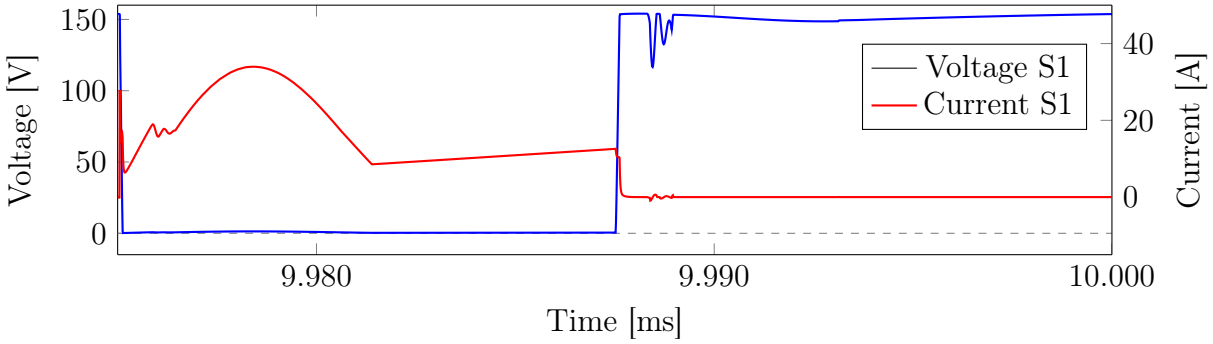

Figure 4.17: The switch current of S1 at 50 % duty cycle

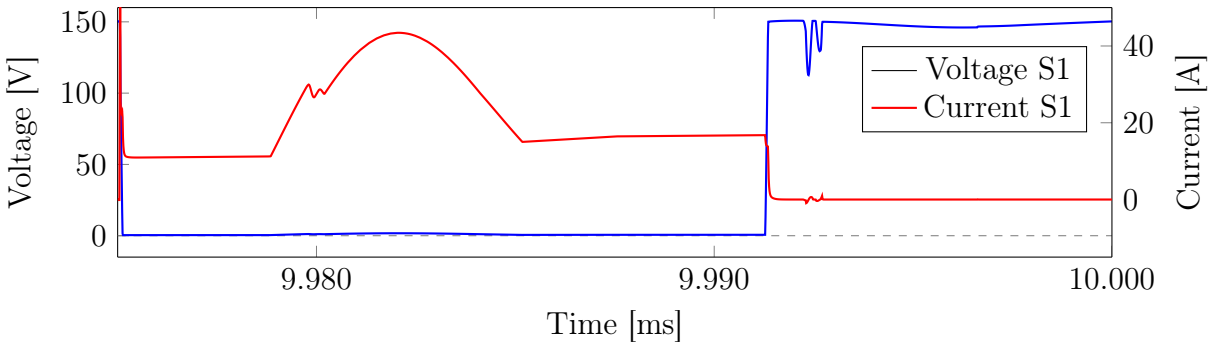

Figure 4.18: The switch current of S1 at 65 % duty cycle

Figures 4.19, 4.20 and 4.21, represent the transition from the off to on state of the switch S1 at a duty cycle of 35 %, 50 % and 65 % for one period.

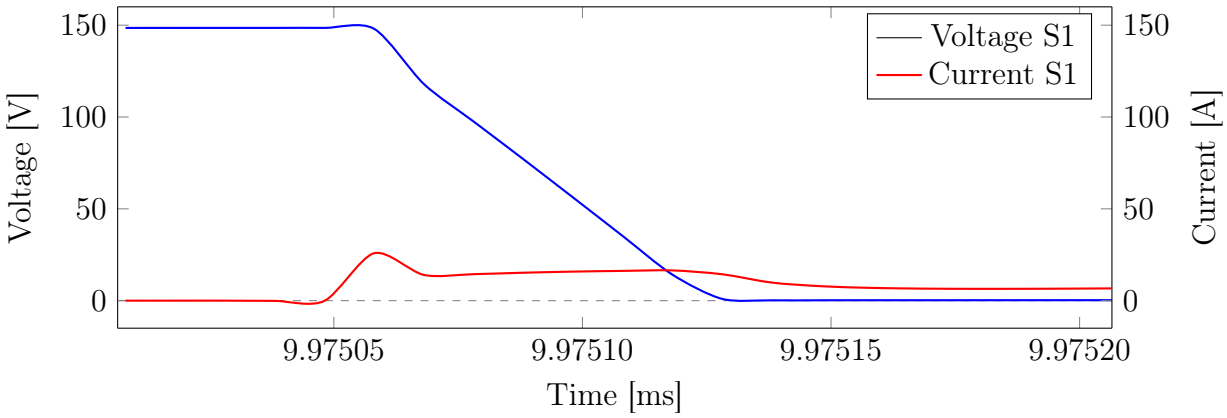

Figure 4.19: The switch current of S1 at 35 % duty cycle

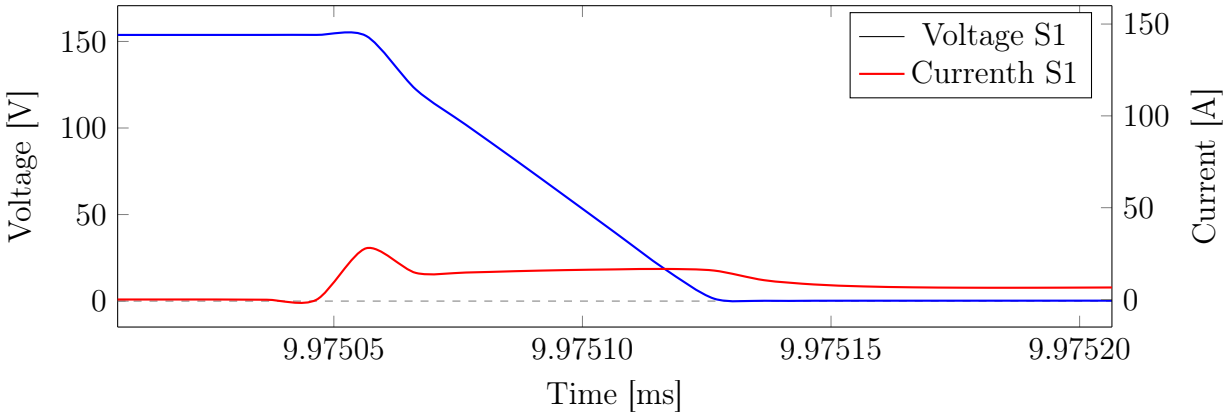

Figure 4.20: The switch current of S1 at 50 % duty cycle

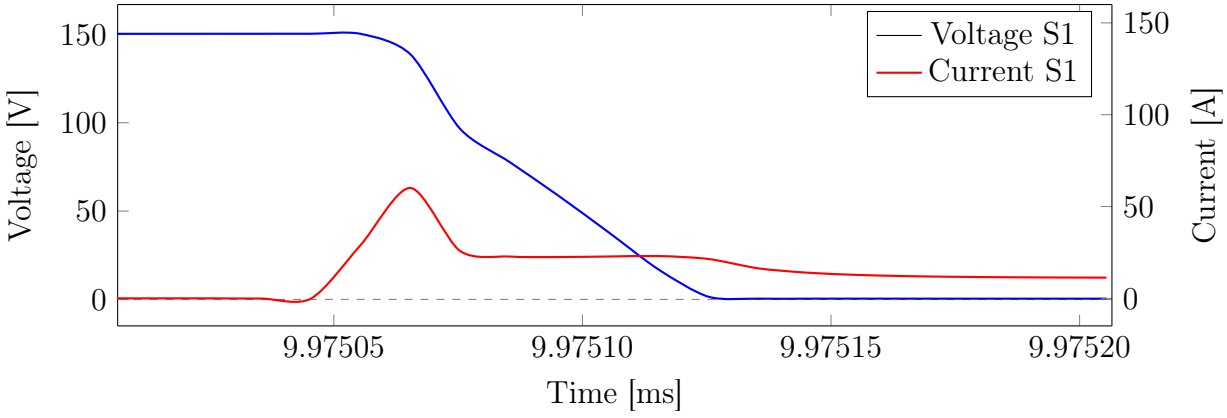

Figure 4.21: The switch current of S1 at 65 % duty cycle

Figures 4.22, 4.23 and 4.24, represent the voltage across and current through the switch S3 at a duty cycle of 35 %, 50 % and 65 % for one period. The shapes of the current signals are similar that of the discussed converter presented in [33].

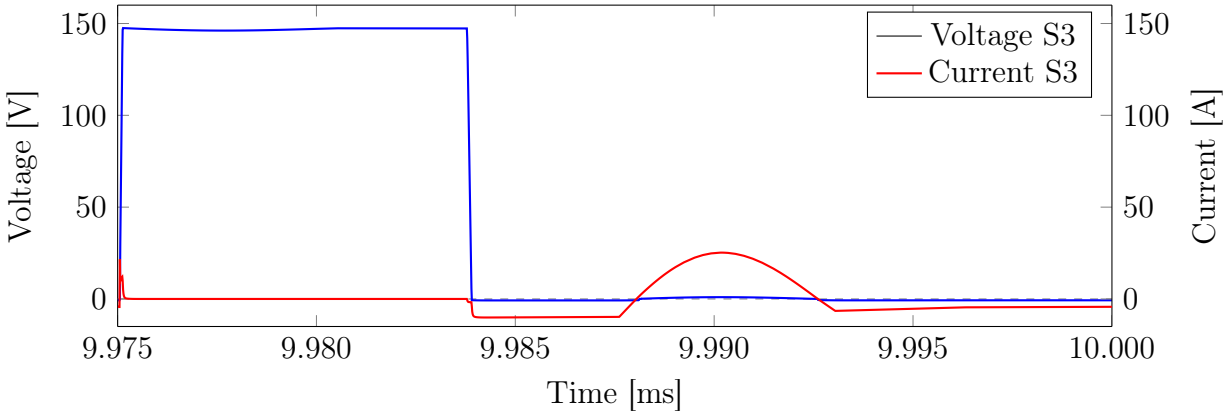

Figure 4.22: The switch current of S3 at 35 % duty cycle

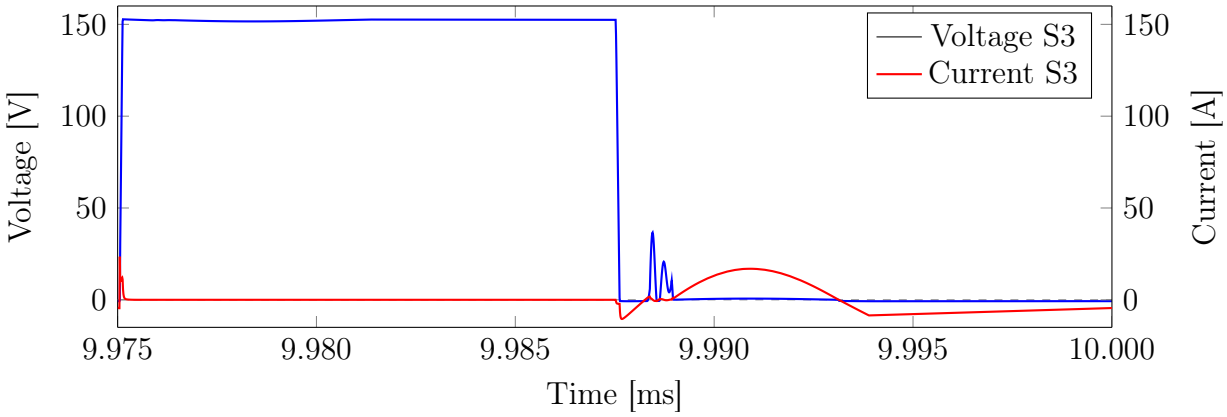

Figure 4.23: The switch current of S3 at 50 % duty cycle

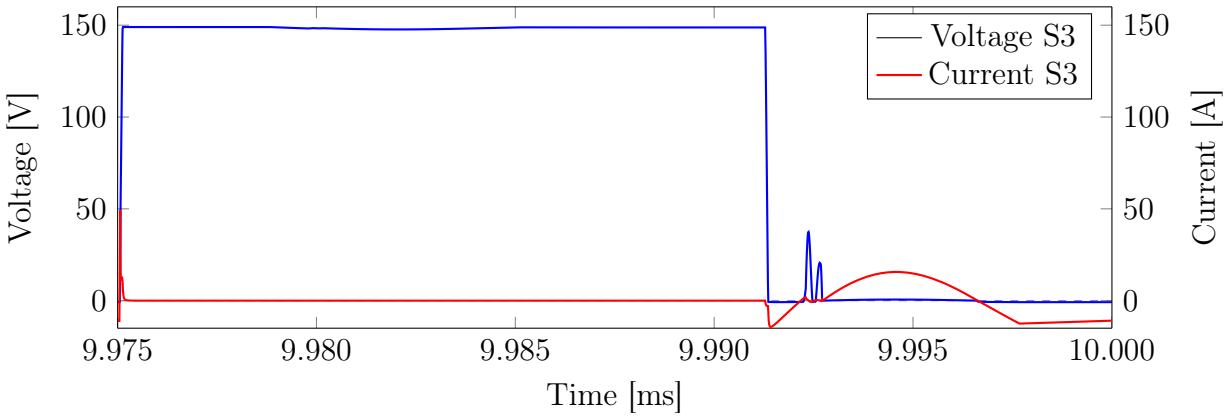

Figure 4.24: The switch current of S3 at 65 % duty cycle

Figures 4.25, 4.26 and 4.27, represent the transition from the off to on state of the switch S3 at a duty cycle of 35 %, 50 % and 65 % for one period.

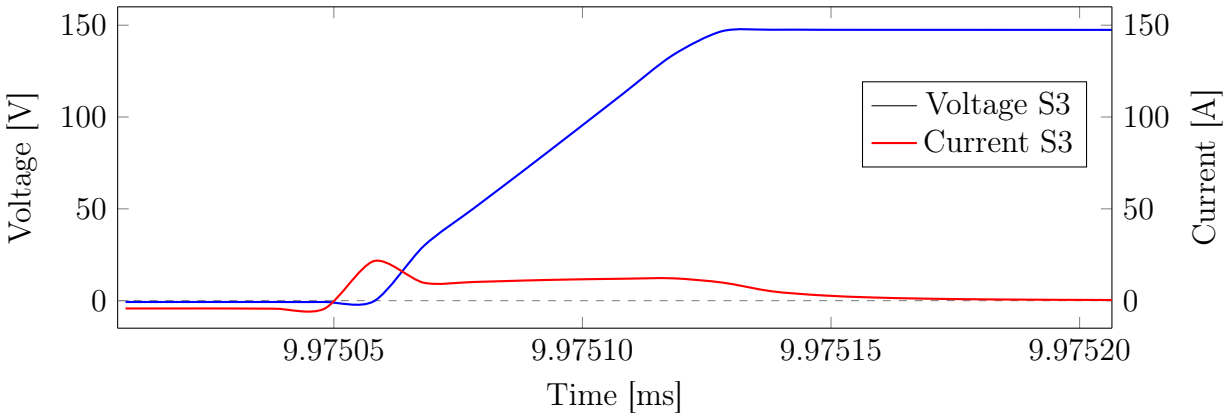

Figure 4.25: The switch current of S3 at 35 % duty cycle

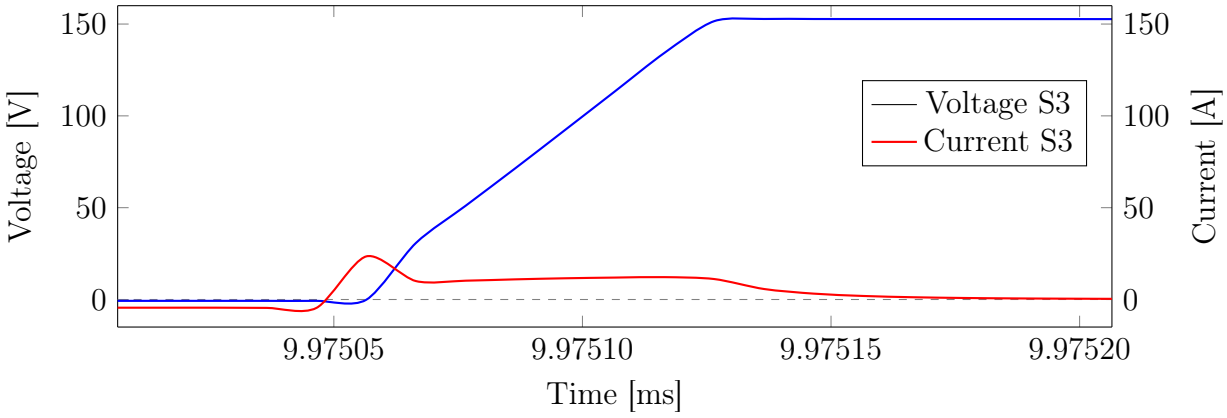

Figure 4.26: The switch current of S3 at 50 % duty cycle

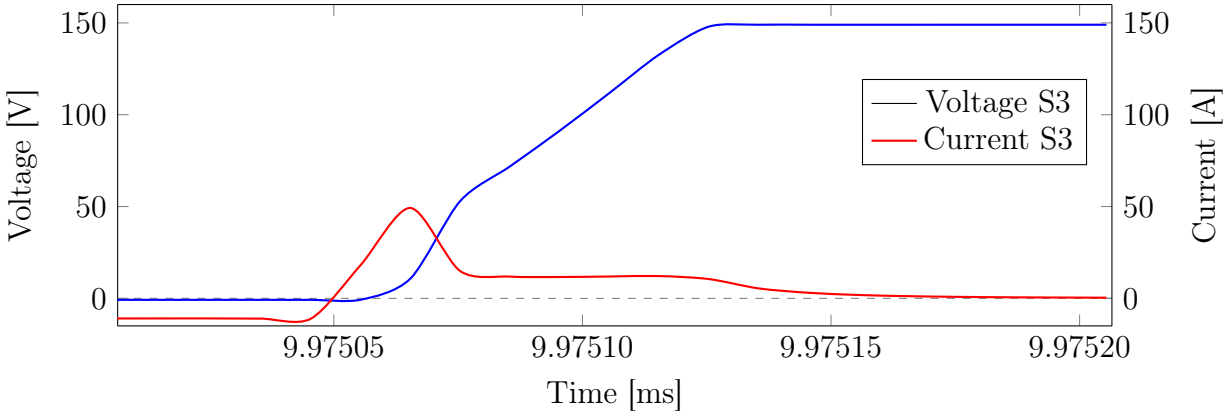

Figure 4.27: The switch current of S3 at 65 % duty cycle

4.5.4 Evaluation of simulated results

The notable characteristics regarding the simulated plots are the large magnitude of the switch currents and some of the disturbances seen in the voltage and current plots.

The switch current is a result of the output current and the ratio between the switching frequencies to the resonating frequency. This is expressed in equation 4.19. Therefore, the large switch current is accounted for.

In the plots using a duty cycle of 50 % and greater, disturbances were noted. For duty cycles less than 50 %, the disturbance was not seen or were not noticeable. The disturbances seem to correlate with the turn-on of the high-side MOSFETs after the dead-time when the low-side MOSFETs turn off.

The currents and voltages plotted in figures 4.16 to 4.18 and 4.22 to 4.24 are similar to the theoretical design waveforms in figures 4.13 and 4.8. Similarities exist in the shape of the waveforms, namely both of theoretical design and the simulation features current signals with sinusoidal nature due to resonance.

4.6 Construction of the converter

4.6.1 PCB design

After simulation of the resonant push-pull converter was constructed. The construction started with a schematic diagram layout in Altium designer leading to a PCB design. The PCB contained the converter, additional measurements circuitry and gate-driver circuitry.

Figure 4.28 shows a schematic diagram of the gate-drive circuitry. The gate-drive circuit consists of the gate-driver IC and its required components. The gate-driver IC take in two control signals from the control module and it is able to drive two MOSFET gate junctions, with complementary signals, through gate resistors. The output signal is then taken to an ADC, which is connecting to the control module.

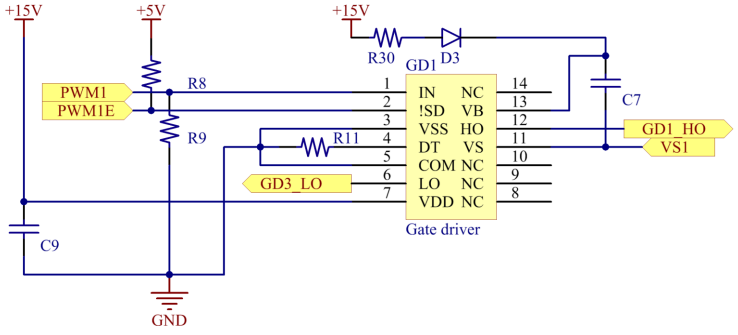

Figure 4.28: Schematic view of the gate-drive circuitry

Figure 4.29 shows a schematic diagram of the measurement circuitry on the input side. The figure on the left-side of the diagram is the voltage measurement circuitry, consisting of a voltage divider and an op-amp. It is connected to the positive input terminal. The figure on the right-side of the diagram is the current measurement circuitry, consisting of an in-amp and the gain resistance. Current is measured through a shunt resistor included in the main PCB. The two terminals of the shunt resistor are connected to the in-amp;

the measured voltage across the resistor is then used. The output signal is then taken to an ADC, which is connecting to the control module.

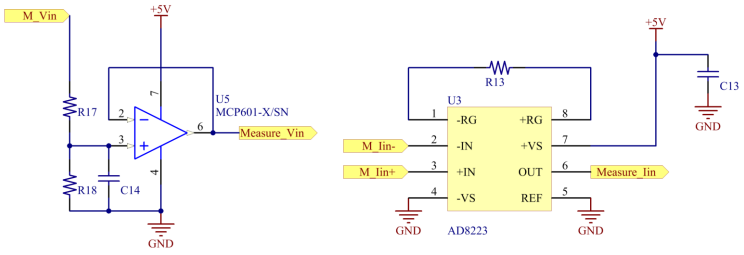

Figure 4.29: Schematic view of the measurement circuitry

The figures 4.30 and 4.31 below depict the resonant push-pull. The converter is shown as a schematic and an electronic PCB document, respectively. The gate resistors used were 51 Ω.

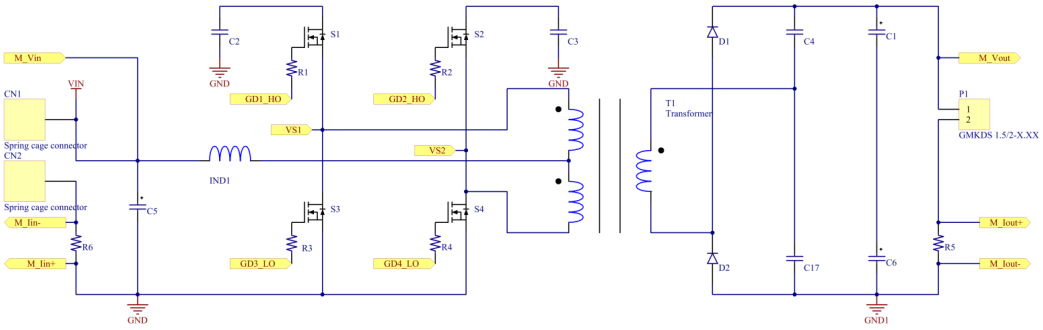

Figure 4.30: Schematic view: The resonant push-pull converter in Altium

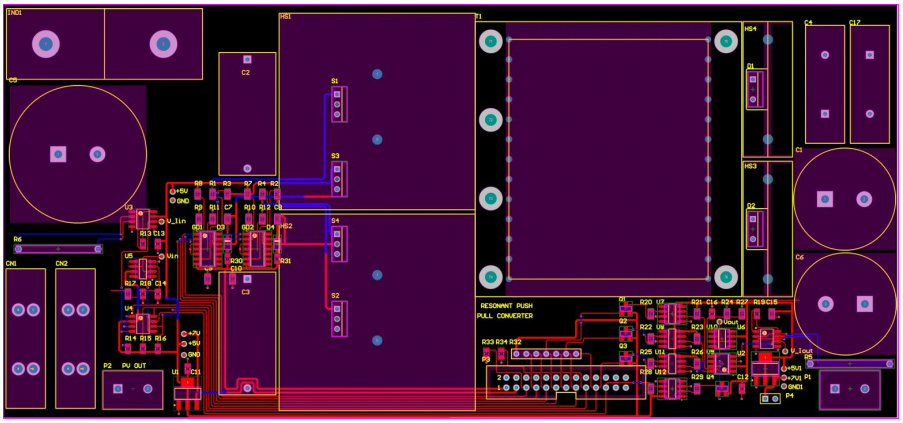

Figure 4.31: Digital view: The resonant push-pull converter in PCB Altium

4.6.2 PCB assembly (Manufacturing)

In this segment, the magnetic components designed are presented similarly to the inductor and the transformer. Furthermore, the full populated PCB of the resonant push-pull converter is presented.

Inductor

Figure 4.32 shows the inductor used in the resonant push-pull converter. An iron-powder core is used with a thick winding. The inductance was measured at 46.457 μH.

Figure 4.32: Photo: The resonant push-pull inductor

Transformer

Figure 4.33 and 4.34 show the assembly of the transformer used in the resonant push-pull converter. An E59 ferrite core was used and it was wound with litz wire. The transformer is shown with only one winding, the secondary winding, for illustration.

After assembly of the transformer, the leakage inductance was measured. The measured leakage inductance was L_{lk} =9.7 μH, which is different from the selected leakage inductance, 1 μH, for the design. The changes in leakage inductance result in a change of the maximum resonant capacitance. The maximum capacitance ensures soft switching over the entire range of switching. The resonant capacitance selected in the design section of the chapter does not have to change as it is less than the calculated maximum resonant

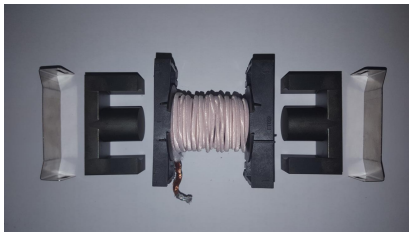

Figure 4.33: Photo: The resonant push-pull transformer with only one winding, disassembled

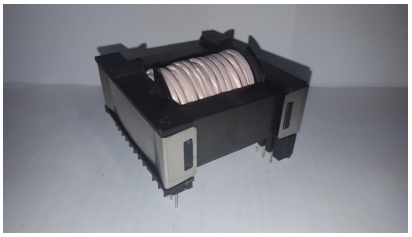

Figure 4.34: Photo: The resonant push-pull transformer with only one winding, assembled

capacitance.

Final PCB

The resonant push-pull is shown below fully populated in figures 4.35-4.39. A bottom enclosure for the PCB is included.

Figure 4.35: Top view of the resonant push-pull converter

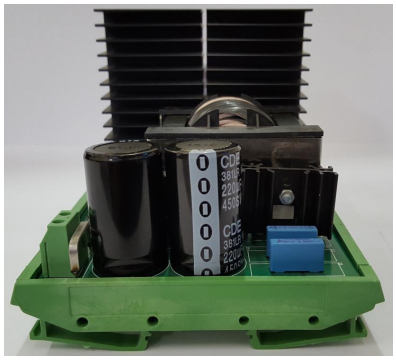

Figure 4.36: Photo: The resonant push-pull converter from the right side

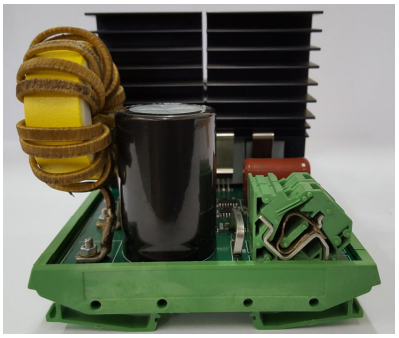

Figure 4.37: Photo: The resonant push-pull converter from the left side

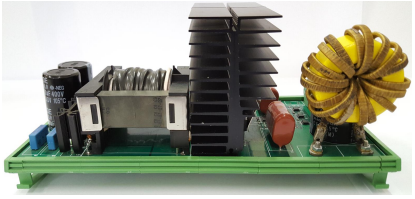

Figure 4.38: Photo: The resonant push-pull converter from the back

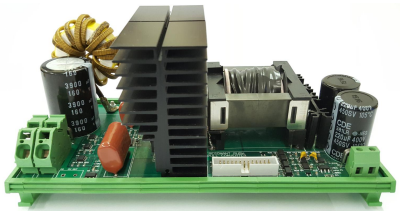

Figure 4.39: Photo: The resonant push-pull converter from the front

4.7 Results

4.7.1 Measurements

After the construction process of the converter was completed, it was tested using a controlled power supply and a solar PV input. The resonant push-pull converter was analysed after it was built, by testing it with different sources at different load; a solar PV array of up to 1500 W and controlled voltage sources. The converter was loaded with adjustable resistors. Tests were conducted to determine whether the output voltage could be achieved with various input voltages. The efficiency of the converter was tested, verifying the design from [33]. At various duty cycles, the inductor voltages and the diode voltages were measured to confirm the design. Lastly, measurements of the clamp capacitors were taken, verifying the voltage ripple. The duty cycle is varied using the MCU or control unit. The measurements were taken using the built-on measurement circuitry, processed through the MCU. Other measurement equipment like multi-meters, voltage, and current meters were also used. All mentioned measurements are presented in this concluding section of chapter 4. Moreover, Appendix B includes additional verification measurements. Figures 4.40 and 4.41 present the measured output voltages for the duty cycles ranging from D = 30 - 70 %. The designed output voltage range is confirmed, that 550 V - 600 V was achievable. The output voltages were measured using MCU.

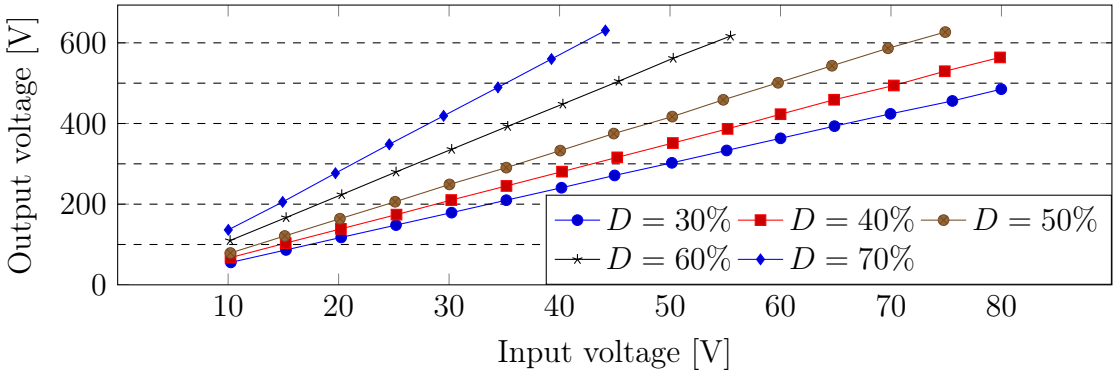

Figure 4.40: The measured output voltages against to the measured input voltages under load (less than 300 W) at various duty cycles

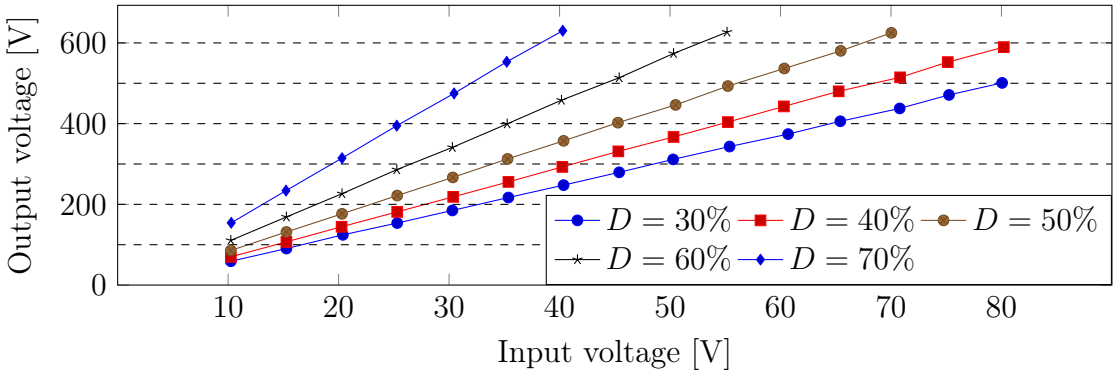

Figure 4.41: The measured output voltages against the measured input voltages under no-load at various duty cycles

In figures 4.42, 4.43 and 4.44 the output voltage measurement from the converter measurement circuitry is verified with the measurements of a multi-meter.

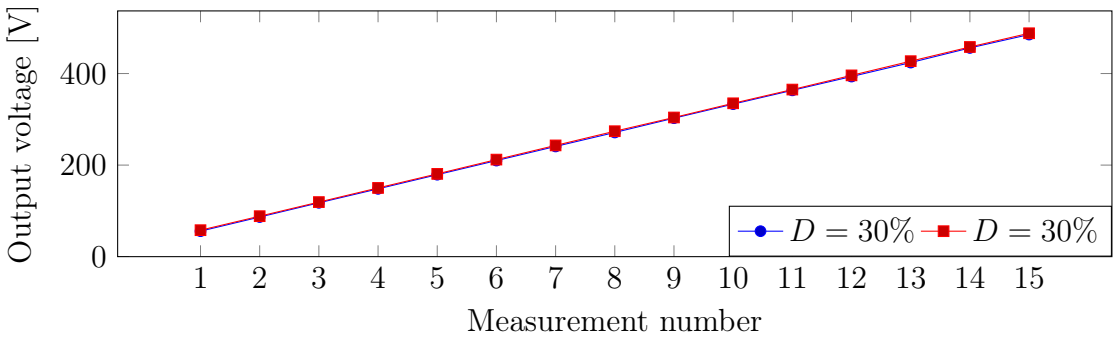

Figure 4.42: Comparison of output voltage measured from MCU and Multi-meter

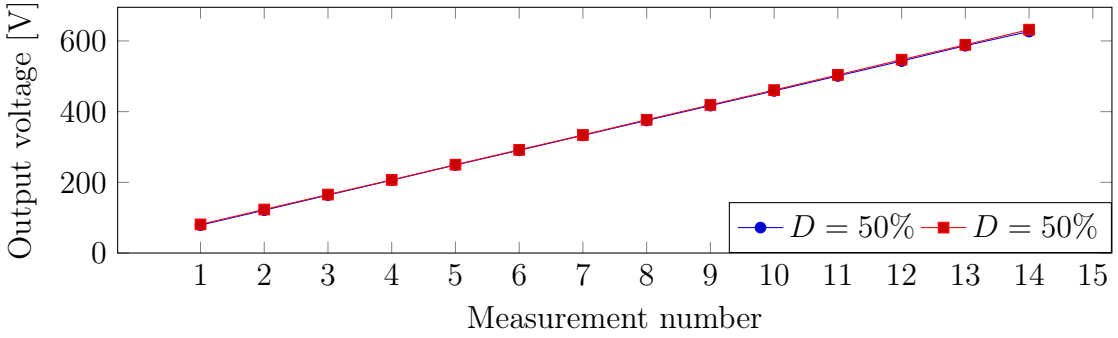

Figure 4.43: Comparison of output voltage measured from MCU and Multi-meter

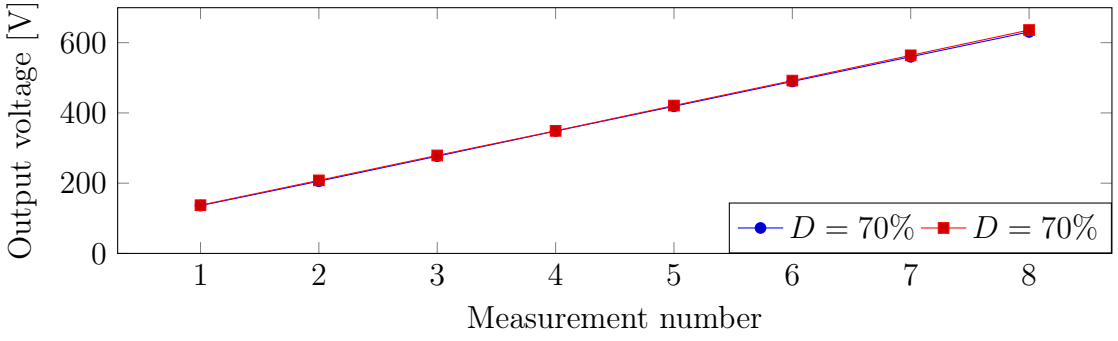

Figure 4.44: Comparison of output voltage measured from MCU and Multi-meter

In figures 4.45, 4.46 and 4.47 the input voltage measurement from the converter measurement circuitry is verified with the measurements of a multi-meter. The measurement circuitry was well calibrated.

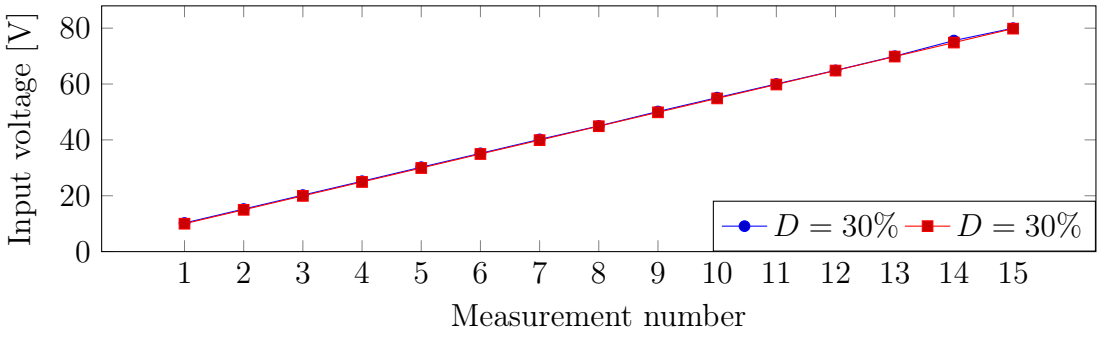

Figure 4.45: Comparison of input voltage measurements from MCU and Multi-meter

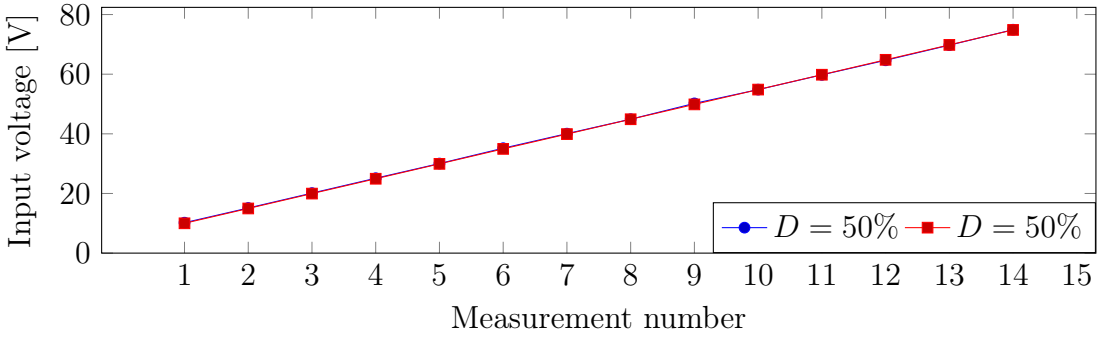

Figure 4.46: Comparison of input voltage measurements from MCU and Multi-meter

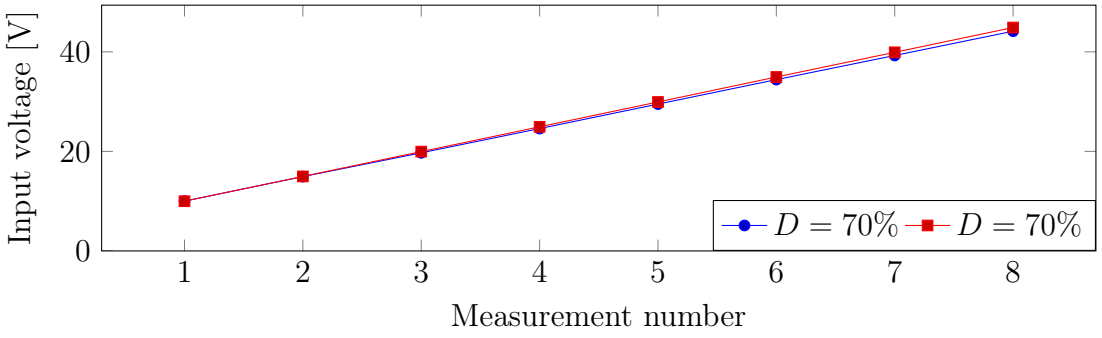

Figure 4.47: Comparison of input voltage measurements from MCU and Multi-meter

In figures 4.48, 4.49 and 4.50 the input current measurement from the converter measurement circuitry is verified with the measurements of a multi-meter. Most measurements compare well when measuring lower currents.

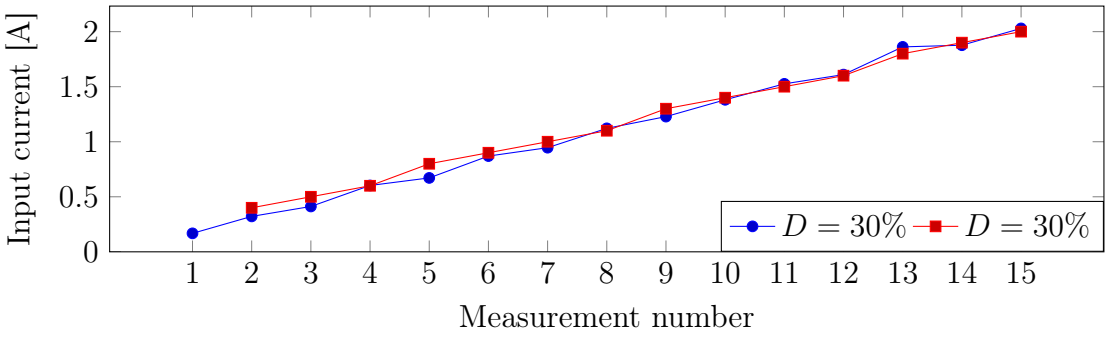

Figure 4.48: Comparison of input current measurements from MCU and Multi-meter

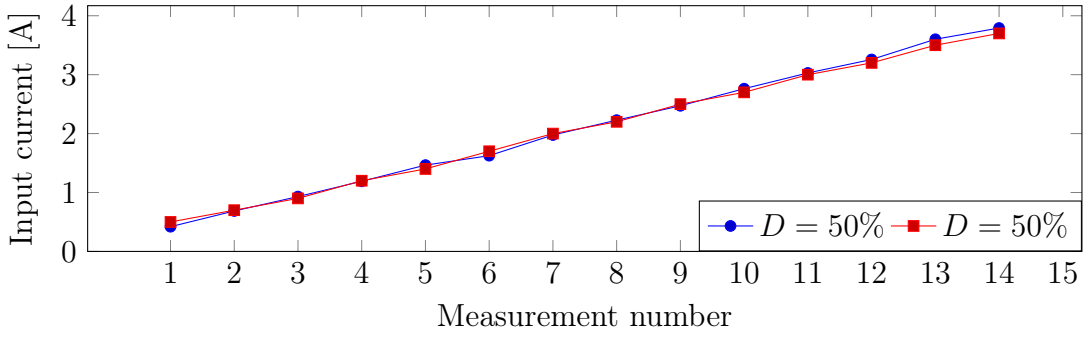

Figure 4.49: Comparison of input current measurements from MCU and Multi-meter

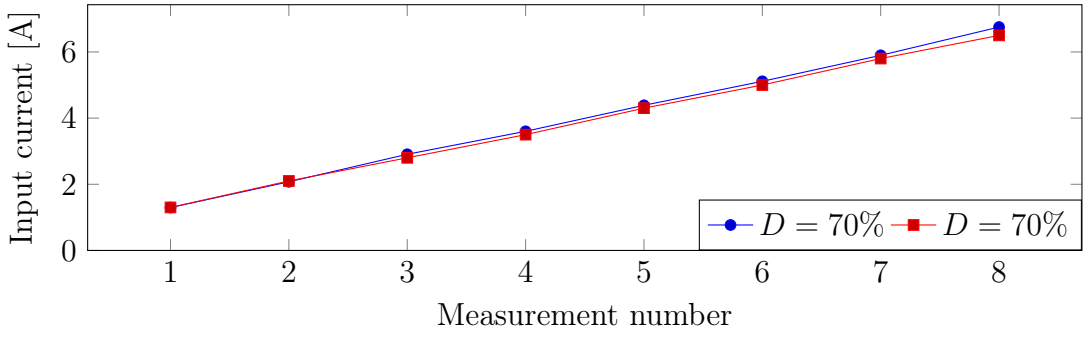

Figure 4.50: Comparison of input current measurements from MCU and Multi-meter

In figures 4.51, 4.52 and 4.53 the output current measurement from the converter measurement circuitry is verified with the measurements of a multi-meter.

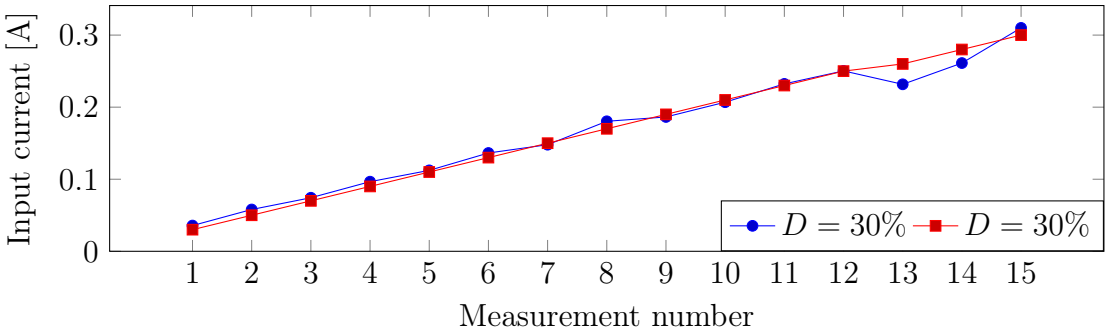

Figure 4.51: Comparison of output current measurements from MCU and Multi-meter

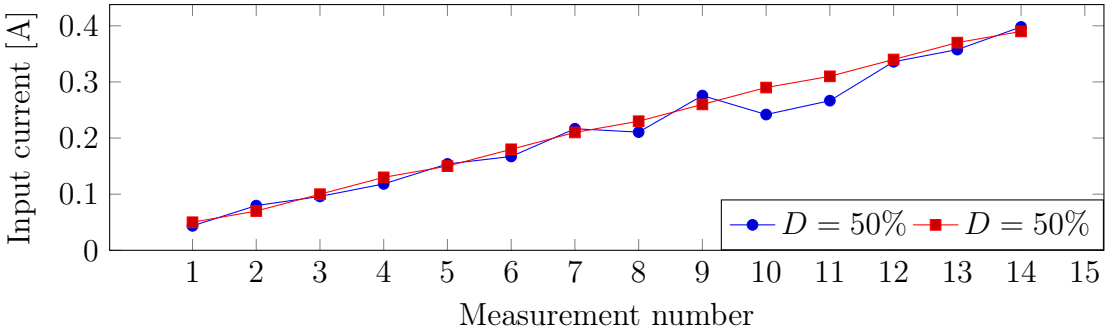

Figure 4.52: Comparison of output current measurements from MCU and Multi-meter

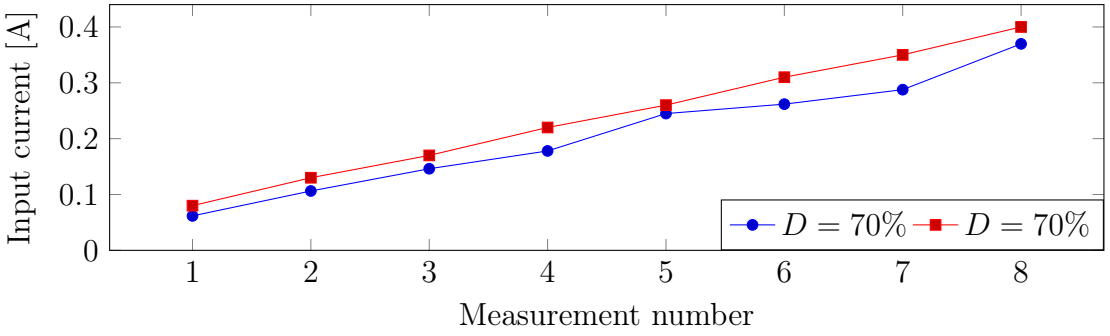

Figure 4.53: Comparison of output current measurements from MCU and Multi-meter

Figure 4.54, 4.55 and 4.56 show the measured inductor voltages at 60 V for 65, 50 and 35 % duty cycle, respectively. The measured inductor voltages correspond to the volt-second balance of the theoretical design, from figures 4.7 for 35 % and 4.12 for 65 % duty cycle.

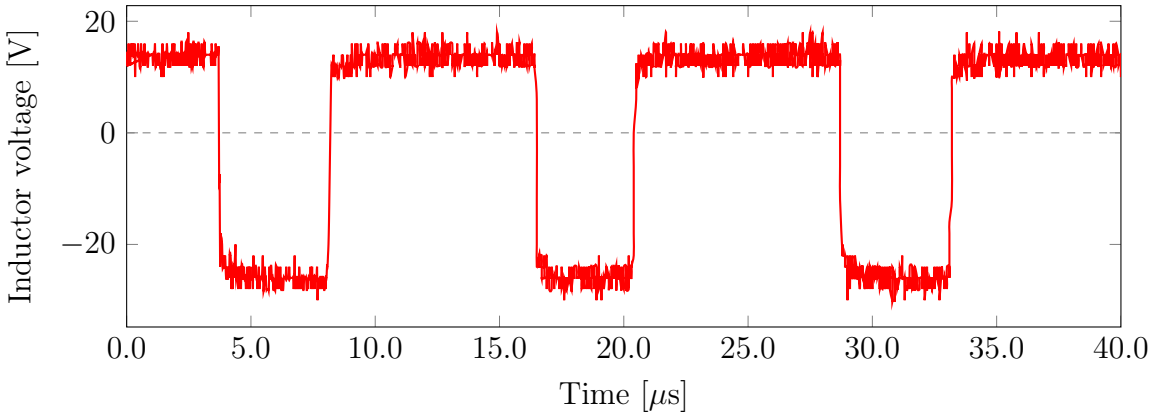

Figure 4.54: Inductor voltage: Input voltage of 60 V at 65 % duty cycle.

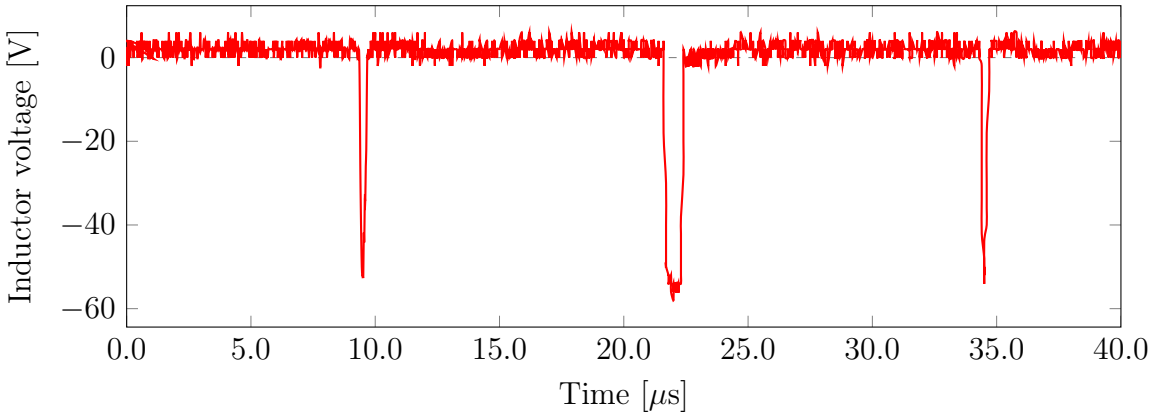

Figure 4.55: Inductor voltage: Input voltage of 60 V at 50 % duty cycle.

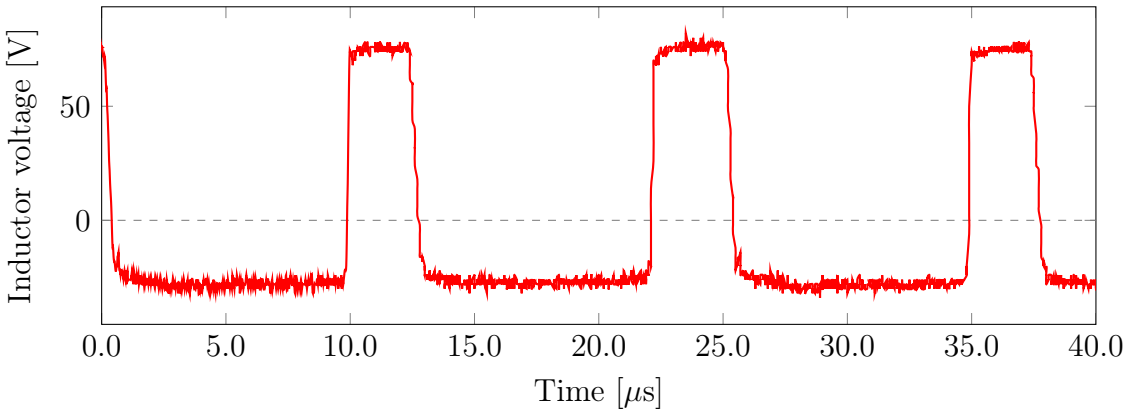

Figure 4.56: Inductor voltage: Input voltage of 60 V at 35 % duty cycle.

Figures 4.57, 4.57 and 4.57 show the voltage across the diode of the output side for 35, 50 and 65 %. These waveforms match theoretical design given by [33].

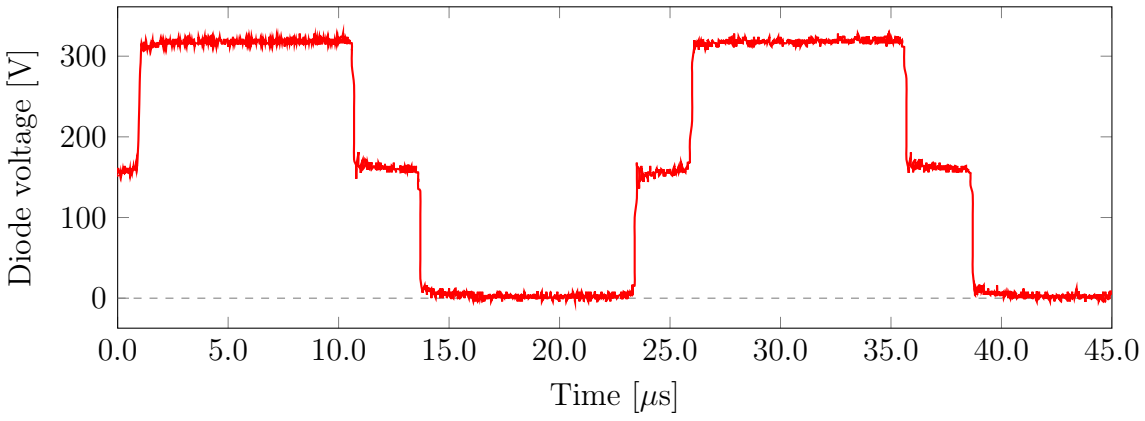

Figure 4.57: Diode voltage: Input voltage of 50 V at 35 % duty cycle.

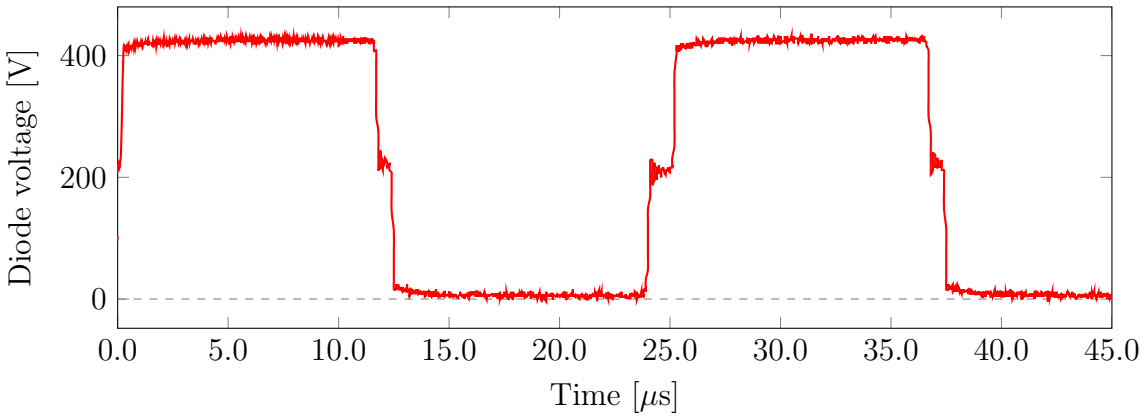

Figure 4.58: Diode voltage: Input voltage of 50 V at 50 % duty cycle.

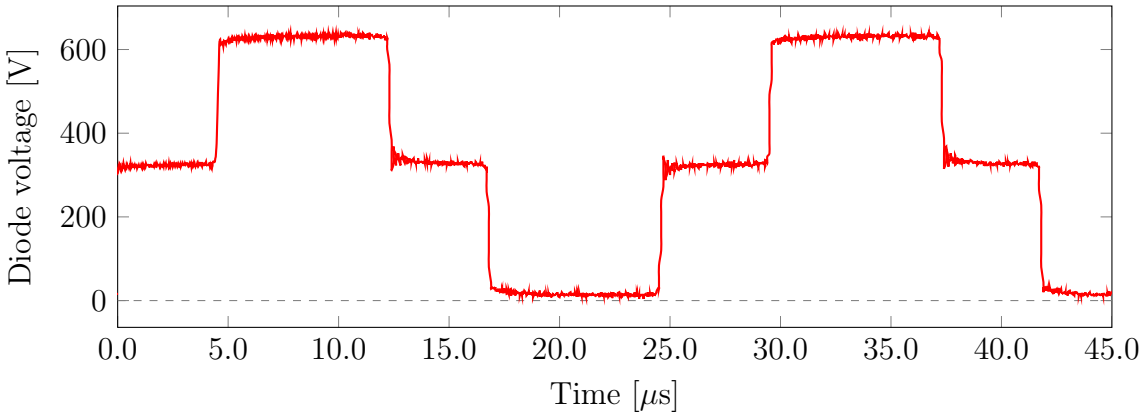

Figure 4.59: Diode voltage: Input voltage of 50 V at 65 % duty cycle.

Figures 4.60, 4.61 and 4.62 show the voltage measured at the clamp capacitor, with the voltage ripple enlarged. Figure 4.60 is from the PV source and figures 4.61 and 4.62 were from the controlled voltage source.

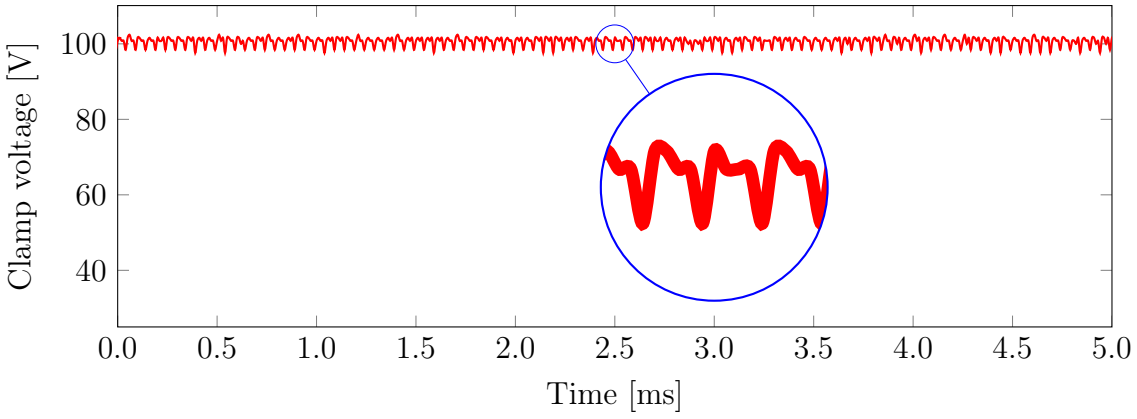

Figure 4.60: Capacitor clamp voltage: Input voltage of 55.7 V and 4.4 A from the PV source

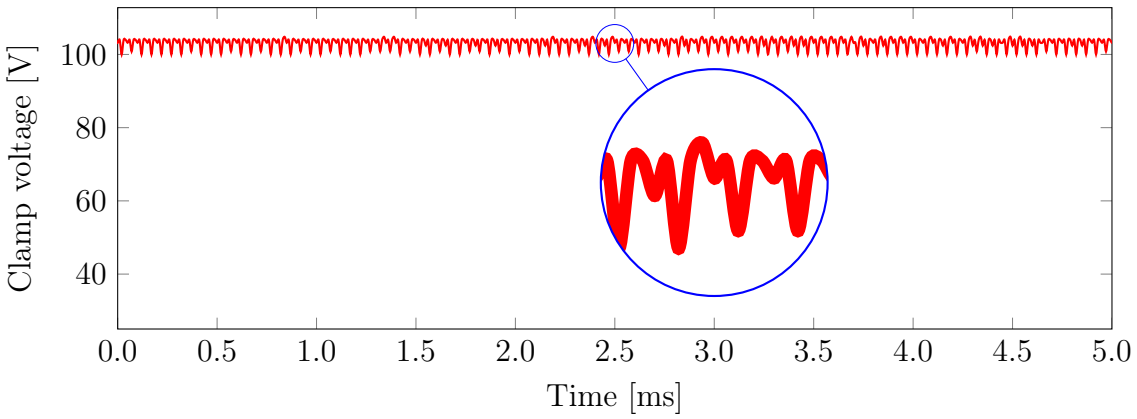

Figure 4.61: Capacitor clamp voltage: Input voltage of 60 V and 9.8 A from the Controlled source

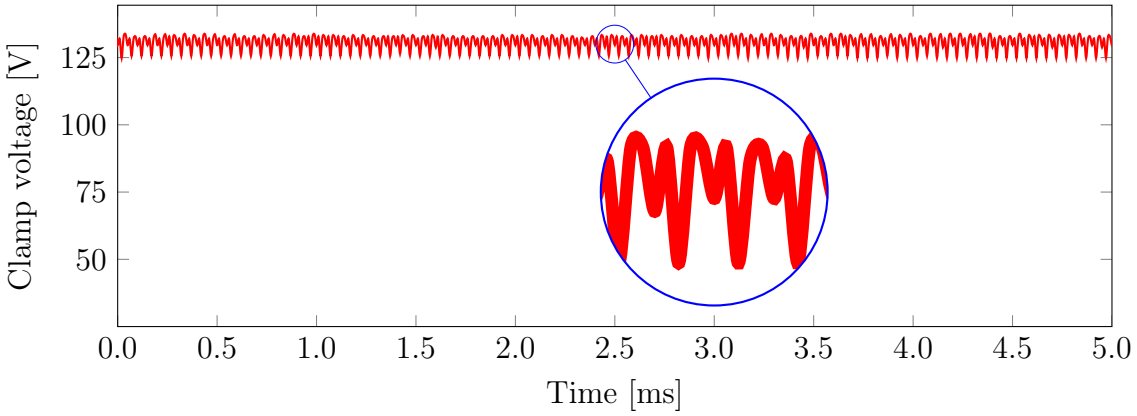

Figure 4.62: Capacitor clamp voltage : Input voltage of 80 V and 14.8 A from the Controlled source

Figure 4.63 shows the converter efficiency, using a controlled source at 50 V, 1000 W and 80V, 1500 W respectively at 550 V as constant output voltage.

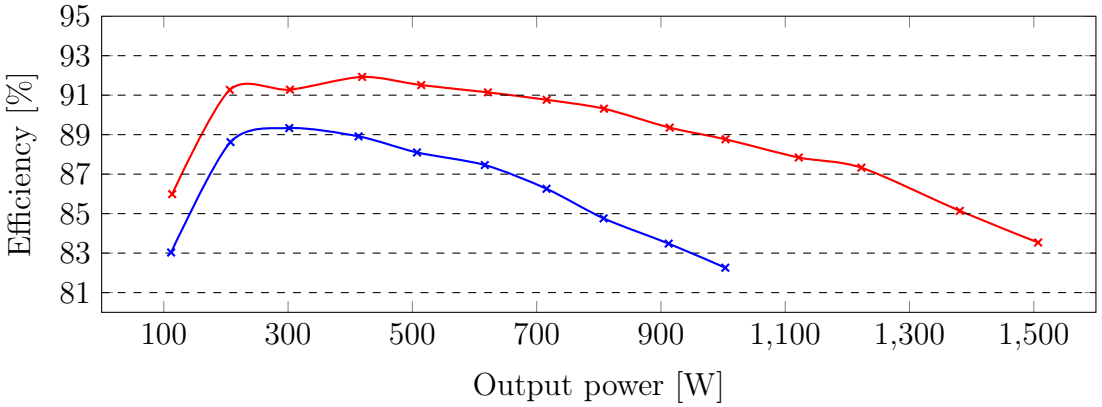

Figure 4.63: Efficiency: Measured with input voltage 80 V and 550 V output voltage and measured with input voltage 50 V and 550 V output voltage

4.7.2 Evaluation of measurements

The results of the converter efficiency were not the same as the converter efficiency presented by [33]. The minimum efficiency measured at 35 V by [33] was 95.5 % at a minimum load of 150 W, 10 % of full load. The measured efficiency of the converter built and operated for the project ranged from 85 - 91 %, measured at 80 V.

The converter used in this project incurred more loss. The losses were ascribed to an inefficient transformer design. During long operation times the MOSFETs, attached to heat-sinks, heated up substantially. Therefore, inefficient heatsink design added to losses as well. Figures 4.40 and 4.40 show that converter could elevate the input voltage to the needed output voltage, a range of 550 V to 600 V.

The inductor and diode voltages measured correspond well to the theoretical design waveforms, except at the duty cycle of 50 %. Clamp voltage ripple ranged from 4 V to 8 V which is sufficiently below 10 % of the clamp voltage. The converter results were adequate compared to the theoretical design since it was operational.

This concludes this chapter regarding the design, operation, construction, and testing of the resonant push-pull DC-DC converter. The following chapter entails the system control, in which the DC-DC converter plays a key role. The chapter focuses more on the control module used.

Chapter 5

System control

5.1 Introduction

This chapter describes the control of the energy flow from the PV source to the load and how it works, through the DC-DC converter. It does this in two main parts. The first main part is the direct control of the DC-DC converter. The second main part describes the implemented algorithms to control the VSD and the DC-DC converter, describing how the energy is managed from PV to the VSD. The communication protocols will also be shown. Figure 5.1 illustrates the interaction between the system parts and flow of energy, above the dashed line. Below the dashed line is the control module central to control of this whole process. The emphasis of this chapter will be on the shown parts, the control module, and the VSD.

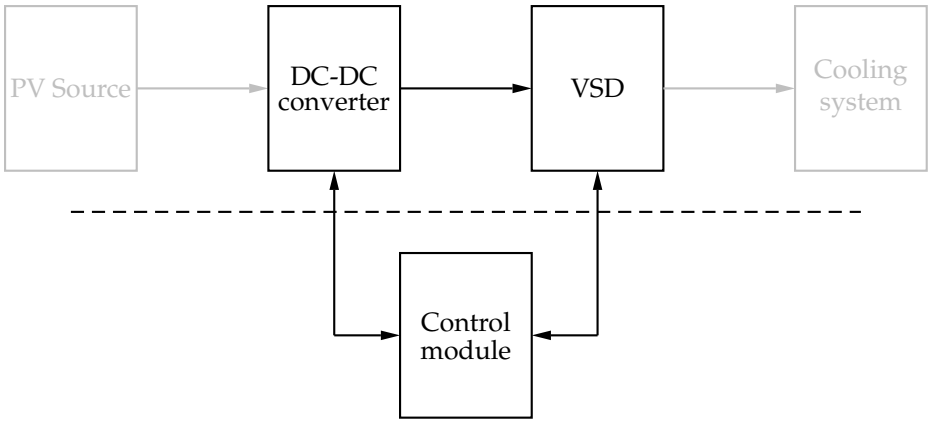

Figure 5.1: Schematic representation of the PV-drive system, indicating an interaction between subsystems.

The VSD, which the load is connected to, needs a specific voltage to operate. To power the VSD with a PV source, the voltage requirement of the VSD needs to be met. Through the DC-DC converter, the voltage requirement for the load is met from the source. The converter is an important element in the flow of energy, as it supplies the energy to power the load through the VSD with the PV source as it is required.

The specific load for this project is a cooling system. This system mainly contains a condenser, evaporator and compressor. The compressor is driven by a motor, either concealed with the compressor or openly driven by it. It is the motor that requires the

adjusted energy from the converter, which is done through a VSD. The converter, then, adjusts its output voltage to power and supply the energy as required to the VSD when it is possible. As previously stated, the VSD is connected to the motor, which then forms, part of the cooling system. Firstly, the control module will be discussed, as it is central to the control of the system and the interaction with the subsystem will be explored.

5.2 Control module

5.2.1 Control module description

The control module is a key component in the drive system, as it is central to its overall operation. It provides the control signals for the converter, takes in the measurements from the converter and processes the data. Serial communication is implemented through the control module to communicate with the VSD through MODBUS and with peripherals through SPI. All power source signals are taken in and distributed by the control module. Figure 5.2 illustrates the control module as a diagram containing the components that make up the module.

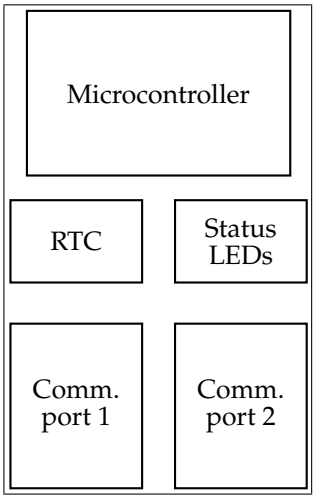

Figure 5.2: Schematic representation of the control module.

As seen from the above figure, the control module consists of a microcontroller, communication ports and a real-time clock (RTC). Of the mentioned parts, the microcontroller is the main and most important part. These parts will be discussed in this chapter. A PCB was designed and manufactured for the control module, and is shown in figure 5.3.

5.2.2 Microcontroller

The microcontroller (MCU) is a programmable electronic system that includes a microprocessor, memory, and peripherals. It is widely used in consumer products such as phones, automobiles, and household appliances to mention a few [64]. Microprocessors are very efficient implementations of digital systems [65].

MCUs have primary functions such as PWM generation, measurement monitoring of voltages, providing control signals, serial communication through universal asynchronous receiver/ transmitter (UART) and computation [40, 65].

Figure 5.3: The control module.

Using a programmable MCU has the advantages of easier system design and debugging; and allows for later additions in peripherals using the MCU for different purposes [65].

Different microcontrollers exist defined by 8-bit, 16-bit and 32-bit word sizes. The 8-bit microcontroller includes on-board memory and peripherals, it was designed for low-cost applications. For more sophisticated implementations the 16-bit microcontroller would be suitable. The 32-bit microcontroller offers very high performance for applications that are computation-intensive [65].

5.2.3 The chosen microcontroller

For this project, a microcontroller was needed to provide PWM signals for multiple channels, implementation of complex algorithms and simultaneous computation; and communication. A MCU from Atmel was chosen, namely the AT32UC3C (UC3C), which is of 32-bit AVR architecture.

The UC3C uses the AVR32UC 32-bit processor running up a maximum frequency of 66 MHz, which makes it a high processor. The processor is designed for cost-sensitive embedded applications, focused on low power consumption, high code density and performance. Incorporated on-chip is Flash and SRAM memories. This MCU was designed for industrial applications, which includes fast communication and motor control [66]. The UC3C contains the following peripherals.

5.2.4 Microcontroller peripherals

The device includes six identical 16-bit Timer/Counter channels, which can be independently set up for a function such as pulse generation and delay timing among others.

The PWM module has four channels that can operate independently or in an interlinking manner, able to be configured to specific polarities and alignments; and able to have multiple channels update at the same time. Dead-time insertion to PWM signals is possible as well [66].

The UC3C has many communication interfaces which include USART and SPI, of which are standard serial interfaces. With the USART interface including an SPI-mode. The UC3C includes ADC and DAC functionality [66].

The UC3C MCU has GPIO lines and also includes several peripheral functions, assigned to the same lines. These functions are selected through the GPIO controller, which assigns the GPIO lines to the peripheral functions [66]. The GPIO pins are able to be used for various purposes, for example in conjunction with LEDs, the GPIO pins are used to turn them on or off. This provides a possibility for status indication.

Basic elements are contained in the MCU as well, like interrupts. An interrupt signals the processor, on a specific occurrence, and forces the execution of specific code. The current position of code-execution, that is interrupted, is saved by the interrupt mechanism to be able to return to the interrupted position after completion of the specific interrupt-execution code [65].

These are some of the functions and peripherals contained by the AT32UC3C. The specific implementation using these functionals of the MCU will be discussed in the following segment.

5.2.5 Specific control capabilities

For the control of the switches, the MCU needed to provide accurate PWM signals since at least two separate signals are required. The UC3U is able to produce a 40 kHz PWM signal that has a maximum resolution range between 10 and 12 bits. Dead-time is needed for converter operation and this functionality is provided for by the UC3C. Dead-time inclusion is important because it allows for operation of multiple switches in groups and ensures that these switches do not create a connection from the source to ground, leading to failure of components.

The MCU needed to process measurements and be able to do calculations based on these measurements to make further programmed decisions. Through communication with an ADC, as an external peripheral, the UC3C is able to accomplish this. Measurement circuitry is contained on two isolated grounds, one common to the MCU and the other not. Signals are transmitted and received through isolation using opto-couplers.

These measurements were done periodically to ensure continuous control. A timer was used to initiate algorithms and measurement taking process. When the set time elapsed an interrupt was set up to trigger.

Throughout the programming of the MCU, interrupts are actually used to implement algorithms and communicate with other devices. Using interrupts means that the MCU does not need to be idle waiting for functions and operations to complete, but is able to initiate functions while the system's cycle continues until again interrupted. The reason for this is the inefficiency of busy-wait states. In this state the CPU waits and checks for a certain occurrence. With interrupts, other computations, and control algorithms can be done executed in parallel by the regular computation [65]. In this implementation,

multiple interrupts are used in conjunction with each other. Namely, a timer interrupt with two different communication interrupts.

Lastly, the RTC was used to keep track of time. This enables the MCU to implement a real-time related function, for example, the start and stop of the system at specific times.

5.2.6 PWM

The PWM signal function of the UC3C contains a setup in which its period, alignment, polarity and the duty cycle can be adjusted. Additional dead time could be added as well. This could be implemented on four channels. Some of the channels could be made synchronous as well, making it able to define channels that are similar in property. In order to change the duty cycle or nature of the signals during the operation the update mode of the PWM function is used. The converter requires four MOSFET gate-junction signals, which the UC3C is capable of providing.

Two of these signals, used for the High-side, needed to be complementary to the low-side. It was accomplished through a gate driver capable of providing this function.

Two synchronous channels for PWM were implemented to be of the same nature, but are out of phase. The two PWM signals are provided to the gate drivers as references. The gate drivers generate two pairs of signals out of phase in reference to each other and the pairs contain one high-side and low-side PWM signal. Dead-time insertion was implemented through the gate drivers, although the UC3U could provide it.

A gate-driver provides the specific voltage signals needed by the source terminal of MOSFETs needed for operation [40]. The specific gate driver used is a half bridge type called "FAN7393AMXCT-ND".

5.2.7 Measurements

The measurements were needed to fully implement regulation and power optimisation algorithms through monitoring voltage and current measurements.

Input and output voltage measurements were used for the regulation of the output voltage. Furthermore, the input and output power measurements, meaning current and voltage measurements, were used to be able to implement maximum power tracking.

These measurements are made through amplifiers and then taken through an analog to digital converter (ADC) that are then fed to the MCU for processing. For the voltage measurements, an op-amp is used with a voltage divider generating a 5 V maximum signal, since the MCU has a voltage limit on the signals it receives. Current measurements are done with in-amps, adjusting the gain of the current with external resistors and using a shunt resistor. The current measurement is, in fact, a voltage measurement across a known resistance and later computed as a current value through Ohm's law. Both these signals are then fed into ADC's, for the MCU to be able to read such signals and process them. Some measurements are done through isolation through opto-couplers since there are two separate ground planes.

5.2.8 ADC

The ADC communicates with the MCU through SPI, which is a communication protocol discussed in following section. The design of the input voltage and current measurement circuitry is presented below.

5.2.9 Current measurement circuit design

The input current of 30 A is measured through an inamp with a 5 $m\Omega$, as the following

$$V_{Shunt} = I_{in} \times R_{Shunt} = 30 \times 5 \times 10^{-3} = 0.150.$$

The Shunt resistor voltage across it is calculated as 150 mV, the gain calculated from the Inamp datasheet is the following

$$Gain = \frac{5}{150 \times 10^{-3}} = 33.3.$$

The gain is 33.3, where 5V corresponds to 150 mV which in turn corresponding to the maximum input current. According to the datasheet [67], the resistor adjusting the gain should be

$$R_G = \frac{80 \times 10^3}{G - 5} = \frac{80 \times 10^3}{33.3 - 5} = 2.8235 \times 10^3.$$

R_G is calculated as 2.8235 $k\Omega$. The output current of 25 A is measured through an inamp with a 5 $m\Omega$, as the following

$$V_{Shunt} = I_{in} \times R_{Shunt} = 2.5 \times 5 \times 10^{-3} = 0.125.$$

The Shunt resistor voltage across it is calculated as 12.5 mV, the gain calculated from the Inamp datasheet is the following

$$Gain = \frac{5}{12.5 \times 10^{-3}} = 400.$$

The gain is 400, where 5 V corresponds to 12.5 mV which in turn corresponding to the maximum input current. According to the datasheet [67], the resistor adjusting the gain should be

$$R_G = \frac{80 \times 10^3}{G - 5} = \frac{80 \times 10^3}{400 - 5} = 0.203 \times 10^3.$$

Therefore, R_G is calculated as 203 Ω.

5.2.10 Voltage measurement circuit design

Input voltage measurements, for a maximum of 5 V corresponding to 150 V input voltage, the op-amp circuit is designed as

$$5 = \frac{R_{18}}{R_{17} + R_{18}} \times 150,$$

leading to a relationship

$$R_{17} = 29R_{18}. \tag{5.1}$$

From equation 5.1 R_{18} is chosen as $R_{18} = 10$ kΩ and R_{17} is calculated as $R_{17} = 300$ kΩ. Output voltage measurements, for a maximum of 4.5 V corresponding to 600 V input voltage, the opamp circuit is designed as

$$4.5 = \frac{R_{27}}{R_{24} + R_{27}} \times 600,$$

leading to relationship

$$R_{24} = 119R_{27}. \tag{5.2}$$

From equation 5.2 R_{27} is chosen as $R_{27} = 3.9$ kΩ and R_{24} is calculated as $R_{24} = 510$ kΩ.

5.2.11 Implemented communication methods

The communication methods that were implemented are discussed before the algorithms, as they form an important part of the algorithms.

RS485 and serial peripheral interface (SPI) were the implemented methods. In order to test the converter, set up the control configurations and communicate with the VSD, a communication protocol was implemented, namely MODBUS through RS485. From a PC to the MCU, commands were sent using MODBUS for testing. Later on, after testing, the MCU was set up to control VSD through MODBUS. The measurements were received through ADC using SPI. Practically on the UC3C, interrupts were used to implement these communication methods.

Modbus is an open-source, serial digital communications for communication between devices protocol created by Modicon. There exist a few variations namely MODBUS ASCII, MODBUS remote terminal unit (RTU) and MODBUS TCP/IP. The common type used is RTU, which has binary encoding and error checking, the cyclic redundancy check (CRC). Operating with only one master device, other slave devices are connected in a daisy chain method, as illustrated below in figure 5.4.

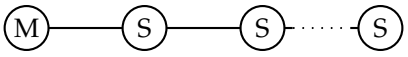

Figure 5.4: Daisy chain connection of master and slave devices

MODBUS RTU was used for implementation and will be regarded as MODBUS further in this chapter. Using the MODBUS protocol holds advantages such as accuracy of communication, the use of open source and the ease of the addition of more devices to communicate with. This makes the protocol widely accepted. MODBUS does have limitations to the number of devices that could be added or used together and has a complex setup. The amount of slave that is possible to be connected with unique IDs is 248 devices, over a distance of 1200 m.

The speed of communication is a Baud rate of 9600 b/s, this is accomplished using the baud rate generator contained in the UC3C. MODBUS has a specific data format made out of the ID of the device, the function that is to be accomplished, the data register's address, the actual data that needs to be used in the function and the CRC bytes. Figure 5.5 contains the structure of MODBUS RTU message.

Figure 5.5: The basic MODBUS RTU message structure

The medium or method of communication through which Modbus was implemented is RS485. It is a common method among industrial devices, a serial communication protocol requiring a clock, receive and transmitter line (Half-duplex). The master device requests information from the slave devices, which transmit information on request.

In addition to MODBUS through RS485, SPI was aslo implemented. SPI systems consist of two data-lines and two control-lines for information transfer. The measurements were transferred using SPI, the information is transferred from the ADC to the MCU.

As the communication methods are now established, the algorithms implemented for energy flow are presented in the following section.

5.3 Energy flow algorithm concepts

5.3.1 Voltage regulation

From the PV source, the load will be supplied through the DC-DC converter and the VSD. The whole operation is controlled by the control module. Since the VSD require a specific operating voltage for it to be on, its specific voltage requirement must be met. Therefore the VSD must be supplied at the required voltage for the VSD to be on and operate. This is a high priority criterion. Only with the voltage conditions of the VSD for operation met further control be implemented regarding input power and output load adjustments.

5.3.2 Input power control

Through the DC-DC converter maximum input power point tracking is done. Load adjustments are made by controlling the output speed of the VSD. These are the three main components that make up the control algorithm implemented focussing on voltage regulation, thereafter, maximum power point tracking and speed control.

This means that input power and output load control is done within the confines of the operating voltage range of the VSD.

The VSD operation and the PV array operating point are related, as any load change has an impact on the source supplying the load. By adjusting the load, the operating point of the source will be adjusted as well. This is the principle of operation when load changes are done without a DC-DC converter, the PV source is directly effected. In the case where a DC-DC converter is used, which is used in this case, this principle cannot be the foundation of the control algorithm as the operating point change on the PV source is indirectly effected by the load change. The PV source is only directly effected by the DC-DC converter.

The DC-DC converter sits between the load and the source. It handles much of the speed adjustment by adjusting the duty cycle for maximum power point tracking. This means that the speed change will not be seen directly by the PV source as an operating point change because the DC-DC converter would compensate for the speed adjustment through a change in duty cycle. This change in duty cycle forces the change in the power point of the PV panel.

5.3.3 Output speed control

As the changes in speed and duty cycle are made, the power changes accordingly. The input parameters are used for the tracking of the power point. For speed adjustments, the output voltage of the converter is used as a measure of energy change. It is used as an indicator of energy change as the implemented speed relates to a certain magnitude of energy.

With the output voltage present, the capacitor charges and a voltage is built up as the input source provides sufficient energy. Without any load, the capacitor voltage will

remain regulated by the control algorithm, but with a load applied, exceeding the energy supply, the capacitor voltage (charge) will decrease.

The voltage (charge) decreases as energy is now being extracted from the capacitor, exceeding the input source energy supply. With the source providing sufficient energy this decrease in charge by the load and increase in charge by the supply will not result in the voltage across the capacitor decreasing. The voltage across the capacitor will only decrease when the supply of energy is insufficient compared to the decrease rate in energy. The voltage is able to be used as an indicator of the power level change.

As the aim is to operate at the maximum power point for the highest speed possible that the input power allows, the speed is increased as long as the output voltage is above a certain lower limit. When this lower limit is reached and surpassed, the speed is decreased to remain within an operational voltage range. The speed limit is then known, but will be continuously tried to be exceeded as the PV panels may be able to supply the output load at another time. This is definitely the case leading up to solar noon.

5.4 Order of the algorithm

5.4.1 Outline of operation and modes

This section explains the function of the operational modes, their need, cause, how they are used and their order. Hereafter follows the basic outline of the control.

The control for the drive system's operation is executed using interrupts and the main control loop. Interrupts are used to execute time based control processes able to initialise and start up the drive system. After a valid start condition has been reached flags are set using interrupts. The flags are used for execution in the main loop regarding the MPPT and VSD control.

The interrupt loop control includes voltages regulation and the setting of flags for control execution in the main control loop. This control consists of several modes namely the no-operation mode, the voltage control mode and load control. All the flags for these modes are set using interrupts. The no-operation mode is discussed first.

5.4.2 No-operation mode

In the no-operation mode (mode 0) the input voltage is verified, looking at whether a valid input voltage is measured. This is done by comparing the input voltage with a pre-set threshold voltage limit. The input voltage needs to be measured greater than the threshold voltage limit for 5 seconds, consecutively, then the mode of operation can change to the next one. Otherwise, the mode of operation remains the same, mode 0, until the valid input condition is met. Failure in meeting the valid input condition results in an idle state in order to start testing for this condition again. Successfully meeting this input voltage threshold condition moves the control process along to the voltage control mode.

5.4.3 Voltage control mode

The voltage control mode consists of voltage increase and regulation. Control decisions are made, every 20 ms, to initially increase the output voltage from 0 V to 550 V. This is done by increasing the duty cycle and is marked as mode 1. Thereafter, once this voltage

level is reached mode 2 is entered concluding voltage increase only based on an upper limit. In mode 2 the output voltage is monitored to be at a maximum of 550 V and if exceeded the output voltage is decreased by decreasing the duty cycle until it is less than 550 V. The mode 3 is then entered if the output voltage is then decreased below 550 V or was measured lower than 550 V in mode 2. Therefore regulating the output voltage. In mode 2 the VSD is turned on/being turned on as well.

5.4.4 MPPT mode

In mode 3, MPPT decisions are able to be made provided the output voltage is measured below 550 V, otherwise, mode 2 is entered again to reduce the output voltage. These MPPT decisions' flags are only set in these modes, 2 and 3. The MPPT execution is not done in the same place. This is the same for the speed load control, only flags are set in the interrupts.

Flags for the load control are set every 200 ms. The VSD flag is set as active, meaning that decisions can be executed in the main loop, when the interrupt control mode 3 is still active. When the VSD flag is set as active to control the load, the MPPT flag is cleared. This is done to ensure that transients are settled after a load-control decision was made and executing the next MPPT decision a cycle later. Both the VSD and MPPT flags are cleared when mode 3 is not active.

The actual execution of these decisions is done in the main control loop. In the main loop, the MPPT flag is checked whether it is active. In the cleared MPPT state no execution is done. In the active MPPT state, a condition for the first perturbation is firstly tested for. When the first perturbation has not been done, the duty cycle is increased. This is then the first perturbation.

Thereafter the duty cycle is increased or decreased based on the previous input power and the current input power. This is done after the first perturbation. These two power measurements are compared and decisions are executed based on the outcome of the comparison. The aim is to use these two parameters to adjust the duty cycle for maximum power input from the PV panels.

Two methods have been investigated: One method uses the direction of change from the first perturbation; in this case, the duty cycle was increased at first which indicates the direction of change. The power was then measured and the PV panels' operating point is adjusted in the same direction for increasing power and when a decrease in power is measured the direction of change is reversed.

The other method uses current and previous input power and voltage measurements to determine direction of duty cycle change. Firstly, the powers are compared and thereafter the voltages are compared to decide whether the duty cycle will be increased or decreased.

Both methods are perturb and observe methods. The method only using power measurements was employed.

5.4.5 VSD mode

No execution of control is made when the VSD flag is cleared. When the VSD flag is set as active in the main loop, load decisions are executed. Conditions are checked to see whether the VSD is on, and if not it is turned on.

Thereafter, the output voltage is measured. For an output voltage greater than 530 V a decision to increase the speed of the load is executed. For an output voltage, less than 530 V, a decision to decrease the speed of the load is executed. The decrease or

increase in speed execution has varying speed increments and decrements depending on the current speed.

A state can be entered where the load is tries to extract too much power, so much that the power can no longer be supplied by the input PV array. In such a state, the output voltage will decrease as the output capacitor is being discharged faster than it is being charged. This is the reason why larger decremented speed adjustments are made, at higher speeds, to ensure that the capacitor energy is not depleted faster than the energy is supplied, hence ensuring the output voltage is not decreasing too fast.

The table 5.1 below indicates the speed increment in terms of the speed range, expressed in frequency.

Table 5.1: Speed adjustments for different speed ranges

Frequency range	Frequency adjustment
0 - 5 Hz	0.5 Hz
5 - 10 Hz	0.5 Hz
10 - 25 Hz	0.2 Hz
25 - 50 Hz	0.1 Hz

The table 5.2 below indicates the speed decrement in terms of the speed range, expressed in frequency.

Table 5.2: Speed adjustments for different speed ranges

Frequency range	Frequency adjustment
0 - 5 Hz	0.1 Hz
5 - 10 Hz	0.5 Hz
10 - 25 Hz	0.5 Hz
25 - 50 Hz	1 Hz

The reason for the varying adjustments of speed is the power dissipated by the load differs non-linearly at different speeds because the torque load profile is variable. This means that for higher speeds more power will be dissipated than lower speeds for the same speed adjustment.

5.4.6 Speed and duty cycle control integration

While the VSD is still off, the DC-DC converter is used to set the operating point of the PV array at the required output voltage. This must be done to power the VSD. Once the VSD is operating, both the DC-DC converter and the VSD can be used to implement control. The DC-DC converter changes the operating point directly by adjusting the duty cycle and the VSD indirectly changes the operating point by adjusting the speed it applies to the load as the duty cycle adjustments are made in reaction to the speed changed. The speed changes occur 10 times slower than that of the duty cycle changes. The control module is used to execute these control processes and guides the integration.

Both of these sub-systems have to work together in extracting the most power from the array, through the implemented algorithms. The DC-DC converter makes sure the operating point leans toward the maximum operating power point of the PV array. The

VSD control the makes sure that the applied speed is increased as long as the PV array is able to supply, otherwise the applied speed is decreased.

This is then the exchange of the adjustments by the DC-DC converter and the VSD. Both of the subsystems work together to operate at the MPP for that specific moment of the day, supplying the most power available to the load, controlled by the control module.

5.4.7 Flow diagrams

The flow diagrams graphically represent the control algorithms and were used to implement these algorithms on the control module. A visualisation of the control process is constructed, through these flow diagrams, to know exactly what will happen when. Numerous functions are implemented in the timer-interrupt and some in the main control loop; this is indicated for the specific function.

Due to the size of the diagrams, some of the flow diagrams were split in half. The full flow diagrams can be found in Appendix F.

The setup of the drive system and integration of subsystems must be noted as well as what action and effect the control has on others subsystems. This system and subsystem will be referred through the explanation of the flow diagrams. Figure 5.6 illustrates the verification process implemented when starting the system.

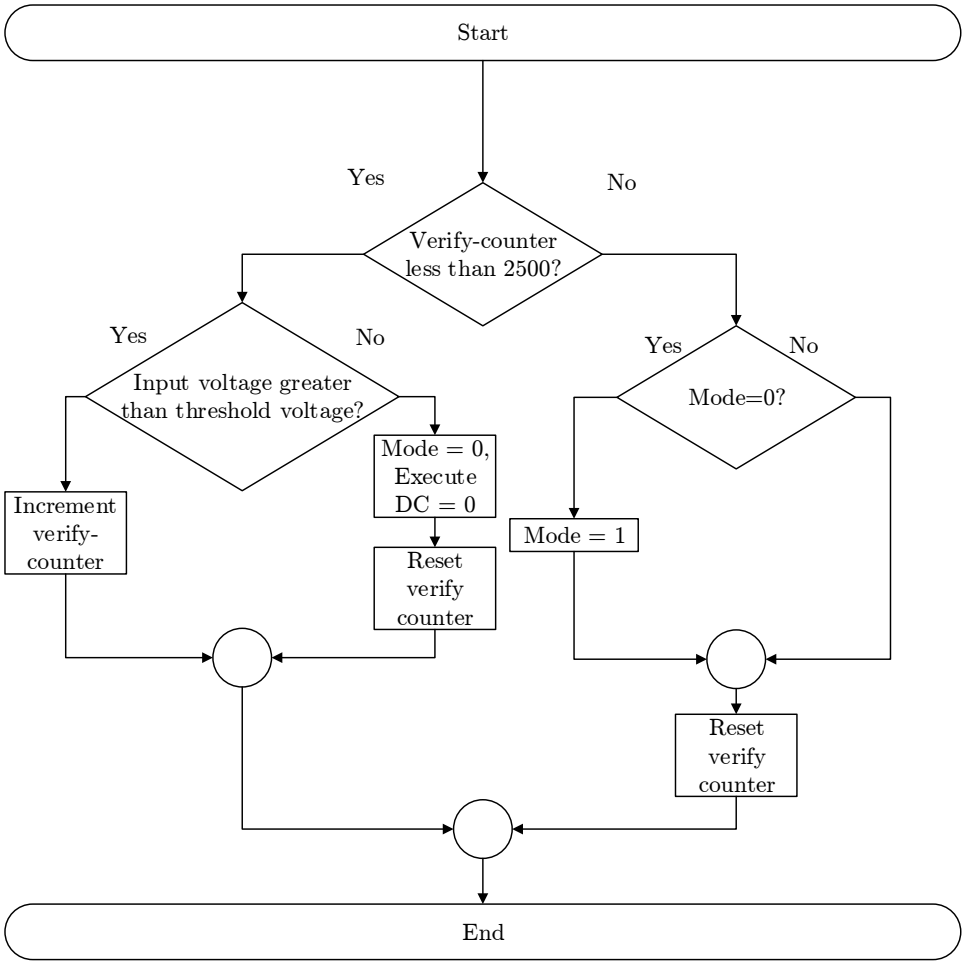

Figure 5.6: Control loop: Verification of input voltage.

The duty cycle is at 0, thus the output is at 0 V. This process was implemented in the timer-interrupt and is triggered periodically. The input voltage is periodically monitored and when it surpasses the set threshold voltage magnitude for a set time the verification is considered successful. After the set time of 5 seconds, wherein verification is continued, the control sequence is continued and the next phase of the sequence is entered. If at any time the input voltage is measured as less than the set threshold voltage, the verification process is restarted: the mode, verification counter used and the duty cycle is set to zero. This part of the control sequence was denoted as mode 0, the verification part.

The verification of the input voltage is important as the PV array voltage is so quickly changed. This is especially the case at sunrise and sunset. Furthermore, an input voltage not satisfactory for operation occurs during the day when weather conditions are cloudy. The verification ensures that operation continues when the weather conditions are adequate.

After the verification part of the control sequence, establishing that the input voltage is stable, voltage control of the output voltage is done. Voltage control is done every 20 ms, having the variables used for the control updated at the same time. Three voltage control modes were constructed as part of the control sequence, each having a purpose. The output voltage limit at which the drive system was controlled by these voltage control modes was 550 V. These modes are implemented in the timer interrupt.

The voltage control mode 1 was used for the sole purpose of increasing the output voltage through the linear increase of the duty cycle of the DC-DC converter. When the duty cycle was increased enough, resulting in an output voltage of 550 V, mode 1 was successful and not continued.

As 550 V is then present from the DC-DC converter output and feeding the VSD, the VSD will switch on and will be powered, but will be idling as no control commands were sent yet. The figure 5.7 shows the flow diagram for the voltage control part one of the control sequence after the verification process.

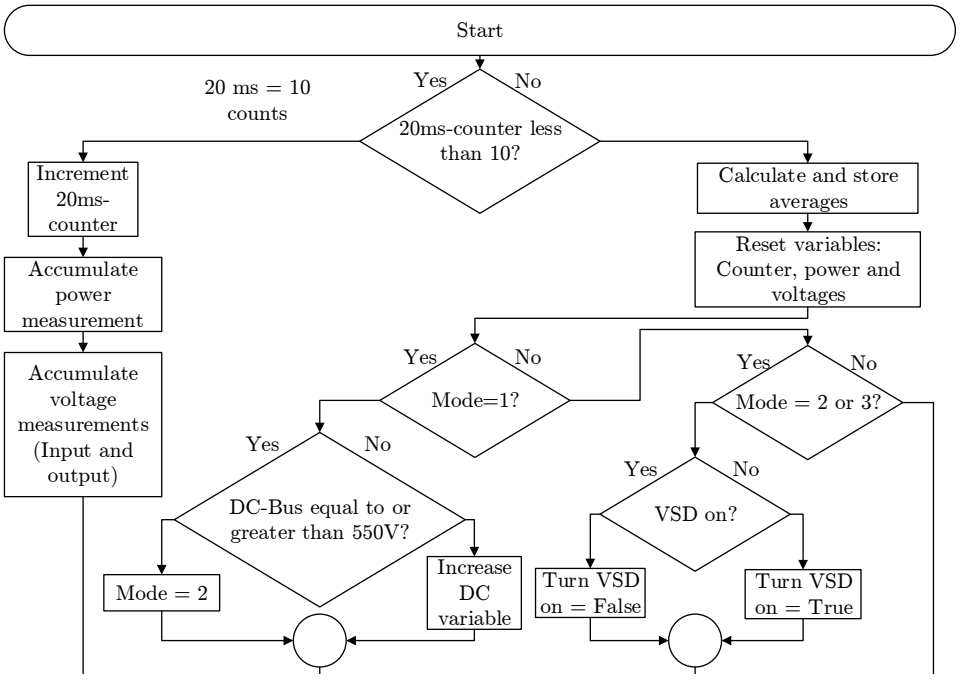

Figure 5.7: Control loop: Voltage control (Part 1).

The control sequence was then ready to proceed with the second and third voltage modes, at this stage the VSD was turned on if it was not already on. These modes were used in conjunction with each other to keep the output voltage at 550 V.

The voltage control mode 2 was used lower the output voltage if it was measured to exceed the limit of 550 V by decreasing duty cycle. When the output voltage was measured less than 550 V voltage control mode 3 was entered. The figure 5.8 shows the flow diagram for the voltage control part two of the control sequence after the verification process.

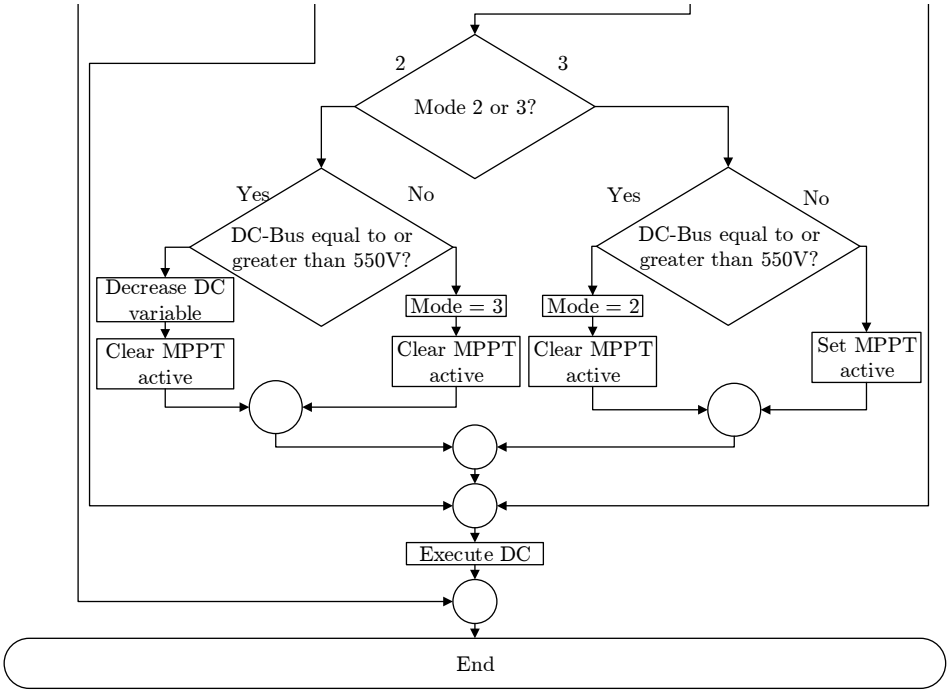

Figure 5.8: Control loop: Voltage control (Part 2).

The voltage control mode 3 was used to regulate the output voltage at 550 V in MPPT mode. When the output voltage is measured at less than 550 V in mode 3 the MPPT function of the system is activated. The voltage control mode is changed to mode 2 when an output voltage that exceeds 550 V is measured and the MPPT function is made inactive.

The purpose of the voltage control modes is to regulate the output voltage at 550 V in different scenarios as explained above. A basic illustration of this is shown in the following chapter where the voltage level is indicated for each voltage control mode. The voltage changes were measured over time illustrating when each control mode is active. In mode 3, the MPPT mode is set active in the timer-interrupt. The MPPT mode control is executed in the main control loop periodically.

The next phase of the control sequence is the load control part shown below in figure 5.9. The verification part ensures that the input voltage is stable, the voltage control part attempts to ensure that the output voltage is at the set 550 V. This attempt is under no-load conditions, meaning that a minimal amount of current is drawn from the DC-DC converter. The load control is implemented in the timer-interrupt.

With the set-up of the drive system, the DC-DC converter feeds into the VSD, therefore the VSD is powered at this point. No output current is drawn by the VSD because the

VSD is not supplying the motor connected to it. As soon as the VSD supplies the motor with power, set by the speed command, current will be drawn from the DC-DC converter.

The purpose of the load control is to set the VSD with speed commands. As the speed commands increase, the current drawn by the VSD increases.

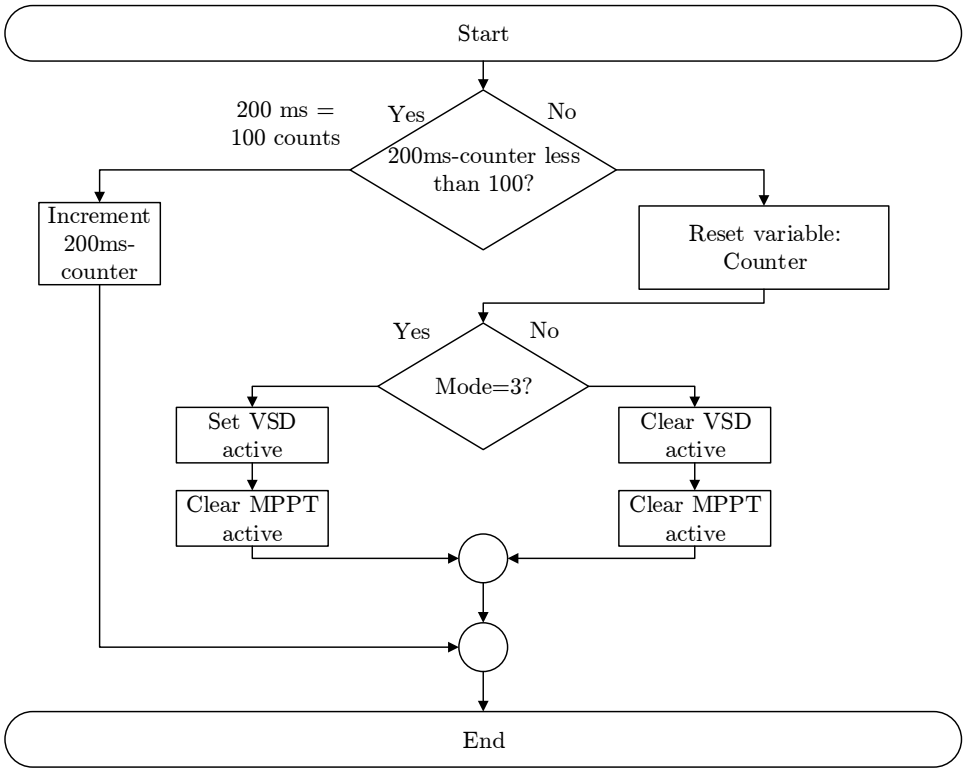

Figure 5.9: Control loop: Load or speed control.

This part of the control is active every 200 ms. It includes a counter-implementation that is reset every 200 ms and checks whether voltage mode 3 is active. If this is the case the VSD speed adjustment function is set active to execute and the MPPT function is made inactive. If voltage mode 3 is not active both the VSD adjustment function and the MPPT function is made inactive.

The voltage control and the load control are not active at the same time to ensure transients are settled. These two control parts work together to make sure the drive system operates at the correct voltage and is loaded appropriately.

The MPPT function is executed in the main control loop every 20 ms. This function is made active when voltage mode 3 is active and made inactive after the execution of the function. Part one of the MPPT algorithm is shown in figure 5.10.

Every execution cycle the code updates the power parameters, although the previous parameters for power is still kept. The updated power parameter is then the current power. With current and previous power parameters the MPPT function executed. These parameters are compared, which gives an indication of power levels over the period of the execution time.

Decisions are then made depending on the difference between the updated and previous power parameters. The two power parameters are compared and a MPPT direction is defined. This MPPT direction is used to either increase or decrease the duty cycle. A

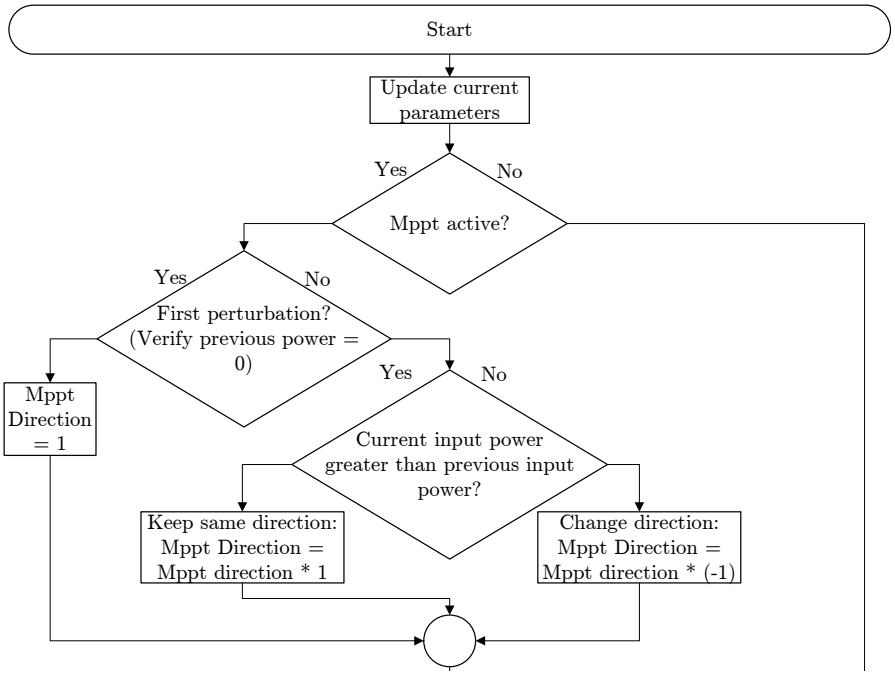

Figure 5.10: Control loop: Maximum power point tracking (Part 1).

MPPT direction that is 1 increases the duty cycle and an MPPT direction that is -1 decreases duty cycle. This means that the polarity of the MPPT direction will decide which action will be implemented. Part two of the MPPT algorithm is shown in figure 5.11.

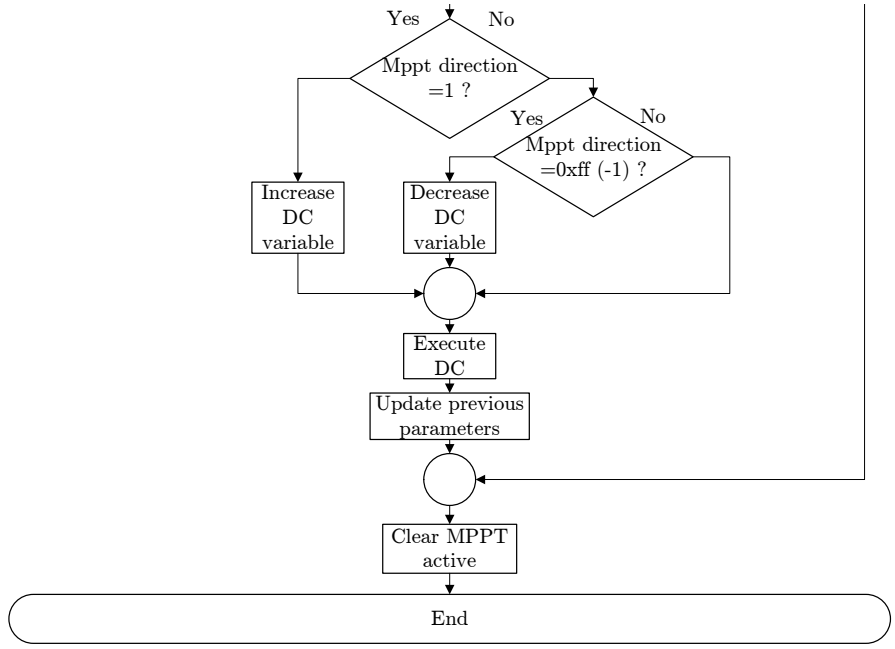

Figure 5.11: Control loop: Maximum power point tracking (Part 2).

Initially, an assumption is made that the previous power parameter is 0 W to orientate and give a reference to compare to. The current power is then compared with the reference previous power and as the difference will be positive the MPPT direction is made 1. The first perturbation is then made once the duty cycle change executes and the previous power parameter is updated.

The cycle repeats when the MPPT function is made active once more. The current power parameters are updated to be used in the comparison. As the first perturbation is done the sequence continues with a comparison of current and previous power parameters.

The comparison is made and if the current power is greater than the previous power the duty cycle must increase. The duty cycle must decrease if the previous power is greater than the current power. This is accomplished by changing the polarity of the MPPT direction. The cycle continues in an attempt to achieve MPPT.

With these changes being made in the duty cycle of the DC-DC converter it effects the PV panel array. The effect is that the operating point of the panel changes and with the MPPT algorithm implemented these are changes made to accomplish the maximum operating point.

The VSD function/load control is executed in the main control loop. This function is made active every 200 ms when voltage mode 3 is active and made inactive after the execution of this function. The execution of this function does happen after the MPPT function. Part one of the VSD function is shown in figure 5.12.

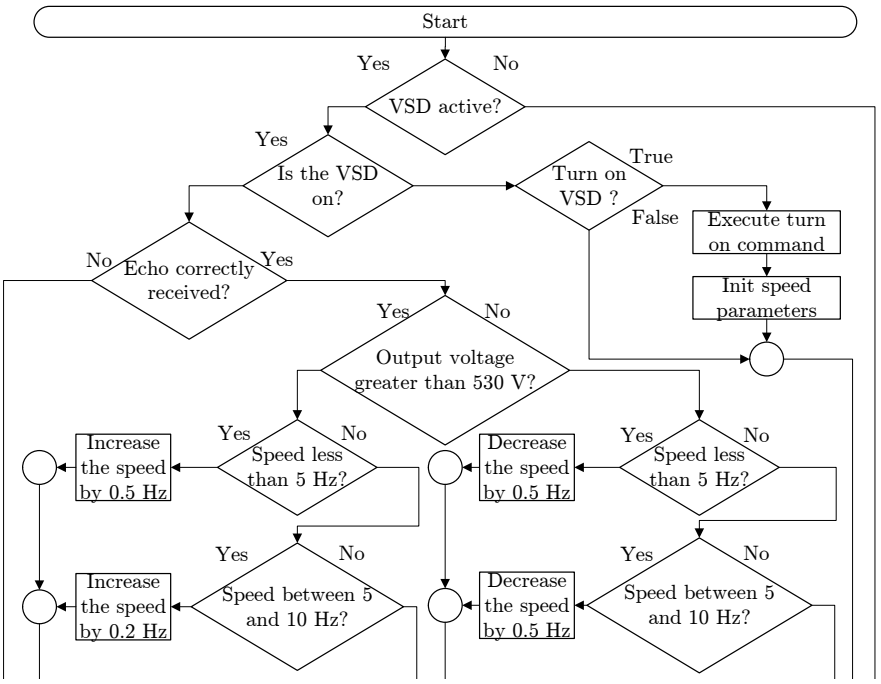

Figure 5.12: Control loop: Speed adjustment (Part 1).

When this function is active verification is done to check whether the VSD is on. If it not on, the VSD will be turned on and initialisation is done in terms of speed commands for the VSD.

Every control cycle the communication health is verified as the VSD does reply when it receives a transmitted message from the control module. If communication health is inadequate the previous message is repeat to establish the communication. Progression is only made when the control module verifies that the sent message was successfully received.

With the control cycle repeating, communications healthy and the VSD active the drive system will be loaded, adjusting the speed of the VSD. The speed is adjusted based on the output voltage magnitude of the DC-DC converter.

A comparison is made with the measured voltage and a set operating voltage of 530 V. The amount of increase or decrease of speed adjustment is based on the actual speed. The speed adjustments vary between speed ranges as the power change is greater at higher speeds for the same speed adjustment made. This will ensure that the rate of power change by the speed adjustments is adequate for that speed range.

If the output voltage is greater than 530 V the speed is increased. Speed adjustment amounts decrease as the actual speed increases. Part two of the VSD function is shown in figure 5.13.

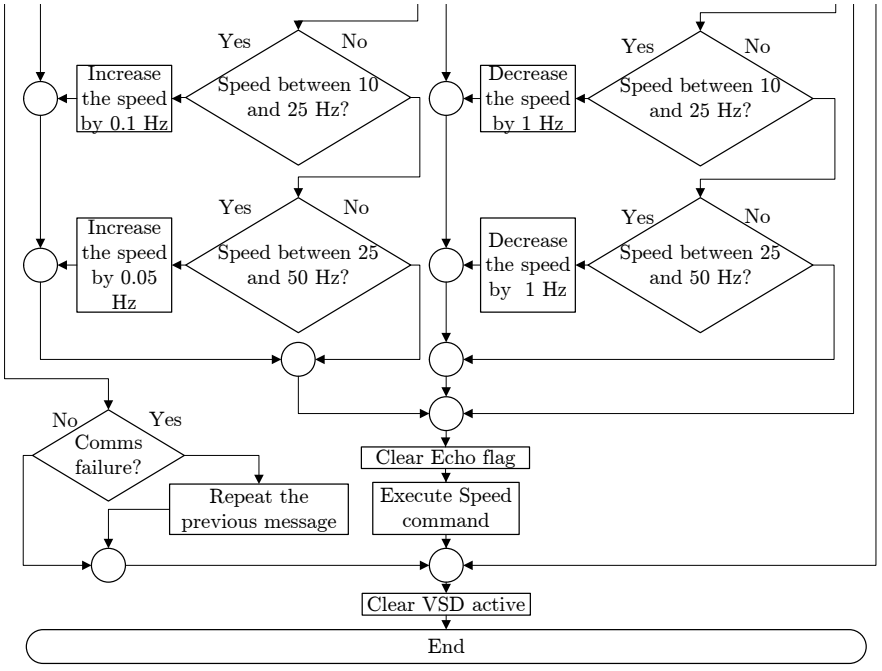

Figure 5.13: Control loop: Speed adjustment (Part 2).

The speed is decreased when the output voltage is less than 530 V. Speed adjustment amounts increases as the actual speed increases. This basic speed control algorithm will ensure that the speed is increased appropriately as long as the output voltage is greater than 530 V. It will ensure that the speed is appropriately decreased in the same manner.

As the output voltage is present across the output capacitor the 550 V regulated voltage will remain operated at, if there is enough energy provided by the PV source. When the limit in power is reached and the load is increasing in speed the capacitor voltage will decrease. The speed will still increase until the 530 V set point is reached, as per the control sequence defined.

Hence, the speed increase will continue until the power limit of the PV panels is reaching for that moment in time. Then the output voltage will decrease for a still increasing speed. At 530 V, the speed will decrease and the output voltage will recover. In the meantime, the MPPT control sequence continues. The control process will attempt to continue to raise and lower the speed and will result in the highest speed possible for that specific moment of the day.

The shutdown sequence, when made active, happens the set time for shutdown is observed. The system must be shutdown safely therefore gradually parameters are decreased. This sequence is shown in figure 5.14.

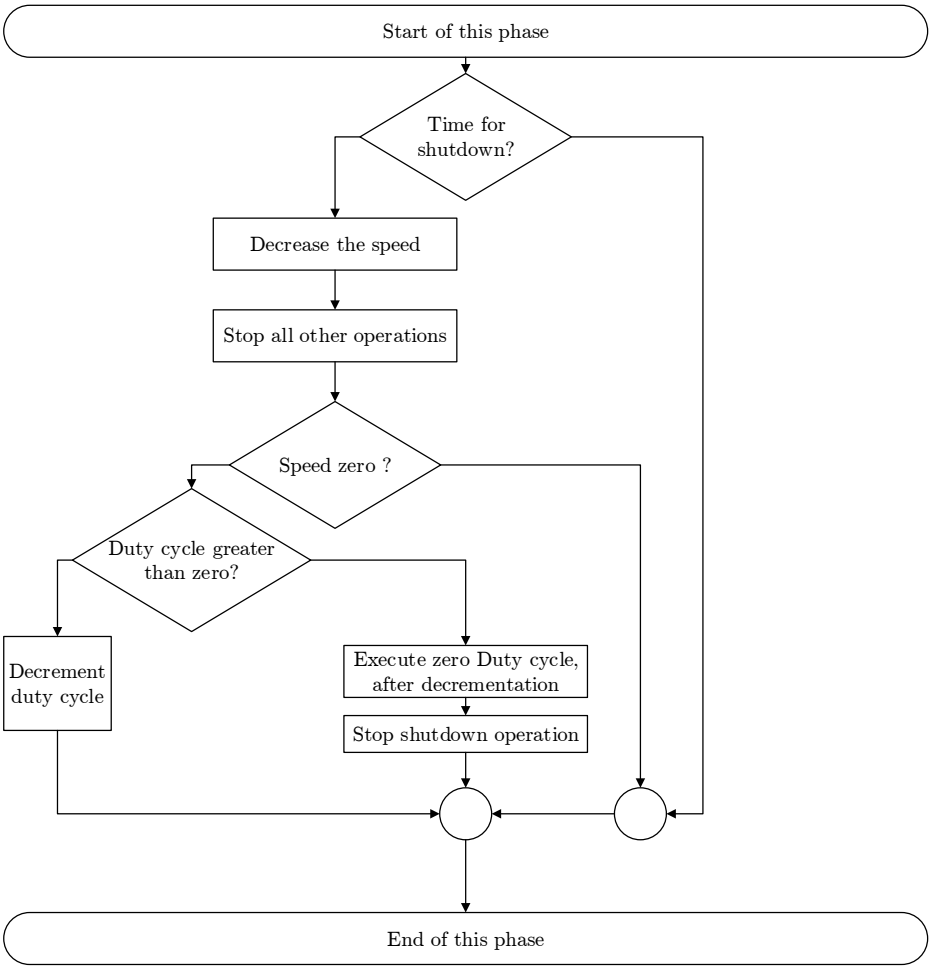

Figure 5.14: Control loop: Shutdown.

Firstly, speed is gradually decreased. All other operations are halted and discontinued. This will ensure that the drive system is properly deload, meaning output current will decrease.

When the speed is measured as zero, thus meaning output current is zero, the duty cycle is decreased gradually. This will ensure that the output voltage of the DC-DC converter is decreased to zero. Upon the indication of a zero duty cycle, the shutdown sequence is made inactive and all operations were safely stopped.

5.5 Control results

The start up of the drive system is shown below by monitoring the output voltage of the DC-DC converter. Figures 5.15, 5.16 show start-up transients at light-load and no-load condition, respectively. Figure 5.17 illustrates the regulation control algorithm. The voltage of 550 V remains regulated after light-load changes.

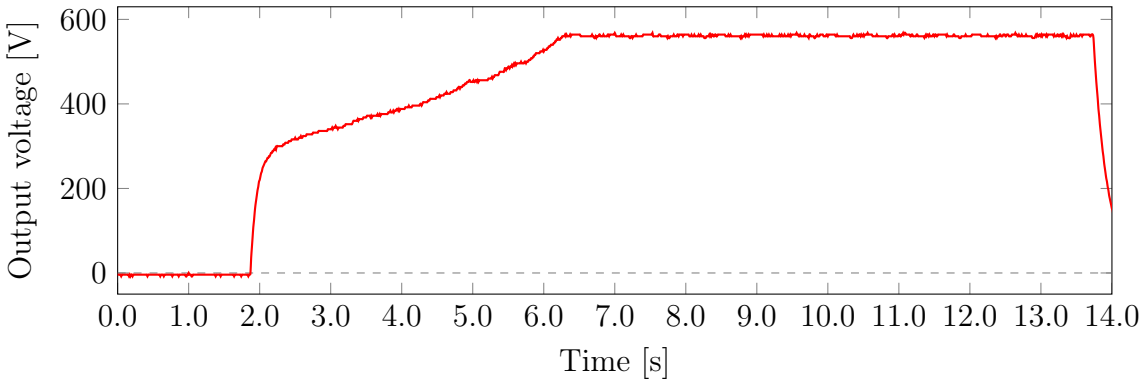

Figure 5.15: Output voltage transient: Start up at the light-load condition.

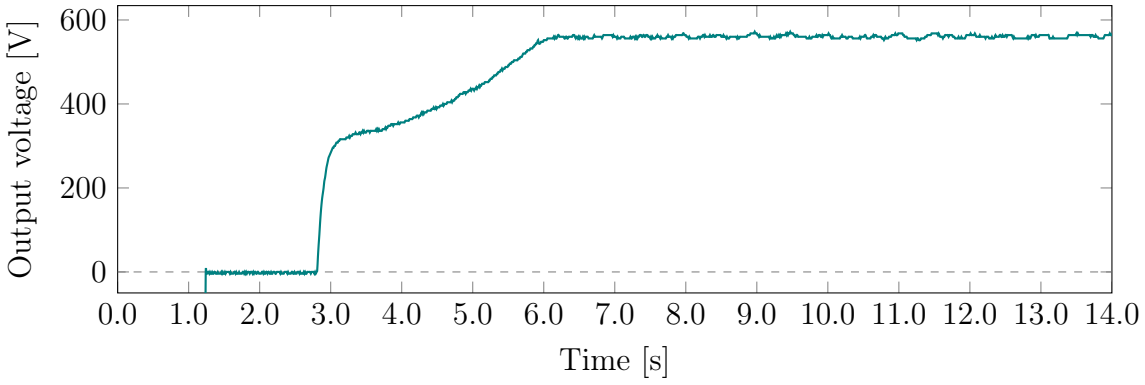

Figure 5.16: Output voltage transient: Start-up at the no-load condition.

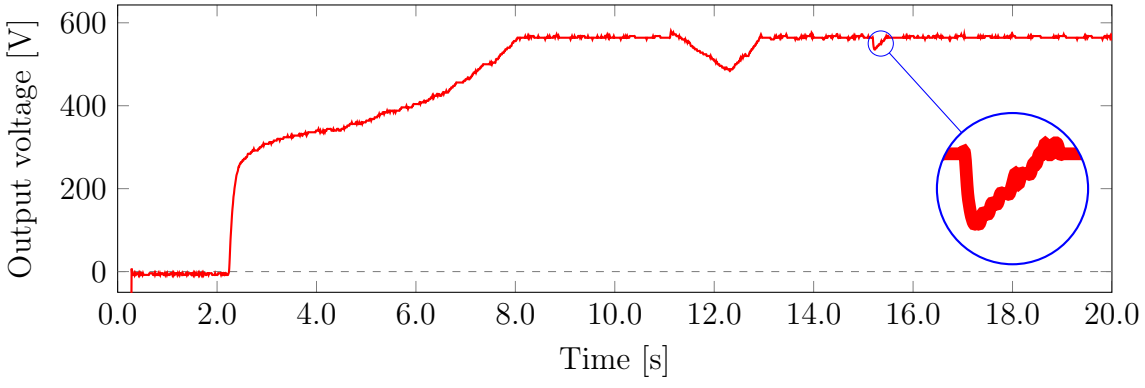

Figure 5.17: Output voltage transient: The voltage regulation with light load changes after start-up. The magnification indicates the load connection.

Chapter 6

Results of implemented application

6.1 Introduction

Chapter 6 describes the implementation of the demonstration and the results of the PV drive system. All the subsystems work together in collaboration to drive the load.

The system is tested and its results are presented for the operation throughout one day. The load used for the system-test is a fan, which is the practical implementation. The energy flow is demonstrated to show the capabilities of the drive system.

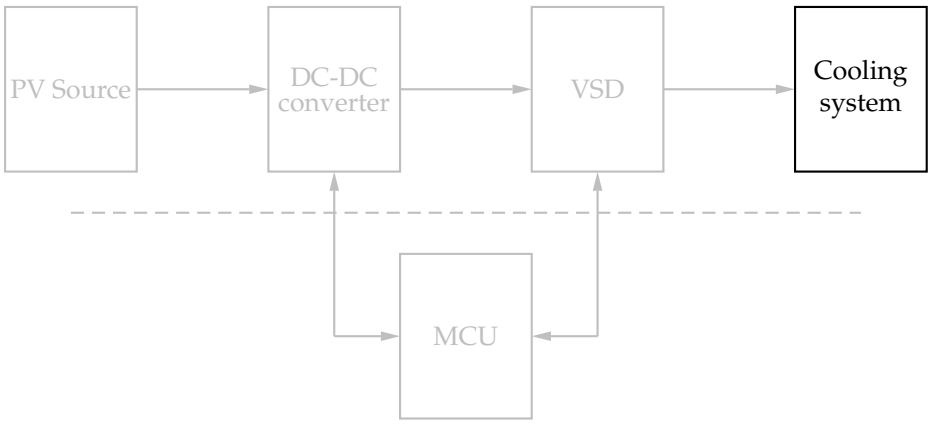

Figure 6.1: Schematic representation of the PV drive system, indicating interaction between various subsystems

The presented PV drive system is designed for a cooling system. The cooling system contains a compressor, which is driven by a motor. Unfortunately, a compressor could not be obtained. Therefore, an obtainable load is used. A fan is the replacement load chosen in order to still demonstrate the drive system.

An induction motor is used to power the fan as it would be used to power the compressor, through the PV drive system. Valid conclusions and observations about the effectiveness of the PV drive system are made, although the load profiles of the fans and compressors differ. This will be taken into account.

6.2 Practical implementation

6.2.1 Brief overview of subsystems' roles and specifications

As the subsystems are thoroughly described in the previous chapters, their roles are briefly stated. Their parameters are specified as well, as they were used in the demonstration.

- PV-source: A PV array of 1 kW was used as the input source. A four-panel PV array was used, configured in two parallel strings with two panels each in series.
- DC-DC converter: The resonant push-pull converter was used to increase the input PV voltage to an output voltage of 550 V.
- VSD: The Powerflex 525 was used, using the 550 VDC output voltage as input, to drive the motor of the fan.
- Control module: The control module was used to implement the main control algorithm, including start and stop of the operation in real-time. All control decisions are implemented automatically without unnecessary external input during the demonstration.
- Load: A fan with an induction motor, from Siemens, was used. The induction motor is rated at 2.2 kW, configured in a Y-configuration.

6.2.2 Aim of demonstration

The aim of the demonstration was to show the operation of the PV drive system connected to the described load, the fan. By demonstrating the PV drive system, as a working system, conclusions could be made about its implementation of the proposed load. Energy flow is recorded throughout the demonstration.

6.2.3 Description of demonstration

The PV drive system is demonstrated by its operation, throughout one day. This system starts up at a set time and begins to operate. During this operation time and power, parameters are recorded in order to illustrate and quantify the operation. At the end of the operating day, the system switches off automatically at a set time. This completes the demonstration. The setup of the equipment used in the demonstration is shown in the following figures.

The Yokogawa power meter, in figure 6.2, was used to measure the power of the PV panels through resistors. These resistors were manually adjusted to operate the panels at MPP.

Figure 6.2: Photo: The Yokogawa digital power meter.

In figure 6.3 are the panels used, 4 of them were used for the demonstration. The rated power of the PV array is a sum total of 1000 W.

Figure 6.3: Photo: The PV panels used as the input source.

The AVR debugger is shown, in figure 6.4, connected to the control module. The debugger used to program the MCU on the control module.

Figure 6.4: Photo: The AVR debugger.

An extra fan used to provide airflow to the DC-DC converter is shown in figure 6.5. Some heatsink temperatures are shown in Appendix E in figure E.6 - E.8.

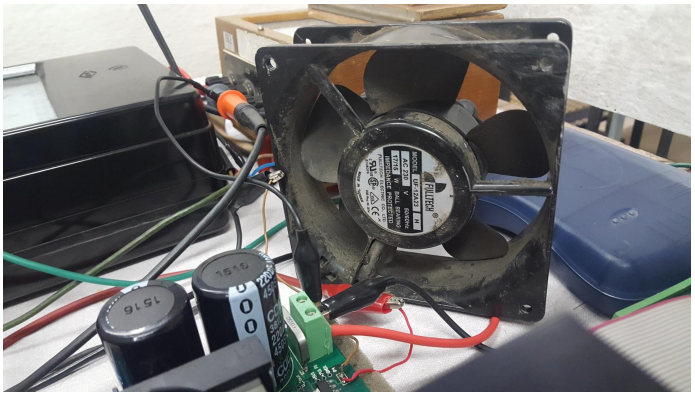

Figure 6.5: Photo: The extra airflow fan.

The multi-meters used to measure the input and the output voltage and current parameters of the DC-DC converter are shown in figure 6.6.

Figure 6.6: Photo: The multi-meters.

The control module is shown, in figure 6.7. It is plugged in and connected to the DC-DC converter with a ribbon cable.

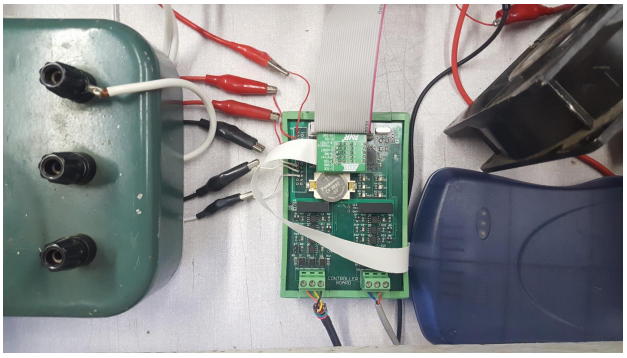

Figure 6.7: Photo: The control module.

In figure 6.8 the resonant push-pull DC-DC converter is shown. Furthermore, in the figure probes used to measure the switch source voltages are shown.

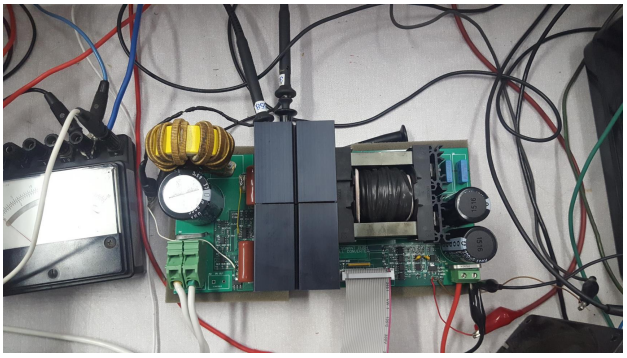

Figure 6.8: Photo: The resonant push-pull DC-DC converter is shown plugged in.

The VSD is shown plugged in, in figure 6.9. It is connected to the output side of the DC-DC converter and to the induction motor in 3-phase.

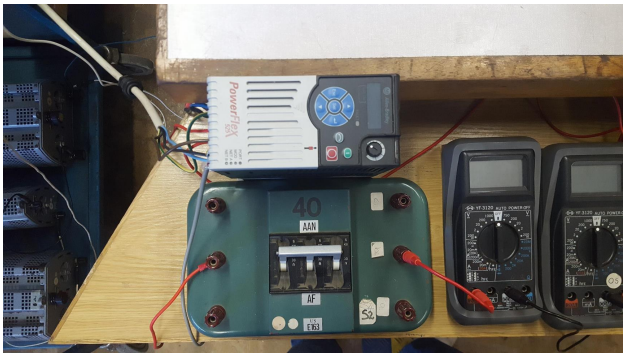

Figure 6.9: Photo: The VSD.

The DC-DC converter is shown, in figure 6.10, connected to the control module. It is surrounded by analog Ampere and Voltage meters.

Figure 6.10: Photo: The whole built setup.

Figures 6.11 shows the power supplies used supplying 5 V, 7 V and 15 V. These are seen to the left and two oscilloscopes which are used to measure and visually illustrate the output voltage and the gate to source voltage of one of the switches, are seen to the right.

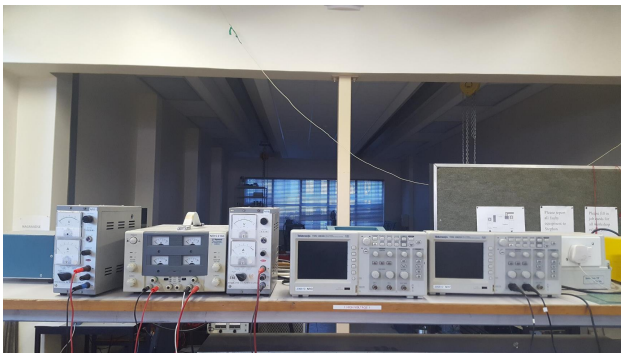

Figure 6.11: Photo: Power sources and oscilloscopes.

It was powered and controlled by the induction motor through a VSD. Figures 6.12-6.15 show the load setup.

Figure 6.12: Photo: The front view of the industrial fan.

Figure 6.13: Photo: The induction motor used to run the fan.

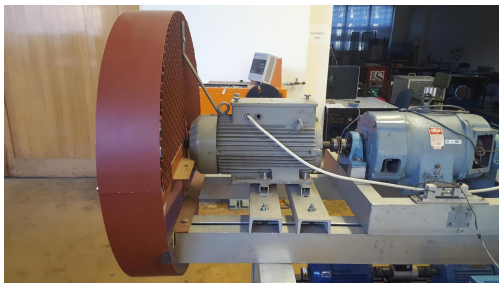

Figure 6.14: Photo: The industrial fan, used as a load.

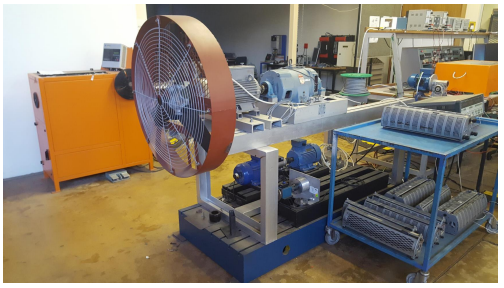

Figure 6.15: Photo: The industrial fan and induction motor, a side view

6.2.4 Results of full load start-up tests

The start-up of the PV system, with PV panels, to full speed, was observed. Figures 6.16 - 6.18 show the control of the PV drive system. Below the voltage and current is shown for this duration. The test was done before noon.

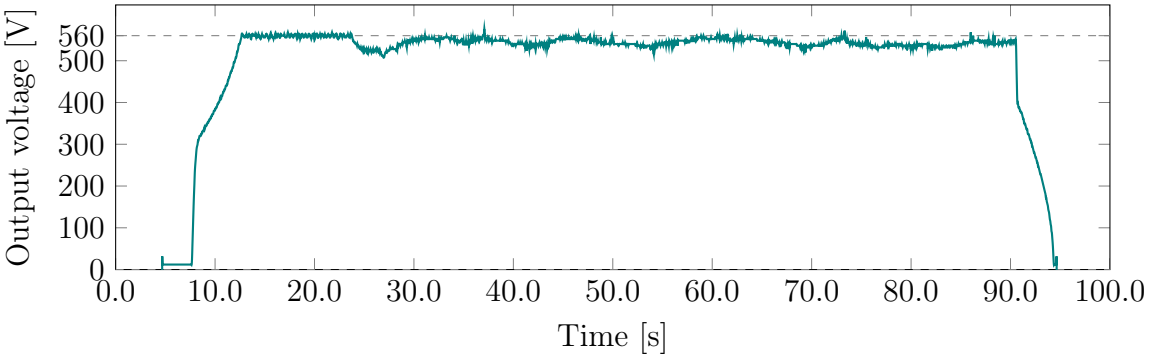

Figure 6.16: Output voltage transient: Start-up of the system increasing the speed to maximum load, in the morning.

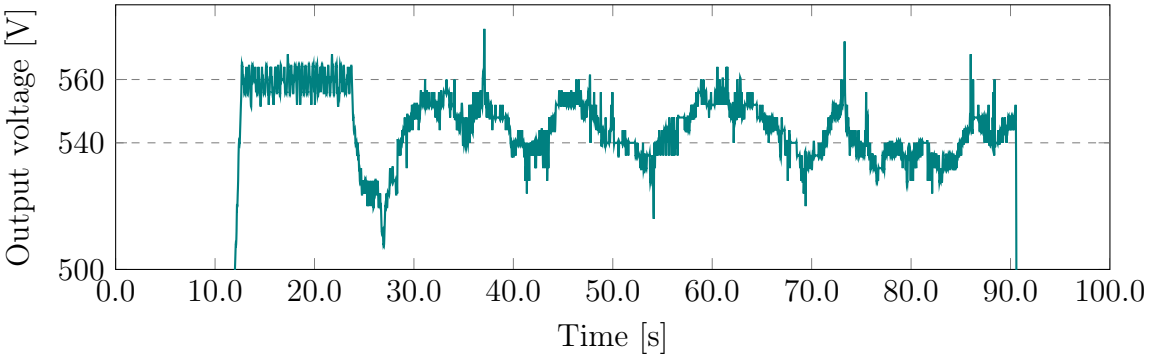

Figure 6.17: Output voltage transient zoomed in: Start-up of the system increasing the speed to maximum load, in the morning.

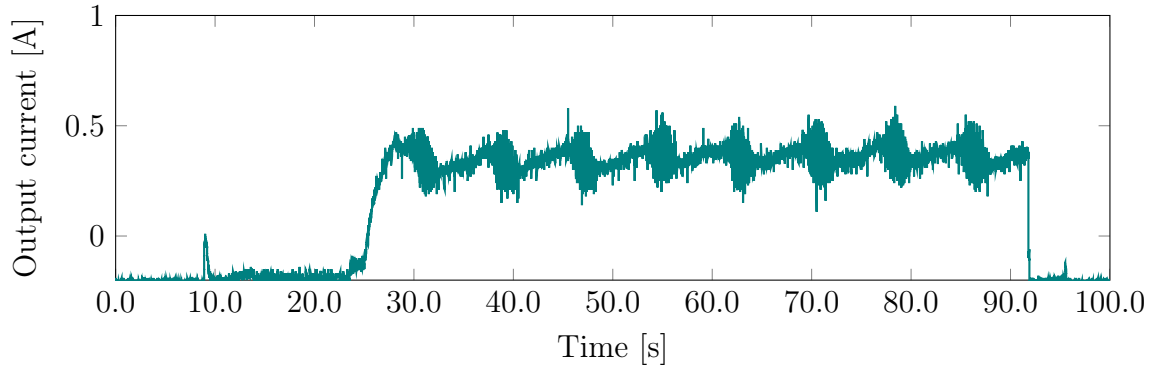

Figure 6.18: Output current transient: Start-up of the system increasing the speed until maximum load, in the morning.

The start-up of the system to full speed was observed. Figures 6.19 - 6.21 show the control of the PV drive system. Below the voltage and current is shown for this duration. The test was done after noon.

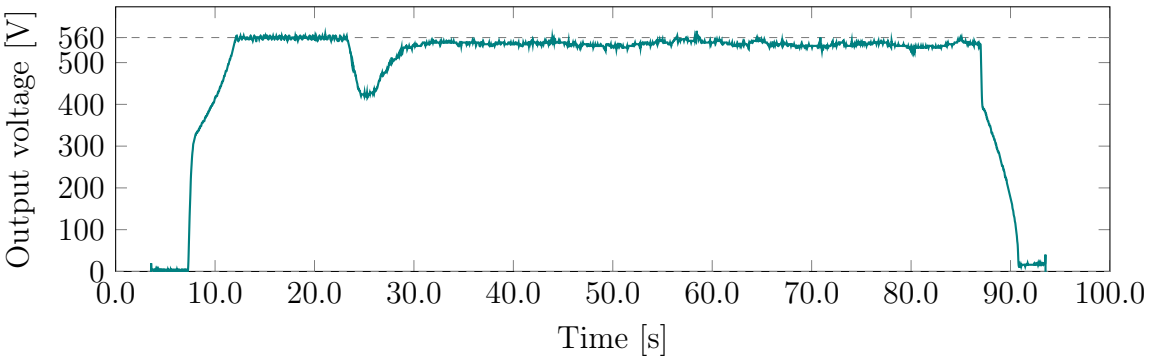

Figure 6.19: Output voltage transient: Start-up of the system increasing the speed until maximum load, in the afternoon.

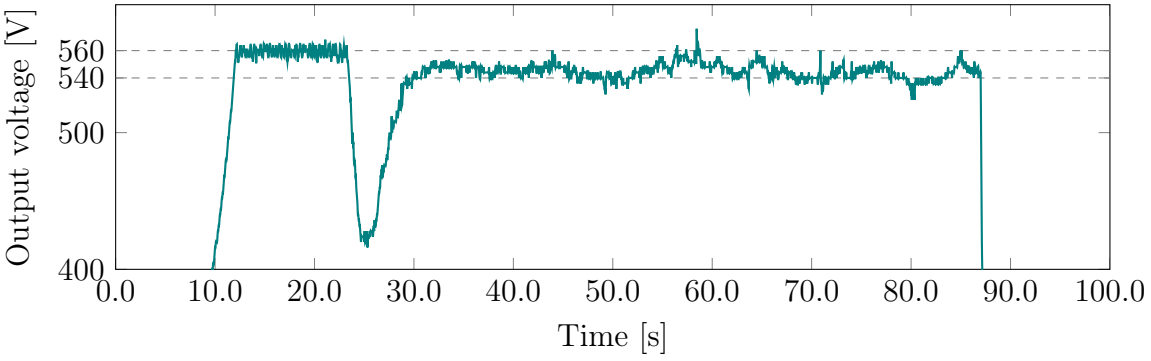

Figure 6.20: Output voltage transient zoomed in: Start-up of the system increasing the speed until maximum load, in the afternoon.

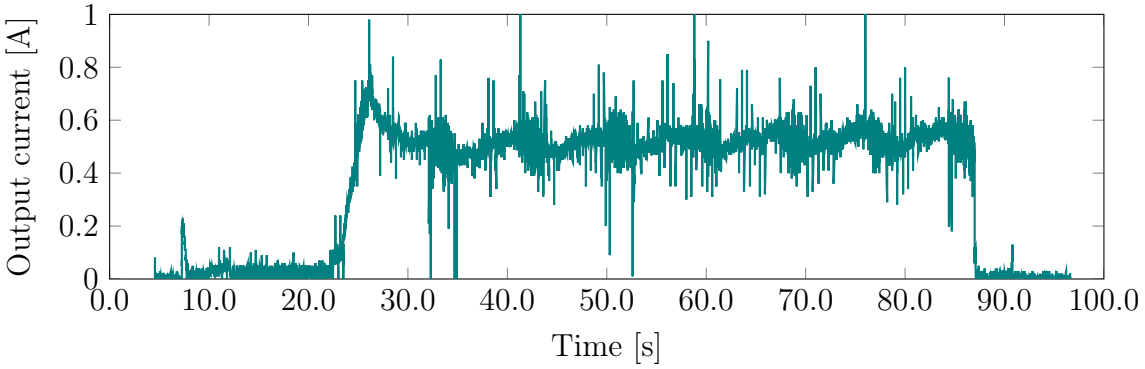

Figure 6.21: Output current transient: Start-up of the system increasing the speed until maximum load, in the afternoon.

6.2.5 Results of full-day operation test

While the PV drive system is in operation it is monitored every 5 to 10 minutes from start-up to shutdown to quantify the energy flow throughout a day. Voltage, current and frequency parameters are recorded while monitoring the system.

In figure 6.22, the operation of the system is shown for one day. A maximum power rating of 681.9 W was recorded during the demonstration at an efficiency 86.85 %.

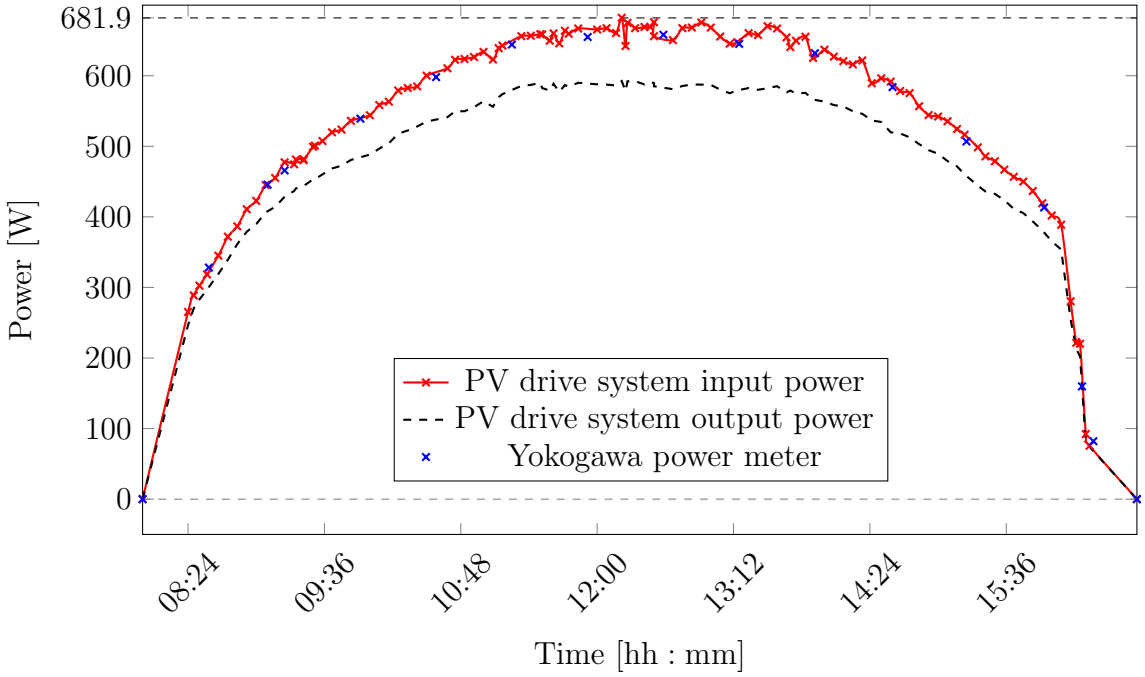

Figure 6.22: The PV drive system is operated throughout a day.

The PV drive system's power, output, and input are shown by the red and black trends, respectively. The Yokogawa power meter trend is shown with the blue trend. All the trends are shown in one figure to compare them.

The Yokogawa power meter was used to measure the power of the PV panels with adjustable resistors as a load. This meter was used as corroborative information to that of the PV drive system power. The PV drive system was operated and regular measurements were made. After every (3rd) PV drive system measurement, a measurement was made with the power meter. That is, the PV drive system was disconnected from the panel and the power meter and the resistors were connected and adjusted to operate at its MPP.

As seen in the figure 6.22 the two measurement types co-align. The two trends fit into each other proving that the PV drive system is operating at MPP.

There are two interesting remarks to make about the graph. Firstly, the start and end points at a magnitude of 0 W were put in for reference and were not actual measurements. Lastly, the last few measurements past the time of 15:36 appear to have a prominently different gradient. This is because the PV array was shaded slightly at that time.

The demonstration showed, in results, that a working system is implementable. The drive system was able to operate and it indicated expected behavior, as shown in figure 6.22. The behavior correlates well to PV applications.

Chapter 7

Conclusion

7.1 Introduction

This chapter draws together the research presented in each chapter. Reflections are made on each chapter stating findings, an evaluation of the project and recommendations.

7.2 Chapter reflections

7.2.1 Chapter 1

In this chapter a background study was given for the thesis, initially relating hunger to food waste, and food waste to refrigeration. Solar PV as an energy source was then discussed and examples of implemented PV applications were given. The research project was then introduced, stating the aspects of the research investigation. These aspects included the research aims, objectives, significance and scope. The chapter ended with a mention of the execution of the project and the outline of the thesis.

7.2.2 Chapter 2

A high-level overview of the project was given in this chapter. This overview described the development process and subsystems of the drive system.

7.2.3 Chapter 3

The focus of this chapter was the DC-DC converter. Converters were introduced. Thereafter, criteria were given for the choice of the converter used in the project. Groups of converters were compared, in search of an advanced converter meeting the stated criteria. These converters were discussed and a converter choice was made. The resonant push-pull converter was chosen as a converter for the project.

7.2.4 Chapter 4

The chosen converter was presented in this chapter. A full description of the converter operation and theoretical design was stated. The design procedure followed for this project was then presented. The design was simulated and its results were given and compared to the theoretical design. The comparison of these results with the design was good.

The construction of the converter was given after the design and simulation, showing key components and the actual converter. The measurements for the built converter were then presented, compared to the simulated results and the theoretical design. These measurements were finally evaluated, discussing the similarities and differences.

7.2.5 Chapter 5

The system control was contained in this chapter, with the focus on three main subsystems; namely the converter, the VSD and the control module. The control module and its aspects were discussed, firstly, in this chapter as it is the central part of the system control. Thereafter, the energy flow of the system control was presented through algorithms stating the implemented control. The chapter was concluded with results showing implemented control processes.

7.2.6 Chapter 6

A demonstration of the PV drive system was given in this chapter. Consequently, the drive system's ability to operate for one full day was shown, practically demonstrating the implemented control algorithms to a successful measure.

7.3 Project evaluation

7.3.1 Research objectives evaluation: Performance

The research objectives were collectively performance based. Therefore, the performance aspects of the project are discussed. Following this section, the research aims to address the financial and performance aspects together.

At the end of the project, the design was done and implementation of a DC-DC converter was made to supply a commercial VSD successfully. Consequently, the low voltage solar PV array could be used to supply the VSD by elevating the PV array voltage using the DC-DC converter. The results are shown in chapter 4.

Furthermore, the control system and control algorithms were well implemented through a central control module, which was micro-controller based. In addition, measurement and communication circuitry was used by the control module to achieve monitoring of vital parameters for control. Additionally, the subsystems -both the DC-DC converter and the VSD - were controlled by the control module for optimal power transfer as discussed in chapter 5.

At the end of construction a combined system of subsystems was established to form the PV drive system. The combined system consisted of the DC-DC converter, the VSD and the micro-controller based control module, integrated together.

It was demonstrated that the combined system was able to supply a variable load with a 1 kW PV array as input source and results were obtained. Furthermore, the variable load was a fan connected to a 2.2 kW rated induction motor powered by the VSD. The operational results, of the PV drive system's demonstration, were successfully corroborated with an external measurement system consisting of resistors and a power meter, shown in chapter 6. As a result the PV drive system is able to be used to power three-phase motors as found in off-the-shelf commercially available cooling systems.

Furthermore, the drive system was operated; its parameters measured and recorded showing optimal operation throughout a full day. Besides the power measurements that were recorded, voltage measurements were taken to show precisely the degree of implemented control through the transient operation for a full day. The system's efficiency during the demonstration was measured as a range between 86.85 % and 91.05 %.

Despite the accomplishment of the mentioned objectives the PV drive system designed had losses and was not tested with actual cooling systems. Thus, commercially available cooling systems were not adapted for use with the PV drive system and was not specifically evaluated for this application in the field of agriculture.

Although a further application could have been made for testing of the system in the specific field of use for small scale farmers, the useful deduction was still made. In effect, the PV drive system was tested with the described setup and yielded results that prove it can be used with equivalent systems, that is to say, equivalent in load magnitude and load profile. In this case, the fan used in the practical demonstration, as a load, had a non-linear load profile. Consequently, a cooling system with a similar load magnitude and load profile would be able to be powered by the PV drive system. This is the evaluation made from by practical demonstration.

Regarding this performance evaluation, the problems that small scale farmer face could be addressed by using the PV drive system to power cooling systems. Therefore, the problem of food waste would be addressed through the ability to power such systems.

With all the above said, most of the objectives were met to a fair degree. From the operational and functioning perspective, the PV drive system implemented with the proposed development process was satisfactory in performance. However, shortcomings were present and are discussed in the following subsection 7.3.4.

7.3.2 Research aims evaluation: Performance and cost

In the evaluation of the research aims, the performance and cost of the built PV drive system needed to be analysed. Thus, with the research objectives indicating performance-based adequacy, the developed system was designed and tested with satisfactory results. In particular, the developed PV drive system was demonstrated using a low voltage input range. However, when compared to similar products in the market, regarding cost, the PV drive system does not fare that well. The PV drive system cost is provided below and thereafter compared to these similar products. It is necessary to mention that the inverters used in the comparison have high voltage input ranges of 450 V to 1000 V with an output voltage of 380 VAC [68].

In addition, the comparison is difficult with these systems as they do not employ identical control methods and are not used for the same application. It must be said that identical systems, in the same application, do not currently exist. However, these systems are used as they are the most comparable. The companies manufacturing these systems have the advantage of procuring components in bulk, as bulk buying lowers total cost. Instead, for this project procurement was done on-line for individual components, increasing the total cost.

The cost factor is quite significant as these PV drive systems would be used by small scale farmers. Therefore, for the target audience, cost effective implementation is important. Evaluating the PV drive system in terms of cost; relevant items and subsystems are taken into account and combined with the total cost. The prices used are the component costs at the time of procurement and manufacturing, which was the 28th of January 2016.

In brief, the PCBs' cost, for all boards used in the implementation, were R 3,157.80. The price for the components of the resonant push pull converter, the measurement and control circuitry, and the control module was a combined R 2,711.74, further detail can be seen in appendix H. Furthermore, the cost of the VSD, namely the Powerflex 525, used in the implementation was R 10,100 [69]. This brings the total cost for the PV drive system to an amount of R 15,969.54 when considering the most relevant cost contributors.

The systems that are similar, to the drive system, are solar pump inverters. The following two solar pump inverters were chosen for comparison based on their equivalent functionality and power rating to the drive system. To mention some of the main functions: these inverters contain built in VSDs, have high efficiencies, are compatible with three-phase motors and include MPPT control algorithms. Firstly, the "Aspire solar pump inverter 2.2 kW" has a cost of R 5460. Secondly, the "Microcare portable 1.5 kW 380 V three phase solar pump inverter" has a cost of R 6156 [70]. Comparing the PV drive system with these two inverters, it is clear to see that these inverters are the more cost effective option to implement; the difference is approximately R 10000.

In summary, the proposed PV drive system is not the most cost effective implementation as there are solar pump inverters on the market that are less expensive with similar functionality, although they operate at high voltage ranges, and are not fully identical in control and application. Regardless, the PV drive system does have a satisfactory performance with a low voltage input range, which was the partial focus of the proposed implementation. In addition, recommendations are made for possible cost and performance improvement.

7.3.3 Research question evaluation

Considering the evaluation of the research objectives and research aims, the research question was answered.

"Is the design and implementation of off-grid PV drive systems feasible for small scale farmer fresh produce cooling, with the proposed development process?" It is not fully feasible, regarding cost, to implement the proposed design for a PV drive system as it is too expensive for small-scale farmers. However, the system could be designed and implemented to a satisfactory degree, regarding performance, for fresh produce cooling for small-scale farmers.

7.3.4 Shortcomings

Although, the drive system performance was adequate, the project implementation had shortcomings which can be improved on. The drawbacks of the project included component design shortfalls and the lack of application-specific implementation.

The testing of the designed drive system showed discrepancies in the achieved efficiencies regarding the resonant push-pull converter that was used. Efficiencies of minimum 95 % were measured by Kwon and Kim [33], which could not be achieved in this project. This efficiency limitation is due to heat losses from the transformers, heatsinks and diodes, which lead to system breakdown over long operational periods. These temperatures are shown in Appendix E. In additions, another main contributor to these heat losses was identified as insufficient airflow during testing. However, this issue was resolved with an external fan, which provided sufficient ventilation thereafter.

Furthermore, noise on the measurement and communications circuitry made it difficult to obtain accurate measurements and communication connections from these subsystems,

respectively. For the measurement circuitry, these issues were more prominent at higher power levels and were considered inherent to the PCB layout of the converter, which included these subsystems on the same PCB. Hardware adjustment attempts were made to reduce the noise by inserting decoupling capacitors where necessary, which provided partial alleviation of the noise. However, the measurement circuitry remained sporadic at higher power levels. After all, software implementations were made to verify the measurements before they were used.

On the other hand, the PV drive system was not demonstrated with the specific application stated for this project, which is small scale farmer fresh produce cooling. Although relevant observations could be made with the load used in the demonstration, more accurate and precise observations could have been made had the demonstration been implemented for the particular application. As mentioned before, the drive system could not be tested for small-scale cooling due to excessive cost implications of refrigeration equipment and construction of equipment housing.

7.4 Recommendations

In retrospect, the recommendations are made regarding the shortcomings of the project. Moreover, comments are made for future improvement.

The design of the converter built for this project did not match up in efficiency as stated in the theoretical design. The converter's transformer and switch heatsinks were observed to be fairly warm in long-term operation. These heat losses in the converter decrease the efficiency of the converter. The converter could not operate at full load without failure with no external fan, thus it is suggested that the converter and component design be reconsidered. Added to this, proper ventilation needs to be considered during testing and operation of the drive system.

On the other hand, an implemented power supply with battery management capabilities is suggested for the control module and supplementary circuits. This will ensure operation of the control module through the night and a more compact drive system; external power supplies will then not be needed. However, this power supply was designed and prototyped for this project, although it was not used throughout the demonstration. A brief description of the power source is given in Appendix B.

Furthermore, demonstration of the PV drive system with the specific application of refrigeration appliances should be attempted. These appliances would need to be adapted to operate with a VSD. This application-specific testing would allow for more accurate conclusions to be made and construction of a cooling room would be needed for this implementation.

Lastly, in comparison with the existing systems on the market, that are less expensive, effort needs to be made in identifying and implementing changes to subsystems that could contribute to a more cost-effective design. In effect, the type of VSD in this project made up most of the cost and should possibly be reconsidered. In addition, an attempt could be made to design an enclosed drive system that includes the DC-DC converter, VSD and control module in one enclosure. It must be said, that the VSD cost for the enclosed PV drive system would still be excessive in cost compared to the two solar pump inverters. The reason being, the higher voltage gain that is needed from using a low voltage PV source as input.

Appendices

Appendix A

List of abbreviations

ADC - Analog to digital converter
CRC - cyclic redundancy checking
EMI - Electromagnetic interference
IBC - Interleaved boost converter
IC - Integrate circuit
LC - inductor capacitor
MCU -Microcontroller unit
MOSFET - Metal oxide semiconductor field effect transistor
MPP - Maximum power point
MPPT - Maximum power point tracking
PCB - Printed circuit board
PV - Photovoltaic PWM - Pulse width modulation
RTC - Real time clock
RTU - Remote terminal unit
SPI - serial peripheral interface
UPS - uninterrupted power supply
VSD - Variable speed drive
WFP - World food programme
ZCS - Zero current switching
ZVS - Zero voltage switching

Appendix B

Power supply

B.0.0.1 Power supply circuit

This circuit was designed and built to mainly provide power to the additional circuits involved in the project, namely the main DC-DC converter switches and the controller circuit. The Flyback converter included a battery-back up system. This was to mainly provide power the DC-DC converter switches through gate drivers in the form of a 15V voltage level, to generate 7V voltage levels for the powering of the main converter measuring circuitry and to, lastly, generate a 5V voltage level to power the controller board. The 5V fed to the micro-controller is very important as this would be the only generate voltage level that would be battery-backed up. The flyback converter also has the back-up circuit built in with it. From the flyback converter, the voltage levels are distributed to the controller board, namely the 15V for the main converter switches, the 7V for the input side of the main converter, a 7V for the output side of the main converter, both for the measuring circuitry and the battery-backed up 5V to keep the micro-controller board running. From the controller board the voltages for the main converter are distributed across to it. The flyback converter is the power source generator of the whole system and is a critical part of the whole design. Figure B.1 shows a 3d-model of the final prototyped flyback converter.

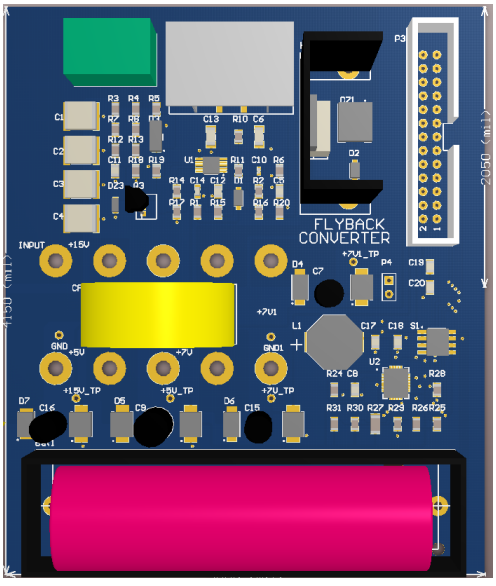

Figure B.1: Photo: The resonant push-pull inductor

Appendix C

Control signals

Gate drive output - 30 %

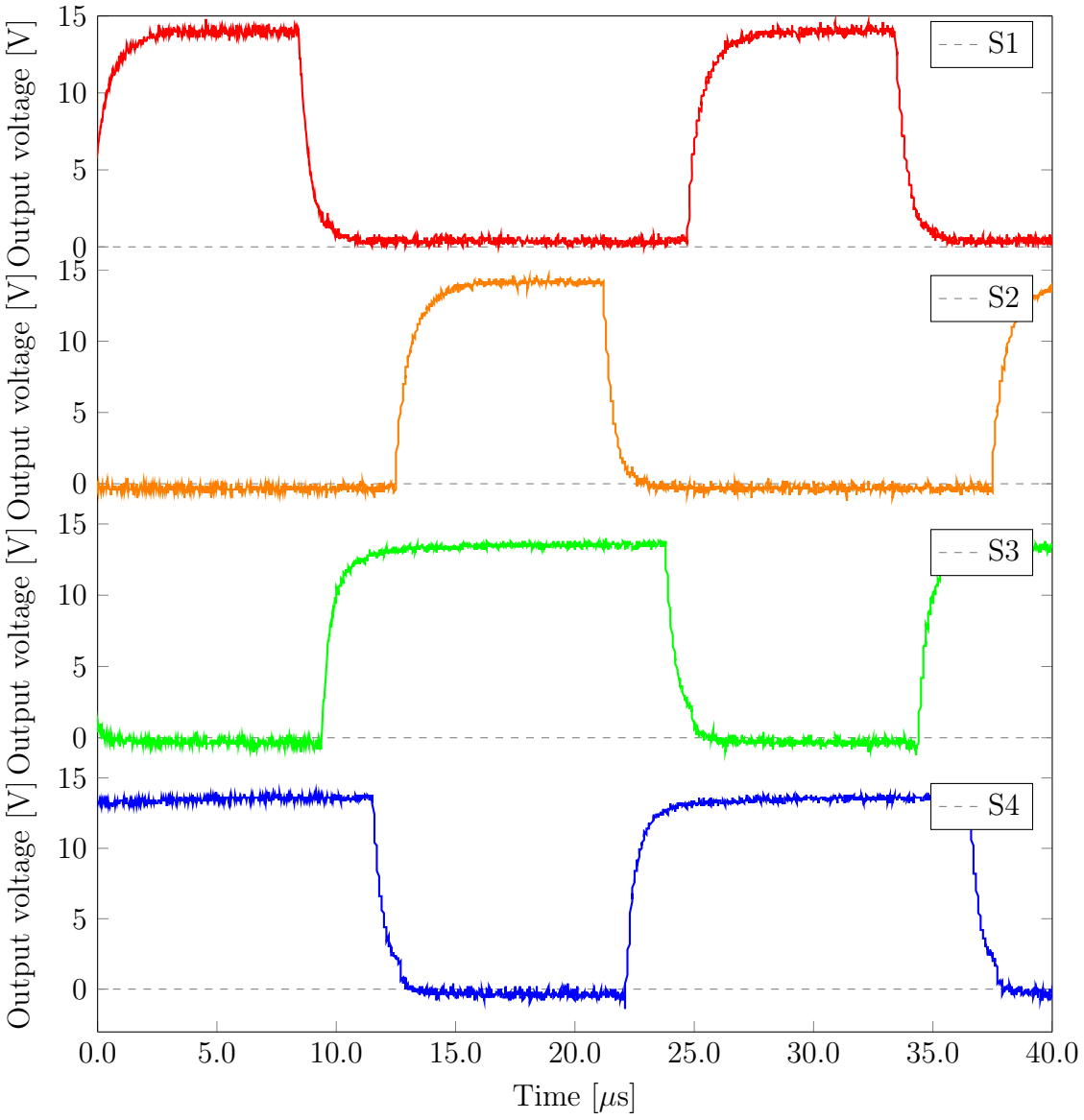

Figure C.1: Control signals: 35 % Duty cycle

Gate drive output - 50 %

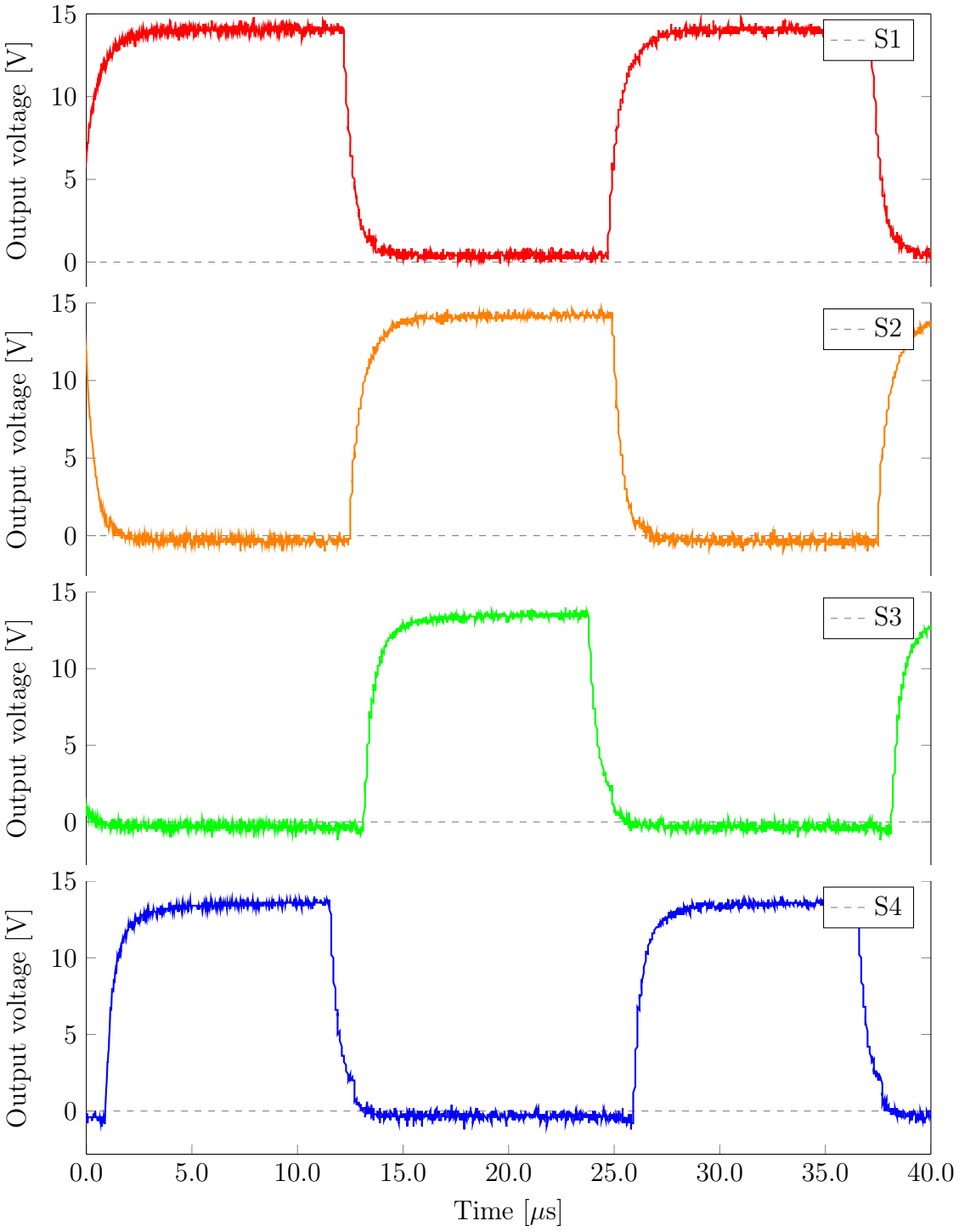

Figure C.2: Control signals: 50 % Duty cycle

Gate drive output - 65 %

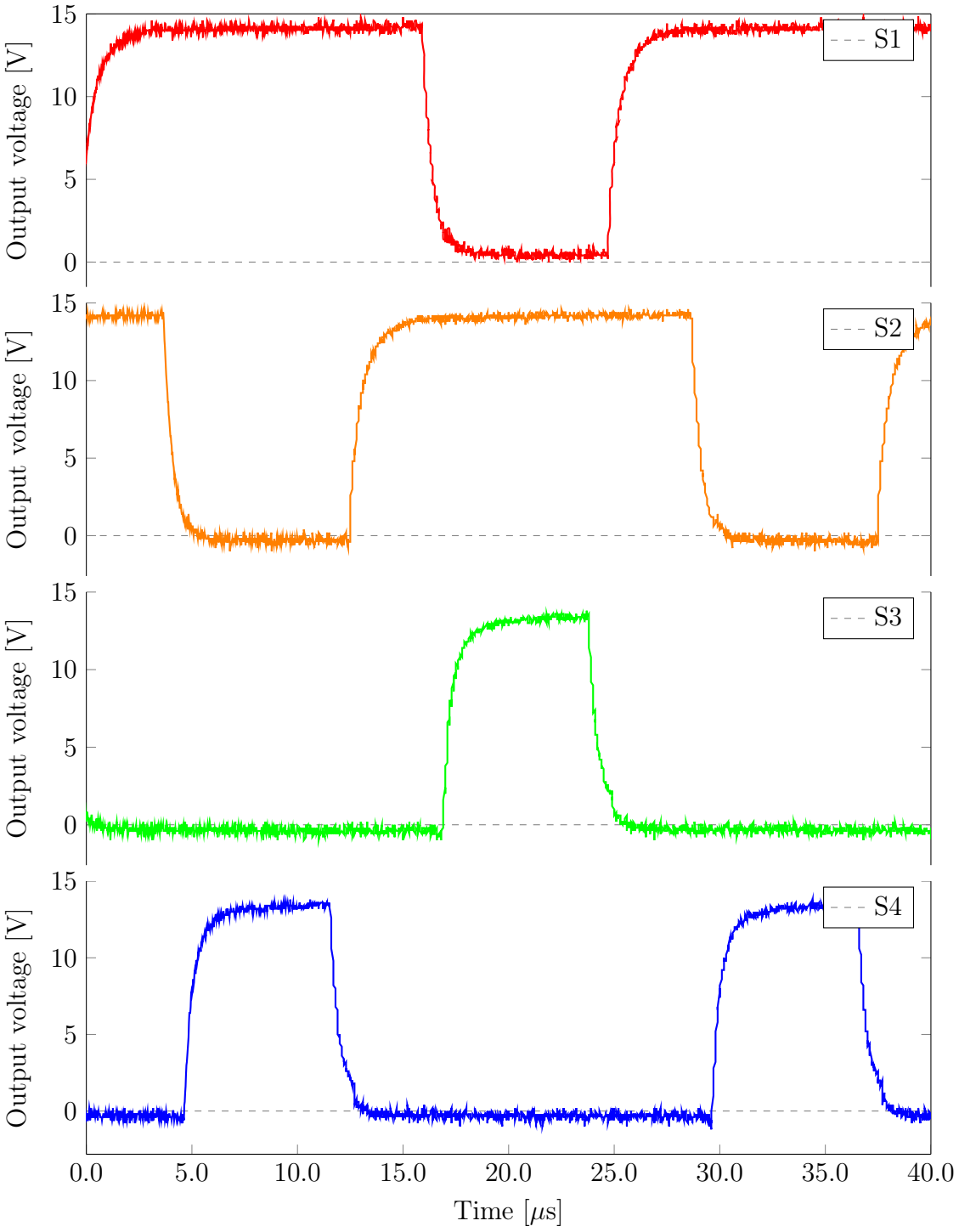

Figure C.3: Control signals: 65 % Duty cycle

The gate-drive output signals to the switch gate junctions were measured in these figures. They can be compared with the control signal presented in [33], the origin of the design. These measurements given in figures C.1, C.2 and C.3 correspond with the given signals.

The dead-time for switch S1 and S3 are measured, and verified as 1 μs. This shown below for duty cycles 35%, 50% and 65%, respectively.

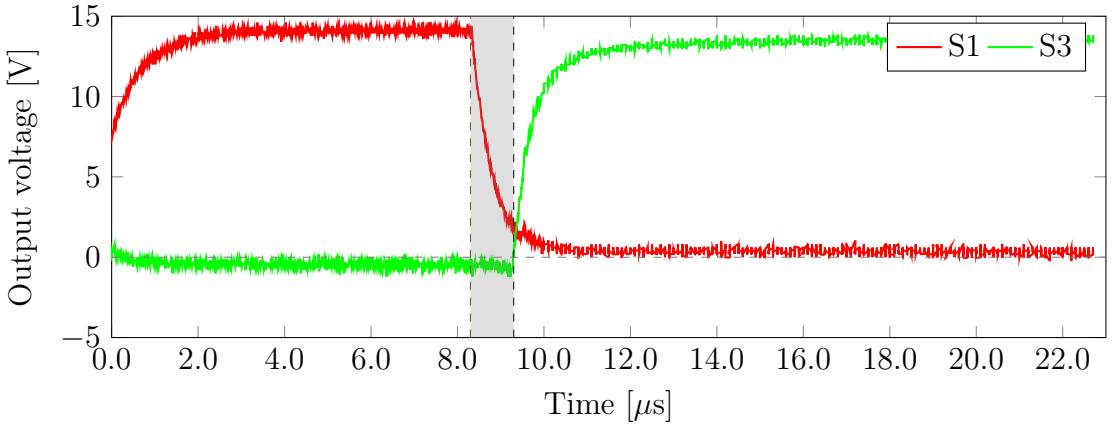

Figure C.4: Control signals: 35 % Duty cycle dead-time between S1 and S3

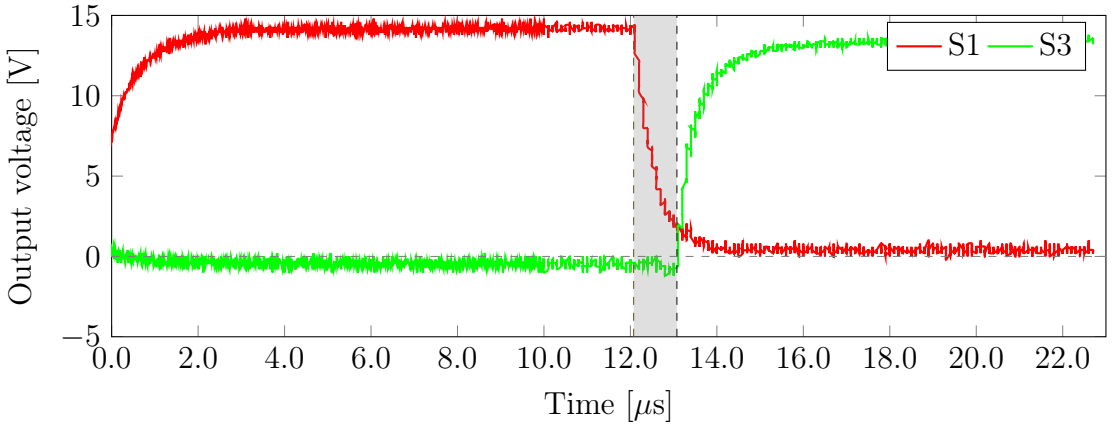

Figure C.5: Control signals: 50 % Duty cycle dead-time between S1 and S3

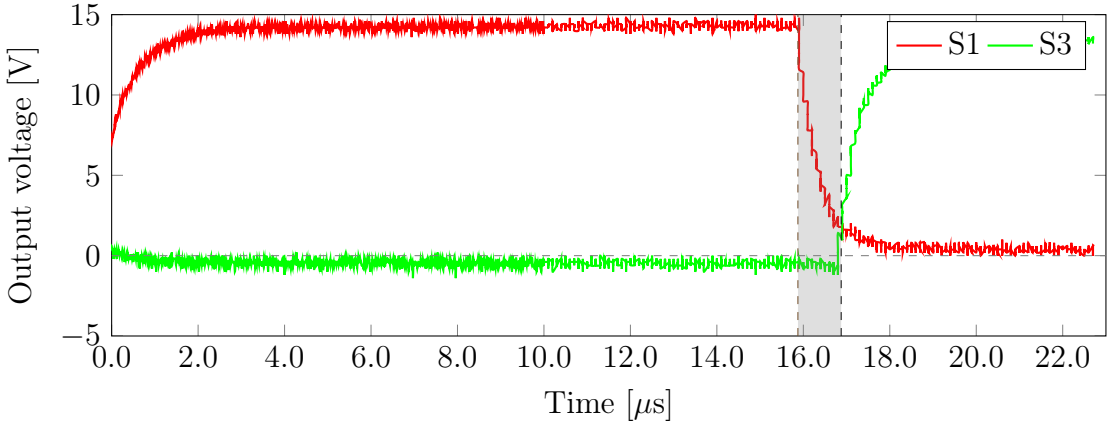

Figure C.6: Control signals: 65 % Duty cycle dead-time between S1 and S3

Appendix D

Motors

D.1 Induction motor vs Brushless DC motor

Between the brushless DC motor and the AC Induction motor, the stators used in both are virtually identical, but the rotors are different. There are certain advantages and disadvantages such as the following, looking at the induction motor first [71].

D.1.1 Induction motor

Induction motors can be directly connected to the utility power. The shaft speed is proportional to the line frequency. Induction machines do not include magnets and the magnetic fields (B) are adjustable, since B is proportional to the ratio of voltage and frequency in an induction machine. Therefore, using an inverter with the induction machine, the magnetic and conduction losses can be mitigated by controlling the inverter to lower the voltage at lighter loads. Inverter control is speed sensor based [71].

But some limitation exists for the induction machine, where the DC motor is favored. Induction motors cannot run off of DC power directly and as mentioned a inverter is needed. In such a case, variable speed can also be accomplished in this manner. Inverter control is speed sensor based for induction machines. Induction machines can operate at 85% of power factor [71].

D.1.2 Brushless DC motor

No starting torque will be produced when a brushless DC motor is connected to a fixed-frequency sources, such at the utility power. DC machines have a greater torque performance, the design includes magnets and is brushless. Using inverters with DC motors, the control will be position sensor based. The DC motor can operate at unity power factor [71].

Looking at the ideal DC motor, the magnetic field strength produced by the permanent magnet is adjustable. To maximize efficiency the magnetic field strength must be adjusted for specific cases. For instance, when the maximum torque is required the magnetic field strength must be adjusted to its maximum as well. Thus making the inverter and motor current as low as possible, to reduce power losses, also known as I^2R losses. Unfortunately, the magnetic field strength is not easily changed in a non-ideal permanent magnet. This means that magnetic and conduction losses are difficult to mitigate [71]. The peak point energy efficiency is greater for a DC motor than for an induction motor,

but the average point energy of an induction motor is greater than that of a DC motor [71].

D.1.3 Comparison between the motors

Comparing both of these machines, certain aspects tend to stand out. Regarding physical size, when brushless DC motor growth is proportional to magnetic losses grow. This is not the case for the induction motor as the magnetic losses do not necessarily grow. The B-field of induction motors is more easily adjusted, therefore the induction motor may be favored for high-performance uses. The induction motor, might also be desired for a better average efficiency, but a higher peak efficiency can be seen in DC motors.[71].

From a cost perspective, permanent magnets used in DC motors are expensive. Induction machines do have added development costs as they are difficult to control and understand. Achieving stability over the entire torque-speed range is more difficult for the induction motor than for the DC motor [71].

D.1.4 The use of three-phase systems

The three following reasons are given for the common use of three-phase systems. Firstly, comparing single-phase generators with three-phase generators, the latter are more efficient based on the power per mass of the unit. They are smoother in operation, meaning less vibration, as well. Secondly, three-phase currents produce a rotating magnetic field in the stator. Therefore they are capable of making machines spin at suited speeds and directions. Lastly, the wiring is used more efficiently in three-phase systems [15].

Appendix E

DC-DC converter : Temperature observation

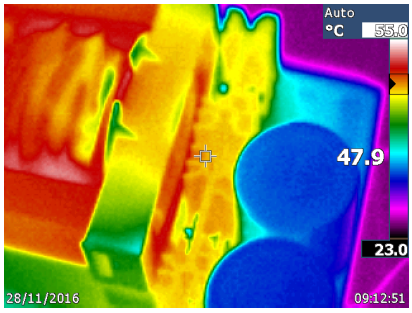

Figure E.1: Temperature distribution: The diodes heatsinks at 47.9 degrees Celsius.

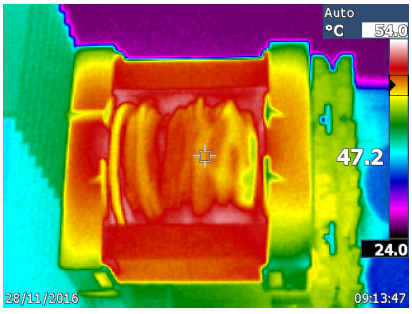

Figure E.2: Temperature distribution: The transformer windings at 47.2 degrees Celsius.

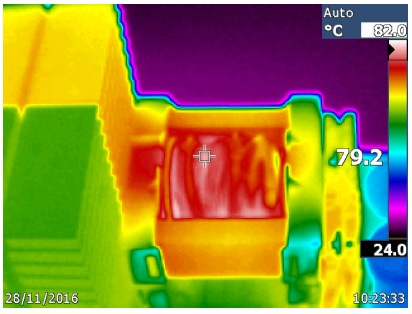

Figure E.3: Temperature distribution: The transformer windings at 79.2 degrees Celsius .

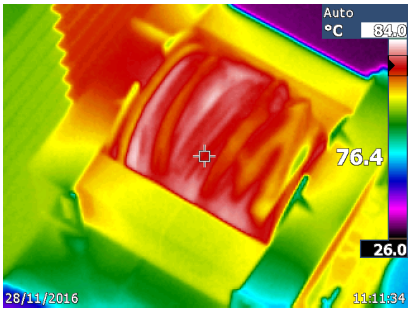

Figure E.4: Temperature distribution: The transformer windings at 76.4 degrees Celsius

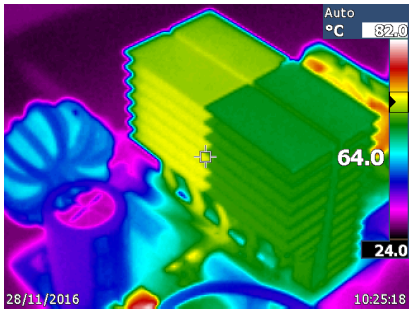

Figure E.5: Temperature distribution: The converter.

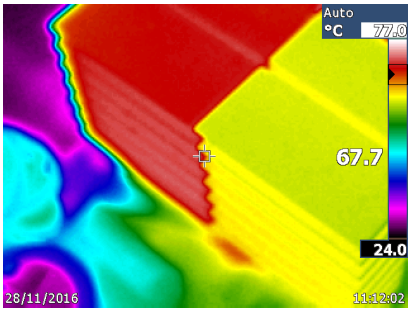

Figure E.6: Temperature distribution: Heatsinks.

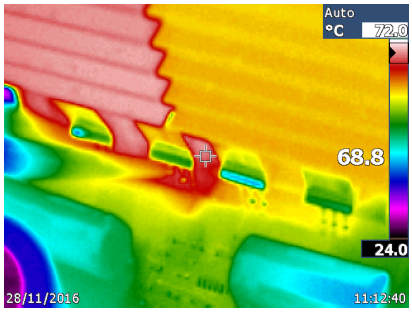

Figure E.7: Temperature distribution: Heatsinks, with temperature of left heatsink as 68.8 degrees.

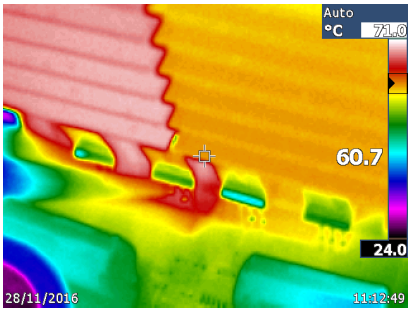

Figure E.8: Temperature distribution: Heatsinks, with temperature of right heatsink as 60.7 degrees.

Appendix F

Flow diagrams: Full view

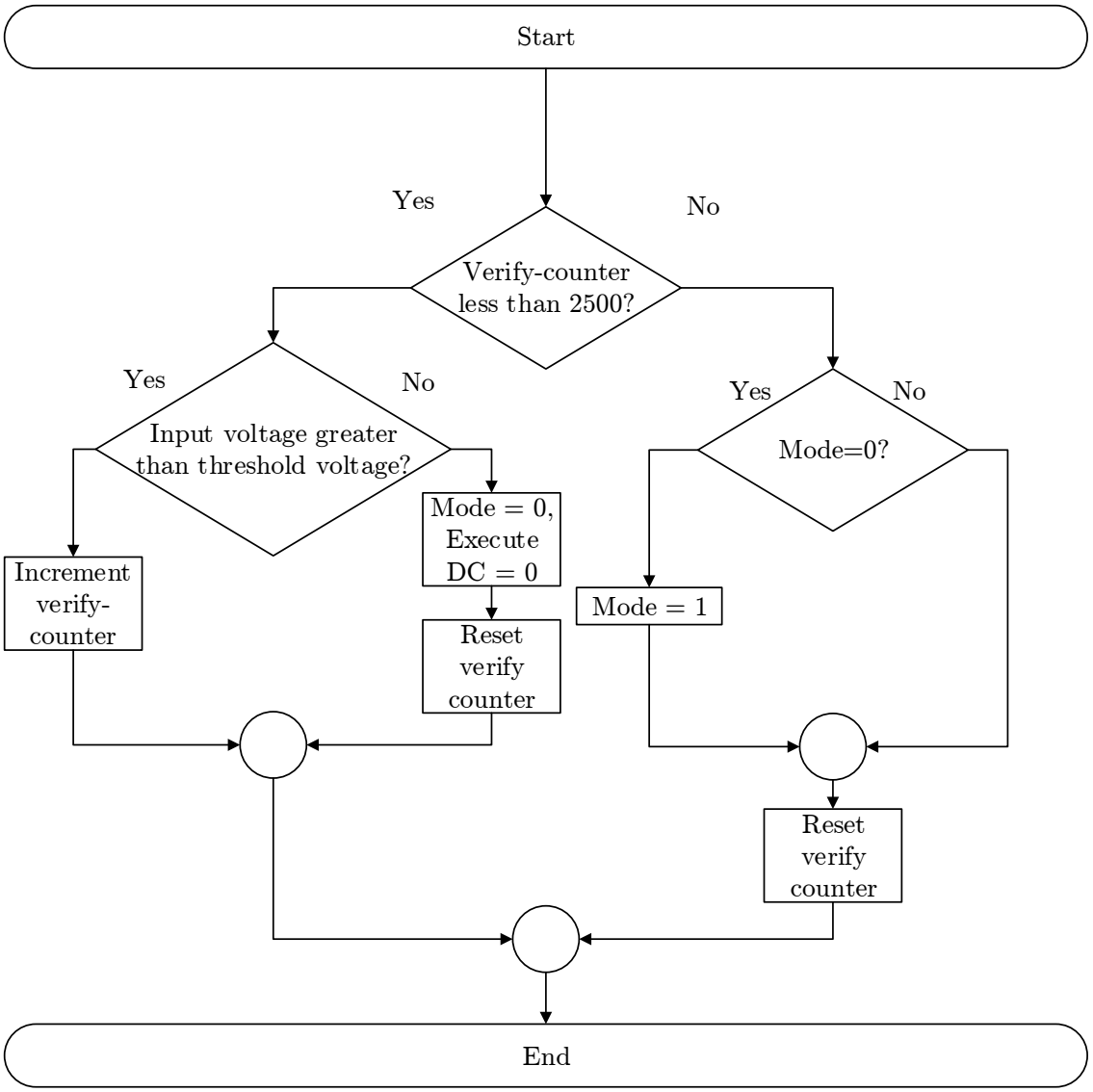

Figure F.1: Control loop: Verification of input voltage.

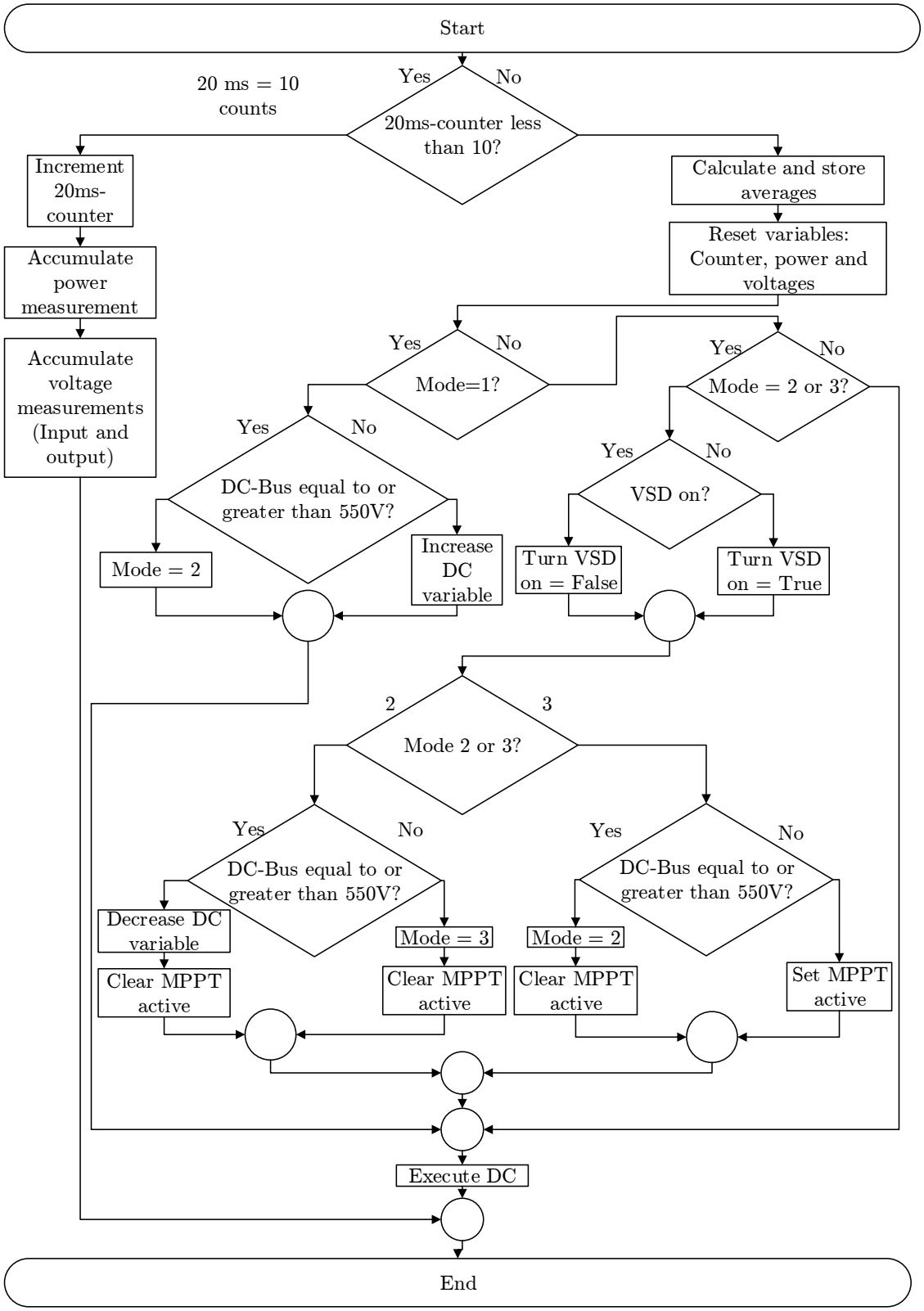

Figure F.2: Control loop: Voltage control.

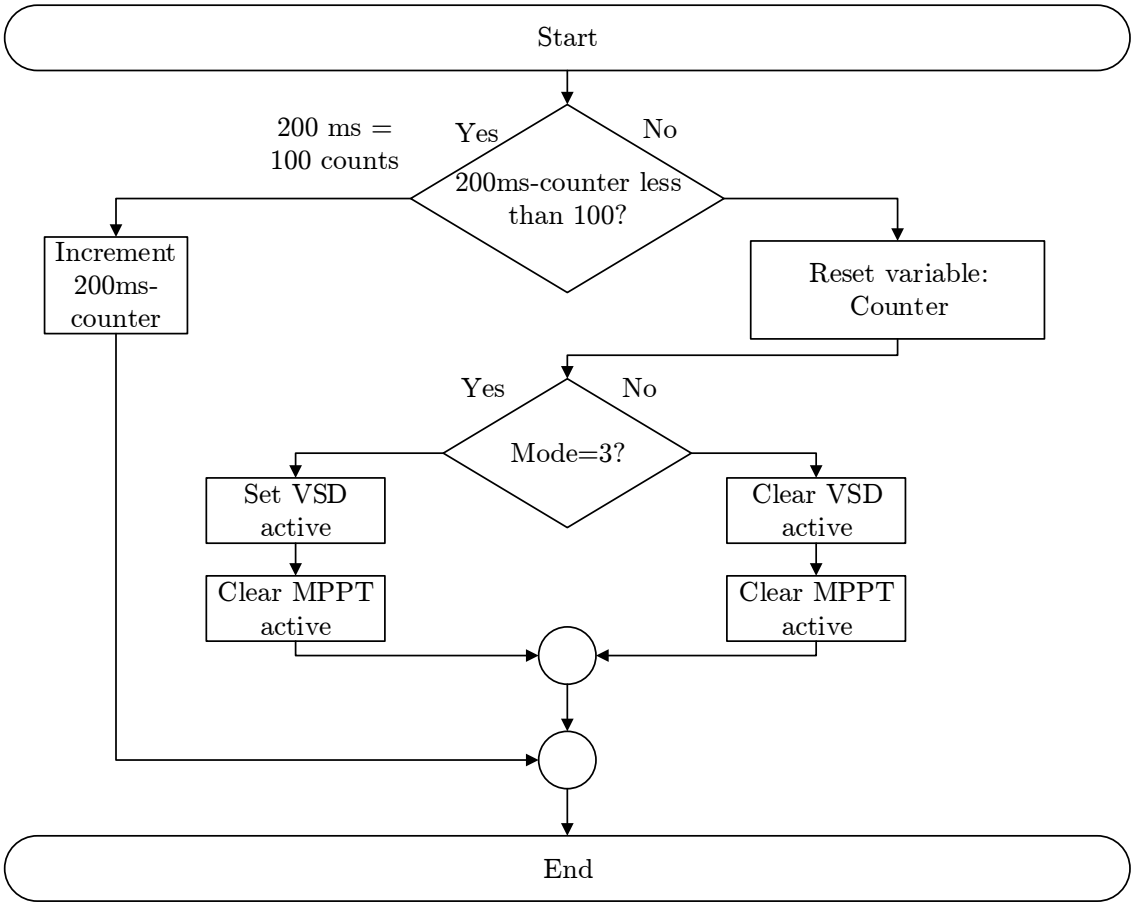

Figure F.3: Control loop: Load or speed control.

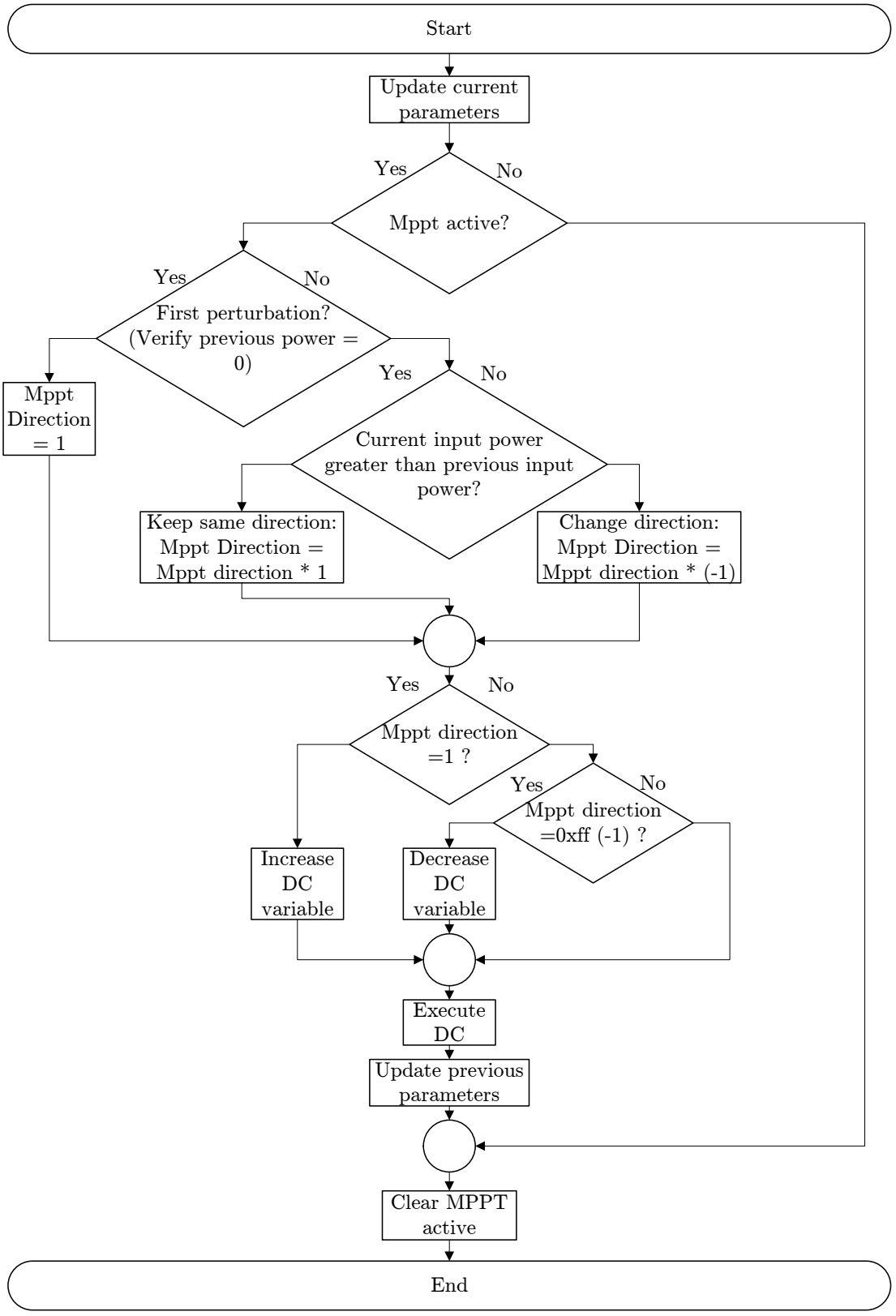

Figure F.4: Control loop: Maximum power point tracking.

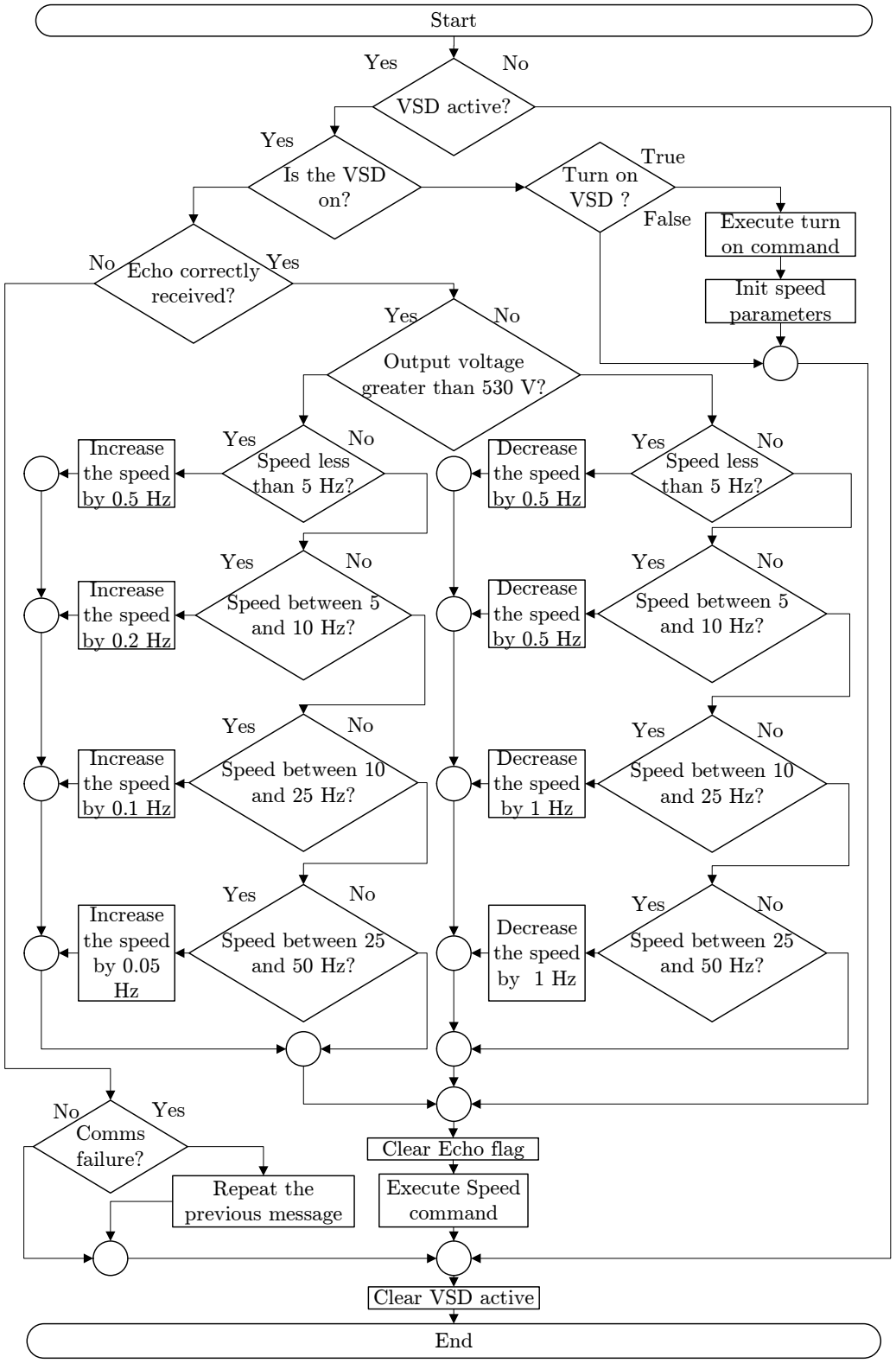

Figure F.5: Control loop: Speed adjustment.

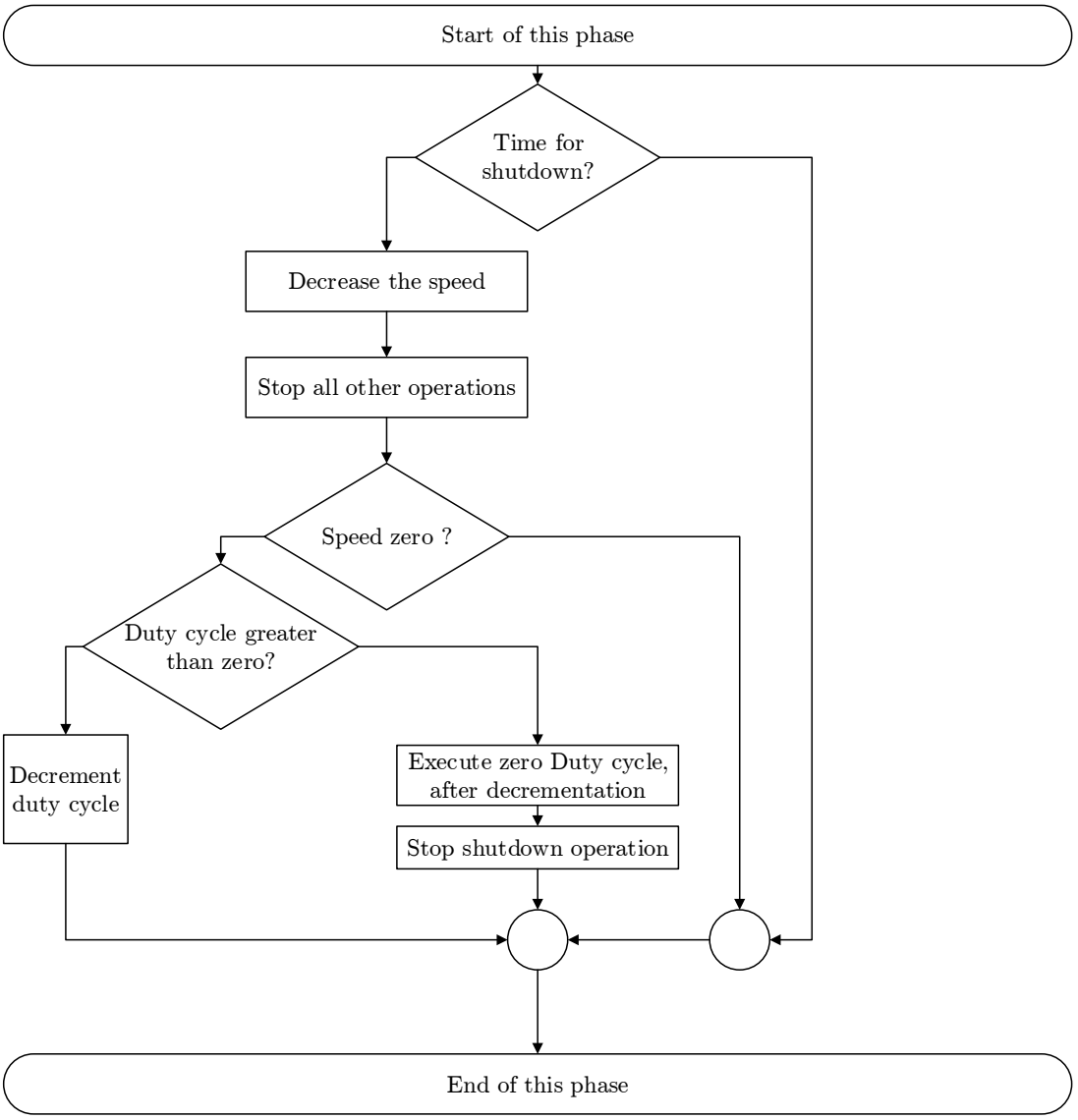

Figure F.6: Control loop: Shutdown.

Appendix G

Component financial information

Figure G.1, on the following page, shows the cost of each component used for the PV drive system excluding the VSD and PCB cost. The total cost for the resonant push-pull converter with the mentioned subsystems accumulates to R 2711.14.

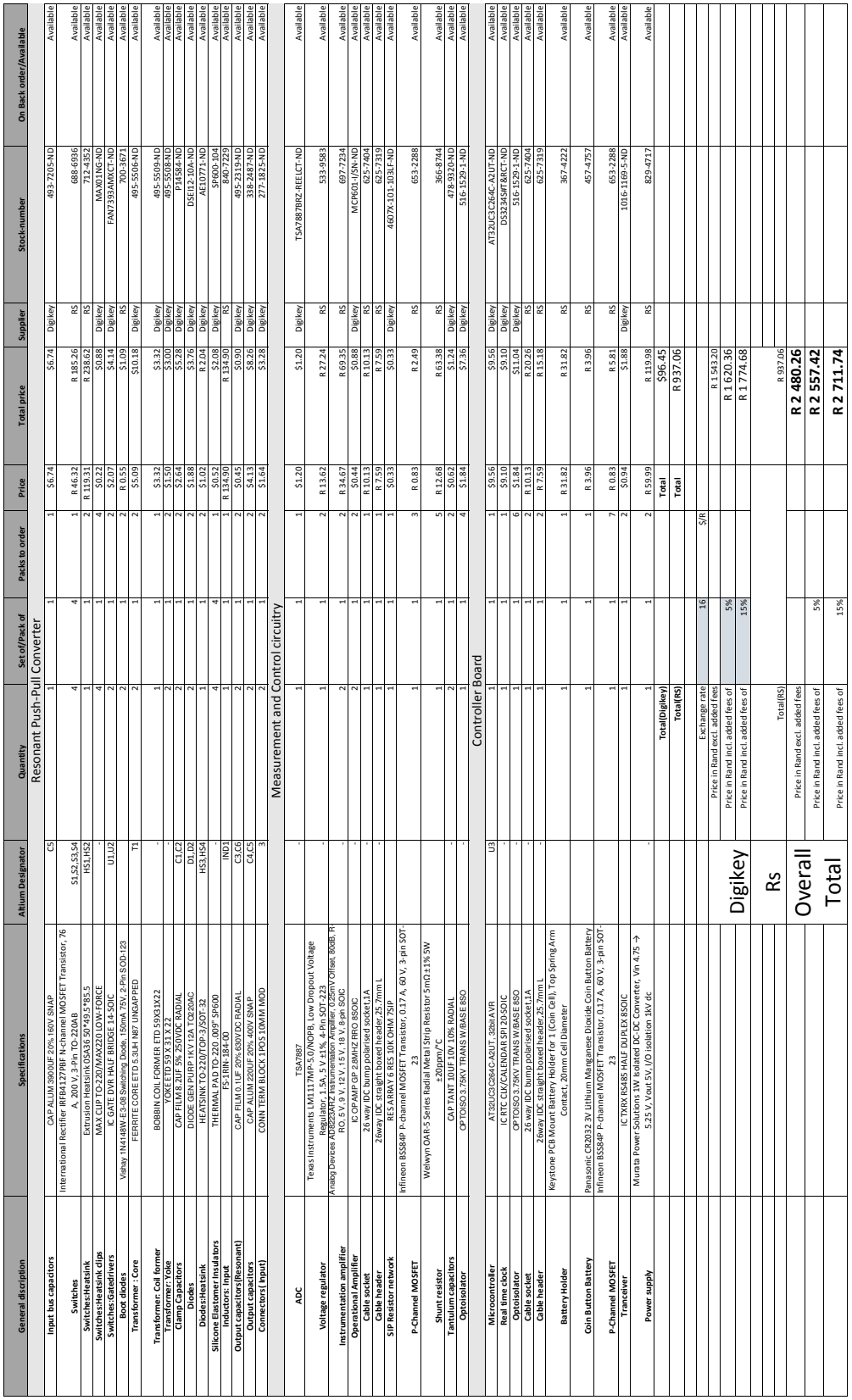

General discription	Specifications	Altium Designator	Quantity	Set of/Pack of	Packs to order	Price	Total price	Supplier	Stock-number	On Back order/Available
Resonant Push-Pull Converter										
Input bus capacitors	CAP ALUM 3900UF 20% 160V SNAP	C5	1	1	1	$6.74	$6.74	Digikey	493-7205-ND	Available
Switches	International Rectifier IRFB4127PBF N-channel MOSFET Transistor, 76 A, 200 V, 3-Pin TO-220AB	S1,S2,S3,S4	4	4	1	R 46.32	R 185.26	RS	688-6936	Available
Switches:Heatsink	Extrusion Heatsink 05A36 50*49.5*85.5	HS1,HS2	1	1	2	R 119.31	R 238.62	RS	712-4352	Available
Switches:Heatsink clips	MAX CLIP TO-220/MAX220 LOW-FORCE	-	4	1	4	$0.22	$0.88	Digikey	MAX01NG-ND	Available
Switches:Gatedrivers	IC GATE DVR HALF BRIDGE 14-SOIC	U1,U2	2	1	2	$2.07	$4.14	Digikey	FAN7393AMXCT-ND	Available
Boot diodes	Vishay 1N4148W-E3-08 Switching Diode, 150mA 75V, 2-Pin SOD-123	-	2	1	2	R 0.55	$1.09	RS	700-3671	Available
Transformer : Core	FERRITE CORE ETD 5.3UH N87 UNGAPPED	T1	2	1	2	$5.09	$10.18	Digikey	495-5506-ND	Available
Transformer: Coil former	BOBBIN COIL FORMER ETD 59X3 1X22	-	1	1	1	$3.32	$3.32	Digikey	495-5509-ND	Available
Transformer: Choke	CAP FILM 8.2UF 5% 250VDC RADIAL	C1,C2	2	1	2	$2.64	$5.28	Digikey	495-5508-ND	Available
Clamp Capacitors	DIODE GEN PURP 1KV 12A TO220AC	D1,D2	2	1	2	$1.88	$3.76	Digikey	P1458A-ND	Available
Diodes	HEATSINK TO-220/TOP-3/SOT-32	HS3,HS4	2	1	2	$1.02	R 2.04	Digikey	DSEI12-10A-ND	Available
Diode:Heatsink	THERMAL PAD TO-220 .009" SP600	-	4	4	1	$0.52	$2.08	Digikey	AE10771-ND	Available
Silicone Elastomer insulators	FS-1 RIN-184.00	IND1	1	1	1	R 334.90	R 334.90	Digikey	SP600-104	Available
Inductors: Input	CAP FILM 0.1UF 20% 630VDC RADIAL	C3,C6	2	1	2	$0.45	$0.90	Digikey	495-2319-ND	Available
Output capacitors(Resonant)	CAP ALUM 220UF 20% 400V SNAP	C4,C5	2	1	2	$4.13	$8.26	Digikey	338-2487-ND	Available
Output capacitors	CONN TERM BLOCK 1POS 10MM MOD	3	2	1	2	$1.64	$3.28	Digikey	277-1825-ND	Available
Connectors(Input)										
Measurement and Control circuitry										
ADC	TSA7887	-	1	1	1	$1.20	$1.20	Digikey	TSA7887HRZ-REELCT-ND	Available
Voltage regulator	Texas Instruments LM1117MP-5.0/NOPB, Low Dropout Voltage Regulator, 1.5A, 5 V ±1%, 4-Pin SOT-223/Offset: 80dB: R	-	1	2	2	R 13.62	R 27.24	RS	533-9583	Available
Instrumentation amplifier	Analog Devices AD8226ARZ, Instrumentation Amplifier, 2.2MHz, 4-Pin SOIC	-	2	1	2	R 34.67	R 69.35	RS	697-7234	Available
Operational Amplifier	RO, 5 V, 9 V, 12 V, 15 V, 18 V, 8-pin SOIC	-	1	1	2	$0.44	$0.88	Digikey	MCP601-I/SN-ND	Available
Cable socket	IC OP AMP GP 2.8MHZ RRO 8SOIC	-	2	1	1	R 10.13	R 10.13	RS	625-7404	Available
Cable header	26 way IDC bump polarised socket 1.A	-	1	1	1	R 10.13	R 10.13	RS	625-7404	Available
SIP Resistor network	26way IDC straight boxed header,25.7mm L	-	1	1	1	R 7.59	R 7.59	RS	625-7319	Available
P-Channel MOSFET	RES ARRAY 6 RES 10K OHM 7SIP	-	1	1	1	$0.33	$0.33	Digikey	4607X-101-103LF-ND	Available
Shunt resistor	Infineon BSS84P P-channel MOSFET Transistor, 0.17 A, 60 V, 3-pin SOT-23		1	1	3	R 0.83	R 2.49	RS	653-2288	Available
Tantulum capacitors	Welwyn OAR-5 Series Radial Metal Strip Resistor 5mΩ ±1% 5W ±20ppm/°C		1	1	5	R 12.68	R 63.38	RS	366-8744	Available
Optoisolator	CAP TANT 10UF 10V 10% RADIAL	-	2	1	2	$0.62	$1.24	Digikey	478-9320-ND	Available
	OPTOISO 2.75KV TRANS W/BASE 8SO	-	1	1	4	$1.84	$7.36	Digikey	516-1529-1-ND	Available
Controller Board										
Microcontroller	AT32UC3C264C-A2UT. 32bit AVR	U3	1	1	1	$9.56	$9.56	Digikey	AT32UC3C264C-A2UT-ND	Available
Real time clock	IC RTC CLK/CALENDAR SPI 20-SOIC	-	1	1	1	$9.10	$9.10	Digikey	DS32345#T&RCT-ND	Available
Optoisolator	OPTOISO 3.75KV TRANS W/BASE 8SO	-	1	1	6	$1.84	$11.04	Digikey	516-1529-1-ND	Available
Cable socket	26 way IDC bump polarised socket 1.A	-	1	1	2	R 10.13	R 20.26	RS	625-7404	Available
Cable header	26way IDC straight boxed header,25.7mm L	-	1	1	2	R 7.59	R 15.18	RS	625-7319	Available
Battery Holder	Keystone PCB Mount Battery Holder for 1 (Coin Cell), Top Spring Arm Contact, 20mm Cell Diameter		1	1	1	R 31.82	R 31.82	RS	367-4222	Available
Coin Button Battery	Panasonic CR2032 3V Lithium Manganese Dioxide Coin Button Battery		1	1	1	R 3.96	R 3.96	RS	457-4757	Available
P-Channel MOSFET	Infineon BSS84P P-channel MOSFET Transistor, 0.17 A, 60 V, 3-pin SOT-23		1	1	7	R 0.83	R 5.81	RS	653-2288	Available
Tranceiver	IC TXRX RS485 HALF DUPLEX 8SOIC		1	1	2	$0.94	$1.88	Digikey	1016-1169-5-ND	Available
Power supply	Murata Power Solutions 1W Isolated DC-DC Converter, Vin 4.75 → 5.25 V, Vout 5V, I/O Isolation 1kV dc	-	1		2	R 59.99	R 119.98	RS	829-4717	Available
						Total	$96.45			
						Total	R 937.06			
							R 937.06			
							R 1 543.20			
							R 1 620.36			
							R 1 774.68			

		Exchange rate	16
		Price in Rand excl. added fees	
Digikey	Rs	Price in Rand incl. added fees of	5%
		Price in Rand incl. added fees of	15%
		Total(RS)	
Overall Total	Price in Rand excl. added fees		
	Price in Rand incl. added fees of	5%	
	Price in Rand incl. added fees of	15%	

$/R	
	R 2 480.26
	R 2 557.42
	R 2 711.74

Figure G.1: Schematic representation of the PV drive system, indicating interaction between various subsystems

Appendix H

Output voltage:Start-up attempts before noon

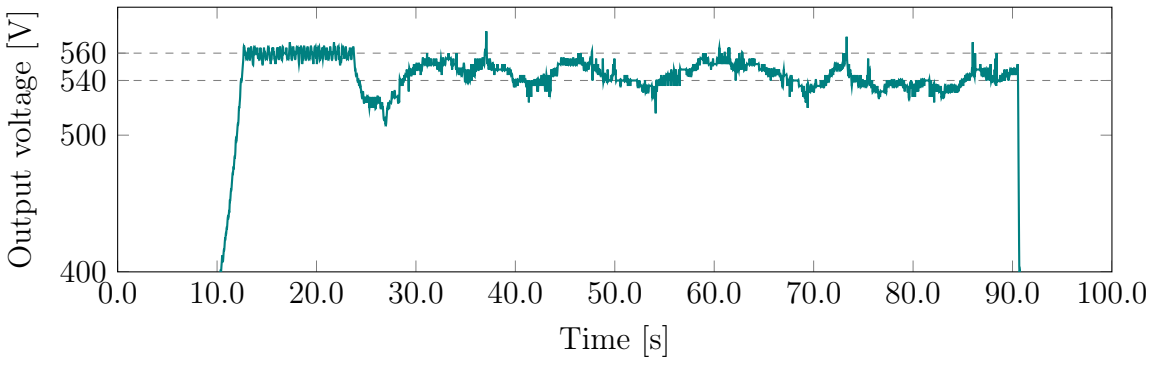

Figure H.1: Output voltage transient zoomed in: Start-up of the system increasing the speed until maximum load, in the morning - Attempt 1.

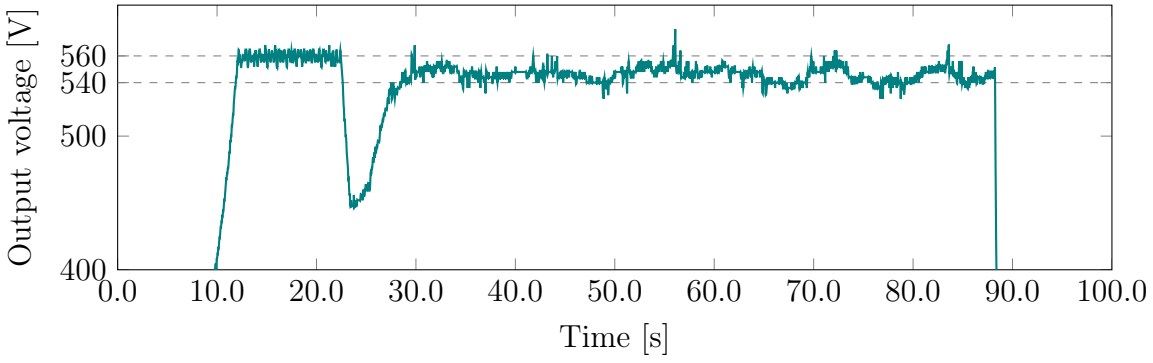

Figure H.2: Output voltage transient zoomed in: Start-up of the system increasing the speed until maximum load, in the morning - Attempt 2.

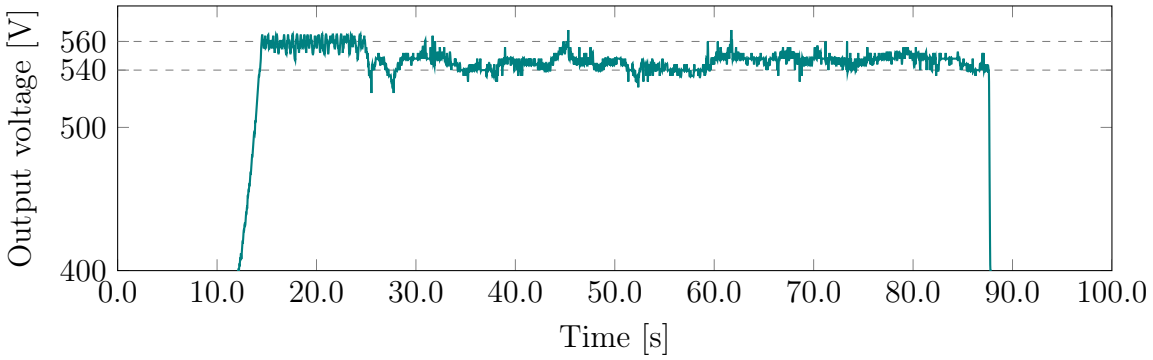

Figure H.3: Output voltage transient zoomed in: Start-up of the system increasing the speed until maximum load, in the morning - Attempt 3.

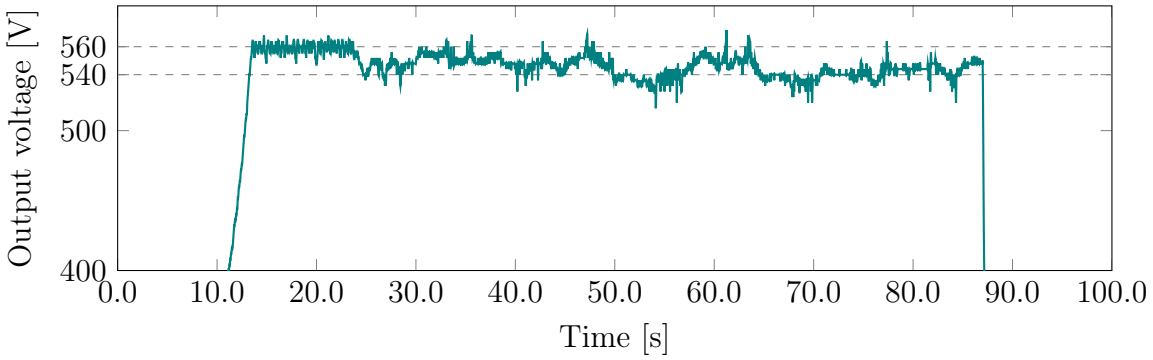

Figure H.4: Output voltage transient zoomed in: Start-up of the system increasing the speed until maximum load, in the morning - Attempt 4.

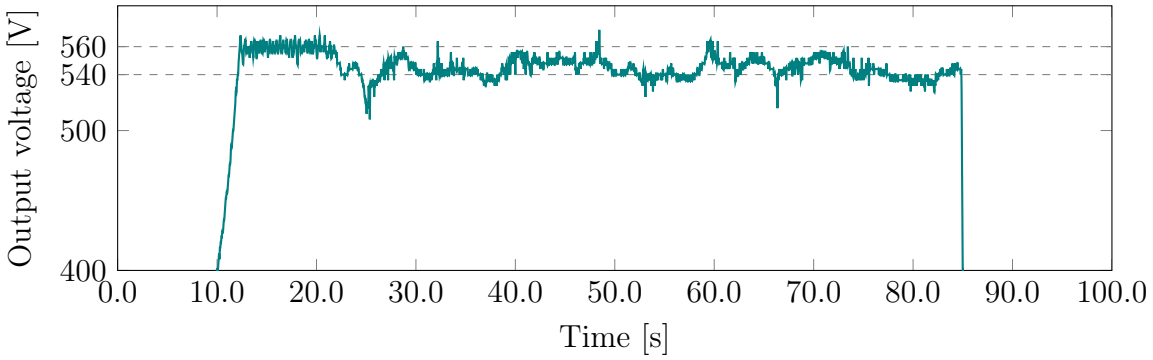

Figure H.5: Output voltage transient zoomed in: Start-up of the system increasing the speed until maximum load, in the morning - Attempt 5.

Appendix I

Output voltage: Start-up attempts after noon

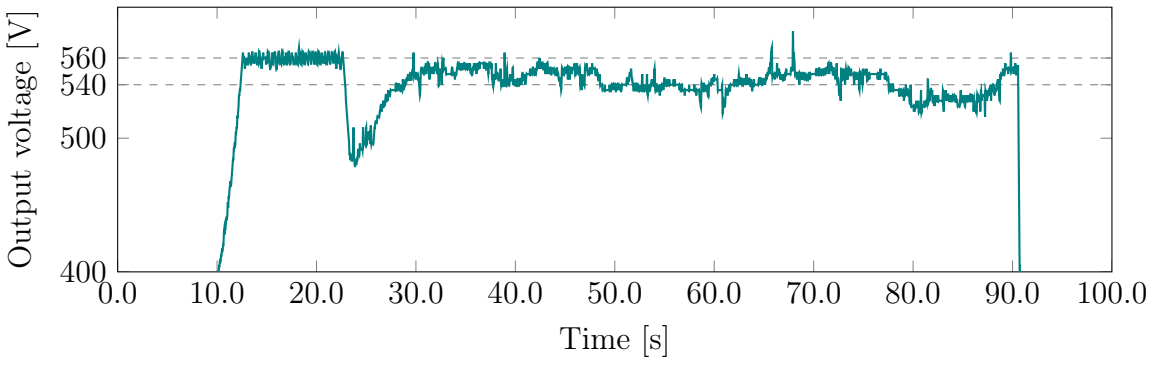

Figure I.1: Output voltage transient zoomed in: Start-up of the system increasing the speed until maximum load, in the morning - Attempt 1.

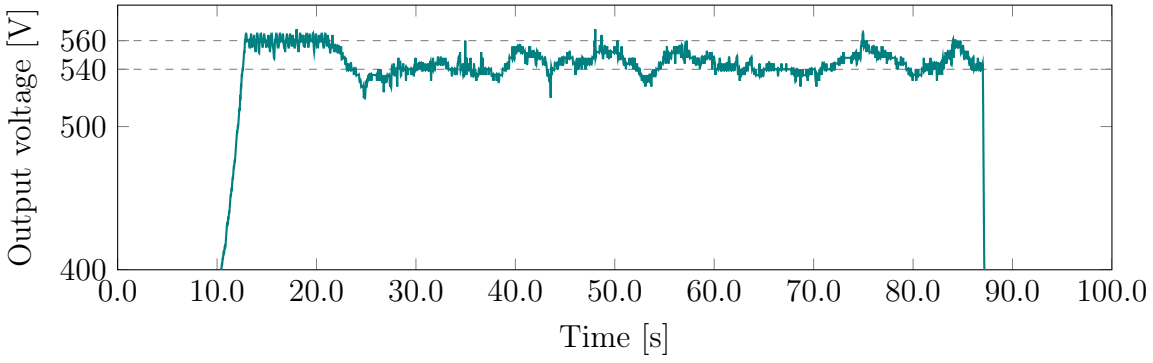

Figure I.2: Output voltage transient zoomed in: Start-up of the system increasing the speed until maximum load, in the afternoon - Attempt 2.

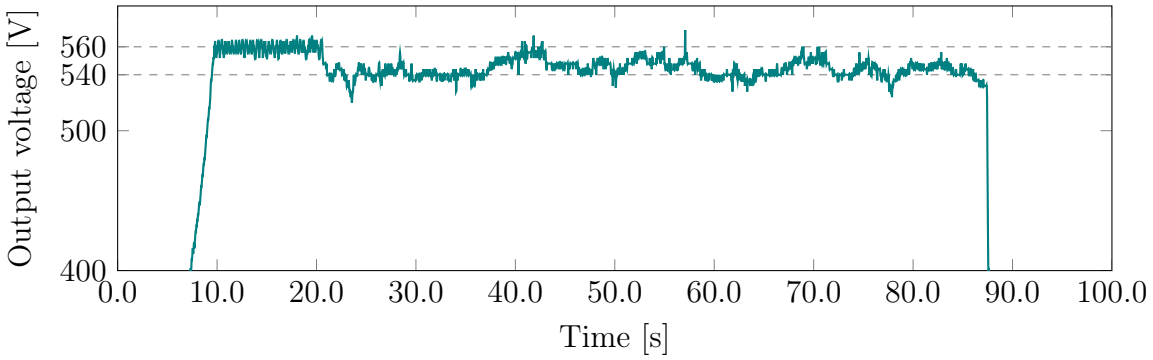

Figure I.3: Output voltage transient zoomed in: Start-up of the system increasing the speed until maximum load, in the afternoon - Attempt 3.

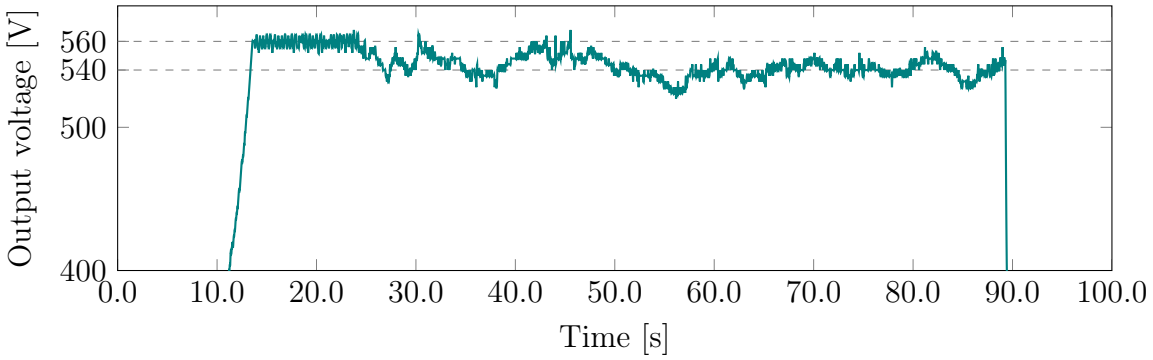

Figure I.4: Output voltage transient zoomed in: Start-up of the system increasing the speed until maximum load, in the afternoon - Attempt 4.

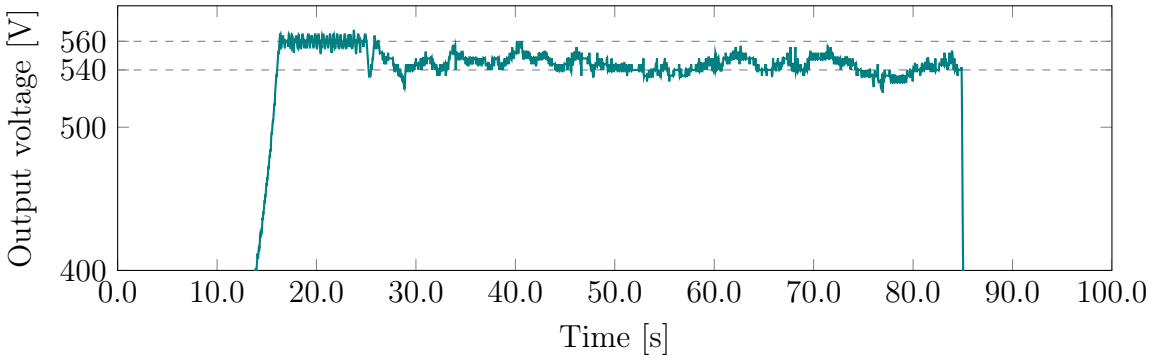

Figure I.5: Output voltage transient zoomed in: Start-up of the system increasing the speed until maximum load, in the afternoon - Attempt 5.

List of References

[1] FAO, IFAD, and WFP, *The State of Food Insecurity in the World: Meeting the 2015 international hunger targets: taking stock of uneven progress*. Food and Agriculture Organization of the United Nations, 2015.

[2] World Bank Staff, *Strategies for Sustained Growth and Inclusive Development*. Washington, DC: The World Bank, 2008.

[3] International Labour Office, *Global Employment Trends 2012: Preventing a deeper jobs crisis*. International Labour Office, 2012.

[4] Y. I. Abdalla, *Causes of Food Insecurity in Southern Africa :*. Master in agriculture, University of Stellenbosch, 2007.

[5] FAO, IFAD, and WFP, "Reducing Poverty and Hunger: The critical role of financing for food, agriculture and rural development.," *Rome, FAO*, 2002.

[6] FAO, "Hunger Statistics _ WFP _ United Nations World Food Programme - Fighting Hunger Worldwide," 2015.

[7] Katharine Earley, "How technology can prevent food waste in developing countries," 2014.

[8] Food and Agriculture Organisation, "4 . Causes and prevention of food losses and waste," *Global Food Losses and Food Waste*, pp. 10–14, 2009.

[9] G. Hundy, A. Trott, and T. Welch, "Food Refrigeration and Freezing," in *Refrigeration and Air-Conditioning*, pp. 177–183, Elsevier, 2008.

[10] G. Bordenave, "Louis Pasteur (1822-1895).," *Microbes and infection / Institut Pasteur*, vol. 5, no. 6, pp. 553–60, 2003.

[11] G. G. Maidment, A. Paurine, and L. South, "Solar Cooling and Refrigeration Systems," *Comprehensive Renewable Energy*, vol. 3, pp. 481–494, 2012.

[12] R. Best and I. Pilatowsky, "Solar assisted cooling with sorption systems : status of the research in Mexico and Latin America Systems frigorifiques sorption utilisant l ' rnergie solaire " etat de la recherche au Mexique et en Amrrique Latine," *International Journal of Refrigeration*, vol. 21, no. 97, pp. 100–115, 1998.

[13] G. Hundy, A. Trott, and T. Welch, "The Refrigeration Cycle," in *Refrigeration and Air-Conditioning*, pp. 15–29, Elsevier, 2008.

[14] G. Hundy, A. Trott, and T. Welch, "Compressors," in *Refrigeration and Air-Conditioning*, pp. 41–65, Elsevier, 4 ed., 2008.

[15] G. M. Masters, *Renewable and Efficient Electric Power Systems, Second edition*. Hoboken, NJ, USA: John Wiley & Sons, Inc., jul 2013.

[16] M. N. Qaiser, M. Usama, B. Ahmad, M. A. Tariq, and H. A. Khan, "Low cost, robust and efficient implementation of MPPT based buck-boost converter for off-grid PV applications," *2014 IEEE 40th Photovoltaic Specialist Conference, PVSC 2014*, pp. 3701–3706, 2014.

[17] S. Mandelli, J. Barbieri, R. Mereu, and E. Colombo, "Off-grid systems for rural electrification in developing countries: Definitions, classification and a comprehensive literature review," *Renewable and Sustainable Energy Reviews*, vol. 58, pp. 1621–1646, 2016.

[18] D. Palit and A. Chaurey, "Energy for Sustainable Development Off-grid rural electrification experiences from South Asia : Status and best practices," *Energy for Sustainable Development*, vol. 15, no. 3, pp. 266–276, 2011.

[19] K. Narula, Y. Nagai, and S. Pachauri, "The role of Decentralized Distributed Generation in achieving universal rural electrification in South Asia by 2030," *Energy Policy*, vol. 47, pp. 345–357, 2012.

[20] P. Cook, "Infrastructure, rural electrification and development," *Energy for Sustainable Development*, vol. 15, no. 3, pp. 304–313, 2011.

[21] M. Welsch, M. Bazilian, M. Howells, D. Divan, D. Elzinga, G. Strbac, L. Jones, A. Keane, D. Gielen, V. S. K. M. Balijepalli, A. Brew-Hammond, and K. Yumkella, "Smart and Just Grids for sub-Saharan Africa: Exploring options," *Renewable and Sustainable Energy Reviews*, vol. 20, pp. 336–352, 2013.

[22] J. T. Murphy, "Making the energy transition in rural East Africa: Is leapfrogging an alternative?," *Technological Forecasting and Social Change*, vol. 68, no. 2, pp. 173–193, 2001.

[23] M. Fahmi, D. Isa, R. Arelhi, and R. RajKumar, "Solar PV system for off-grid electrification in rural area," *3rd IET International Conference on Clean Energy and Technology (CEAT) 2014*, pp. 49 (6 .)–49 (6 .), 2014.

[24] S. Baurzhan and G. P. Jenkins, "Off-grid solar PV: Is it an affordable or appropriate solution for rural electrification in Sub-Saharan African countries?," *Renewable and Sustainable Energy Reviews*, vol. 60, pp. 1405–1418, 2016.

[25] M. Bouzguenda, A. Al Omair, A. Al Naeem, M. Al-Muthaffar, and O. B. Wazir, "Design of an off-grid 2 kW solar PV system," *2014 9th International Conference on Ecological Vehicles and Renewable Energies, EVER 2014*, pp. 1–6, 2014.

[26] G. Lahn and P. Stevens, "Burning Oil to Keep Cool: the Hidden Energy Crisis in Saudi Arabia," 2011.

[27] M. A. Jones, I. Odeh, M. Haddad, A. H. Mohammad, and J. C. Quinn, "Economic analysis of photovoltaic (PV) powered water pumping and desalination without energy storage for agriculture," *Desalination*, vol. 387, pp. 35–45, 2016.

[28] M. A. Vitorino, M. B. De Rossiter Corrêa, C. B. Jacobina, and A. M. N. Lima, "An effective induction motor control for photovoltaic pumping," *IEEE Transactions on Industrial Electronics*, vol. 58, no. 4, pp. 1162–1170, 2011.

[29] Y. Fan, L. Luo, and B. Souyri, "Review of solar sorption refrigeration technologies: Development and applications," *Renewable and Sustainable Energy Reviews*, vol. 11, no. 8, pp. 1758–1775, 2007.

[30] I. F. P. Research Institute (IFPRI), "Food security in a world of natural resource scarcity The role of agricultural technologies," tech. rep., International Food Policy Research Institute, Washington, DC, 2016.

[31] E. Zhou, "Integration of a PV-Battery Hybrid System with the Main Power Grid," pp. 0–4, 2016.

[32] S. P. Energy, "Solar Products _ Gel Deep Cycle Batteries _ AGM Deep Cycle Batteries _ Lead Acid Batteries _ Victron Quattro Inverters_Chargers _ Batteries _ Victron."

[33] B.-H. Kwon and E.-H. Kim, "High step-up resonant push-pull converter with high efficiency," *IET Power Electronics*, vol. 2, pp. 79–89, jan 2009.

[34] N. Mohan, T. M. Undeland, and W. P. Robbins, *Power Electronics: Converters, Applications and Design*. New Jersey: John Wiley & Sons, 3rd ed., 2003.

[35] P. Randewijk, "Three-Phase Variable Speed Drive (Image)."

[36] V. Barends, *Developing a Suitable Carbon Calculator for Smallholder Mixed Farming Systems in Western Cape , South Africa by*. Master in agriculture, University of Stellebosch, 2016.

[37] A. El-Shaer, M. T. Y. Tadros, and M. A. Khalifa, "Effect of Light intensity and Temperature on Crystalline Silicon Solar Modules Parameters," *Ijetae*, vol. 4, no. 8, pp. 311–318, 2014.

[38] S. J. Chapman, *Electric Machinery Fundamentals*. McGraw-Hill, fourth ed., 2005.

[39] S. Ang, *Power switching converters*. New York: Marcel Dekker, Inc, one ed., 1995.

[40] N. Kularatna, *Power electronics design handbook: Low-power components and applications*. Woburn: Butterworth-Heinemann, one ed., 1998.

[41] H. d. T. Mouton, "Electronics 414 (Power Electronics) Lecture Notes," 2013.

[42] S. E.Lyshevski, *Electromechanical Systems and Devices*. Boca Raton: CRC Press, 1st ed., 2008.

[43] E. Sanchis-Kilders, a. Ferreres, E. Maset, J. Ejea, V. Esteve, J. Jordan, R. Garcia, and a. Garrigos, "High power passive soft switched interleaved boost converters," *2004 IEEE 35th Annual Power Electronics Specialists Conference (IEEE Cat. No.04CH37551)*, vol. 1, pp. 426–432, 2004.

[44] G. Spiazzi, P. Mattavelli, and A. Costabeber, "High step-up ratio flyback converter with active clamp and voltage multiplier," *IEEE Transactions on Power Electronics*, vol. 26, no. 11, pp. 3205–3214, 2011.

[45] P. Muthukrishnan and R. Dhanasekaran, "Dc- Dc Boost Converter for Solar Power Application," *Theoretical and Applied Information Technology*, vol. 68, no. 3, pp. 630–636, 2014.

[46] R. Gules, L. L. Pfitscher, and L. C. Franco, "An interleaved boost DC-DC converter with large conversion ratio," *IEEE International Symposium on Industrial Electronics*, vol. I, pp. 411–416, 2003.

[47] P. W. Lee, Y. S. Lee, D. K. W. Cheng, and X. C. Liu, "Steady-state analysis of an interleaved boost converter with coupled inductors," *IEEE Transactions on Industrial Electronics*, vol. 47, no. 4, pp. 787–795, 2000.

[48] H. Kosai, J. Scofield, S. McNeal, B. Jordan, and B. Ray, "Design and performance evaluation of a 200C interleaved boost converter," *IEEE Transactions on Power Electronics*, vol. 28, no. 4, p. 1691, 2013.

[49] a. Tomaszuk and a. Krupa, "High efficiency high step-up DC/DC converters - a review," *Bulletin of the Polish Academy of Sciences: Technical Sciences*, vol. 59, no. 4, pp. 475–483, 2012.

[50] R. P. T. Bascope, G. J. M. Sousa, C. G. C. Branco, L. D. S. Bezerra, C. M. T. Cruz, and R. G. A. Cacau, "A new step-up high voltage gain dc-dc converter," in *2010 9th IEEE/IAS International Conference on Industry Applications - INDUSCON 2010*, pp. 1–6, IEEE, nov 2010.

[51] X. Fang, "A novel Z-source DC-DC converter," *Proceedings of the IEEE International Conference on Industrial Technology*, pp. 8–11, 2008.

[52] Q. Zhao and F. C. Lee, "High-efficiency, high step-up dc-dc converters," *IEEE Transactions on Power Electronics*, vol. 18, no. 1 I, pp. 65–73, 2003.

[53] R. Redl, N. Sokal, and L. Balogh, "A novel soft-switching full-bridge DC/DC converter: Analysis, design considerations, and experimental results at 1.5 kW, 100 kHz," in *21st Annual IEEE Conference on Power Electronics Specialists*, pp. 162–172, IEEE, 1990.

[54] O. Krykunov, "Comparison of the DC/DC-converters for Fuel Cell Applications," *International Journal of Electrical and Electronics Engineering*, vol. 1, no. 1, pp. 71–79, 2007.

[55] M. Rashid and D. Czarkowski, "DC-DC Converters," *Power Electronics Handbook. Devices, Circuits, and Applications*, vol. 2, no. c, pp. 245–259, 2006.

[56] M. Nymand and M. A. Andersen, "A new approach to high efficiency in isolated boost converters for high-power low-voltage fuel cell applications," in *2008 13th International Power Electronics and Motion Control Conference*, pp. 127–131, IEEE, sep 2008.

[57] M. Nymand and M. A. E. Andersen, "High-efficiency isolated boost DCDC converter for high-power low-voltage fuel-cell applications," *IEEE Transactions on Industrial Electronics*, vol. 57, no. 2, pp. 505–514, 2010.

[58] F. Nome and I. Barbi, "A ZVS clamping mode-current-fed push-pull DC-DC converter," *IEEE International Symposium on Industrial Electronics. Proceedings. ISIE'98 (Cat. No.98TH8357)*, vol. 2, pp. 617–621, 1998.

[59] Epcos, "Ferrites and Accessories EPCOS Data Book 2013," 2012.

[60] M. A. Swihart, "Inductor cores - Material and Shape Choices."

[61] D. Murthy-Bellur, N. Kondrath, and M. Kazimierczuk, "Transformer winding loss caused by skin and proximity effects including harmonics in pulse-width modulated DC-DC flyback converters for the continuous conduction mode," *IET Power Electronics*, vol. 4, no. 4, p. 363, 2011.

[62] S. Ang, *Power-Switching Converters, Second Edition*. Boca Raton: CRC press, 2005.

[63] A. N. Lemmon, M. S. Mazzola, J. R. Gafford, and C. Parker, "Ensuring volt-second balance in high-power-density phase-shifted full-bridge converter design," *Conference Proceedings - IEEE Applied Power Electronics Conference and Exposition - APEC*, pp. 2919–2925, 2014.

[64] Future Electronics, "Microcontrollers, what is a microcontroller? 8 bit, 16 bit & 32 bit microcontrollers - Future Electronics."

[65] M. Wolf, *Computers as components: principles of embedded computing system design*. 2012.

[66] Atmel Corporation, "At32Uc3C," pp. 1–1316, 2012.

[67] A. Devices, "Single-Supply , Low Cost Instrumentation Amplifier," 2008.

[68] V. P. T. Corporation, "Aspire Solar Pump Inverter," 2017.

[69] C. D. C. P. Ltd, "CraigCor Distribution Company Ltd Services," 2017.

[70] Sustainable, "Microcare Portable 1," 2017.

[71] W. Rippel, "Induction Versus DC Brushless Motors," 2007.